SELF-ASSEMBLING PEPTIDE HYDROGEL: DESIGN, CHARACTERIZATION AND APPLICATION

by

HONGZHOU HUANG

B.S., Xiamen University, Xiamen, China, 2007

AN ABSTRACT OF A DISSERTATION

submitted in partial fulfillment of the requirements for the degree

DOCTOR OF PHILOSOPHY

Department of Grain Science and Industry
College of Agriculture

KANSAS STATE UNIVERSITY
Manhattan, Kansas

2012

Abstract

Rational design of peptide molecules to undergo spontaneous organization as a higher-ordered supramolecular structure is an attractive and fast-growing field for developing new functional biomaterials. Hydrogel, with its high water content and three-dimensional architecture, is formed by a self-assembling peptide and has great potential for broad biomedical applications. The key challenge in controlling the functional properties of final biomaterials can be met by designing the peptide primary structure carefully at the beginning and developing a comprehensive understanding of peptide self-assembly pathways.

In this study, we first designed a Ca^{2+} responsive peptide (eD_2) using identified functional native domains from a spider flagelliform silk protein and the Ca^{2+} binding domain of lipase Lip A from *Serratia marcescens*. Instead of directly linking the two peptide sequences, we rationally inserted the ion-binding motif into the silk structure sequence and made the new peptide inherit the physical characteristics of both model sequences and assemble into nanofibers when triggered by Ca^{2+}. Next, we introduced the amphiphilic property to the eD_2 peptide by conjugating its N-terminus with a strong hydrophobic sequence from a trans-membrane segment of human muscle L-type calcium channel. This self-assembly peptide, called h9e, was responsive to Ca^{2+}, solution pH, and selected proteins for hydrogel formation. Interestingly, the turning segment GSII of h9e was considered to play a critical role in construction of the finial matrix. This hypothesis was further demonstrated by exploiting a series of amphiphilic diblock model peptides with different conformational flexibility. The kinetic rate of peptide assembly was suggested as one of the key influences for peptide supramolecular assembly morphology. To better understand the peptide self-assembly process during hydrogel formation, the conformational, morphological, and mechanical properties of h9e molecules in different dimethylsulfoxide/H_2O solutions were monitored by 1D and 2D proton nuclear magnetic resonance (NMR), electron microscopy, and a rheometer. The h9e peptide hydrogel formed with Ca^{2+} and albumin exhibited superior physiological and specific injectable properties, which provides a more realistic tool for 3D cell culture and drug delivery.

This study generates new knowledge and contributes to the field by leading to a better understanding the self-assembly hydrogel formation and designing peptides with unique properties for biomedical applications such as cell culture, drug delivery, and tissue engineering.

SELF-ASSEMBLING PEPTIDE HYDROGEL: DESIGN, CHARACTERIZATION AND APPLICATION

by

HONGZHOU HUANG

B.S., Xiamen University, Xiamen, China, 2007

A DISSERTATION

submitted in partial fulfillment of the requirements for the degree

DOCTOR OF PHILOSOPHY

Department of Grain Science and Industry
College of Agriculture

KANSAS STATE UNIVERSITY
Manhattan, Kansas

2012

Approved by:

Major Professor
Xiuzhi Susan Sun

Copyright

Abstract

Rational design of peptide molecules to undergo spontaneous organization as a higher-ordered supramolecular structure is an attractive and fast-growing field for developing new functional biomaterials. Hydrogel, with its high water content and three-dimensional architecture, is formed by a self-assembling peptide and has great potential for broad biomedical applications. The key challenge in controlling the functional properties of final biomaterials can be met by designing the peptide primary structure carefully at the beginning and developing a comprehensive understanding of peptide self-assembly pathways.

In this study, we first designed a Ca^{2+} responsive peptide (eD_2) using identified functional native domains from a spider flagelliform silk protein and the Ca^{2+} binding domain of lipase Lip A from *Serratia marcescens*. Instead of directly linking the two peptide sequences, we rationally inserted the ion-binding motif into the silk structure sequence and made the new peptide inherit the physical characteristics of both model sequences and assemble into nanofibers when triggered by Ca^{2+}. Next, we introduced the amphiphilic property to the eD_2 peptide by conjugating its N-terminus with a strong hydrophobic sequence from a trans-membrane segment of human muscle L-type calcium channel. This self-assembly peptide, called h9e, was responsive to Ca^{2+}, solution pH, and selected proteins for hydrogel formation. Interestingly, the turning segment GSII of h9e was considered to play a critical role in construction of the finial matrix. This hypothesis was further demonstrated by exploiting a series of amphiphilic diblock model peptides with different conformational flexibility. The kinetic rate of peptide assembly was suggested as one of the key influences for peptide supramolecular assembly morphology. To better understand the peptide self-assembly process during hydrogel formation, the conformational, morphological, and mechanical properties of h9e molecules in different dimethylsulfoxide/H_2O solutions were monitored by 1D and 2D proton nuclear magnetic resonance (NMR), electron microscopy, and a rheometer. The h9e peptide hydrogel formed with Ca^{2+} and albumin exhibited superior physiological and specific injectable properties, which provides a more realistic tool for 3D cell culture and drug delivery.

This study generates new knowledge and contributes to the field by leading to a better understanding the self-assembly hydrogel formation and designing peptides with unique properties for biomedical applications such as cell culture, drug delivery, and tissue engineering.

Table of Contents

List of Figures

List of Tables

Acknowledgements

First and above all, I praise God, almighty creator and my Redeemer, who guides my life and bestowed wisdom and perseverance upon me during this research project.

I would like to show my deep gratidute to the following people for helping me complete this thesis. Sincere appreciation is expressed to Dr. Xiuzhi Susan Sun, my major advisor, whose continuous passion for work and life, patient guidance, and generous support became great encouragement for my professional development as well as my life throughout the whole period of this degree. I especially thank Dr. Om Prakash, my co-major advisor, for his valuable suggestions, guidance in the NMR project and kindly providing many meeting opportunities. I thank Dr. Jianhan Chen for his patience and guidance during the research project and manuscript writing process. I thank Dr. Dan Boyle, who helped me to accomplish many imaging studies. Special thanks to Dr. Christine Aikens for serving as chairperson of my exam committee. My appreciation also extends to Dr. Annelise Nguyen, Dr. Jishu Shi, and Dr. Julia Laskin for their generous support and valuable suggestions for my research projects.

It is a pleasure to thank all members in Dr. Sun's group for their generous help, constant support, and previous friendship. Special thanks to Dr. Jeanne Shera and Dr. Karthik Venkateshan for their valuable suggestions and technical assistance at the beginning of this project. I would like to thank Ms. Susan Kelly for her continuous help and support. Thanks also to all the members of the Department of Grain Science and Industry at Kansas State University for their friendship and support.

I thank my faith families in the Manhattan Chinese Christian Fellowship for their prayer and encouragement with faith, hope, and love.

Last, but not least, I am grateful to my family. Without their love and understanding, it would not have been possible for me to complish this thesis. My heartfelt appreciation goes to my lovely wife, Xiaojing Zhang, for her patience, perspective, encouragement, and endless love. I warmly thank and appreciate my parents and my parents-in-law for their material and spiritral support in all aspects of my life.

"I keep asking that the God for our Lord Jesus Christ, the glorious Father, may give you the spirit of wisdom and revelation, so that you may know him better." (Ephesians 1:17)

Chapter 1 - Introduction

1.1 Overview

A peptide is a short (typically containing fewer than 50 monomer units) sequence of amino acids linked through peptide bonds. Amino acids present in peptides may be divided into two groups based on whether the R groups attached to the α-carbon atoms are polar or nonpolar. These side chains of each amino acid residue affect the peptides solubility and association with hydrophilic (water loving, polar amino acids) and/or hydrophobic (water repulsive, nonpolar amino acids) solvents and environments. Amphiphilic peptides have both polar and nonpolar amino acids.

The process of peptides undergoing a spontaneous assembly into ordered nanostructures is known as peptide self-assembly. Not all peptides self assemble. This process is dependent upon peptide molecular structure and chemistry. Peptide self-assembly is observed in many natural phenomena of functional biological structures and processes such as cell membrane formation, protein-protein interaction, and DNA expression.[1-5] Studying molecular self-assembly is not only critical to understanding the biological functions of a wide range of biomolecules and mechanisms of many human diseases, but also inspires material scientists to design and synthesize building blocks with the capability to self-assemble into well-ordered nanostructures for developing new functional biomaterials at the molecular level.[6-8] This "bottom-up" concept for the fabrication of higher-ordered supramolecular structure was first raised by Richard Feynmen at an American Physical Society meeting in 1959.[9] The driving forces behind molecular self-assembly are largely based on non-covalent interactions including hydrogen bonds, electrostatic interactions (ionic bonds), and hydrophobic and van der Waals interactions.[10] A lack of information to link these driving forces with molecular structures and assembly pathways restricts the development of self-assembly biomaterials. Because of the rapid development of characterization techniques for study materials' physical properties, structural information, morphological properties, and biological functions from the molecular level since the 1990s, the design of biomolecular constituents for self-assembly and applications as bio-functional materials has become a quickly growing field.[11-13]

Because of amphililic peptides environmentally responsive properties and biocompatibilities, these peptides have become an attractive building block for rationally

designing molecules with potential to self-assemble into biomaterials of potential bio-medical uses .[14-16] Like many discoveries in science, the discovery of the first self-assembling peptide was serendipitous. In 1989, Shuguang Zhang found that a left-handed Z-DNA binding protein in yeast, zuotin, contained a repetitive motif.[17] By synthesizing this 16-residue peptide and studying its biophysical properties, Zhang found this peptide possessed a self-assembly property.[18] Inspired by this natural structure, a class of ionic self-complementary peptides called "Peptide Lego" was designed by Zhang's group.[19-21] Over the past few decades, several different peptide design strategies have been developed, and some of them such as the coiled-coil motif, [22] peptide amphiphilies,[23] and the β-hairpin structure[24] are becoming sophisticated and cooperate with various functional groups for different applications. Designing peptide-based biomaterial with precise modification of protein functional domains is an interesting and valuable topic. The inseparable connection between the function and the corresponding structure of native protein inspires researchers to determine and design peptide sequences that can mimic the desired functions in nature. Although the design principle and peptide self-assembly rules of this strategy are difficult to establish, some repeat sequence of functional motif and compatible structure of domain swapping provide several hints to designing functional peptide materials based on our current knowledge.[25-27]

Hydrogel is one of the most common architectures formed through peptide self-assembly.[28] The formation of a hydrogel involves peptides spontaneously organizing into nanofibers that form a supramolecular structure consisting of a three-dimensional matrix, which can hold up to 99.9% water content. Hydrogels are not fluids and present as a semi-solid material. Because of its high water content, most characteristics such as molecular structure and biological functions such as cell/molecular activities of a broad range of cells, proteins, and other bioactive molecules can be retained[29] within the hydrogel matrix. Depending on the biophysical characteristics of peptide molecules, the soluble peptides-to-hydrogel transition could be made environmentally sensitive and respond to temperature, solution pH, metal ions, or light.[30-32] With these properties, peptide-based hydrogel has great potential for a wide range of applications including three-dimensional (3D) cell culture (grow cell in a matrix environment) for tissue engineering, controlled release and targeted delivery, antimicrobial agents, skin care, cosmetic products, as a few examples of applications.[33-36]

Although the field of designing peptide-based biomaterials is growing quickly and more and more applications are being reported, determining the finial supramolecular structure and its corresponding function remains a grand challenge. In this study, we rationally combined a Ca^{2+} binding domain of lipase Lip A from *Serratia marcescens* with a spider flagelliform silk peptide domain. By doing this we hoped to produce a rationally designed peptide that forms the filamentous or fiber structure under the trigger of Ca^{2+}. In addition, we added a hydrophobic motif of a trans-membrane segment of human muscle L-type calcium channel to the N-terminal of this nanofiber-forming sequence mentioned above. We hypothesized that this new peptide has amphiphilic properties and can self-assemble into hydrogel materials under the trigger of various environmental factors such as Ca^{2+}, pH, and albumins. We also hypothesized that the finial morphology of a peptide supramolecule is related to the self-assembly kinetics of peptide monomers and environmental conditions. A series of amphiphilic peptides with different turning sequences were designed to test this hypothesis. In addition, the hydrogel forming process was monitored by nuclear magnetic resonance, transimission electron microscope, and oscillational rechological test to better understand the relationship of peptide conformational structure, supramolecular morphology and hydrogel mechanical properties. Finally, we used this peptide hydrogel as a 3D cell culture matrix, which is one example of its potential for various medical applications.

1.2 Objectives

The main objective of this research is to rationally design peptide molecules with potential to self-assemble into supramolecular structures like hydrogels under controllable triggers for potential bio-medical uses. Because Ca^{2+} is a ubiquitous cellular signal affecting nearly every aspect of cellular life, we start by using a Ca^{2+} binding sequence and a spider silk functional domain from native proteins and aim to design a hydrogel-forming peptide with controlled trigger methods and specific characters for biomedical applications. The specific objectives are:

1. To rationally design a Ca^{2+}-triggered nanofiber-forming peptide by combining identified functional native domains from spider flagelliform silk protein and the Ca^{2+} binding domain of lipase Lip A from *Serratia marcescens* ; Chapter 3

2. To rationally combine the Ca^{2+}-sensitive peptide from objective 1 and hydrophobic from a trans-membrane segment of human muscle L-type calcium channel to design a hydrogel-forming peptide with controlled trigger methods (Ca^{2+} or adjust pH) and specific physical properties such as shear thinning and rapid recovery in gel strength; Chapter 4
3. To design a series of amphiphilic diblock model peptides with different turning sequences and demonstrate the possibility of controlling the supra-assembly morphology by modulating peptide turning sequence flexibility and environmental pH; Chapter 5
4. To monitor the conformation and morphological and mechanical properties of a hydrogel-forming peptide (peptide in objective 2) by using nuclear magnetic resonance, transimission electron microscope, and oscillational rechological test during hydrogelation in different dimethylsulfoxide (DMSO)/H_2O solutions; Chapter 6
5. To trigger peptide hydrogel formation with our rational designed peptide in objective 2 by metal ion (Ca^{2+}) and albumin proteins and explore the possibility of utilizing this trigger controlled hydrogel as a 3D cell culture matrix. Chapter 7 & 8

1.3 References

1. Cui, F.; Li, Y.; Ge, J. Self-assembly of mineralized collagen composites. Mat. Sci. Eng. R-Reports 2007, 57, 1-27.

2. Cho, N.; Jackman, J. A.; Liu, M.; Frank, C. W. pH-Driven Assembly of Various Supported Lipid Platforms: A comparative study on silicon oxide and titanium oxide. Langmuir 2011, 27, 3739-3748.

3. Morgado, I.; Faendrich, M. Assembly of alzheimer's a beta peptide into nanostructured amyloid fibrils. Curr. Opin. Col. Int. Sci. 2011, 16, 508-514.

4. Sun, X. S. Soy protein polymers and adhesion properties. J. Bio. Mat. Bio. 2011, 5, 409-432.

5. Afonin, K. A.; Grabow, W. W.; Walker, F. M.; Bindewald, E.; Dobrovolskaia, M. A.; Shapiro, B. A.; Jaeger, L. Design and self-assembly of siRNA-functionalized RNA nanoparticles for use in automated nanomedicine. Nat. Prot. 2011, 6, 2022-2034.

6. Junk, A.; Riess, F. From an idea to a vision: There's plenty of room at the bottom. Am. J. Phy. 2006, 74, 825-830.

7. Madia, W. J. Building the future an atom at a time: Realizing Feynman's vision. Metal. Mater. Trans. A-Phys. Metal. Mater. Sci. 2006, 37A, 2905-2918.

8. Yadugiri, V. T.; Malhotra, R. 'Plenty of room' - fifty years after the Feynman lecture. Curr. Sci. 2010, 99, 900-907.

9. Feynman, R. There is plenty of room at the bottom. Eng. Sci. 1960, 23, 22-36.

10. Cavalli, S.; Albericio, F.; Kros, A. Amphiphilic peptides and their cross-disciplinary role as building blocks for nanoscience. Chem. Soc. Rev. 2010, 39, 241-263.

11. McBane, J. E.; Sharifpoor, S.; Labow, R. S.; Ruel, M.; Suuronen, E. J.; Santerre, J. P. Tissue engineering a small diameter vessel substitute: engineering constructs with select biomaterials and cells. Curr. Vasc. Pharm. 2012, 10, 347-360.

12. Oss-Ronen, L.; Seliktar, D. Polymer-conjugated albumin and fibrinogen composite hydrogels as cell scaffolds designed for affinity-based drug delivery. Acta Biomater. 2011, 7, 163-170.

13. Li, N.; Niu, L.; Qi, Y.; Yiu, C. K. Y.; Ryou, H.; Arola, D. D.; Chen, J.; Pashley, D. H.; Tay, F. R. Subtleties of biomineralisation revealed by manipulation of the eggshell membrane. Biomaterials 2011, 32, 8743-8752.

14. Hauser, C. A. E.; Zhang, S. Designer self-assembling peptide nanofiber biological materials. Chem. Soc. Rev. 2010, 39, 2780-2790.

15. Caplan, M. R.; Moore, P. N.; Zhang, S. G.; Kamm, R. D.; Lauffenburger, D. A. Self-assembly of a beta-sheet protein governed by relief of electrostatic repulsion relative to van der Waals attraction. Biomacromolecules 2000, 1, 627-631.

16. Gelain, F.; Lomander, A.; Vescovi, A. L.; Zhang, S. Systematic studies of a self-assembling peptide nanofiber scaffold with other scaffolds. J. Nanosci. Nanotech. 2007, 7, 424-434.

17. Zhang, S.; Lockshin, C.; Herbert, A.; Winter, E.; Rich, A. Zuotin, a putative z-dna binding-protein in saccharomyces-cerevisiae. EMBO J. 1992, 11, 3787-3796.

18. Zhang, S.; Holmes, T.; Lockshin, C.; Rich, A. spontaneous assembly of a self-complementary oligopeptide to form a stable macroscopic membrane. Proc. Natl. Acad. Sci. U. S. A. 1993, 90, 3334-3338.

19. Loo, Y.; Zhang, S.; Hauser, C. A. E. From short peptides to nanofibers to macromolecular assemblies in biomedicine. Biotechnol. Adv. 2012, 30, 593-603.

20. Luo, Z.; Wang, S.; Zhang, S. Fabrication of self-assembling D-form peptide nanofiber scaffold d-EAK16 for rapid hemostasis. Biomaterials 2011, 32, 2013-2020.

21. Khoe, U.; Yang, Y.; Zhang, S. Self-assembly of nanodonut structure from a cone-shaped designer lipid-like peptide surfactant. Langmuir 2009, 25, 4111-4114.

22. Ryadnov, M.; Woolfson, D. Engineering the morphology of a selfassembling protein fibre. Nature Materials 2003, 2, 329-332.

23. Hartgerink, J.; Beniash, E.; Stupp, S. Self-assembly and mineralization of peptide-amphiphile nanofibers. Science 2001, 294, 1684-1688.

24. Schneider, J.; Pochan, D.; Ozbas, B.; Rajagopal, K.; Pakstis, L.; Kretsinger, J. Responsive hydrogels from the intramolecular folding and self-assembly of a designed peptide RID B-7888-2009. J. Am. Chem. Soc. 2002, 124, 15030-15037.

25. McDaniel, J. R.; Callahan, D. J.; Chilkoti, A. Drug delivery to solid tumors by elastin-like polypeptides. Adv. Drug Deliv. Rev. 2010, 62, 1456-1467.

26. Ringler, P.; Schulz, G. Self-assembly of proteins into designed networks. Science 2003, 302, 106-109.

27. Nagarkar, R. P.; Hule, R. A.; Pochan, D. J.; Schneider, J. P. Domain swapping in materials design. Biopolymers 2010, 94, 141-155.

28. Jonker, A. M.; Loewik, D. W. P. M.; van Hest, J. C. M. Peptide- and protein-based hydrogels. Chemistry of Materials 2012, 24, 759-773.

29. Zhang, S. Wet or let die. Nat. Mater. 2004, 3, 7-8.

30. Massodi, I.; Moktan, S.; Rawat, A.; Bidwell, Gene, L. III; Raucher, D. Inhibition of ovarian cancer cell proliferation by a cell cycle inhibitory peptide fused to a thermally responsive polypeptide carrier. Int. J. Cancer 2010, 126, 533-544.

31. Aggeli, A.; Bell, M.; Carrick, L.; Fishwick, C.; Harding, R.; Mawer, P.; Radford, S.; Strong, A.; Boden, N. pH as a trigger of peptide beta-sheet self-assembly and reversible switching between nematic and isotropic phases. J. Am. Chem. Soc. 2003, 125, 9619-9628.

32. Charati, M. B.; Lee, I.; Hribar, K. C.; Burdick, J. A. Light-sensitive polypeptide hydrogel and nanorod composites. Small 2010, 6, 1608-1611.

33. Dawson, E.; Mapili, G.; Erickson, K.; Taqvi, S.; Roy, K. Biomaterials for stem cell differentiation. Adv. Drug Deliv. Rev. 2008, 60, 215-228.

34. Koutsopoulos, S.; Unsworth, L. D.; Nagaia, Y.; Zhang, S. Controlled release of functional proteins through designer self-assembling peptide nanofiber hydrogel scaffold. Proc. Natl. Acad. Sci. U. S. A. 2009, 106, 4623-4628.

35. Chen, C.; Pan, F.; Zhang, S.; Hu, J.; Cao, M.; Wang, J.; Xu, H.; Zhao, X.; Lu, J. R. Antibacterial activities of short designer peptides: a link between propensity for nanostructuring and capacity for membrane destabilization. Biomacromolecules 2010, 11, 402-411.

36. Kanlayavattanakul, M.; Lourith, N. Lipopeptides in cosmetics. Inter. J. Cosm. Sci. 2010, 32, 1-8.

Chapter 2 - Literature Review

2.1 Design of Peptide-Based Materials

"What would the properties of materials be if we could really arrange the atoms the way we want them? … When we get to the very, very small world, we have a lot of new things that would happen that present completely new opportunities for design," said Richard Feynman, winner of the Nobel Prize in Physics in 1965, when he presented a lecture titled "There's plenty of room at the bottom" at an American Physical Society meeting in 1959.[1] This is considered the seminal event in nanotechnology because it inspired the concept of a bottom-up approach of higher-ordered supramolecular structure via self-assembly of individual atoms and molecules.[2-4]

In nature, self-assembly is ubiquitous and reflects the spontaneous organization of numerous individual entities into a range of supramolecular architectures exemplified by structures formed by collagen,[5] lipid bilayers,[6] and folding of protein[7, 8] or nucleic acids[9] into their functional forms. Although non-covalent interactions such as hydrogen bonds, electrostatic interactions (ionic bonds), and hydrophobic and van der Waals interactions are weak and relatively insignificant in isolation, together they play critical roles in mediating the self-assembly pathways of well-defined structures and influencing molecule-to-molecule interactions.[10] These inspirations of nature have become better understood in the last few decades because of rapid development of electron microscope technology, nuclear magnetic resonance (NMR), X-ray diffraction, and small angle scattering.[11-14] Functional biomaterials for tissue engineering,[15] drug delivery,[16] and biomineralisation[17] have been designed through this bottom-up self-assembly strategy; researchers from biology, chemistry, and various engineering areas are attracted to this rapidly advancing field.

Fifty years after Richard Feynman's lecture, the age of nanotechnology for self-assembly biomaterials has truly arrived.

2.1.1 Peptide Lego

"Peptide Lego" was the concept introduced by Shugung Zhang regarding the design of ionic self-complementary peptides as building blocks to fabricate novel higher-ordered architectures.[18] Like Lego bricks, which contain pegs and holes in a precisely determined manner,

peptides with β-sheet structure were designed with two distinct surfaces: one is hydrophobic and the other was hydrophilic, in a well-ordered fashion.[19, 20] Similar to spontaneous protein folding *in vivo*, the hydrophobic residues drove self-assembly by shielding themselves from water and packing through intermolecular hydrophobic force. The alternation of positively and negatively charged amino acid residues on the hydrophilic side cast the unique "Lego" structural feature of these peptides.[21, 22] Based on the regular intervals of the repeated charged residues, Zhang classified arrangements of the complementary ionic sides of "Peptide Lego" into several moduli:[18] modulus I, modulus II, modulus III, modulus IV, etc., and mixtures thereof. For example, the arrangement of positively (+) and negatively (-) charged amino acids in modulus I alternates with one residue (e.g. + - + - + - + - or - + - + - + - +), which was increased to two, three, and four residues for modulus II, III, and IV, respectively (e.g. + + - - + + - -, + + + - - - and + + + + - - - - etc.). Also, the orientation of charged residues were reversed (e.g. + - + - + - + - and - + - + - + - +), and the different charged modulus were also mixed to yield entirely different designs.

Like many discoveries in science, the discovery of the first member of "Peptide Lego" was serendipitous and curiosity-driven. In 1989, while working on yeast genetics and protein chemistry in Alexander Rich's Laboratory, Zhang identified a left-handed Z-DNA binding protein in yeast, which he named zuotin (*zuo* means left in Chinese, and *tin* refers to protein in biology).[23] The sequence of this protein presented an interesting repetitive 16-residue motif, AEAEAKAKAEAEAKAK (EAK 16-II). Driven by curiosity, Zhang custom-made this peptide and studied its morphological and structural properties in aqueous solution. Surprisingly, Zhang and his colleagues found this peptide spontaneously assembled into an insoluble macroscopic membrane upon the addition of salt.[24] The results of this study were new compared to literatures at the time which further stimulated extensive studies in this area.[25-27] This discovery has lead to the rational design of many self-assembling peptide-based materials, and some of them have become today's most attractive biomaterials.[28-30]

With the development of Peptide Lego, evidence showed that, besides the whole poly-peptide sequence, properties of peptide-based materials were also greatly affected by some smaller design units such as a structural segment.[31-33] Based on these findings, recent peptide designs have placed more and more attention on carefully modifying smaller design units to

achieve the desired functional material. Just as Feynman predicted in 1959, the smaller we get, the more opportunities we have. A class of β-hairpin peptides designed by Joel Schneider's group is a good example.[34-37] In 2002, Schneider and colleagues reported a responsive hydrogel-forming peptide, MAX1 (VKVKVKVK-V^{D}PPT-KVKVKVKV-NH_2).[34] They inserted intermittent tetra-peptide V^{D}PPT, which was designed to adopt type II' turn structure,[38, 39] into two high β-sheet propensity modulus I Peptide Lego, VKVKVKVK and KVKVKVKV. This presented as a reversed orientation of charged residues. Under unfolding conditions, the peptide solution was free-flowing with random coil secondary structure. When the environmental pH was higher than 9.0, under the help of the β-turning segment, the peptide intra-molecularly folded into an amphiphilic β-hairpin structure. This structure lined two Lego β-branches parallel with one face of hydrophobic valine residues and the other face of hydrophilic lysine residues.[34] Subsequently, the monomeric peptides self-assembled both laterally and facially via hydrogen bond formation and hydrophobic association of the valine rich faces, respectively, and lead to a hydrogel formation. Interestingly, the physical cross-links of this peptide hydrogel were disturbed by a shear-thinning property and occured 30 min after cessation of shear. It was also shown that about 80% of elastic properties of this self-assembled hydrogel quickly recovered. Furthermore, Schneider and colleagues modified the Peptide Lego segments by replacing valine residues on positions 7 and 16 and lysine on position 15 of the β-branches with threonine and glutamic acid, respectively, and created a serial of hydrogel-forming peptides: MAX2 (VKVKVKVK-V^{D}PPT-KVKTKVKV-NH_2),[40] MAX3 (VKVKVKTK-V^{D}PPT-KVKTKVKV-NH_2),[40] and MAX8 (VKVKVKVK-V^{D}PPT-KVEVKVKV-NH_2).[41, 42] Threonine was an isostructural with valine but classed as polar amino acid for bearing a hydroxyl group. With threonine incorporated in both positions 7 and 16, the MAX3 peptide exhibited a special thermo-reversible hydrogel-forming property that was not observed in other MAX peptides. Increasing the temperature served to trigger a conformational transition of the peptide from unfolding random coil structure to a folding β-hairpin that consequently self-assembled into a hydrogel network. Cooling the resulting hydrogel caused unfolding of the peptide monomial structure and dissociation of peptide assembly into a low-viscosity (free-flowing) solution. Similarly, peptide MAX8 was also driven from MAX1 by replacing the lysine residue on position 15 with glutamic acid residue. This substitution reduced the electrostatic repulsion between adjacent peptides and gave rise to a faster folding and self-assembly kinetics with more rigid hydrogel formation.[42]

2.1.2 Coiled-Coil Motif (α-helical assembly)

Coiled-coil is a ubiquitous structure in nature that covers about 3% of all protein-encoding regions among the known genomes.[43] Largely associated with directing, specifying, and cementing protein-protein interactions, α-helical coiled coil is considered to play a primary structural/functional role for many biological processes, including ATP synthesis, transmembrane signaling, transcription of gene expression, and formation and remodeling of the extracellular matrix.[44-47] Discovery of the coiled-coil motif goes back to the 1920s when William Astbury studied the X-ray diffraction patterns of some natural fibers. He identified three main structures: α-form from un-stretched native wool, β-form from stretched denatured wool, and γ-form from the collagen of tendons.[48] Linus Pauling and Lawrence Bragg found that the meridional arc of 5.15 Å was observed as a common feature of α-form structure and found in a whole class of fibrous proteins.[48] In 1952–1953, Pauling and Francis Crick independently submitted reports to *Nature* within weeks of one another to express their speculation that the 5.15 Å diffraction patterns could be caused by the packing of two or more α-helical strands.[49, 50] Meanwhile, Crick postulated a "knobs-into-holes" interaction to interpret the residue-to-residue association of adjacent helices based on the 7/2 (7 residues over 2 turns) configuration of helix laterally packing.[51, 52] Instead of simply helix-to-helix contact, the "knobs-into-holes" fashion suggests that a hydrophobic side chain from one of the binding helices, referred as the "knob," interlocks within a cluster of four side chains, forming a diamond-shaped "hole" from the partnering helix. In 1972, based on the amino acid sequence analysis of the C-terminal of rabbit skeletal tropomyosin, a three-dimensional model of tropomyosin coiled-coil was built with regular packing patterns at intervals of seven residues.[53] This was first time the heptad repeat pattern $((abcdefg)_n, n \geq 3)$ of coiled-coil structure was identified. After that, several high-resolution X-ray crystal coiled-coil structures, including the structure of hemagglutinin glycoprotein were reported in 1981[54] and 15 Å resolution structure of tropomyosin report in 1986,[55] were described and revealed the theoretical predictions of helix packing residues based on a heptad repeat. From that time on, the 7/2 periodicity $(abcdefg)_n$ heptad repeat coiled-coil structure became a repeatable model found in a variety of coiled-coil-containing proteins. With the identification of "leucine zippers" (leucine occupies the d position of heptad repeat and shows at every seventh position of α-helix) in several transcription factors in 1991,[56] clearer

sequence-to-structure relationships of heptad repeat were achieved and aroused the inspiration of using heptad repeat as basic design principle for coiled-coil biomaterials.[57-59]

Unlike the β-structured systems where inter-chain backbone hydrogen bonding introduces uncertainty to control the peptide self-assembly process, the majority of backbone hydrogen bonding in coiled-coil structure was tied up along the lateral orientation within the helix.[60, 61] This structural pattern reduced the potentially promiscuous backbone-to-backbone interactions, making the coiled-coil motif a discrete building block; however, this pattern also led to a requirement of careful selection and arrangement of amino acids at each heptad position to rationally promote the side-chain interactions and peptide self-assembly for higher-order biomaterials. Hydrophobic amino acids are normally selected to be placed on positions a and g in a heptad repeat and form the hydrophobic core of the coiled-coil helical bundle through hydrophobic-hydrophobic interactions with residues on positions a' and g' of the partnering helix, $(a'b'c'd'e'f'g')_n$. Experimental studies demonstrated that the combination of isoleucine at position a and leucine at position d provided the most stable hydrophobic core for dimeric leucine zippers.[62-64] Position e and g of the heptad repeat were solvent exposed; therefore, polar residues with complementary charged side-chains were preferred in these two sites for a stable inter-chain salt bridge through electrostatic interactions. Residues at the b, c, and f positions were located on the surface of the coiled-coil helix. Amino acids with charged groups also were applied in these positions to increase the solubility of the biomaterials and to control the aggregation of helices. In addition, the overall coiled-coil stability was increased by increasing the number of heptad repeats.[61] The number of helices in a coiled-coil (degree of oligomerization), the homo- or heterodimerization of the coiled-coil structure, and the orientation of the helices all depended on the nature and geometry of the side-chains of the packing core composed of residues at positions a, d, e, and g.[60]

Moreover, shifting one charged residue from C-termini to N-termini, Woolfson's group built a class of a four-heptad framework for self-assembling fibers (SAFs), whose sequence was g-$(abcdefg)_3$-abcdef.[65-67] Opening the N- and C-termini as free amine and free acid groups made this coiled-coil have "sticky ends." The end-to-end salt bridges linked the N- and C-termini of the neighboring peptides and further extended coiled-coil aligned with the long axis of fibers. In 2009 *Nature Materials*, based on their SAFs compositions, Woolfson's group reported the first self-assembly hydrogel with a purely α-helical structure, called hydrogelating SAF (hSAF) .[68] In

this design, they kept the critical amino acids at a, d, e, and g positions of the original SAFs design to maintain the dimer interface of the coiled-coil and introduced both hydrophobic and polar amino acids at position b, c, and f. The sequences of the complementary hSAF peptides were hSAF p1: K-IXXLKXK-IXXLKXE-IXXLEXE-NXXLEX and hSAF p2: K-IXXLKXK-NXXLKXE-IXXLEXE-IXXLEX, where X represented alanine ($hSAF_{AAA}$) or glutamine ($hSAF_{QQQ}$) residues at positions b, c, and f. Although self-supporting physical hydrogels with more than 99% water content were found in both $hSAF_{AAA}$ and $hSAF_{QQQ}$ peptides, they suggested two different mechanisms of gelation. Interestingly, the hydrogel properties were consequently affected by these different fibril-to-fibril interactions: $hSAF_{QQQ}$ formed a gel through a hydrogen-bonded network, which melted on heating, whereas $hSAF_{AAA}$, whose hydrogel network was established by hydrophobic collapse, showed an increase in gel strength upon warming. This phenomenon exhibits a great example for rational design of peptide sequences for desired functional biomaterial through the coiled-coil design principle.

2.1.3 Peptide Amphiphiles (PA)

Lipid-modified proteins are widespread and play crucial roles in many biological processes.[69-71] For example, lipid moiety aids in sorting the protein to the membrane domain, which allows interactions of water-soluble protein with cell membranes and promotes the biological functions of proteins.[72] In recent decades, substantial efforts have been made to understand the effects of noncovalent interactions for molecular self-assembly.[21, 31, 67, 73, 74] With the development of the solid-phase synthesis method that gives access to combine hydrophobic alkyl chains into the N- or C-termini of a peptide sequence, the contribution of hydrocarbon chains to accelerate ordered aggregation of lipid-peptide conjunctions becomes clearer.[75-76] For example, in 1998, Gregg Fields and Matthew Tirrell synthesized serial amphiphilic peptides with mono-alkyl hydrocarbon chains modified in N terminal.[77] A 16 residues peptide was designed as LAEIEALKAEIEALKA, according to the heptad repeat principle of $(EIEALKA)_n$ motif, which was demonstrated to associate into a highly α-helical coiled-coil structure when the sequence had more than 23 residues.[78] There was a random coil secondary structure of this 16-residue peptide in solution; however, binding hexanoic acid (C_6) or palmitic acid (C_{16}) mono-alkyl chain at the N-terminal of this peptide promoted the formation of the α-helical secondary structure.[77, 79]

Using the hydrocarbon chain as a hydrophobic domain to rationally control the self-assembly pathway has been greatly advanced by the group of Samuel Stupp from Northwestern University. This group first launched the Peptide Amphiphiles (PA) peptide design concept in 2001.[80-83] Their original design constructed the peptide sequence with five critical structural segments. From N terminue to C terminus, these segmants included a alkyl tail, consecutive cysteine for intermolecular interactions, flexible linker region, calcium binding phosphorylated serine reside, and integrin receptor (a cellular protein that binds to the extracellular matrix) ligand RGD. This 16-carbon alkyl chain pocesses hydrophobic characteristics and by conjugating it to the N-terminus of the polar functional peptide domain made the whole molecule amphiphilic. This amphiphilic property was considered to be one of the most important design elements to allow the cylindrical nanostructure to self-assembly. In the last decade, Stupp's group designed and synthesized a broad range of functional biomaterials and adopted a series of biophysical, morphological, mechanical, and biological studies to confirm the basic aspects of its design principle.[84-88] Conceptually, the compositions of PAs had the following four key structural features:[88] Region 1 was a hydrophobic tail that typically consisted of alkyl groups with varying chain lengths. Palmitic acid, a 16-carbon chain, was the most popular hydrophobic block for this design. Region 2 was a short peptide, typically composed of hydrophobic amino acids, for intermolecular hydrogen bond formation. This short peptide was directly adjacent to the alkyl tail, β-sheet structure preferred and highly associated with the overall shape of self-assembled nanostructure and mechanical properties of the resulting nanofiber networks. Region 3 consisted of charged amino acids that ensured the solubility of peptide materials in an aqueous environment. The number of charged amino acids was critical for maintaining solubility, while not disturbing the peptide self-assembly. The final region of PAs was located at the C terminus and contained different peptide epitopes. This segment was exposed to the surface of the cylindrical geometry after peptide self-assembly. This region was modified for different purposes and allowed the final biomaterial to exhibit various bioactive signals. According to this design principle, many peptide-based biomaterials were synthesized and tested for applications in cell scaffolding, drug delivery, and regeneration of bone and nervous system.[89-93]

2.1.4 Design Based On Protein Domain

A protein domain is considered a part of the primary protein sequence that spontaneously folds into an independent, compact three-dimensional structure accompanying certain functional or stable structural characters.[94-95] In nature, the inseparable connection between the protein function and the corresponding structure of its domains exhibits the perfect model to fabricate functional biomaterials with desirable overall properties through precise design of its molecular structure;[96-97] however, the design principle and rules governing pathways of peptide self-assembly have not been established, which make the exerting of peptide design with protein domain extremely difficult. On the other hand, some protein domains have distinct physical and biological properties and display repeating peptide sequences, and thus are eligible for rationally designed peptide materials based on our current knowledge.[98, 99] For example, a class of elastin-like polypeptides (ELP) were designed according to a repeating unit from mammalian elastin protein: $(VPGXG)_n$, where X represented any amino acid other than proline and n was the number of repeats.[100] These peptides performed a special thermal responsive property: below the transition temperature (T_t), ELPs were highly soluble, but above T_t, they aggregated rapidly. T_t was strongly affected by X residue as well as the number of repeating units. With different conjugations, many thermally sensitive peptide vehicles were produced for target drug delivery system.

For various biological functions, the conformational shift of some protein domains when binding to targeted metal ions turned out to be an essential process.[101,102] Besides the repeating motif of peptide primary structure, this metal-ion triggered structural changing property provided a fresh inspiration to design responsive peptide based biomaterials. Consider calcium binding motif GGXGXDXUX, where X was any amino acid and U was hydrophobic amino acid, as an example.[103] This fragment was selected from the enzyme serralysin of *Serratia marcescens* and presents a right-handed β-helical structure with calcium ions binding between turning segment (GGXGXD) and adjacent β-strands (XUX).[104] Using this domain, Philippe Ringler and Georg Schulz designed a protein lattice with switchable mesh in 2003.[105] They first made a β-helix containing 5 repeats of characteristic motif GGXGXDXUX, then conjugated its N and C termini with one globular monomeric 468-residue protein 6-phospho-β-galactosidase (PGAL). The total 998-residue tandem fusion protein PGAL-β-PGAL presented a dumbbell shape with a 3-nm distance between two PGAL groups when the β-helical spacer was shrunk by adding calcium

ions. After adding 10 mM ethylenediaminetetraacetic acid (EDTA) to the solution, the micrographic images showed the distance of PGAL was increased from 3 nm to 13 nm, which indicated that calcium ions were removed and a β-helical spacer presented a random and relaxed structure. Such a metal ion–sensitive motif has potential application for future construction of switchable nanostructure.

Domain swapping was reflected in the mechanism of oligomerization for two or more protein molecules to aggregate into a dimer or higher-ordered structure by exchanging their identical structural domains.[106-109] The term "3D domain swapping" was first used to describe a diphtheria toxin dimer that was constructed by a globular domain exchange of two monomers.[106] This complementary assembly of tertiary and quaternary structural elements was found in many naturally occurring proteins[110-112] including human cystatin C, human prion protein, and immunoglobulin-binding domain B1 mutant. This explored a new idea to design discrete units for complementary assembly into more complex architecture. In 2009, Schneider and colleagues applied a similar concept to modify their β-hairpin peptides and created a class of strand swapping β-hairpin for peptide hydrogel.[113, 114] Unlike the symmetrical structure of MAX1, $(VK)_4$-V^DPPT-$(KV)_4$-NH_2, which contains identic chain length on each β-strand, the newly designed peptides retain the β-turning segment (V^DPPT) but introduced asymmetry of the whole molecule by varying the chain length on each β-strand region: SSP1 $(VK)_2$-V^DPPT-$(KV)_6$-NH_2, SSP2 $(VK)_3$-V^DPPT-$(KV)_5$-NH_2 and SSP3 $(VK)_5$-V^DPPT-$(KV)_3$-NH_2. In an aqueous solution, these asymmetrical peptides were triggered to fold into a facially amphiphilic β-hairpin conformation by changing the environmental pH. Because of the different peptide length in the β-strand region, the folded hairpins exhibited an exchangeable tail that was swapped with another β-hairpin and became a conformational complemented dimmer. These stand-swapped dimmers assembled through valine-rich hydrophobic faces for well-defined fibrils and a mechanically rigid peptide hydrogel. Interestingly, varying degrees of β-strand asymmetry led to various fibril morphology in nanoscale and different hydrogel rheological properties in macroscale. With advancements of biotechnology, the design principles and self-assembly pathways of various natural materials have become clear and feasible. Inspired by these natural phenomena, more and more maturely designed biomaterials with controlled finial structures and target properties are expected in the near future.

2.2 Peptide Hydrogel

Hydrogel is a distinct three-dimensional scaffold with interstitial spaces that retains a significant amount of water.[115] Because of their high water content, these hydrogels potentially could surve as suitable environment substitutesfor maintaining characteristics and functions of a broad range of cells, tissues, proteins, and other bioactive molecules, as well as for *in vitro*study of some biological interactions at the molecular level.[116-119] These biocompatible properties indicate the great potential to use hydrogel as a biomaterial. In the 1950s, Wichterle and Lim proposed to design a new type of biomaterial that held a shape and was biochemically stable and nutrient- and metabolites-permeable in an aqueous environment with softness comparable to surrounding tissue[120]. Based on this idea, they made the first hydrogel in 1953 by copolymerization of 2-hydroxyethyl methacrylate and ethylene dimethacrylate and reported a seminal paper in *Nature* in 1960.[120, 121] In the report, Wichterle and Lim further summarized the structural characteristics of this type of biomaterial as a three-dimensional structure that permited desirable water content and was constructed by building blocks containing hydrophilic groups.[121]

In the development of peptide-based biomaterials, hydrogels are one of the most common architectures from peptide molecules because of their amphiphilic characteristics and self-assembly capabilities.[122, 123] According to the natural properties, hydrogels can be categorized in a number ways, such as neutral/ionic hydrogels or natural/synthetic hydrogels.[124, 125] One important classification of peptide hydrogels is to distinguish their cross-linking forces as chemical gels or physical gels.[125] The fibrils of hydrogel scaffolds are cross-linked through covalent interactions for chemical gels. Chemical hydrogels undergo significant volume change during the solution-to-gel transition, and the cross-linking density can be varied to control the overall properties of the final gel. On the other hand, the network of physical hydrogels is held through an entanglement of fibrils or non-covalent interactions among peptide segments or the peptide-metal ion complex. Because the spontaneous association of peptide molecules is critical to leading assembly for the finial hydrogel matrix, the physical hydrogel is also recognized as "self-assembling hydrogel".[126] This spontaneous process brings some advantages to self-assembling peptide hydrogels because it is suitable for injection, stable in organic solvents or cross-linking agents, and able to be incorporated with bioactive molecules, which promote the applications of physical hydrogel in a number of fields like tissue engineering, drug delivery and biological sensing.[41, 76, 118, 123] Moreover, the spontaneous self-assembly process depends on the

biophysical characteristics of peptide molecules and presents “smart” responses to various environmental factors. Environmentally sensitive hydrogels are classified into thermo-sensitive hydrogels, pH-sensitive hydrogels, and light-sensitive hydrogels.

2.2.1 Thermo-Sensitive Hydrogel

Thermo-sensitive hydrogel is one of the most studied environmentally sensitive hydrogels in the pharmaceutical field.[127-129] Dependent on temperature, the volume of hydrogel could swell/de-swell. The solution-to-hydrogel transitions could also be modulated by temperature. These switchable physical transitions have gained considerable attention for use as thermo-sensitive on-off controls for drug delivery, biosensors, and cell culture.[127, 130] Based on the relationship of temperature changes and hydrogel swelling-shrinking transitions, a thermo-sensitive hydrogel can be further identified as a positive or negative thermo-sensitive system.[125, 131] A positive thermo-sensitive hydrogel/solution would shrink/hydrogelate when the environmental temperature is cooled below its upper critical solution temperature (UCST). In contrast, a negative thermo-sensitive hydrogel has a lower critical solution temperature (LCST). With a negativethermo-sensitive hydrogel below its LCST, hydrogen bonding dominates the molecular association between the hydrophilic segments and increases the material solubility of these negative thermo-sensitive molecules; however, as the temperature increases above the LCST, the hydrophobic interactions take over the intermolecular association and lead to shrinkage or hydrogelation of the system. In 1978, Toyoichi Tanaka reported the first thermo-sensitive hydrogel, poly(N-iso-propylacrylamide) (PNIPAAm).[132] After the modification of its LCST close to body temperature, this molecule became one of the most extensively studied thermo-sensitive polymers for controlled drug delivery systems.[133-135]

The hyperthermia technologyis a method to local and regional deposition of heat to affected parts such as a tumor or a specific organ.[136] This achievement provides an opportunity to use negative thermo-sensitive hydrogel with LCST for targeted drug delivery. Through rational design and careful modification of their thermo-sensitive range from 37 to 42 ℃, some elastin-like peptides are prepared with drug conjugation and injected as a free-flowing solution into the body. Then these peptides self-assemble into a stable hydrogel around the target position where the enthetic hyperthermia heat is applied.[100, 137, 138] Synergized application of site specific hyperthermia and thermo-sensitive peptide hydrogel provide great potential for site specific

delivery of a drug to a target position.[139] Besides elastin-like peptide, others, such as leucine zippers, silk-like peptides ($(GAGAGS)_n$, n=2 to 168), and collagen-like peptides ($(Gab)_n$, a=often proline (P), b=often hydroxyproline (P^{OH}), n=100 to 500), also have potential thermo-sensitive properties.[140]

2.2.2 pH-Sensitive Hydrogel

The pH-sensitive hydrogels could switch the on/off control for swelling/de-swelling or solution-to-hydrogel transitions dependent on the changes of environmental pH.[131, 141-143] Because of the acidic and basic side-chains of certain amino acids as well as the amide and carboxylic group at the N and C termini, many peptide-based materials also exhibit pH-sensitive properties.[144, 145] Depending on the overall charges of the whole molecules at neutral pH, peptide hydrogels can be ionic or cationic. As a result of changing the external pH, the pendant groups are adjusted to be ionized, protonated, or neutralized. This process is highly relative to the intra- and intermolecular electrostatic repulsions, suddenly or gradually changing the hydrophilicity of the whole peptide network and consequently resulting in the swelling/de-swelling or solution-to-hydrogel transitions of many pH-sensitive peptide-based hydrogels. For example, an 11-residue β-peptide, QQRFEWEFEQQ, has been designed as a pH-sensitive material because of the ionizable glutamate and arginine side-chains.[146] Below its critical concentration (10 mg/mL), this peptide was soluble at a neutral pH; however, when the pH decreases to below 4.2, peptide molecules folded as anti-parallel β-sheet tapes and self-assemble into a hydrogel. Interestingly, because most ionic groups were shielded by metal ions as well as protons, this peptide solution was also adopted the hydrogel state above the critical peptide concentration when salt concentration is increased to 140 mM. In addition, polar, but uncharged, amino acids such as threonine, serine, and tyrosine were also important for pH-sensitive peptide folding and self-assembly through intra- and intermolecular hydrogen bonding. A 16-residue amphophilic peptide, RATEA16, CH_3CONH-RATARAEA-RATARAEA-$CONH_2$, containing 4 cationic and 2 anionic residues, could underwent a pH-reversible three-phase transition from viscous solution to elastic hydrogel to precipitate.[145] The threonine residues turned out to be very important for hydrogel formation under physiological conditions. Furthermore, Schneider's group designed two groups of peptides:[144] one with an altering peptide net charge and the other with a glutamic acid substituting lysine residue at different positions within the peptide sequence. Their results

indicated that the folding and self-assembling behavior of pH-sensitive peptide was related not only to the net charge of overall peptide molecules, but also to the exact position of the salt-bridge formed.

2.2.3 Light-Sensitive Hydrogel

Compared with hydrogels sensitive to other stimuli such as temperature or pH, which are limited by diffusion of heat or hydrogen ions, light-sensitive hydrogels have specific advantages of instant imposition and accurate amounts of light/energy delivery.[131] To introduce UV or visible light-sensitive properties into a polymer network, some light-sensitive ligands are normally conjugated into the building units. For example, a leuco derivative molecule, bis(4-di-methylamino)phenylmethyl leucocyanide, is selected for UV-sensitive hydrogel because it can be ionized and produce triphenylmethyl cations, which increase the osmotic pressure of the solution and lead to the hydrogel phase transitions.[147] A similar design strategy has been applied to some peptide-based materials. Darcy Burns and colleagues reported a helix peptide JRK, acetyl-EACARVAibAACEAAARQ-NH_2, which was intramolecularly cross-linked with a light-sensitive compound, diiodoacetamide-azobenzene.[148] The helix-coil conformational transition of this peptide was controlled by photoisomerization. Besides the light-sensitive molecules, some nanoparticles also helped peptide molecules become responsive to light. Manoj Charati et al. found that incorporation of gold nanorods (Au-NRs) with a hydrogel-forming leucine-zipper peptide led the peptide/Au-NR gel to melt when the material was exposed to NIR light.[149] Significant heat was accumulated under the exposure of NIR light and resulted in a complete dissociation of the physical crossing of the hydrogel scaffold. In contrast, no heating or melting occurred in the peptide hydrogel without Au-NRs, and the gel shape was preserved well during light exposure. In addition, some other light sources also showed potential to trigger peptide self-assembly. In 2010, Stupp's group reported that a spontaneous X-ray triggered peptide filament networks in *Science*:[87] the peptide amphiphiles (C_{16}-A_6E_3) crystallized and self-assembled into a supramolecular filament with 3D networks when they were exposed under an X-ray beam. Although not many light-sensitive peptide-based hydrogels have been reported, the in-depth exploration of peptide properties and how they correspond with stimulating factors will yield more peptide-based biomaterials with light sensitivity and other "smart" responses will be developed in the near future.

2.3 Characterization Techniques

To determine the functionality of peptide-based biomaterials, many physical and biochemical techniques have been developed to characterize the designed peptide from the atom and molecular levels to bulky structural levels. In this chapter, some popular and useful techniques are highlighted in biophysical, structural, morphological, and rheological areas. For individual application of each specific peptide, some additional techniques may be needed to make a comprehensive characterization.

2.3.1 Biophysical Properties

The biophysical properties of peptide-based biomaterials include peptide concentration, molecular weight, sequence, particle size, binding behavior, and thermodynamic properties. Many techniques originally designed for protein characterization may be used to characterize hydrogels.

High-performance liquid chromatography (HPLC) is one of the most useful methods for purifying, identifying, and quantifying peptide solutions.[150-152] Using chromatographic columns as a stationary phase and miscible combination of water with various organic solvents as a mobile phase, individual components of the mixture could be separated by an HPLC system according to their characteristic retention time. Based on a different component-separating concept, HPLC can be classified as normal-phase, reserved-phase, size-exclusion, and ion-exchange chromatography.

Sodium dodecyl sulfate polyacrylamide gel electrophoresis (SDS-PAGE) is a widespread method in biological and biochemical research to determine the approximate size of a protein or large peptide.[153, 154] By adding the anionic detergent SDS, the shape of the protein is linearized, and the original protein charge is shielded by many and evenly distributed negative charges of SDS. Therefore, during electrophoretic mobility, the proteins are separated based on their particle sizes or molecular weights.

A more accurate method of determining peptide molecular weight is mass spectrometry (MS).[155, 156] Using an electron ionization or chemical ionization method, testing samples are ionized and accelerated to magnetic or electric fields, and the elemental compositions of a sample are analyzed based on their mass-to-charge ratio. Electrospray ionization (ESI) and matrix-assisted laser desorption/ionization (MALDI) are the two most common methods of

producing ions for liquid and solid biological samples. According to analysis methods, MS could be identified as Time-Of-Flight (TOF), quadruple mass filter, ion traps, and Fourier Transform Ion Cyclotron Resonance (FTICR) mass spectrometry. TOF is a method to use the same electric potential to accelerate sample ions and analyze the time for each compound to reach the detector. Instead of using the static electric field, quadrupole mass filter, and ion traps, use oscillating electrical fields to create a selectable path for ions to pass through a radio frequency quadrupole field built by 4 parallel rods. Injecting ions into a penning trap and circuiting them in a static electric/magnetic field, FTICR detects the frequency of an ion's cycling and provides highly sensitive analysis data through a deconvoluted Fourier transform signal.[157] In addition, chromatographic techniques such as liquid chromatography, gas chromatography, and ion mobility spectrometry could be combined with MS to increase its mass resolving and mass determining capabilities.

Dynamic light scattering (DLS) is a photon correlation spectroscopy used to determine the particle size and size distribution of polypeptide in aqueous solution.[158, 159] As long as the particles are smaller than the wavelength of light source, the light beam would be scattered in all directions after it hit the small particles. Because the particles are small enough to undergo a Brownian motion, the scattered light exhibits a constantly changed distance between them and undergoes a constructive and destructive interference by the surrounding particles. By measuring the time-dependent intensity fluctuation of scattered light, the diffusion coefficient of the particles can be determined. According to Einstein's theory about the relationship of diffusion and particle size, the hydrodynamic diameter of testing particles could be calculated. With the help of DLS software, the population of particles with different diameters could be obtained. The peptide aggregation via heating, pH changing, or lighting could be conveniently studied through DLS.

To study the binding behavior of soluble molecules, isothermal titration calorimetry (ITC) provides a physical technique to detect the thermodynamic interactions.[160, 161] Using two identical cells with high amounts of thermal conducting material, an isothermal titration calorimeter holds a sample with targeted molecules in one cell and the corresponding buffer without molecules in the other cell. During the test, ligands are titrated into the sample cell and bind to the target molecules. These exothermic or endothermic interactions will further influence the requirement of power input/output of the reference cell to maintain the equal temperatures

between the sample and reference cells. Thermodynamic parameters such as the binding affinity, enthalpy, entropy, free energy, and binding stoichiometry can be measured and calculated based on calorimetric data.

Similar to ITC, differential scanning calorimetry (DSC) is another thermoanalytical technique to measure the physical transformation of biomaterials as a function of temperature.[162] During the heating or cooling process, the different energy requirement for the sample and reference to maintain the same temperature could be monitored throughout the experiment. The folding and unfolding of protein molecules could be determined with this method.

2.3.2 Structural Properties

The primary structure of a peptide is referred to as a monomeric sequence, which would spontaneously fold into a certain secondary structure. Based on the atomic coordinates, spatially describing the peptide monomeric structure in three dimensions is considered its tertiary structure. An arrangement of multiple peptides could further become the quaternary structure. Because the functionalities of most peptides are highly related to their structures, studying the peptide structure from molecular and supramolecular levels becomes critical to understanding the biochemical and biophysical properties of peptide-based biomaterials.

Circular dichroism (CD) spectroscopy is a quick and effective method that relies on the peptide-specific absorption of left and right circularly polarized light to determine peptide secondary structures.[163, 164] According to different light sources, the wavelength ranges of CD could cover from 170 nm (synchrotron) to the far UV region (180–240 nm) and to the near UV regions (260–320 nm) and reflect different conformational information such as peptide bonds, aromatic amino acid side-chains, and tertiary structure of the peptide. The percentage of different types of regular secondary structure such as helix, sheet, and turning also could be quantitatively calculated according to some algorithms or basic datasets to estimate the secondary structural composition of peptide.[165] Additionally, because the sample preparation and the operation requirements of CD are simple, the conformational changes of protein under varying experimental parameters such as pH, temperature, salinity, and the presence of various cofactors could be monitored by CD spectroscopy.

Fourier transform infrared spectroscopy (FTIR) is an infrared spectrum technique to identify unknown materials and detect the quantity and material compositions of a mixture.[166, 167]

It could be used to characterize the secondary structure of peptide molecules. When IR radiation passes through a sample, the sample molecules would absorb the frequencies, which is the same as the vibrations between the bonds of the atoms, and let the rest of the radiation transmit. Because of the unique atom arrangement and combination of different molecules, the infrared spectrum provides the "fingerprint" information for qualitative analysis of every different kind of material. With some modern software algorithms, FTIR could be applied to quantitative analysis based on the size of the peaks in the spectrum. For peptide structural studies, the backbone conformation of peptide molecules provides the characteristic absorption bands at the amide I and amide II regions, which cover the range from 1400 to 1700 cm^{-1}. Secondary structure of peptide molecules can be described based on these characteristic bands.

Nuclear magnetic resonance (NMR) spectroscopy is a preeminent technique to provide detailed structural information of organic chemical molecules including peptide, protein, and DNA in their relaxed environment without specific sample modification or deconstruction during the experiment.[168, 169] All isotopes with an odd number of protons and/or neutrons present a non-zero spin, which causes a corresponding magnetic moment. In the presence of an external magnetic field, spin shows two different energy states: lower energy state (aligned with the external field) and higher energy state (opposite the external field). In NMR spectroscopy, a radio frequency pulse that corresponds to the observed nucleus is applied under a static magnetic field to shift spins from a lower energy state to a higher energy state. Based on the population relaxation time and transverse relaxation time of the nucleus returning to the thermal equilibrium state, the system collects the free induction decay and uses Fourier transform for a characteristic resonance signal. Because the nucleus resonance is highly affected by the magnetic field created by surrounding nuclei, chemical shifting and J-coupling provide useful structural information in a one-dimensional NMR spectrum. For more complex molecules, the effectiveness of NMR can be improved by using hyperpolarization or two-dimensional NMR such as correlation spectroscopy (COSY), nuclear overhauser effect spectroscopy (NOESY), total correlation spectroscopy (TOCSY), and heteronuclear correlation experiments.

X-ray crystallography is another option to determine the comprehensive structural information of peptide-based biomaterials.[170-172] To get a diffraction pattern of regularly spaced spots, a crystal material is placed on a goniometer and rotated gradually under the X-ray beam. The beam of light spreads in various directions and provides angle and intensity information to

build a three-dimensional picture of the density of electrons within the crystal. According to these electron patterns, structures and functions of many biological molecules such as proteins, peptides, and DNA have been detailed at the atomic level, including size of atom and the lengths and types of chemical bonds. Besides X-ray, electrons or neutrons also could be used to produce similar diffraction patterns based on different material conditions. Furthermore, besides the atomic scale structural information, the size, shape, and orientation are also crucial to biomaterial study. Small angle scattering (SAS) is a useful technique for these investigations.[173, 174] Instead of deflection from a straight trajectory, SAS collects the deflection from 0.1 to 10 °and covers the scale range up to thousands of angstroms. Two of the most commonly used SAS techniques are small-angle neutron scattering and small-angle X-ray scattering.

2.3.3 Morphological Properties

Like Richard Feynman said in his famous lecture in 1959, "It is very easy to answer many of these fundamental biological questions; you just look at the thing!"[1] Morphological observation is the key to answering a large number of biological questions and to predicting the functionality and biophysical properties of many biomaterials. Because peptide molecules are nano-scale, which is outside the resolution of optical microscopes, electron microscopy and atomic force microscopy become the chief techniques to study the morphological properties of peptide-based biomaterials.

Using electrons as an illumination or imaging source, transmission electron microscopy (TEM) operates on the same basic principles as light microscopy but provides resolution that is tens of thousands times better.[175-177] Electrons are emitted from the anode of the microscope and move toward to samples through a vacuum column. Unlike light microscopy, which uses solid lenses to focus the light, TEM focuses the electrons into a beam with electromagnetic lenses. The electron beam then travels through condenser and objective apertures with different sizes to hit studied samples at controlled beam intensity. This image is then magnified and focused on a fluorescent screen for direct observation or detected by an imaging device such as a CCD camera. To obtain a high-quality image, a specific sample preparation method must be conducted to increase the image contrast. Negative stain is one useful method for this purpose. Negative staining materials such as uranyl acetate, ammonium molybdate, and uranyl formate attach samples and perform electron scattering properties, which increase the contrast of molecular

structures. On the other hand, instead of introducing staining molecules to samples, anothermethod is using a specific sample holder that allows samples to be held at a liquid nitrogen temperature and to be embedded in vitreous ice. This technique is called electron cryo-microscopy (CryoTEM) and could be used to observe macromolecular assemblies such as a peptide hydrogel matrix.[178, 179] With an additional raster system and suitable detectors, TEM could be further developed as other electron microscopy instruments such as a scanning transmission electron microscope (STEM) and a high-resolution transmission electron microscope (HR-TEM). Furthermore, when an electron beam is scanned in a raster pattern and hits the surface of samples, secondary electrons and back-scattered electrons can be emitted. By detecting such an electron signal, scanning electron microscopy (SEM) could be used to study the surface characters of biomaterials.

Atomic Force Microscopy (AFM) is another higher-resolution technique to determine the surface characteristics of materials and tip-sample interaction force.[180, 181] It uses a sharp probe with a nano-scale tip to scan the sample surface. During the test, the force between the probe tip and sample surface leads to a deflection of the scanning probe. This deflection is then detected by a laser beam system and causes the adjustment of the feedback system; for example, the probe-to-sample distance can be adjusted by z direction movement of the sample holder to maintain a constant force between tip and sample. AFM can be operated in a static mode or a dynamic mode where the scanning probe is vibrated. AFM can provide a three-dimensional surface profile and even higher resolution. Because no specific treatments are required for the AFM sample and its working environment, such as ambient air or liquid, is very relaxed, AFM is a good imaging tool to study biological macromolecules and even living organisms without exerting artificial influence in the final images.

2.3.4 Rheological Properties

A fundamental understanding of rheological properties of peptide-based biomaterials is particularly important to evaluate their potential applications.[34, 114, 182] Especially for peptide-based hydrogels, bulk mechanical and viscoelastic properties, dynamic rheological behavior, and gelation time are all relative to their biotechnological uses such as three-dimensional cell scaffolding and drug delivery systems.[20, 123] Oscillatory shear measurement of a dynamic rheological system is a powerful technique to study the mechanical properties of biomaterials

from solution to semi-solid state.[182, 183] Parameters such as storage modulus (G'), loss modulus (G''), complex modules (G*), complex viscosity (η*) and loss factor (tan δ) would be measured as a function of strain, frequency, temperature and time to estimate the physical state and mechanical characters of tested materials. According to the basic rheological principle, the complex notation defines G*=G'+iG'' and tan δ =G''/G', considering G' and G'' as the real and imaginary components of G*. For viscoelastic materials, G' represents the deformation energy stored in tested material during the shearing process and G'' represents the energy dissipated during shearing process. In other words, G' and G'' indicate the stiffness and liquid-like components of a viscoelastic material, respectively. When G' is larger than G'' (tan δ <1), the material behaves more like an elastic solid; however, when G'' is larger than G' (tan δ >1) the liquid-like behavior predominates. An extreme situation is when δ = 0˚ and the material presents as an elastic solid; conversely, when δ = 90˚, the material is a Newtonian viscous fluid. Therefore, δ could be used to quantify the viscoelasticity of a material. For peptide hydrogel, the gelation point is the crossover point of G' and G''.

2.4 Application of Peptide-Based Materials

2.4.1 3D Cell Culture for Tissue Engineering

With an in-depth understanding of influences of cell culture environment in physiology and pathophysiology studies, several striking differences in subtle cellular processes such as proliferation, apoptosis, differentiation, gene expression, migration, and drug sensitivities have been revealed between traditional platforms and hydrogel matrix cell culture systems.[184-186] On the other hand, the expensive, time-consuming, and ethical issues with animal models as *in vivo* 3D systems have become a drawback on drug discovery, regenerative medicine, and other biomedical development. The peptide-based hydrogel is an attractive candidate to bridge the gap between *in vitro* cell culture platforms and *in vivo* animal systems. Unlike polysaccharide-based hydrogel (e.g. alginate) or a synthetic polymer–based scaffold (e.g. polystyrene and polycaprolactone), peptide-based hydrogel presents mimic the native extracellular matrix (ECM) by showing similar fibril and porous sizes within the matrix.[185,186] Additionally, some commercially available protein-based hydrogels such as Matrigel are reconstituted basement membranes extracted from the Engelbreth Holm Swarm (EHS) mouse tumor that contains various growth factors and enzymes that may change or influence the growth and native

functions of given cultured cells.[187] Such inconvenience could be improved by peptide-based hydrogel, because the synthetic peptide molecules make the self-assembled matrix homogeneous and can be suitable for various cell types.

The first commercially available peptide-based 3D cell culture hydrogel was PuraMatrix,[188, 189] which was based on a 16-residue peptide sequence $(RADA)_4$-$CONH_2$. The peptide solution was acidic and was triggered to hydrogel by changing the environmental pH to physiological conditions. Water content of this hydrogel reached around 99.5%, and the nanopores in the peptide scaffold ranged from a few nanometers to a few hundred nanometers. Similar research has been done by many different groups. Schneider and colleagues used their MAX8 hydrogel to encapsulate C3H10t1/2 mesenchymal stem cells.[35] Because of the fast hydrogel forming process and the mechanical rigidity of the hydrogel scaffold, z-stack laser scanning confocal microscopy images showed that cells were homogenously suspended in 3D. Based on the special shearing-thinning and fast recovery properties of MAX8 hydrogel, the gel/cell constructs could be targeted for delivery via syringe. One recent report showed that a tripeptide (Fmoc-RGD) containing the cell adhesion motif RGD could also form a peptide when the N-termini was conjugated with the Fmoc [N-(fluorenyl)-9-methoxycarbonyl] aromatic unit.[189] After dissolving in water at 35–40 ˚C, the peptide solution was cooled to room temperature and stood overnight to self-assemble as a self-supporting hydrogel through the stacking interactions of aromatic groups. Bovine fibrobleasts were demonstrated to grow in this Fmoc-RGD hydrogel matrix.

2.4.2 Controlled Release and Delivery System

Peptide-based hydrogels also could be applied as auxiliary carriers for drugs or genes.[190-192] To understand the influence of the molecular mass, hydrodynamic radii and isoelectric points of encapsulated molecules on molecular release kinetics of hydrogel matrix, Zhang and colleagues used $(RADA)_4$-$CONH_2$ peptide hydrogel to encapsulate a variety of proteins including lysozyme, trypsin inhibitor, bovine serum albumin (BSA), and immunoglobulin G (IgG).[193] By directly measuring the diffusion coefficients through single-molecule fluorescence correlation spectroscopy and comparing the release kinetic with other diffusion models and data from the literature, Zhang and colleagues suggested that the size of the protein was the primary factor affecting the molecular diffusion from peptide hydrogel. Changing the hydrogel matrix

density might be a method to control molecular release kinetics. The conformation and functionality of encapsulated proteins were not changed after they were released from hydrogel matrix. Similar research to Zhang et al. was done by Schneider and colleagues using MAX1 and MAX8 peptides to encapsulate FITC-dextran macromolecules.[191] They demonstrated that the release kinetics of macromolecules was affected by the hydrogel mesh size, which was adjustable through modulating the peptide concentration or altering the peptide sequence. Depending on different sizes of macromolecules, the release of half-lives ranged from 8 hours to over a month.

Besides hydrogel, some trans-membrane peptides are excellent candidates for drug delivery systems.[194, 195] Because of their amphiphilic properties, these peptides can facilitate drug internalization by direct conjugation with drugs or initiating their self-assembly in the presence of drugs and encapsulating drugs within the assembling vehicles.[196,197] Using cell membrane receptors as a mode and combining drug binding properties with environmentally sensitivetrigger peptide sequences, peptide vehicles might be rationally designed to deliver and release a drug to the target site.Recently, Erkki Ruoslahti's group from the University of California-Santa Barbara, reported designing a tumor-homing peptide, iRGD (CRGDK-RGPD-EC), to deliver drugs deep into the tumor parenchyma for cancer treatment.[194, 196, 197] By binding to the αv integrins on the tumor endothelium, this peptide was proteolytically cut and exposed a binding motif for neuropilin-1 for cell or tissue penetration. The sensitivity of antitumor drugs or tumor-imaging agents was significantly enhanced by conjugating or directly mixing with iRGD peptides.

2.4.3 Antimicrobial Activities

Because of the increasing resistance of microbes to conventional antibiotics, functional peptides are considered potential bactericidal or static candidates through their ability to interact and/or disrupt bacterial cell membranes.[198-200] Peptide lengths vary from several to a few dozen amino acid residues. Charged amino acids such as lysine, arginine, aspartic acid, and glutamic acid are mostly selected for the hydrophilic region.[201] Based on their structural features, peptides can attach to or insert into microbial membrane bilayers and play antimicrobial functions.[202] Under this principle, serial peptides with sequence A_mK (m=3, 6, or 9) were designed as antimicrobial agents.[202] Depending on the length of the alanine tail, the peptides performed

membrane penetration leading to bacterial aggregation. The longer the hydrophobic tail, the stronger bacterial killing capacity presented. Peptide Amphiphiles, consisting of a lipid tail and an amino acid functional head, also showed a remarkable capability for bacterial growth inhibition.[203, 204] A peptide serial C_{16}-KXK (X=A, G, L or K) was designed and exhibited powerful antimicrobical activity on both Gram-positive and Gram-negative bacteria and fungus.[205] Interestingly, some peptide hydrogels also performed antimicrobial functions; for example, by modifying several residues of MAX1, Schneider designed a new peptide called MARG1 (VKVKVRVK-V_DPPT-KVKVRVKV-NH_2).[206] This peptide could self-assemble into injectable hydrogel in cell culture medium with a certain salt concentration (Na^+ > 100 mM). MARG1 showed antibacterial behavior against Methicillin-resistant Staphylococcus aureus (MRSA) on contact.

2.4.4 Others

Skin care and cosmetic products are other areas with great potential for peptide applications.[207, 208] Peptide amphiphiles act as surfactants. They perform biological functions such as anti-wrinkle and anti-microbial activities.[207, 208] When applied to fibroblast cell culture, a peptide amphiphile, C_{16}-KTTKS, stimulated the synthesis of collagen, elastin, and glucosaminoglycans.[207] These molecules are the critical components of the skin matrix.[207] Peptides like C_{16}-GQPR and C_{16}-GHK were used as important active ingredients for the commercial skin care product Matrixyl™ 3000.[208]

A template for nanofabrication and biomineralisation is another potential application for self-assembling peptides;[209, 210] for example, using a nanofiber-forming peptide as a template in a Cd^{2+} containing solution, the nucleation and growth of CdS nanocrystal were formed when hydrogen sulfide was diffused into the system.[211] By using similar peptide nanofibers to coat bone implanted materials, Stupp's group found that nanofiber occupied the pores of the metallic foam and facilitate the mineralization of hydroxyapatite, which consequently helped bone tissue regenerate.[212]

With the development of peptide design and characterization, as well as increasingly interdisciplinary cooperation, many potential applications of peptide-based biomaterials are under investigation, such as using peptide-based biomaterials as hemostats, adhesion agents, and

membrane protein stabilization agents.[213-215] More peptide-based biomaterials are coming in near future.

2.4 References

1. Feynman, R. There is plenty of room at the bottom. Eng. Sci. 1960, 23, 22-36.

2. Junk, A.; Riess, F. From an idea to a vision: There's plenty of room at the bottom. Am. J. Phy. 2006, 74, 825-830.

3. Madia, W. J. Building the future an atom at a time: Realizing Feynman's vision. Metal. Mater. Trans.A-Phys. Metal. Mater. Sci. 2006, 37A, 2905-2918.

4. Yadugiri, V. T.; Malhotra, R. 'Plenty of room' - fifty years after the Feynman lecture. Curr. Sci. 2010, 99, 900-907.

5. Cui, F.; Li, Y.; Ge, J. Self-assembly of mineralized collagen composites. Mat. Sci. Eng. R-Reports 2007, 57, 1-27.

6. Cho, N.; Jackman, J. A.; Liu, M.; Frank, C. W. pH-driven assembly of various supported lipid platforms: a comparative study on silicon oxide and titanium oxide. Langmuir 2011, 27, 3739-3748.

7. Morgado, I.; Faendrich, M. Assembly of Alzheimer's A beta peptide into nanostructured amyloid fibrils. Curr. Opin. Col. Int. Sci. 2011, 16, 508-514.

8. Sun, X. S. Soy protein polymers and adhesion properties. J. Bio. Mat. Bio. 2011, 5, 409-432.

9. Afonin, K. A.; Grabow, W. W.; Walker, F. M.; Bindewald, E.; Dobrovolskaia, M. A.; Shapiro, B. A.; Jaeger, L. Design and self-assembly of siRNA-functionalized RNA nanoparticles for use in automated nanomedicine. Nat. Prot. 2011, 6, 2022-2034.

10. Cavalli, S.; Albericio, F.; Kros, A. Amphiphilic peptides and their cross-disciplinary role as building blocks for nanoscience. Chem. Soc. Rev. 2010, 39, 241-263.

11. Knoops, K.; Schoehn, G.; Schaffitzel, C. Cryo-electron microscopy of ribosomal complexes in cotranslational folding, targeting, and translocation. Wiley Interdisciplinary Reviews-Rna 2012, 3, 429-441.

12. Di Matteo, S. Resonant x-ray diffraction: multipole interpretation. J. Phys. D-Applied Physics 2012, 45, 163001.

13. Hodzic, A.; Llusa, M.; Fraser, S. D.; Scheibelhofer, O.; Koller, D. M.; Reiter, F.; Laggner, P.; Khinast, J. G. Small- and wide-angle X-ray scattering (SWAXS) for quantification of aspirin content in a binary powder mixture. Int. J. Pharm. 2012, 428, 91-95.

14. Wang, W.; Murthy, N. S.; Grubb, D. T. Central small-angle diffuse scattering from fibers is made of two components. J. Poly. Sci. Part B-Polymer Physics 2012, 50, 797-804.

15. McBane, J. E.; Sharifpoor, S.; Labow, R. S.; Ruel, M.; Suuronen, E. J.; Santerre, J. P. Tissue engineering a small diameter vessel substitute: engineering constructs with select biomaterials and cells. Curr. Vasc. Pharm. 2012, 10, 347-360.

16. Oss-Ronen, L.; Seliktar, D. Polymer-conjugated albumin and fibrinogen composite hydrogels as cell scaffolds designed for affinity-based drug delivery. Acta Biomater. 2011, 7, 163-170.

17. Li, N.; Niu, L.; Qi, Y.; Yiu, C. K. Y.; Ryou, H.; Arola, D. D.; Chen, J.; Pashley, D. H.; Tay, F. R. Subtleties of biomineralisation revealed by manipulation of the eggshell membrane. Biomaterials 2011, 32, 8743-8752.

18. Zhang, S. Fabrication of novel biomaterials through molecular self-assembly. Nat. Biotechnol. 2003, 21, 1171-1178.

19. Zhao, X.; Zhang, S. Designer self-assembling peptide materials. Macromolecular Bioscience 2007, 7, 13-22.

20. Hauser, C. A. E.; Zhang, S. Designer self-assembling peptide nanofiber biological materials. Chem. Soc. Rev. 2010, 39, 2780-2790.

21. Caplan, M. R.; Moore, P. N.; Zhang, S. G.; Kamm, R. D.; Lauffenburger, D. A. Self-assembly of a beta-sheet protein governed by relief of electrostatic repulsion relative to van der Waals attraction. Biomacromolecules 2000, 1, 627-631.

22. Gelain, F.; Lomander, A.; Vescovi, A. L.; Zhang, S. Systematic studies of a self-assembling peptide nanofiber scaffold with other scaffolds. J. Nanosci. Nanotech. 2007, 7, 424-434.

23. Zhang, S.; Lockshin, C.; Herbert, A.; Winter, E.; Rich, A. Zuotin, a Putative Z-Dna Binding-Protein in Saccharomyces-Cerevisiae. EMBO J. 1992, 11, 3787-3796.

24. Zhang, S.; Holmes, T.; Lockshin, C.; Rich, A. Spontaneous assembly of a self-complementary oligopeptide to form a stable macroscopic membrane. Proc. Natl. Acad. Sci. U. S. A. 1993, 90, 3334-3338.

25. Zhang, S.; Rich, A. Direct conversion of an oligopeptide from a beta-sheet to an alpha-helix: A model for amyloid formation. Proc. Natl. Acad. Sci. U. S. A. 1997, 94, 23-28.

26. Holmes, T.; de Lacalle, S.; Su, X.; Liu, G.; Rich, A.; Zhang, S. Extensive neurite outgrowth and active synapse formation on self-assembling peptide scaffolds. Proc. Natl. Acad. Sci. U. S. A. 2000, 97, 6728-6733.

27. Vauthey, S.; Santoso, S.; Gong, H.; Watson, N.; Zhang, S. Molecular self-assembly of surfactant-like peptides to form nanotubes and nanovesicles. Proc. Natl. Acad. Sci. U. S. A. 2002, 99, 5355-5360.

28. Loo, Y.; Zhang, S.; Hauser, C. A. E. From short peptides to nanofibers to macromolecular assemblies in biomedicine. Biotechnol. Adv. 2012, 30, 593-603.

29. Luo, Z.; Wang, S.; Zhang, S. Fabrication of self-assembling D-form peptide nanofiber scaffold d-EAK16 for rapid hemostasis. Biomaterials 2011, 32, 2013-2020.

30. Khoe, U.; Yang, Y.; Zhang, S. Self-assembly of nanodonut structure from a cone-shaped designer lipid-like peptide surfactant. Langmuir 2009, 25, 4111-4114.

31. Castelletto, V.; Hamley, I. W.; Harris, P. J. F.; Olsson, U.; Spencer, N. influence of the solvent on the self-assembly of a modified amyloid beta peptide fragment. I. morphological investigation. J. Phys. Chem. B 2009, 113, 9978-9987.

32. Lee, O.; Stupp, S. I.; Schatz, G. C. Atomistic molecular dynamics simulations of peptide amphiphile self-assembly into cylindrical nanofibers. J. Am. Chem. Soc. 2011, 133, 3677-3683.

33. Meng, Q.; Kou, Y.; Ma, X.; Liang, Y.; Guo, L.; Ni, C.; Liu, K. Tunable self-assembled peptide amphiphile nanostructures. Langmuir 2012, 28, 5017-5022.

34. Schneider, J.; Pochan, D.; Ozbas, B.; Rajagopal, K.; Pakstis, L.; Kretsinger, J. Responsive hydrogels from the intramolecular folding and self-assembly of a designed peptide. J. Am. Chem. Soc. 2002, 124, 15030-15037.

35. Haines-Butterick, L.; Rajagopal, K.; Branco, M.; Salick, D.; Rughani, R.; Pilarz, M.; Lamm, M. S.; Pochan, D. J.; Schneider, J. P. Controlling hydrogelation kinetics by peptide design for three-dimensional encapsulation and injectable delivery of cells. Proc. Natl. Acad. Sci. U. S. A. 2007, 104, 7791-7796.

36. Branco, M. C.; Pochan, D. J.; Wagner, N. J.; Schneider, J. P. The effect of protein structure on their controlled release from an injectable peptide hydrogel. Biomaterials 2010, 31, 9527-9534.

37. Gungormus, M.; Branco, M.; Fong, H.; Schneider, J. P.; Tamerler, C.; Sarikaya, M. Self assembled bi-functional peptide hydrogels with biomineralization-directing peptides. Biomaterials 2010, 31, 7266-7274.

38. Bean, J.; Kopple, K.; Peishoff, C. Conformational-Analysis of Cyclic Hexapeptides Containing the D-Pro-L-Pro Sequence to Fix Beta-Turn Positions. J. Am. Chem. Soc. 1992, 114, 5328-5334.

39. Stanger, H.; Gellman, S. Rules for antiparallel beta-sheet design: D-Pro-Gly is superior to L-Asn-Gly for beta-hairpin nucleation. J. Am. Chem. Soc. 1998, 120, 4236-4237.

40. Pochan, D.; Schneider, J.; Kretsinger, J.; Ozbas, B.; Rajagopal, K.; Haines, L. Thermally reversible hydrogels via intramolecular folding and consequent self-assembly of a de Novo designed peptide. J. Am. Chem. Soc. 2003, 125, 11802-11803.

41. Branco, M. C.; Pochan, D. J.; Wagner, N. J.; Schneider, J. P. Macromolecular diffusion and release from self-assembled beta-hairpin peptide hydrogels. Biomaterials 2009, 30, 1339-1347.

42. Branco, M. C.; Nettesheim, F.; Pochan, D. J.; Schneider, J. P.; Wagner, N. J. Fast Dynamics of semiflexible chain networks of self-assembled peptides. Biomacromolecules 2009, 10, 1374-1380.

43. Rackham, O. J. L.; Madera, M.; Armstrong, C. T.; Vincent, T. L.; Woolfson, D. N.; Gough, J. The evolution and structure prediction of coiled coils across all genomes. J. Mol. Biol. 2010, 403, 480-493.

44. Gruber, M.; Lupas, A. Historical review: Another 50th anniversary - new periodicities in coiled coils. Trends Biochem. Sci. 2003, 28, 679-685.

45. Walshaw, J.; Gillespie, M. D.; Kelemen, G. H. A novel coiled-coil repeat variant in a class of bacterial cytoskeletal proteins. J. Struct. Biol. 2010, 170, 202-215.

46. Kurochkina, N.; Choekyi, T. Helix-helix interfaces and ligand binding. J. Theor. Biol. 2011, 283, 92-102.

47. Sprang, S.; Fletterick, R. Structure of Glycogen Phosphorylase-a at 2.5 a Resolution. J. Mol. Biol. 1979, 131, 523-551.

48. Astbury, W. T. Some problems in the X-ray analysis of the structure of animal hairs and other protein fibres. Trans. Fara. Soc. 1933, 29, 193-205.

49. Crick, F. H. Is alpha-keratin a coiled coil? Nature 1952, 170, 882-883.

50. Pauling, L.; Corey, R. B. Structure of the nucleic acids. Nature 1953, 171, 346.

51. Crick, F. The Fourier Transform of a Coiled-Coil. Acta Crystallogr. 1953, 6, 685-689.

52. Crick, F. The packing of alpha-helices - simple coiled-coils. acta crystallogr. 1953, 6, 689-697.

53. Sodek, J.; Hodges, R.; Smillie, L.; Jurasek, L. Amino-acid sequence of rabbit skeletal tropomyosin and its coiled coil structure. Proc. Natl. Acad. Sci. U. S. A. 1972, 69, 3800-3804.

54. Wilson, I. A.; Skehel, J. J.; Wiley, D. C. Structure of the haemagglutinin membrane glycoprotein of influenza virus at 3 Å resolution. Nature 1981, 289, 366-373.

55. Phillips, G.; Fillers, J.; Cohen, C. Tropomyosin Crystal-Structure and Muscle Regulation. J. Mol. Biol. 1986, 192, 111-128.

56. Oshea, E.; Klemm, J.; Kim, P.; Alber, T. X-Ray Structure of the Gcn4 leucine zipper, a 2-stranded, parallel coiled coil. Science 1991, 254, 539-544.

57. Jing, P.; Rudra, J. S.; Herr, A. B.; Collier, J. H. Self-assembling peptide-polymer hydrogels designed from the coiled coil region of fibrin. Biomacromolecules 2008, 9, 2438-2446.

58. Wagner, D.; Phillips, C.; Ali, W.; Nybakken, G.; Crawford, E.; Schwab, A.; Smith, W.; Fairman, R. Toward the development of peptide nanofilaments and nanoropes as smart materials. Proc. Natl. Acad. Sci. U. S. A. 2005, 102, 12656-12661.

59. Dong, H.; Paramonov, S. E.; Hartgerink, J. D. Self-assembly of alpha-helical coiled coil nanofibers. J. Am. Chem. Soc. 2008, 130, 13691-13695.

60. Woolfson, D. N. Building fibrous biomaterials from alpha-helical and collagen-like coiled-coil peptides. Biopolymers 2010, 94, 118-127.

61. Apostolovic, B.; Danial, M.; Klok, H. Coiled coils: attractive protein folding motifs for the fabrication of self-assembled, responsive and bioactive materials. Chem. Soc. Rev. 2010, 39, 3541-3575.

62. Kouzarides, T.; Ziff, E. The role of the leucine zipper in the fos jun interaction. Nature 1988, 336, 646-651.

63. Landschulz, W.; Johnson, P.; Mcknight, S. The leucine zipper - a hypothetical structure common to a new class of dna-binding proteins. Science 1988, 240, 1759-1764.

64. Oshea, E.; Rutkowski, R.; Kim, P. Evidence that the leucine zipper is a coiled coil. Science 1989, 243, 538-542.

65. Ryadnov, M.; Woolfson, D. Engineering the morphology of a selfassembling protein fibre. Nature Materials 2003, 2, 329-332.

66. Papapostolou, D.; Smith, A. M.; Atkins, E. D. T.; Oliver, S. J.; Ryadnov, M. G.; Serpell, L. C.; Woolfson, D. N. Engineering nanoscale order into a designed protein fiber. Proc. Natl. Acad. Sci. U. S. A. 2007, 104, 10853-10858.

67. Mahmoud, Z. N.; Grundy, D. J.; Channon, K. J.; Woolfson, D. N. The non-covalent decoration of self-assembling protein fibers. Biomaterials 2010, 31, 7468-7474.

68. Banwell, E. F.; Abelardo, E. S.; Adams, D. J.; Birchall, M. A.; Corrigan, A.; Donald, A. M.; Kirkland, M.; Serpell, L. C.; Butler, M. F.; Woolfson, D. N. Rational design and application of responsive alpha-helical peptide hydrogels. Nat. Mater. 2009, 8, 596-600.

69. Janeway, C.; Wigzell, H. Interaction of T-Cells with a Lipid-Modified Hapten-Protein Conjugate. Scand. J. Immunol. 1977, 6, 711-712.

70. Johansson, K.; Jagersten, C.; Christiansson, A.; Wieslander, A. Protein-Composition and Extractability of Lipid-Modified Membranes from Acholeplasma-Laidlawii. Biochemistry 1981, 20, 6073-6079.

71. Eisenhaber, B.; Sammer, M.; Lua, W. H.; Benetka, W.; Liew, L. L.; Yu, W.; Lee, H. K.; Koranda, M.; Eisenhaber, F.; Adhikari, S. Nuclear import of a lipid-modified transcription factor. Cell Cycle 2011, 10, 3897-3911.

72. Boyer, M.; Wise, K. Lipid-modified surface protein antigens expressing size variation within the species mycoplasma-hyorhinis. Infect. Immun. 1989, 57, 245-254.

73. Ringler, P.; Schulz, G. E. Self-assembly of proteins into designed networks. Science 2003, 302, 106-109.

74. Ozbas, Salt-triggered peptide folding and consequent self-assembly into hydrogels with tunable modulus. Macromolecules 2004, 37, 7331.

75. Ten Brink, H. T.; Meijer, J. T.; Geel, R. V.; Damen, M.; Lowik, D. W. P. M.; Van Hest, J. C. M. Solid-phase synthesis of C-terminally modified peptides. Journal of Peptide Science 2006, 12, 686-692.

76. Trent, A.; Marullo, R.; Lin, B.; Black, M.; Tirrell, M. Structural properties of soluble peptide amphiphile micelles. Soft Matter 2011, 7, 9572-9582.

77. Yu, Y.; Tirrell, M.; Fields, G. Minimal lipidation stabilizes protein-like molecular architecture. J. Am. Chem. Soc. 1998, 120, 9979-9987.

78. Su, J.; Hodges, R.; Kay, C. Effect of chain-length on the formation and stability of synthetic alpha-helical coiled coils. Biochemistry 1994, 33, 15501-15510.

79. Forns, P.; Lauer-Fields, J.; Gao, S.; Fields, G. Induction of protein-like molecular architecture by monoalkyl hydrocarbon chains. Biopolymers 2000, 54, 531-546.

80. Hartgerink, J.; Beniash, E.; Stupp, S. Self-assembly and mineralization of peptide-amphiphile nanofibers. Science 2001, 294, 1684-1688.

81. Jiang, H.; Guler, M. O.; Stupp, S. I. The internal structure of self-assembled peptide amphiphiles nanofibers. Soft Matter 2007, 3, 454-462.

82. Stupp, S. I. Self-assembly and biomaterials. Nano Letters 2010, 10, 4783-4786.

83. Matson, J. B.; Newcomb, C. J.; Bitton, R.; Stupp, S. I. Nanostructure-templated control of drug release from peptide amphiphile nanofiber gels. Soft Matter 2012, 8, 3586-3595.

84. Silva, G.; Czeisler, C.; Niece, K.; Beniash, E.; Harrington, D.; Kessler, J.; Stupp, S. Selective differentiation of neural progenitor cells by high-epitope density nanofibers RID B-6737-2009. Science 2004, 303, 1352-1355.

85. Zhang, S.; Greenfield, M. A.; Mata, A.; Palmer, L. C.; Bitton, R.; Mantei, J. R.; Aparicio, C.; de la Cruz, M. O.; Stupp, S. I. A self-assembly pathway to aligned monodomain gels. Nat. Mater. 2010, 9, 594-601.

86. Pashuck, E. T.; Cui, H.; Stupp, S. I. Tuning supramolecular rigidity of peptide fibers through molecular structure. J. Am. Chem. Soc. 2010, 132, 6041-6046.

87. Cui, H.; Pashuck, E. T.; Velichko, Y. S.; Weigand, S. J.; Cheetham, A. G.; Newcomb, C. J.; Stupp, S. I. Spontaneous and x-ray-triggered crystallization at long range in self-assembling filament networks. Science 2010, 327, 555-559.

88. Sur, S.; Pashuck, E. T.; Guler, M. O.; Ito, M.; Stupp, S. I.; Launey, T. A hybrid nanofiber matrix to control the survival and maturation of brain neurons. Biomaterials 2012, 33, 545-555.

89. Cui, H.; Webber, M. J.; Stupp, S. I. Self-assembly of peptide amphiphiles: from molecules to nanostructures to biomaterials. Biopolymers 2010, 94, 1-18.

90. Hung, A. M.; Stupp, S. I. Simultaneous self-assembly, orientation, and patterning of peptide-amphiphile nanofibers by soft lithography. Nano Letters 2007, 7, 1165-1171.

91. Standley, S. M.; Toft, D. J.; Cheng, H.; Soukasene, S.; Chen, J.; Raja, S. M.; Band, V.; Band, H.; Cryns, V. L.; Stupp, S. I. Induction of cancer cell death by self-assembling nanostructures incorporating a cytotoxic peptide. Cancer Res. 2010, 70, 3020-3026.

92. Mata, A.; Geng, Y.; Henrikson, K. J.; Aparicio, C.; Stock, S. R.; Satcher, R. L.; Stupp, S. I. Bone regeneration mediated by biomimetic mineralization of a nanofiber matrix. Biomaterials 2010, 31, 6004-6012.

93. Huang, Z.; Newcomb, C. J.; Bringas, P., Jr.; Stupp, S. I.; Snead, M. L. Biological synthesis of tooth enamel instructed by an artificial matrix. Biomaterials 2010, 31, 9202-9211.

94. George, R.; Heringa, J. An analysis of protein domain linkers: their classification and role in protein folding. Protein Eng. 2002, 15, 871-879.

95. LEVITT, M.; CHOTHIA, C. Structural patterns in globular proteins. Nature 1976, 261, 552-558.

96. Angkawidjaja, C.; Paul, A.; Koga, Y.; Takano, K.; Kanava, S. Importance of a repetitive nine-residue sequence motif for intracellular stability and functional structure of a family I.3 lipase. FEBS letters 2005, 579, 4707.

97. Yamada, Y.; Hozumi, K.; Aso, A.; Hotta, A.; Toma, K.; Katagiri, F.; Kikkawa, Y.; Nomizu, M. Laminin active peptide/agarose matrices as multifunctional biomaterials for tissue engineering. Biomaterials 2012, 33, 4118-4125.

98. Okuyama, K. High-resolution structures of collagen-like peptides [(Pro-Pro-Gly)(4)-Xaa-Yaa-Gly-(Pro-Pro-Gly)(4)]: implications for triple-helix hydration and Hyp(X) puckering. Biopolymers 2009, 91, 361-372.

99. Megeed, Genetically engineered silk-elastinlike protein polymers for controlled drug delivery. Adv. Drug Deliv. Rev. 2002, 54, 1075.

100. McDaniel, J. R.; Callahan, D. J.; Chilkoti, A. Drug delivery to solid tumors by elastin-like polypeptides. Adv. Drug Deliv. Rev. 2010, 62, 1456-1467.

101. Gifford, J. L.; Walsh, M. P.; Vogel, H. J. Structures and metal-ion-binding properties of the Ca^{2+}-binding helix-loop-helix EF-hand motifs. Biochem. J. 2007, 405, 199-221.

102. Nelson, M. R.; Chazin, W. J. Structures of EF-hand Ca^{2+}-binding proteins: Diversity in the organization, packing and response to Ca^{2+} binding. Biometals 1998, 11, 297-318.

103. Meier, R.; Drepper, T.; Svensson, V.; Jaeger, K.; Baumann, U. A calcium-gated lid and a large beta-roll sandwich are revealed by the crystal structure of extracellular lipase from Serratia marcescens. J. Biol. Chem. 2007, 282, 31477-31483.

104. Baumann, U.; Bauer, M.; Letoffe, S.; Delepelaire, P.; Wandersman, C. Crystal-structure of a complex between serratia-marcescens metalloprotease and an inhibitor from Erwinia-Chrysanthemi. J. Mol. Biol. 1995, 248, 653-661.

105. Ringler, P.; Schulz, G. Self-assembly of proteins into designed networks. Science 2003, 302, 106-109.

106. Bennett, M.; Schlunegger, M.; Eisenberg, D. 3D domain swapping - a mechanism for oligomer assembly. Protein Science 1995, 4, 2455-2468.

107. Heringa, J.; Taylor, W. Three-dimensional domain duplication, swapping and stealing. Curr. Opin. Struct. Biol. 1997, 7, 416-421.

108. Liu, Y.; Eisenberg, D. 3D domain swapping: As domains continue to swap. Protein Science 2002, 11, 1285-1299.

109. Dehouck, Y.; Biot, C.; Gilis, D.; Kwasigroch, J.; Rooman, M. Sequence-structure signals of 3D domain swapping in proteins. J. Mol. Biol. 2003, 330, 1215-1225.

110. Szilagyi, A.; Zhang, Y.; Zavodszky, P. Intra-chain 3D segment swapping spawns the evolution of new multidomain protein architectures. J. Mol. Biol. 2012, 415, 221-235.

111. Spadaccini, R.; Ercole, C.; Gentile, M. A.; Sanfelice, D.; Boelens, R.; Wechselberger, R.; Batta, G.; Bernini, A.; Niccolai, N.; Picone, D. NMR Studies on structure and

dynamics of the monomeric derivative of BS-RNase: new insights for 3D domain swapping. Plos One 2012, 7, e29076.

112. Aravind, P.; Suman, S. K.; Mishra, A.; Sharma, Y.; Sankaranarayanan, R. Three-dimensional domain swapping in nitrollin, a single-domain beta gamma-crystallin from nitrosospira multiformis, controls protein conformation and stability but not dimerization. J. Mol. Biol. 2009, 385, 163-177.

113. Nagarkar, R. P.; Hule, R. A.; Pochan, D. J.; Schneider, J. P. Domain swapping in materials design. Biopolymers 2010, 94, 141-155.

114. Hule, R.; Nagarkar, R.; Hammouda, B.; Schneider, J.; Pochan, D. Dependence of self-assembled peptide hydrogel network structure on local fibril nanostructure. Macromolecules 2009, 42, 7137-7145.

115. Peppas, N.; Hilt, J.; Khademhosseini, A.; Langer, R. Hydrogels in biology and medicine: From molecular principles to bionanotechnology. Adv. Mater. 2006, 18, 1345-1360.

116. Geckil, H.; Xu. F.; Zhang, X.; Moon, S.; Demirci, U. Engineering hydrogels as extracellular matrix mimics. Nanomedicine 2010, 5, 469-484.

117. Lee, K.; Mooney, D. Hydrogels for tissue engineering. Chem. Rev. 2001, 101, 1869-1879.

118. Drury, J.; Mooney, D. Hydrogels for tissue engineering: scaffold design variables and applications. Biomaterials 2003, 24, 4337-4351.

119. Calvert, P. Hydrogels for soft machines. Adv. Mater. 2009, 21, 743-756.

120. Kopecek, J.; Yang, J. Revie - Hydrogels as smart biomaterials. Polym. Int. 2007, 56, 1078-1098.

121. Wichterle, O.; Lim, D. Hydrophilic gels for biological use. Nature 1960, 185, 117-118.

122. Garty, S.; Kimelman-Bleich, N.; Hayouka, Z.; Cohn, D.; Friedler, A.; Pelled, G.; Gazit, D. Peptide-modified "smart" hydrogels and genetically engineered stem cells for skeletal tissue engineering. Biomacromolecules 2010, 11, 1516-1526.

123. Chawla, K.; Yu, T.; Liao, S. W.; Guan, Z. Biodegradable and biocompatible synthetic saccharide-peptide hydrogels for three-dimensional stem cell culture. Biomacromolecules 2011, 12, 560-567.

124. Jonker, A. M.; Loewik, D. W. P. M.; van Hest, J. C. M. Peptide- and protein-based hydrogels. Chemistry of Materials 2012, 24, 759-773.

125. Peppas, N.; Bures, P.; Leobandung, W.; Ichikawa, H. Hydrogels in pharmaceutical formulations. Eur. J. Pharm. Biopharm. 2000, 50, 27-46.

126. Xu, C.; Kopecek, J. Self-assembling hydrogels. Polymer Bulletin 2007, 58, 53-63.

127. Wright, E.; Conticello, V. Self-assembly of block copolymers derived from elastin-mimetic polypeptide sequences. Adv. Drug Deliv. Rev. 2002, 54, 1057-1073.

128. Mano, J. F. Stimuli-responsive polymeric systems for biomedical applications. Adv. Eng. Mater. 2008, 10, 515-527.

129. Park, K.; Na, K.; Jung, S.; Kim, S.; Park, K.; Cha, K.; Chung, H. Insulinoma cell line (MIN6) adhesion and spreading mediated by Arg-Gly-Asp (RGD) sequence conjugated in thermo-reversible gel. J. Biosci. Bioeng. 2005, 99, 598-602.

130. Bidwell,Gene L.,,III; Fokt, I.; Priebe, W.; Raucher, D. Development of elastin-like polypeptide for thermally targeted delivery of doxorubicin. Biochem. Pharmacol. 2007, 73, 620-631.

131. Qiu, Y.; Park, K. Environment-sensitive hydrogels for drug delivery. Adv. Drug Deliv. Rev. 2001, 53, 321-339.

132. Tanaka, T. Collapse of gels and the critical endpoint. Phys. Rev. Let. 1978, 40, 823.

133. Zhang, X.; Wu, D.; Chu, C. Synthesis, characterization and controlled drug release of thermosensitive IPN-PNIPAAm hydrogels. Biomaterials 2004, 25, 3793-3805.

134. Hou, Y.; Matthews, A. R.; Smitherman, A. M.; Bulick, A. S.; Hahn, M. S.; Hou, H.; Han, A.; Grunlan, M. A. Thermoresponsive nanocomposite hydrogels with cell-releasing behavior. Biomaterials 2008, 29, 3175-3184.

135. Wei, H.; Zhang, X.; Cheng, C.; Cheng, S.; Zhuo, R. Self-assembled, thermosensitive micelles of a star block copolymer based on PMMA and PNIPAAm for controlled drug delivery. Biomaterials 2007, 28, 99-107.

136. Han, H. D.; Choi, M. S.; Hwang, T.; Song, C. K.; Seong, H.; Kim, T. W.; Choi, H. S.; Shin, B. C. Hyperthermia-induced antitumor activity of thermosensitive polymer modified temperature-sensitive liposomes. J. Pharm. Sci. 2006, 95, 1909-1917.

137. Viglianti, B. L. Target molecular therapies: methods to enhance and monitor tumor drug delivery. Abdom. Imaging 2009, 34, 686-695.

138. Ohnishi, T.; Takahashi, A. Signal transduction of radiation and/or hyperthermic cancer therapies. Curr. Sign. Trans. Ther. 2010, 5, 231-236.

139. Massodi, I.; Moktan, S.; Rawat, A.; Bidwell,Gene L.,,III; Raucher, D. Inhibition of ovarian cancer cell proliferation by a cell cycle inhibitory peptide fused to a thermally responsive polypeptide carrier. Int. J. Cancer 2010, 126, 533-544.

140. Aluri, S.; Janib, S. M.; Mackay, J. A. Environmentally responsive peptides as anticancer drug carriers. Adv. Drug Deliv. Rev. 2009, 61, 940-952.

141. Jung, pH-Sensitive polymer nanospheres for use as a potential drug delivery vehicle. Biomacromolecules 2007, 8, 3401.

142. Torres-Lugo, M.; Peppas, N. Molecular design and in vitro studies of novel pH-sensitive hydrogels for the oral delivery of calcitonin. Macromolecules 1999, 32, 6646-6651.

143. Akala, E.; Kopeckova, P.; Kopecek, J. Novel pH-sensitive hydrogels with adjustable swelling kinetics. Biomaterials 1998, 19, 1037-1047.

144. Rajagopal, K.; Lamm, M. S.; Haines-Butterick, L. A.; Pochan, D. J.; Schneider, J. P. Tuning the pH Responsiveness of beta-Hairpin Peptide Folding, Self-assembly, and hydrogel material formation. Biomacromolecules 2009, 10, 2619-2625.

145. Zhao, Y.; Yokoi, H.; Tanaka, M.; Kinoshita, T.; Tan, T. Self-assembled pH-responsive hydrogels composed of the RATEA16 peptide. Biomacromolecules 2008, 9, 1511-1518.

146. Aggeli, A.; Bell, M.; Carrick, L.; Fishwick, C.; Harding, R.; Mawer, P.; Radford, S.; Strong, A.; Boden, N. pH as a trigger of peptide beta-sheet self-assembly and reversible switching between nematic and isotropic phases. J. Am. Chem. Soc. 2003, 125, 9619-9628.

147. Mamada, A.; Tanaka, T.; Kungwatchakun, D.; Irie, M. Photoinduced phase-transition of gels. Macromolecules 1990, 23, 1517-1519.

148. Burns, D.; Flint, D.; Kumita, J.; Feldman, H.; Serrano, L.; Zhang, Z.; Smart, O.; Woolley, G. Origins of helix-coil switching in a light-sensitive peptide. Biochemistry (N. Y.) 2004, 43, 15329-15338.

149. Charati, M. B.; Lee, I.; Hribar, K. C.; Burdick, J. A. Light-sensitive polypeptide hydrogel and nanorod composites. Small 2010, 6, 1608-1611.

150. Mant, C. T.; Kovacs, J. M.; Kim, H.; Pollock, D. D.; Hodges, R. S. Intrinsic amino acid side-chain hydrophilicity/hydrophobicity coefficients determined by reversed-phase high-performance liquid chromatography of model peptides: comparison with other hydrophilicity/hydrophobicity scales. Biopolymers 2009, 92, 573-595.

151. Moritz, R.; Ji, H.; Schutz, F.; Connolly, L.; Kapp, E.; Speed, T.; Simpson, R. A proteome strategy for fractionating proteins and peptides using continuous free-flow electrophoresis coupled off-line to reversed-phase high-performance liquid chromatography. Anal. Chem. 2004, 76, 4811-4824.

152. Yoshida, T. Peptide separation by hydrophilic-interaction chromatography: a review. j. biochem. Biophys. Methods 2004, 60, 265-280.

153. Fried, M.; Crothers, D. M. Equilibria and kinetics of lac repressor-operator interaction by polyacrylamide electrophoresis. Nucleic Acid Research 1981, 9: 6505-6525.

154. Righetti, P. G.; Candiano, G. Recent advances in electrophoretic techniques for the characterization of protein biomolecules: A poker of aces. Journal of Chromatography a 2011, 1218, 8727-8737.

155. Domon, B.; Aebersold, R. Review - mass spectrometry and protein analysis. Science 2006, 312, 212-217.

156. Merchant, M.; Weinberger, S. Recent advancements in surface-enhanced laser desorption/ionization-time of flight-mass spectrometry. Electrophoresis 2000, 21, 1164-1177.

157. Marshall, A.; Hendrickson, C.; Jackson, G. Fourier transform ion cyclotron resonance mass spectrometry: A primer. Mass Spectrom. Rev. 1998, 17, 1-35.

158. Moussaid, A.; Pusey, P. Multiple scattering suppression in static light scattering by cross-correlation spectroscopy. Phys. Rev. E 1999, 60, 5670-5676.

159. Schatzel, K. suppression of multiple-scattering by photon cross-correlation techniques. J. Mod. Optics 1991, 38, 1849-1865.

160. Ladbury, J.; Chowdhry, B. Sensing the heat: The application of isothermal titration calorimetry to thermodynamic studies of biomolecular interactions. Chem. Biol. 1996, 3, 791-801.

161. Leavitt, S.; Freire, E. Direct measurement of protein binding energetics by isothermal titration calorimetry. Curr. Opin. Struct. Biol. 2001, 11, 560-566.

162. Sturtevant, J. Biochemical applications of differential scanning calorimetry. Annu. Rev. Phys. Chem. 1987, 38, 463-488.

163. Rost, B.; Sander, C. Prediction of protein secondary structure at better than 70-percent accuracy. J. Mol. Biol. 1993, 232, 584-599.

164. Stephens, P.; Devlin, F.; Chabalowski, C.; Frisch, M. Ab-Initio calculation of vibrational absorption and circular-dichroism spectra using density-functional force-fields. J. Phys. Chem. 1994, 98, 11623-11627.

165. Kelly, S.; Jess, T.; Price, N. How to study proteins by circular dichroism. Biochim. Biophys. Acta-Proteins Proteo. 2005, 1751, 119-139.

166. Arrondo, J.; Muga, A.; Castresana, J.; Goni, F. Quantitative studies of the structure of proteins in solution by fourier-transform infrared-spectroscopy. Prog. Biophys. Mol. Bio. 1993, 59, 23-56.

167. Jackson, M.; Mantsch, H. the use and misuse of ftir spectroscopy in the determination of protein-structure. Crit. Rev. Biochem. Mol. Biol. 1995, 30, 95-120.

168. Bock, K.; Pedersen, C. C-13 Nuclear magnetic-resonance spectroscopy of monosaccharides. Adv. Carbohydr. Chem. Biochem. 1983, 41, 27-66.

169. Vliegenthart, J.; Dorland, L.; Vanhalbeek, H. High-resolution, H-1-nuclear magnetic-resonance spectroscopy as a tool in the structural-analysis of carbohydrates related to glycoproteins. Adv. Carbohydr. Chem. Biochem. 1983, 41, 209-374.

170. Uson, I.; Sheldrick, G. Advances in direct methods for protein crystallography. Curr. Opin. Struct. Biol. 1999, 9, 643-648.

171. Wormald, M.; Petrescu, A.; Pao, Y.; Glithero, A.; Elliott, T.; Dwek, R. Conformational studies of oligosaccharides and glycopeptides: Complementarity of NMR, X-ray crystallography, and molecular modelling. Chem. Rev. 2002, 102, 371-386.

172. Putnam, C. D.; Hammel, M.; Hura, G. L.; Tainer, J. A. X-ray solution scattering (SAXS) combined with crystallography and computation: defining accurate macromolecular structures, conformations and assemblies in solution. Q. Rev. Biophys. 2007, 40, 191-285.

173. Chen, S. Small-angle neutron-scattering studies of the structure and interaction in micellar and microemulsion systems. Annu. Rev. Phys. Chem. 1986, 37, 351-399.

174. Koch, M.; Vachette, P.; Svergun, D. Small-angle scattering: a view on the properties, structures and structural changes of biological macromolecules in solution. Q. Rev. Biophys. 2003, 36, 147-227.

175. Nitzan, A. Electron transmission through molecules and molecular interfaces. Annu. Rev. Phys. Chem. 2001, 52, 681-750.

176. Pennycook, S. J.; Varela, M.; Lupini, A. R.; Oxley, M. P.; Chisholm, M. F. Atomic-resolution spectroscopic imaging: past, present and future. J. Electron Microsc. 2009, 58, 87-97.

177. Bando, Y. Microstructure analysis of advanced ceramics by high-resolution analytical transmission electron-microscopy. J. Electron Microsc. 1995, 44, 115-123.

178. Holmes, K.; Angert, I.; Kull, F.; Jahn, W.; Schroder, R. Electron cryo-microscopy shows how strong binding of myosin to actin releases nucleotide. Nature 2003, 425, 423-427.

179. van Heel, M.; Gowen, B.; Matadeen, R.; Orlova, E.; Finn, R.; Pape, T.; Cohen, D.; Stark, H.; Schmidt, R.; Schatz, M.; Patwardhan, A. Single-particle electron cryo-microscopy: towards atomic resolution. Q. Rev. Biophys. 2000, 33, 307-369.

180. Giessibl, F. Advances in atomic force microscopy. Reviews of Modern Physics 2003, 75, 949-983.

181. Hansma, H.; Hoh, J. Biomolecular imaging with the atomic-force microscope. Annu. Rev. Biophys. Biomol. Struct. 1994, 23, 115-139.

182. Yan, C.; Pochan, D. J. Rheological properties of peptide-based hydrogels for biomedical and other applications. Chem. Soc. Rev. 2010, 39, 3528-3540.

183. Yan, C.; Altunbas, A.; Yucel, T.; Nagarkar, R. P.; Schneider, J. P.; Pochan, D. J. Injectable solid hydrogel: mechanism of shear-thinning and immediate recovery of injectable beta-hairpin peptide hydrogels. Soft Matter 2010, 6, 5143-5156.

184. Dawson, E.; Mapili, G.; Erickson, K.; Taqvi, S.; Roy, K. Biomaterials for stem cell differentiation. Adv. Drug Deliv. Rev. 2008, 60, 215-228.

185. Feder-Mengus, C.; Ghosh, S.; Reschner, A.; Martin, I.; Spagnoli, G. C. New dimensions in tumor immunology: what does 3D culture reveal? Trends Mol. Med. 2008, 14, 333-340.

186. Cushing, M. C.; Anseth, K. S. Hydrogel cell cultures. Science 2007, 316, 1133-1134.

187. Kleinman, H.; Martin, G. Matrigel: Basement membrane matrix with biological activity. Semin. Cancer Biol. 2005, 15, 378-386.

188. McGrath, A. M.; Novikova, L. N.; Novikova, L. N.; Wiberg, M. BD (TM) PuraMatrix (TM) peptide hydrogel seeded with Schwann cells for peripheral nerve regeneration. Brain Res. Bull. 2010, 83, 207-213.

189. Zhou, M.; Smith, A. M.; Das, A. K.; Hodson, N. W.; Collins, R. F.; Ulijn, R. V.; Gough, J. E. Self-assembled peptide-based hydrogels as scaffolds for anchorage-dependent cells. Biomaterials 2009, 30, 2523-2530.

190. Zha, L.; Banik, B.; Alexis, F. Stimulus responsive nanogels for drug delivery. Soft Matter 2011, 7, 5908-5916.

191. Branco, M. C.; Pochan, D. J.; Wagner, N. J.; Schneider, J. P. The effect of protein structure on their controlled release from an injectable peptide hydrogel. Biomaterials 2010, 31, 9527-9534.

192. King, W. J.; Mohammed, J. S.; Murphy, W. L. Modulating growth factor release from hydrogels via a protein conformational change. Soft Matter 2009, 5, 2399-2406.

193. Koutsopoulos, S.; Unsworth, L. D.; Nagaia, Y.; Zhang, S. Controlled release of functional proteins through designer self-assembling peptide nanofiber hydrogel scaffold. Proc. Natl. Acad. Sci. U. S. A. 2009, 106, 4623-4628.

194. Hossen, M. N.; Kajimoto, K.; Akita, H.; Hyodo, M.; Ishitsuka, T.; Harashima, H. Ligand-based targeted delivery of a peptide modified nanocarrier to endothelial cells in adipose tissue. J. Controlled Release 2010, 147, 261-268.

195. Sugahara, K. N.; Teesalu, T.; Karmali, P. P.; Kotamraju, V. R.; Agemy, L.; Girard, O. M.; Hanahan, D.; Mattrey, R. F.; Ruoslahti, E. Tissue-penetrating delivery of compounds and nanoparticles into tumors. Cancer Cell 2009, 16, 510-520.

196. Teesalu, T.; Sugahara, K. N.; Kotamraju, V. R.; Ruoslahti, E. C-end rule peptides mediate neuropilin-1-dependent cell, vascular, and tissue penetration. Proc. Natl. Acad. Sci. U. S. A. 2009, 106, 16157-16162.

197. Sugahara, K. N.; Teesalu, T.; Karmali, P. P.; Kotamraju, V. R.; Agemy, L.; Greenwald, D. R.; Ruoslahti, E. Coadministration of a tumor-penetrating peptide enhances the efficacy of cancer drugs. Science 2010, 328, 1031-1035.

198. Boman, H. Peptide Antibiotics and their Role in Innate Immunity. Annu. Rev. Immunol. 1995, 13, 61-92.

199. Brogden, K. Antimicrobial peptides: Pore formers or metabolic inhibitors in bacteria? Nat. Rev. Micro. 2005, 3, 238-250.

200. Zasloff, M. Antimicrobial peptides of multicellular organisms. Nature 2002, 415, 389-395.

201. Zhao, X.; Pan, F.; Xu, H.; Yaseen, M.; Shan, H.; Hauser, C. A. E.; Zhang, S.; Lu, J. R. Molecular self-assembly and applications of designer peptide amphiphiles. Chem. Soc. Rev. 2010, 39, 3480-3498.

202. Chen, C.; Pan, F.; Zhang, S.; Hu, J.; Cao, M.; Wang, J.; Xu, H.; Zhao, X.; Lu, J. R. Antibacterial activities of short designer peptides: a link between propensity for nanostructuring and capacity for membrane destabilization. Biomacromolecules 2010, 11, 402-411.

203. Scott, R. W.; DeGrado, W. F.; Tew, G. N. De novo designed synthetic mimics of antimicrobial peptides. Curr. Opin. Biotechnol. 2008, 19, 620-627.

204. Roy, S.; Das, P. K. Antibacterial hydrogels of amino acid-based cationic amphiphiles. Biotechnol. Bioeng. 2008, 100, 756-764.

205. Makovitzki, A.; Baram, J.; Shai, Y. Antimicrobial lipopolypeptides composed of palmitoyl di- and tricationic peptides: In vitro and in vivo activities, self-assembly to nanostructures, and a plausible mode of action. Biochemistry 2008, 47, 10630-10636.

206. Salick, D. A.; Pochan, D. J.; Schneider, J. P. Design of an injectable beta-hairpin peptide hydrogel that kills methicillin-resistant staphylococcus aureus. Adv Mater 2009, 21, 4120-4123.

207. Kanlayavattanakul, M.; Lourith, N. Lipopeptides in cosmetics. Inter. J. Cosm. Sci. 2010, 32, 1-8.

208. Robinson, L. R.; Fitzgerald, N. C.; Doughty, D. G.; Dawes, N. C.; Berge, C. A.; Bissett, D. L. Topical palmitoyl pentapeptide provides improvement in photoaged human facial skin. Inter. J. Cosm. Sci. 2005, 27, 155-160.

209. Dickerson, M. B.; Sandhage, K. H.; Naik, R. R. Protein- and peptide-directed syntheses of inorganic materials. Chem. Rev. 2008, 108, 4935-4978.

210. Hsu, L.; Cvetanovich, G. L.; Stupp, S. I. Peptide amphiphile nanofibers with conjugated polydiacetylene backbones in their core. J. Am. Chem. Soc. 2008, 130, 3892-3899.

211. Sone, E.; Stupp, S. Semiconductor-encapsulated peptide-amphiphile nanofibers. J. Am. Chem. Soc. 2004, 126, 12756-12757.

212. Sargeant, T. D.; Guler, M. O.; Oppenheimer, S. M.; Mata, A.; Satcher, R. L.; Dunand, D. C.; Stupp, S. I. Hybrid bone implants: Self-assembly of peptide amphiphile nanofibers within porous titanium. Biomaterials 2008, 29, 161-171.

213. Luo, Z.; Wang, S.; Zhang, S. Fabrication of self-assembling D-form peptide nanofiber scaffold d-EAK16 for rapid hemostasis. Biomaterials 2011, 32, 2013-2020.

214. Shen, X.; Mo, X.; Moore, R.; Frazier, S.; Iwamoto, T.; Tomich, J.; Sun, X. Adhesion and structure properties of protein nanomaterials containing hydrophobic and charged amino acids. J. Nanosci. Nanotech. 2006, 6, 837-844.

215. Prive, G. G. Lipopeptide detergents for membrane protein studies. Curr. Opin. Struct. Biol. 2009, 19, 379-385.

Chapter 3 - Rational Design of Responsive Self-Assembling Peptides from Native Protein Sequences[1]

3.1 Abstract

This study used β-spiral motif from spider flagelliform silk protein and the Ca^{2+} binding domain of lipase Lip A from Serratia marcescens. After carefully comparing the primary structures of both sequences, we rationally designed a newly sequenced eD_2 by "hiding" the ion binding sequence in the silk structure sequence. This helped avoid redundancy, and the new sequence had properties of both model sequences. In water, eD_2 formed uniform spherical agglomerates with a β-spiral structure. Triggered by Ca^{2+}, eD_2 formed nanofibers with higher compliance and thermal stability. We demonstrated the specialties of this novel peptide design by changing the pH, using other metal ions, and mutating the model sequence.

3.2 Introduction

Peptides have become attractive molecules for fabricating biomaterials by using a "bottom-up" approach.[1] Studies of peptide structure, assembly properties, and dynamic behavior in response to external parameters have led to rational novel design of peptide biomaterials.[2-6] For example, hydrogel formation was achieved by designing model peptides with alternating charged and noncharged amino acids or blocks of hydrophobic and hydrophilic copolymers.[7-11] On the other hand, identified functional domains of native proteins were also potential models for peptide design.[12-14] Rational design of peptides involving functional domain sequences of native proteins is a promising approach for development of functional biomaterials. Herein, we report a responsive self-assembling peptide designed by rationally combining two native functional sequences from spider flagelliform silk protein and lipase Lip A from Serratia marcescens. After carefully comparing the primary structures of both sequences, we produced a newly designed sequence eD_2 by "hiding" the Ca^{2+} binding domain of lipase Lip A in the β-

[1] Results have been published. Huang, H,; Sun, X. S. Rational design of responsive self-assembling peptides from native protein sequences. Biomacromolecules. 2010, 11, 3390-3394. (Reuse by permission of American Chemical Socity)

spiral motif from spider flagelliform silk protein; this procedure avoided redundancy. We expected the newly designed peptide to contain functions of both native sequences.

One model sequence selected was a β-spiral motif of spider flagelliform silk protein,[15, 16] $[GPGGX]_n$ (X = any amino acid). $[GPGGX]_n$ provided the elasticity in the extremely high tensile strength of spider silk, which indicated this motif has high potential for use as a biomaterial in tissue engineering for human tissue repair like bone, blood vessel or organs that requires tensile property. Modifying the X residue changed the quantity of secondary structure and stability of this spider silk motif.[17, 18]. Glycine (G) provided flexible properties,[19, 20] and proline (P) influenced the secondary structure and mechanical properties of spider silk motifs by affecting the crystal cross-link density and hydrogen bonding network.[21, 22]

Another model sequence was GXGXDXUX (U = hydrophobic residue), a Ca^{2+} binding domain of lipase Lip A from *Serratia marcescens*,[23, 24] in which aspartate (D) residue was required for ion binding.[25] The primary structure of this sequence was similar to that of $[GPGGX]_n$ (Figure 3.1). The objective of this study was to rationally combine these two motifs by replacing the X residues of $[GPGGX]_n$ with D and defined the newly designed peptide as GPGGDGPGGD (eD_2). The Ca^{2+} binding sequence was hidden in the first eight residues of eD_2. We hypothesized that the eD_2 peptides assembled into nanofibers triggered by Ca^{2+} ions.

3.3 Experimental Section

3.3.1 Peptide Synthesis

Peptides were synthesized on a CEM Liberty microwave peptide synthesizer (CEM Corporation, Matthews, NC) according to the automated base-labile 9-fluorenylmethoxycarbonyl (Fmoc) strategy with Fmoc-protected amino acids (EMD Biosciences, San Diego, CA). Peptides were cleaved using 95% trifluoroacetic acid (Sigma-Aldrich, Milwaukee, WI), 2.5% triisopropylsilane (Sigma), and 2.5% deionized water. After synthesis, peptides were washed three times with anhydrous ether (Fisher Biotech, Fair Lawn, NJ) anddissolved in distilled water. The peptide solution was frozen at -80 ˚C in a freezer overnight and then was freeze-dried for 48 hours using a Labconco freeze dry system (Labconco, Kansas City, MO). The pH value of the peptide in water solution was 3.6. Molecular weight of the synthesized peptide was confirmed by matrix-assisted laser desorption/ionization time-of-flight mass spectroscopy on an Ultraflex II instrument (Bruker Daltronics, Billerica, MA). The peptide purity wa confirmed by a Beckman

System Gold high performance liquid chromatography (HPLC, Beckman Coulter, Inc., Fullerton, CA) on a phenomenex synergi 4μ Hydro-RP column (Phenomenex, Inc., Torance, CA) with the following gradient: 10-90% B in 20 min (A: 99.9% H_2O, 0.1% TFA; B: 90% acetonitrile, 9.9% H_2O, 0.1% TFA). 1 wt % peptide solution was prepared with DI water. The Ca^{2+}, Na^{+}, Mg^{2+} and Zn^{2+} concentrations were 100 mM unless spefified otherwise.

3.3.2 Transmission Electron Microscopy (TEM)

Peptide solutions were obsorbed onto Formvar/carbon-coated 200-mesh copper grids (Electron Microscopy Sciences, Fort Washington, PA) and stained with 2% (w/v) uranyl acetate (Ladd Research Industries, Inc., Burlington, VT) for 60 s at ambient conditions before being imaged. The samples were imaged with a CM100 TEM (FEI Company, Hillsboro, OR) at 100 kv. The digital camera system is a Hamamatsu digital camera model C8484-05G. The particle size was measured by using Image J software (rsbweb. nih. gov) with more than 10 measurements.

3.3.3 Particle Size Distribution Analysis

A ZetaPALS (Brookhaven Instruments Corporation, Holtsville, NY) was used to measure the particle size distribution of eD2 in water; 1% (w/v) eD2 was diluted in HPLC-grade water. The samples were measured at 25 ℃ and 658 nm wavelength.

3.3.4 Scanning Electron Microscopy (SEM)

Morphology of freeze-dried peptides with and without Ca^{2+} was observed by SEM. Samples were sputter coated with 60% Au/40% Pd using a DESK II sputter/etch unit (Denton Vacuum, LLC., Moorestown, NJ). Images were taken on a Hitachi S-3500N SEM (Hitachi Science Systems, Ltd., Hitachinaka, Japan) at an accelerating voltage of 20 keV with a Robinson backscatter detector. The SEM morphology of peptides with and without Ca^{2+} after thermogravimetric analysis (TGA) test was also obtained as a comparison. The pore size of TGA cinder was measured by using Image J software (rsbweb. nih. gov) with more than 10 measurements.

3.3.5 Circular Dichroism (CD) Spectroscopy

The CD spectra of h9e basic solution, acidic hydrogel, and Ca^{2+} hydrogel were recorded at ambient conditions on a Jasco J-815 spectrometer (Jasco Corporation, Tokyo, Japan). The concentration of samples was 0.5 mM. Spectra were recorded from 190 to 260 nm with a 1 nm bandwidth and 50 nm min^{-1} scanning speed and averaged over five accumulations. The pass length of the cuvette was 1 mm. Baselines of the blank solution without peptide were subtracted from the sample data.

3.3.6 Creep Recovery Compliance Analysis

Peptides in water and Ca^{2+} solution were freeze-dried. The creep and recovery compliance was determined with a rheometer system C-VOR 150 (Malvern instruments, Malvern, Worcestershire WR141XZ, United Kingdom) under the oscillation mode of measuring system PP8. The gap size was 0.5 mm, stress was 5000 Pa, and creep and recovery time were both 50 s.

3.3.7 Thermogravimetric Analysis (TGA)

Thermal stability of the peptide solutions was characterized with the Pyris 1 TGA (PerkinElmer Pyris1 TGA, Norwalk, CT) with a temperature scan ranging from 30 to 500 ℃ at 5 ℃ min^{-1}.

3.3.8 Differential Scanning Calorimetry (DSC) Analysis

A 20% (w/v) peptide solution was sealed in the high-volume pan and characterized with a DSC Q200 (TA instrument, New Castle, DE). The temperature was equilibrated at 0 ℃ and isothermal for 1 min and then ramped to 250 ℃ at 10.0 ℃/min.

3.4 Results and Discussion

In water, most eD_2 molecules formed uniform spherical agglomerates with a diameter of 10 to 20 nm (Figure 3.2a), but some larger agglomerates with a diameter of 70 to 150 nm were also observed. The ZetaPALS data support this mid-range polydispersity with a dispersed value of 0.347. Peptide molecules aggregated due to the molecular hydrophobic effect and formed a spherical morphology (Figure 3.2a). The CD spectra revealed the secondary structure of eD_2 in an aqueous environment (Figure 3.2b). The inflection around 220 nm and the negative band

close to 200 nm indicate a β-spiral structure, which suggests that our newly designed peptide conserved the emblematical secondary structure of the model sequence $[GPGGX]_n$ [15,16, 26-30] even though eD_2 has only two repeat GPGGX fragments.

When Ca^{2+} solution (20 mM) was added to the peptide solution (volume ratio: 50/50), the pH of the peptide solution changed from 3.6 to 4.3, which was slightly higher than its isoelectric pH of 3.9. We observed that peptide molecules self-assembled as nanofibers (Figure 3.2d). Interestingly, the CD spectra did not show the significant structural transformation of eD_2 after Ca^{2+} solution was added (Figure 3.2b). However, the spectral intensity of eD_2 with Ca^{2+} slightly increased around 200 and 220 nm, indicating that Ca^{2+} ions may further stabilize the β-spiral structure. A possible strategy for this peptide nanofibre formation is that two eD_2 molecules each bound to one Ca^{2+} ion at the 5th and 10th Asp residues, respectively, and stacked in a perpendicular direction as a peptide filament, which didn't change the secondary structure of eD_2 molecules but further stabilized it by binding with Ca^{2+} ions. The Proline ring was arranged on the surface of peptide filaments, which combined in a parallel arrangement to form thicker nanofibres due to the hydrophobic effect (Figure 3.2d). The observed width of a single filament (about 3 nm, data not showed) matches the length of a peptide from N-terminal to C-terminal, which supports this peptide assembly strategy. Binding with Ca^{2+} ions, the newly designed eD_2 performed similarly to the model sequence GXGXDXUX and adopted an orderly assembly as nanofibres. When the concentration of Ca^{2+} solution was increased to 200 mM, the eD_2 nanofibres compacted into high-density rod shapes a few hundred nanometers in width and several micrometers in length (Figure 3.2e). The CD spectra suggest that the intensity at 200 and 220 nm increased as the concentration of Ca^{2+} solution increased (inserted spectra of Figure 3.2b), indicating that packing of peptide molecules could be tightened by increasing the link between peptides and ions.[18]

Differences were also present in the SEM images of freeze-dried eD_2 with and without Ca^{2+}. The sputter coating method may cause artifact on sample surface,[31] but the fiber and porous morphological structure of samples could be observed under SEM. The original peptide without Ca^{2+} formed a network with thin fibers (arrows in Figure 3.2c) and discontinuous film morphology (Figure 3.2c). With the addition of Ca^{2+}, the peptides formed a tunable and interconnected porous morphology with a smooth texture (Figure 3.2f). The creep and recovery compliance of eD_2 in these two conditions showed that eD_2 with Ca^{2+} had much higher

compliance (Figure 3.2g). The instantaneous compliance of the original eD_2 was $1.8252*10^{-7}$ Pa^{-1}. This value increased to $5.7068*10^{-5}$ Pa^{-1} when the tunable morphology formed with Ca^{2+}. Under the stress of 5000 Pa for 50 s, eD_2 with Ca^{2+} reached the linear Newtonian compliance region. Its structure was broken as a result of ruptured bonds flowing past one another. After the stress force was removed, the horizontal linear line was found in eD_2 with Ca^{2+}, suggesting the peptide structure was completed destroyed during the creep time. However, the original eD2 showed an obvious recovery after the stress force was removed (Figure 3.2g). Because one of our model sequences was from the elastic functional region of spider silk, eD_2 was expected have high tension. When eD_2 bound with Ca^{2+}, tunable structure was formed, contributing the higher creep compliance. But once the combination was broken, tunable structure was not recoverable.

As mentioned previously, the intensity of CD spectra increased after Ca^{2+} solution was added. To further study the Ca^{2+} binding stability of eD_2, we used TGA to analyze 20% (w/v) eD_2 solution with and without Ca^{2+}. Plots of the weight-change derivative (Figure 3.3a) showed that in addition to the water peak, there were two major peaks at 240 and 340 ℃ for the original eD_2 solution. When Ca^{2+} was added, these two major peaks shifted to 320 and 380 ℃, respectively (inserted plot of Figure 3.3a), indicating that Ca^{2+} binding induced higher thermal stability. The fluctuation at 170 ℃ of eD_2 in Ca^{2+} solution could be caused by Cl_2 because we added $CaCl_2$ as the source of Ca^{2+}. Upon observing the cinders after TGA, we were surprised to find the expansion of eD_2 with Ca^{2+}; its hight was about 10 mm which is close to five times as what we added in the pan (2 mm hight) (Figure 3.3b). This phenomenon was not observed in samples without Ca^{2+}. The cinder of peptides with Ca^{2+} formed a thick, sponge-like conformation, whereas cinder without Ca^{2+} formed a thin sheet. Small pores were observed on the surface of both cinders, but the pore sizes were distinct: 0.5 to 3 μm for eD_2 with Ca^{2+} and 10 to 100 μm for eD2 without Ca^{2+} (inserted figure of Figure 3.3c, d). In the inner conformation of cinders, pore sizes of both peptides were larger than surface pore sizes: 10 to 80 μm for eD_2 with Ca^2 and 50 to 200 μm for eD_2 without Ca^{2+} (Figure 3.3c, d). We used DSC to test both peptide solutions, but no phase transition was found when the temperature ramped from 0 to 250 ℃. When temperature was increased, eD_2 molecules aggregated as a fibre network with Ca^{2+} ions, forming a kind of sealed structure that would expand when water or other gas, such as HCl or Cl_2, tried to escape during heating (scheme in Figure 3.3e).

As a peptide-ion binding reaction, the coincidence of space conformation between eD_2 and Ca^{2+} ions could be an important factor in addition to electrostatic force reactions and is why the two model sequences, $[GPGGX]_n$ and GXGXDXUX, led to nanofibre formation with Ca^{2+}. To further characterize the newly designed peptide, we adjusted the pH of solution to change the electrical environment and used other metal ions to observe the aggregation of eD_2 molecules. As pH was adjusted to neutral or higher by 1M NaOH solution, many big spherical agglomerates were observed (Figure 3.4a). These agglomerates bound together and formed the amorphic aggregation. Obviously, this aggregation was different from the linear arrangement of eD_2 molecules with Ca^{2+}. Again, the CD spectra showed no structural transformation (Figure 3.4b), but the intensity decreased after the pH adjustment, indicating that the deprotoned Asp residues disturb the β-spiral structure. We used Na^{+}, Mg^{2+}, and Zn^{2+} to replace Ca^{2+} as the trigger that induces nanofibre formation. The TEM images show that none of these three metal ions induced peptides to assemble as nanofibres (Figure 3.4c, d, e), which indicates that eD_2 peptides have special ion-selective properties. There was no significant difference in the CD spectra of these three ions and those of Ca^{2+} (data not shown).

To further demonstrate the approach of mapping the ion binding functional domain onto the structural domain, we designed two additional peptides. GFGGDGFGGD (eFD_2), which replaces the proline (P) of eD_2 with phenylalanine (F), mutated the $[GPGGX]_n$ structural domain but retained the ion binding domain. Accordingly, GPGGVGPGGV (eV_2) mutated the ion binding domain by replacing D residue with valine (V) and retained the structural domain. The CD spectra showed that only eD_2 and eV_2 adopted the β-spiral structure, whereas eFD_2, which replaced proline with phenylalanine lost the emblematical secondary structure exhibited in the model sequence $[GPGGX]_n$ (Figure 3.2b). Adding Ca^{2+} did not induce the structural transformation in either of the mutant peptides. As seen in the TEM images, eV_2 formed spherical agglomerates similar to those of eD_2 in both water and Ca^{2+} solution (data not shown), but eFD_2 had amorphous morphology in water and aggregated as spherical agglomerates with Ca^{2+} (Figure 3.5a, b). The differences in morphology and secondary structure between eD_2 and the two mutated sequences suggest that eD_2 is uniquely able to map the ion binding functional domain onto the structural domain.

3.5 Conclusions

We rationally used two native functional sequences from spider silk and calcium-binding motifs to design and synthesize a novel peptide, termed eD_2. The eD_2 inherited properties of both model sequences, adopted a β-spiral structure, and formed nanofibers triggered by Ca^{2+}. Compliance and thermal stability of eD_2 were increased by forming a tunable structure with Ca^{2+}. We demonstrated the specialties of this peptide by changing the pH, using other metal ions, and mutating the model sequence. The properties of eD_2 indicated that this newly designed peptide has high potential for use as nanowire or a biosensor or could be combined with other sequences to induce fiber structure controlled with Ca^{2+}.

3.6 Acknowledgments

We thank Dr. Dan Boyle (Department of Biology, Kansas State University) for performing TEM analysis, Mr. Kent Hampton (Department of Entomology, Kansas State University) for performing SEM analysis, Dr. John Tomich (Department of Biochemistry, Kansas State University) for use of the CD spectroscope, and the University of Kansas Mass Spectrometry Lab for HPLC and mass spectrometric analysis. Funding for this work was provided by the Targeted Excellence Program and Center for Biobased Polymers by Design at Kansas State University. Contribution no. 10-127-J from the Kansas Agricultural Experiment Station.

3.7 References

1. Cavalli, S.; Albericio, F.; Kros, A. Amphiphilic peptides and their cross-disciplinary role as building blocks for nanoscience. Chem. Soc. Rev. 2010, 39, 241-263.

2. Langer, R.; Tirrell, D. A. Designing materials for biology and medicine. Nature 2004, 428, 487-492.

3. Lee, K. Y.; Mooney, D. J. Hydrogels for tissue engineering. Chem Rev. 2001, 101, 1869-1879.

4. Petka, W. A.; Harden, J. L.; McGrath, K. P.; Wirtz, D.; Tirrell, D. A. Reversible hydrogels from self-assembling artificial proteins. Science 1998, 281, 389-392.

5. Aggeli, A.; Bell, M.; Boden, N.; Keen, J. N.; Knowles, P. F.; Mcleish, T. C. B.; Pitkeathly, M.; Radford, S. E. Responsive gels formed by the spontaneous self-assembly of peptides into polymeric beta-sheet tapes. Nature 1997, 386, 259-262.

6. Hartgerink, J. D.; Beniash, E.; Stupp, S. I. Self-assembly and mineralization of peptide-amphiphile nanofibers. Science 2001, 294, 1684-1687.

7. Zhang, S. Fabrication of novel biomaterials through molecular self-assembly. Nat. Biotechnol. 2003, 21, 1171-1178.

8. Schneider, J. P.; Pochan, D. J.; Ozbas, B.; Rajagopal, K.; Pakstis, L.; Kretsinger, J. Responsive hydrogels from the intramolecular folding and self-assembly of a designed peptide. J. Am. Chem. Soc. 2002, 124, 15030-15037.

9. Caplan, M. R.; Moore, P. N.; Zhang, S.; Kamm, R. D.; Lauffenburger, D. A. Self-assembly of a beta-sheet protein governed by relief of electrostatic repulsion relative to van der waals attraction. Biomacromolecules 2000, 1, 627-631.

10. Rapaport, H.; Grisaru, H.; Silberstein, T. Hydrogel scaffolds of amphiphilic and acidic beta-sheet peptides. Adv. Funct. Mater. 2008, 18, 2889-2896.

11. Nowak, A. P.; Breedveld, V.; Pakstis, L.; Ozbas, B.; Pine, D. J.; Pochan, D.; Deming, T. J. Rapidly recovering hydrogel scaffolds from self-assembling diblock copolypeptide amphiphiles. Nature 2002, 417, 424-428.

12. Hardy, J. G.; Römer, L. M.; Scheibel, T. R. Polymeric materials based on silk proteins. Polymer 2008, 49, 4309-4327.

13. Yang, M.; Yamauchi, K.; Kurokawa, M.; Asakura, T. Design of silk-like biomaterials inspired by mussel-adhesive protein. Tissue Eng. 2007, 13, 2941-2947.

14. Scotter, A. J.; Guo, M.; Tomczak, M. M.; Daley, M. E.; Campbell, R. L.; Oko, R. L.; Bateman, D. A.; Chakrabartty, A.; Sykes, B. D.; Davies, P. L. Metal ion-dependent, reversible, protein filament formation by designed beta-roll polypeptides. BMC Struct. Biol. 2007, 7, 63.

15. Lewis, R. V. Spider silk: Ancient ideas for new biomaterials. Chem. Rev. 2006, 9, 3762-3774.

16. Hayashi, C. Y.; Lewis, R. V. Spider flagelliform silk: Lessons in protein design, gene structure, and molecular evolution. BioEssays 2001, 8, 750-756.

17. Teulé, F.; Furin, W. A.; Cooper, A. R.; Duncan, J. R.; Lewis, R. V. Modifications of spider silk sequences in an attempt to control the mechanical properties of the synthetic fibers. J. Mater. Sci. 2007, 21, 8974-8985.

18. Hayashi, C. Y.; Lewis, R. V. Evidence from flagelliform silk cDNA for the structural basis of elasticity and modular nature of spider silks. J. Mol. Biol. 1998, 5, 773-784.

19. Hall, J. C. Glycine. J. Parenter. Enter. Nutr. 1998, 6, 393-398.

20. Serrano L.; Neira, J. L.; Sancho, J.; Fersht, A. R. Effect of alanine versus glycine in alpha-helices on protein stability. Nature 1992, 6368, 453-455.

21. Savage, K. N.; Gosline, J. M. The effect of proline on the network structure of major ampullate silks as inferred from their mechanical and optical properties. J. Exp. Biol 2008, 12, 1937-1947.

22. Rauscher, S.; Baud, S.; Miao, M. Keeley, F. W.; Pomès, R. Proline and glycine control protein self-organization into elastomeric or amyloid fibrils. Structure 2006, 11, 1667-1676.

23. Foo, C.; Wong P.; Bini, E.; Huang, L. J.; Lee, S. Y.; Kaplan, D. L. Solution behavior of synthetic silk peptides and modified recombinant silk proteins. Applied Physics. A, Materials Science Processing 2006, 2, 193-203.

24. Lewis, R. V. Spider silk: Ancient ideas for new biomaterials. Chem. Rev. 2006, 9, 3762-3774.

25. Angkawidjaja, C.; Paul, A.; Paul, Y.; Koga, Y.; Takano, K.; Kanaya, S. Importance of a repetitive nine-residue sequence motif for intracellular stability and functional structure of a family I.3 lipase. FEBS Lett. 2005, 21, 4707-4712.

26. Zhou, Y.; Wu, S.; Conticello, V. P. Genetically directed synthesis and spectroscopic analysis of a protein polymer derived from a flagelliform silk sequence. Biomacromolecules 2001, 1, 111-125.

27. Renugopalakrishnan, V. A 27-mer tandem repeat polypeptide in bovine amelogenin: Synthesis and CD spectra. J. Pept. Sci. 2002, 4, 139-143.

28. Hayashi, C. Y.; Shipley, N. H.; Lewis, R. V. Hypotheses that correlate the sequence, structure, and mechanical properties of spider silk proteins. Int. J. Biol. Macromol. 1999, 2-3, 271-275.

29. Halford, N. G.; Tatham, A. S.; Sui, E.; Daroda, L.; Dreyer, T.; Shewry, P. R. Identification of a novel beta-turn-rich repeat motif in the D-hordein of barley. Biochim. Biophys. Acta. 1992, 2, 118-122.

30. Ohgo, K.; Kawase, T.; Ashida, J.; Asakura, T. Solid-state NMR analysis of a peptide (gly-pro-gly-gly-ala)(6)-gly derived from a flagelliform silk sequence of nephila clavipes. Biomacromolecules 2006, 4, 1210-1214.

31. Stephens, T. C. A comparison of the appearance of various high resolution sputter coatings. Microsc. Microanal. 2005, 11, 770-771.

Figure 3.1 Diagram showing how the elastic calcium-binding peptide (GPGGDGPGGD) (eD_2) was derived from the calcium-binding domain and elastic region of spider silk.

G = glycine, P = proline, X = any amino acid, D = aspartate, and U = large hydrophobic residue.

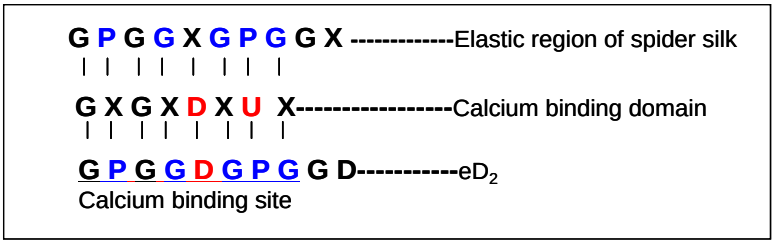

Figure 3.2 Properties of eD2 in water and Ca^{2+} solution.

a. TEM image of eD_2 in water **b.** CD spectra of eD_2, eFD2, eV_2 (without Ca^{2+}: fill, with Ca^{2+}: open, eD_2: black, eFD_2: red, eV_2: blue, inserted spectra: eD_2 with different Ca^{2+} concentration (500 μM: orange, 5 mM: black, 50 mM: purple) **c.** SEM image of original eD_2 (arrow: thin firber) **d.** TEM image of eD_2 in 10 mM Ca^{2+} solution and the assembly of eD_2 in water and Ca^{2+} solution **e.** TEM image of eD_2 in 100 mM Ca^{2+} solution **f.** SEM image of eD_2 with Ca^{2+} **g.** creep and recovery compliance of eD_2 with (open) and without Ca^{2+} (solid).

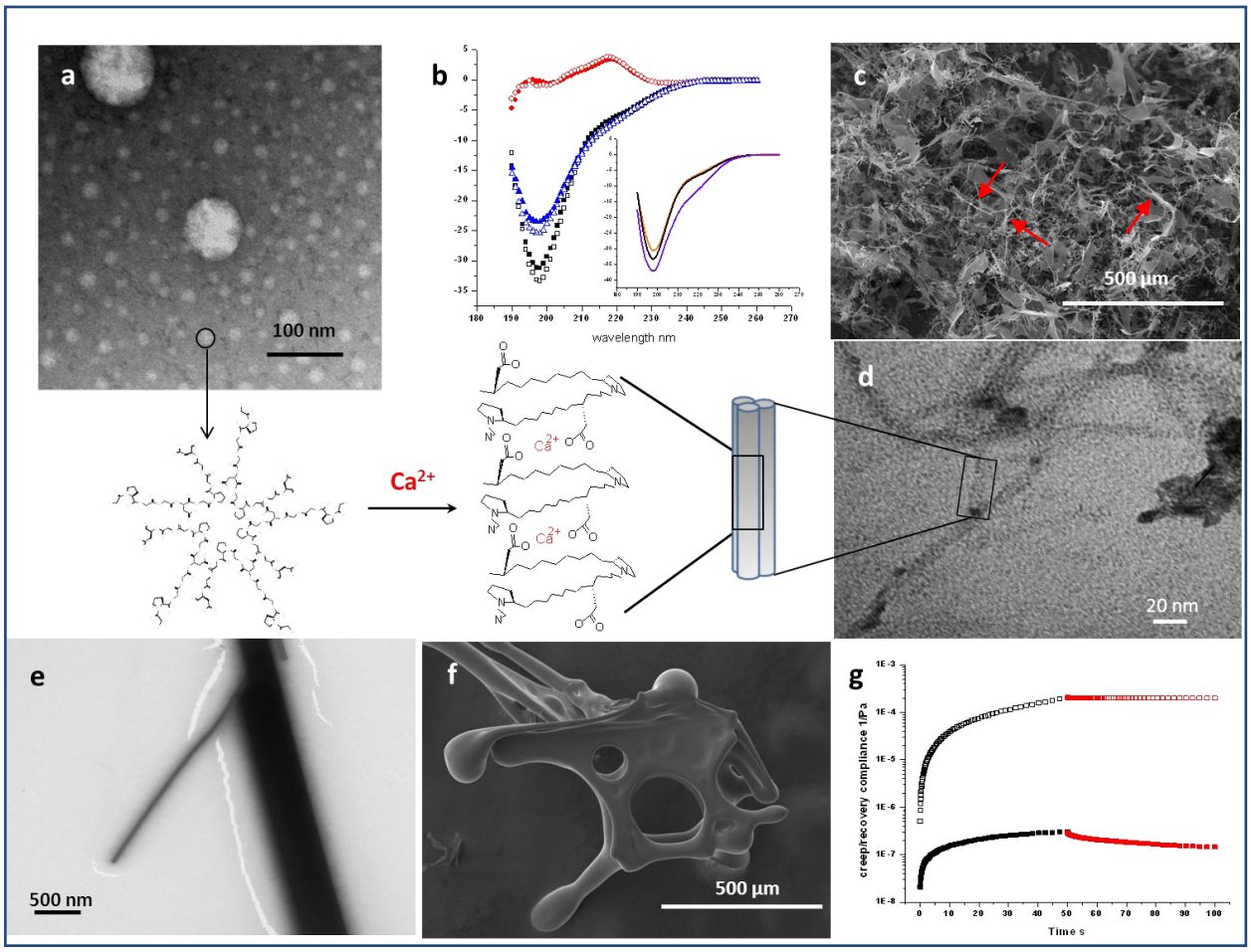

Figure 3.3 TGA test for eD2 in water and Ca2+ solution

a. weight-change derivative of eD2 in water and Ca2+ solution (inserted plot: enlarged curve from 200 to 600 ℃. **b.** cinder of eD2 in Ca2+ solution. **c, d.** SEM image of cinders of eD2 in water and Ca2+ solution respectively (inserted figures: the surface images of the cinders) **e.** the expansion of eD2 network structure in Ca2+ solution

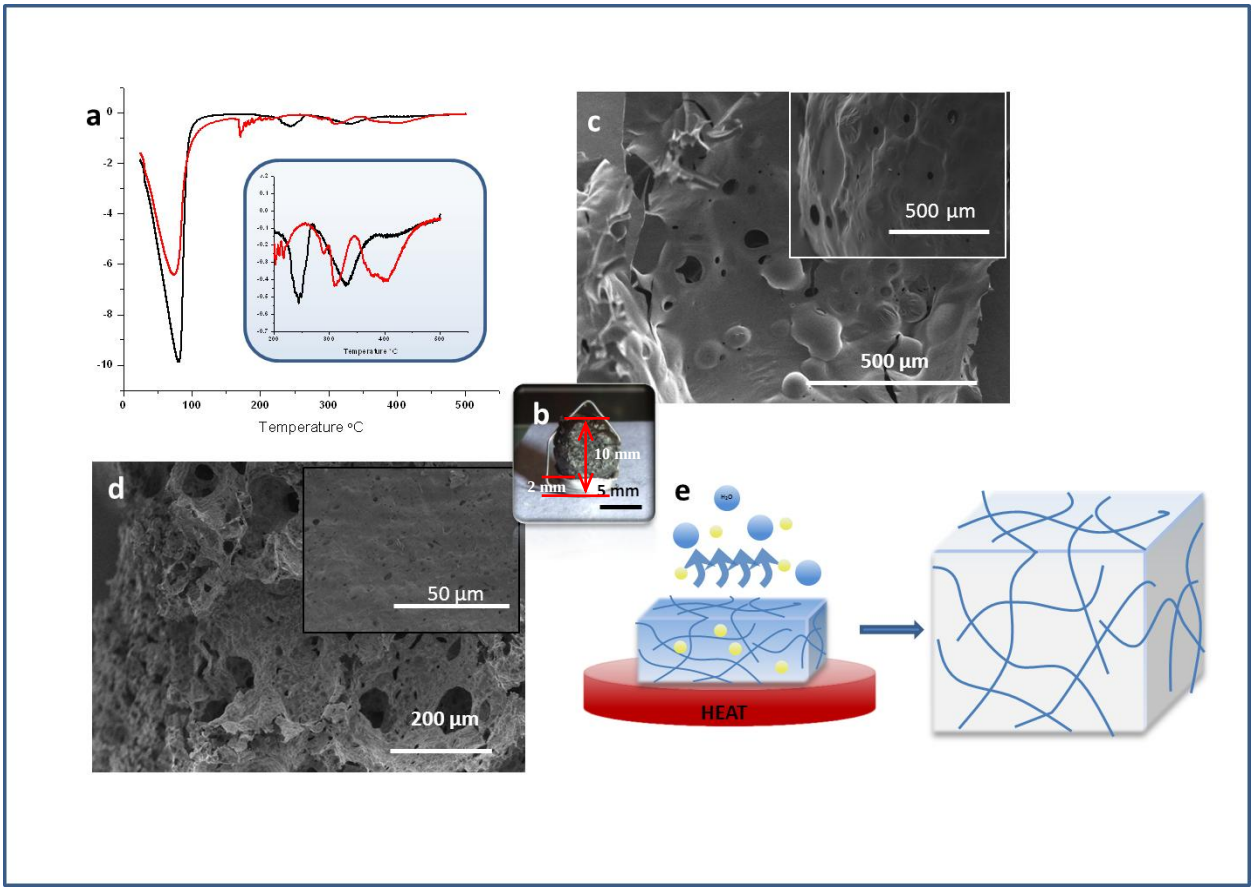

Figure 3.4 eD_2 in different electrical environments.

a. TEM of eD_2 in neutral pH **b.** CD spectra of eD_2 in water (black: without pH adjustment, red: pH adjusted to neutral) **c.** TEM of eD_2 in Na^+ solution **d.** TEM of eD_2 in Mg^{2+} solution **e.** TEM of eD_2 in Zn^{2+} solution

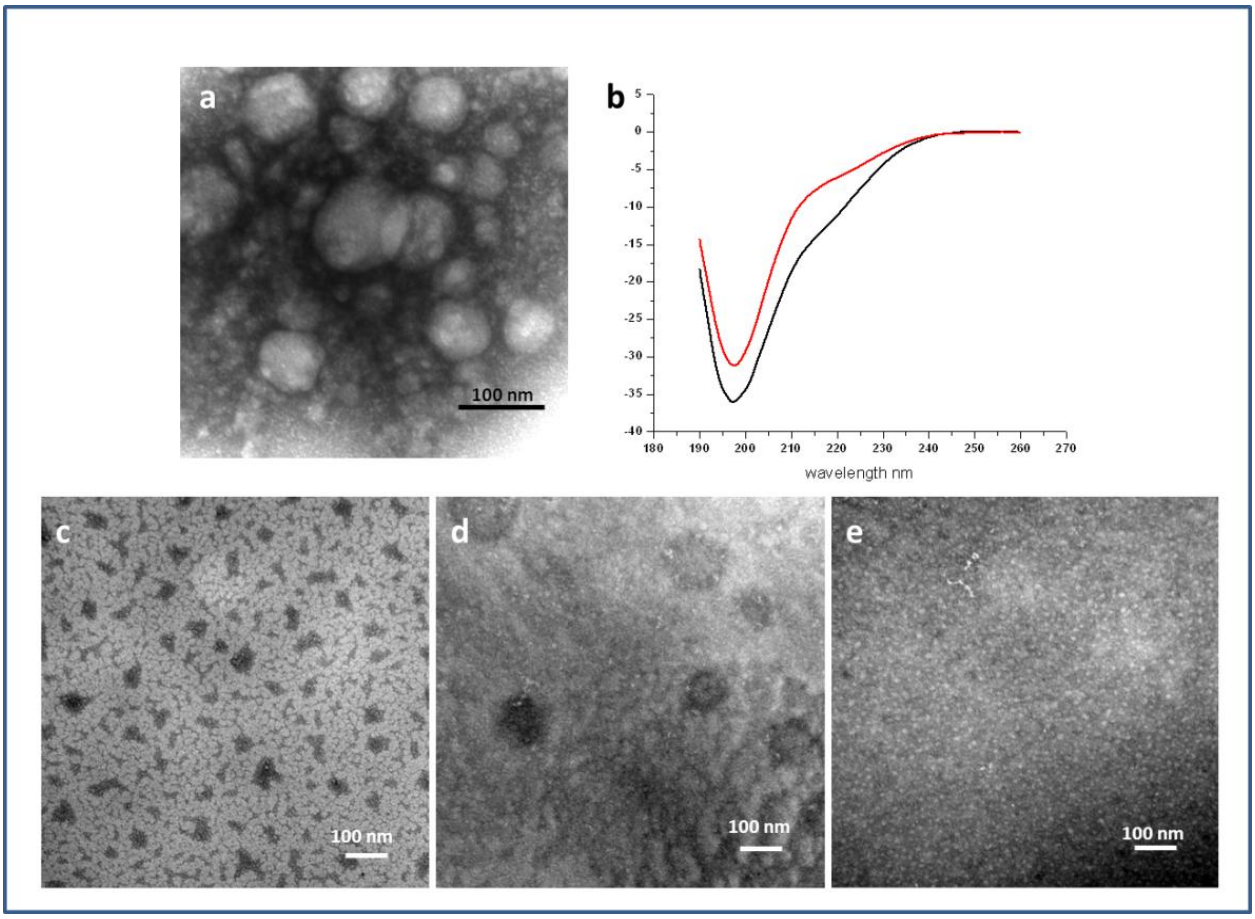

Figure 3.5 TEM of eFD2 a. eFD2 in water b. eFD2 in Ca2+ solution

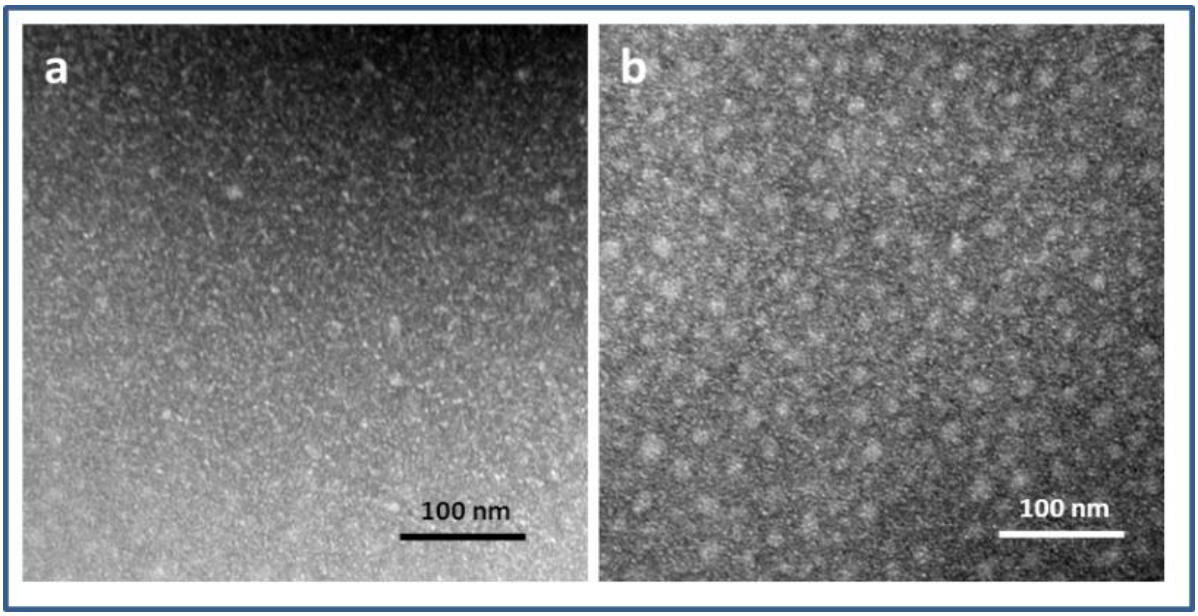

Chapter 4 - Design of a Shear-Thinning Recoverable Peptide Hydrogel from Native Sequences[2]

4.1 Abstract

Injectable peptide hydrogels have great potential for drug delivery and tissue engineering applications. Most published hydrogel-forming sequences contain either alternating-charged and non-charged residues or amphiphilic blocks. Here, we report a self-assembling peptide, h9e (FLIVIGSIIGPGGDGPGGD), designed by combining two native sequences from an elastic segment of spider silk and a trans-membrane segment of human muscle L-type calcium channel. The turning segment GSII of h9e promoted hydrogel formation in both Ca^{2+} solution and acidic pH conditions at water content greater than 99.5%. Although h9e Ca^{2+} hydrogel and h9e acidic hydrogel have the same sequence, they have distinct physical properties. The h9e Ca^{2+} hydrogel perform a specific shear-thinning and rapid-strength-recovering mechanical property which has potential for wide biomedical applications.

4.2 Introduction

Using peptide hydrogels as injectable materials for drug delivery systems and tissue engineering applications has been an important discovery made over the past few decades.[1-6] Because of its high water content and polymer network, most proteins could maintain their biological activities in peptide hydrogel.[7] A sol-gel transition occurs when peptide molecules self-assemble into a well-defined nanofibre network that traps water molecules. Because this transition occurs at specific temperature and pH, peptide hydrogel precursors may be injected into the body in the liquid phase and converted into hydrogel when physiological condition such as pH or temperature changed,[8-11] which is important for injectable applications. A special type of injectable hydrogel has shear thinning and rapid recovery characteristics.[12-14] The storage modulus of this kind of hydrogel decreases sharply under the shearing force but recovers after

[2] Results have been published. Huang, H.; Shi, J.; Laskin, J.; Liu, Z.; McVey, D. S.; Sun, X. S. Design of a shear-thinning recoverable peptide hydrogel from native sequences and application for influenza H1N1 vaccine adjuvant. Soft Matter. 2011, 7, 8905-8912. (Reused by permission of The Royal Society of Chemistry)

the force is removed. Although the mechanism of this shear thinning and recovery phenomena is still under debate, this hydrogel-forming peptides have high potential for use as injectable materials for medical applications.[15]

Within the last decade, many novel designed hydrogels have been achieved by amphiphilic peptides.[16-20] With a propensity of fiber structure, peptide monomers fabricate the nanofibre structure under the hydrophobic aggregation and the further crossing as a nanofibre network for hydrogel formation. On the other hand, the identified functional domains of native proteins were also selected and modified as potential models for peptide design in recent years.[21-23] Since these sequences exist in the biological system and were identified because of their potential for certain functions, we hypothesized that rational design of peptides involving native functional domain sequences is a promising approach for development of functional biomaterials.

Instead of choosing artificial designed model peptide monomer, the objective of this study is to make a Ca^{2+} induced shear-thinning and rapid recoverable hydrogel forming peptide FLIVIGSIIGPGGDGPGGD (h9e) from rational combining two native sequences. The hydrophilic segment GPGGDGPGGD (eD_2), designed from a β-spiral motif of spider flagelliform silk protein, has the potential to drive peptide monomer aggregation to nanofibre structure triggered by Ca^{2+}.[24] The hydrophobic motif, FLIVIGSII (h9), was derived from the third trans-membrane segment of subunit IV in the dihydropyridine sensitive human muscle L-type calcium channel.[25] According to our previous study, solutions of peptides Kh5K (KKK-FLIVI-KKK) and Kh9K (KKK-FLIVIGSII-KKK) which have core FLIVI (h5) and FLIVIGSII (h9) flanked by tri-lysine segments are characterized by high adhesion shear strength and unusual biophysical properties.[26] The initial design of peptides examined in this study was performed by combining both h5 and h9 segments with eD_2 as two amphiphilic peptides FLIVIGPGGDGPGGD (h5e) and h9e. We hypothesized that the hydrophobic cores h5 and h9 will accelerate the strength of nanofiber backbone and both amphiphilic peptides will form hydrogel upon addition of Ca^{2+}. However, with Ca^{2+} ions, the hydrogel was only observed in h9e peptide. To further understand the contribution of each native region of h9e for hydrogel formation, a serial of peptides were synthesized by modifying the primary structure of h9e. The characters of h9e hydrogel were identified by morphological and structure observation and mechanical property tests in different environmental conditions.

4.3 Experimental Section

4.3.1 Peptide Synthesis

Peptides were synthesized on a CEM Liberty microwave peptide synthesizer (CEM Corporation, Matthews, NC) according to the automated base-labile 9-fluorenylmethoxycarbonyl (Fmoc) strategy with Fmoc-protected amino acids (EMD Biosciences, San Diego, CA). Peptides were cleaved using 95% trifluoroacetic acid (Sigma-Aldrich, Milwaukee, WI), 2.5% triisopropylsilane (Sigma), and 2.5% deionized water. After synthesis, peptides were washed three times with anhydrous ether (Fisher Biotech, Fair Lawn, NJ) and dissolved in acetonitrile and distilled (DI) water (50/50 v/v). The peptide solution was freezed in a -80 ˚C refrigerator overnight and then was freeze-dried for 48 hours by using the Labconco freeze dry system (Labconco, Kansas City, MO). Molecular weight of the synthesized peptide was confirmed by matrix-assisted laser desorption/ionization time-of-flight mass spectroscopy on an Ultraflex II instrument (Bruker Daltronics, Billerica, MA). The peptide purity wa confirmed by a Beckman System Gold high performance liquid chromatography (HPLC, Beckman Coulter, Inc., Fullerton, CA) on a phenomenex synergi 4 µ Hydro-RP column (Phenomenex, Inc., Torance, CA) with the following gradient: 10-90% B in 20 min (A: 99.9% H_2O, 0.1% TFA; B: 90% acetonitrile, 9.9% H_2O, 0.1% TFA). 2.5, 5 and 10 mM peptide solution was prepared with basic solution (100 mM NaOH). 100 mM $CaCl_2$ solution and 100 mM HCl solution were prepared to add into peptode solution for hydrogel formation.

4.3.2 Transmission Electron Microscopy (TEM)

Peptide solutions were prepared on Formvar/carbon-coated 200-mesh copper grids (Electron Microscopy Sciences, Fort Washington, PA) and stained with 2% (w/v) uranyl acetate (Ladd Research Industries, Inc., Burlington, VT) for 60 s at ambient conditions before being imaged. The samples were imaged with a CM100 TEM (FEI Company, Hillsboro, OR) at 100 kv. The digital camera system is a Hamamatsu digital camera model C8484-05G. The particle size was measured by using Image J software (rsbweb. nih. gov) with more than 10 measurements.

4.3.5 Mass Spectrometry (MS)

MS experiments were performed using LTQ-Orbitrap (Thermo Electron Bremen, Germany) equipped with an electrospray ionization source. Samples were injected through a pulled fused silica capillary (50 μm ID) at a flow rate of 0.3 to 0.5 μL/min using a spray voltage of 4 kV. The system was operated in the positive ion mode with a resolving power of 60,000 at *m/z* 400. MS/MS experiments were performed using a 2 to 3 amu isolation window. The collision energy was adjusted for each species to obtain ca. 70 to 90% fragmentation of the precursor ion. High-resolution mass analysis enabled unambiguous identification of the resulting fragments.

Stock solutions of peptides were prepared by dissolving 0.85 mg and 0.94 mg of h5e (MW 1370.6951) and h9e (MW 1740.9167), respectively, in 500 μl HPLC grade water and adding 60 to 80 μl of 0.25 M NaOH to obtain solutions with pH 8. Solutions for MS experiments were prepared by mixing 10 μl of the stock solution with 10 μl of 0.1 M $CaCl_2$ and adding 200 μl of 50:50 (v:v) H_2O/acetonitrile.

4.3.6 Circular Dichroism (CD) Spectroscopy

The CD spectra of h9e acidic hydrogel, and Ca^{2+} hydrogel were recorded at ambient conditions using a Jasco J-815 spectrometer (Jasco Corporation, Tokyo, Japan). The concentration of samples was 1 mM (0.17 wt%). CD spectra were recorded from 190 to 260 nm with 1 nm bandwidth and 20 nm min^{-1} scanning speed, then averaged over two accumulations. Baselines were recorded using basic, acidic, and Ca^{2+} solutions without peptide. (on page 48, the CD measure was performed with 50 nm min^{-1} scanning speed and averaged over five accumulations. Both methods provide accurate results)

4.3.7 Fourier Transform Infrared Spectroscopy (FTIR)

The Ca^{2+} and acidic hydrogels of h9e were prepared and freeze-dried. The FTIR spectra were recorded on a PerkinElmer spectrum 400 FT-IR/FT-NIR spectrometer (PerkinElmer Inc, Waltham, MA) in the range of wavenumbers from 400-4000 cm-1. The accumulation was 16 sans and the peaks were identified by deconvolution.

4.3.8 Oscillational Rheology Test

The storage moduli, G' (which represent the elastic character of the material), and loss moduli, G'' (which repersnt the viscous character of the material),of h9e acidic and Ca^{2+} hydrogels were determined on a rheometer system C-VOR 150 (Malvern instruments, Malvern, Worcestershire WR141XZ, United Kingdom) with a 20 mm diameter parallel plate geometry through frequency sweep (strain 1%, frequency 0.01 to 10 Hz, temperature 25 ℃), amplitude sweep (strain 1 to 500%, frequency 1Hz, temperature 25 ℃), and temperature profile (strain 1%, frequency 1Hz, Temperature 5, 20, 37, 50, 75, and 90 ℃) measurements. The multiple amplitude sweep experiments were conducted to test the moduli recovery of peptide hydrogels. The time gap between every two tests was 10, 30, and 60 s for h9e Ca^{2+} hydrogel.

4.4 Results and Discussion

The lyophilized h5e and h9e peptide were dissolved in 100 mM NaOH solution. Under TEM examination, the matrix morphology was observed in the h5e solution (Figure 4.1a), while the h9e solution contained predominantly dimers of short nanofibers of about 10 nm width (Figure 4.1 e). Changing the pH value to acidic or adding Ca^{2+} solution made the h5e solution become cloudy with sedimentation. The h5e molecules aggregated into large insoluble particles that could be observed with the naked eye. However, the same process triggered h9e solution into hydrogels. These different behaviors between these two peptides were unexpected. Compared their primary structures, beside the hydrophobic core h5 (sequence: FLIVI) and the fiber structure induced region eD_2, turning segment GSII of hydrophobic core h9 (sequence: FLIVI-GSII), the only difference in the sequence of h5e and h9e, indicated a key role in hydrogel formation.

Mass spectrometry (MS) experiments were conducted to identify possible precursors of the peptide assembly in a Ca^{2+} solution of h5e and h9e peptides (Figure 4.1f). Mass spectrum obtained for both peptides was dominated by Ca^{2+} adducts indicating high affinity of h5e and h9e to calcium. MS/MS experiments were conducted to gain insight on the mode of binding of calcium to h5e and h9e peptides. In agreement with earlier work[27, 28] fragmentation of peptide molecules cationized on calcium produces a number of backbone fragments including y-, b-, a-, z- and c-ions. It has been demonstrated that the a-ion formation is promoted by calcium binding and occurs C-terminal to the Ca^{2+} binding site.[27] Examination of MS/MS spectra obtained for

different calcium adducts of the h5e and h9e peptides (Table 4.1, 3.2) shows that in $[M+Ca]^{2+}$ ion calcium is most likely coordinated by the carboxyl group of the internal D residue is and solvated by the C-terminal D. Fragmentation behavior changed in an interesting way for $[h9e+2Ca]^{4+}$ (Table 4.1). Cleavages indicative of Ca^{2+} binding were observed in the SII and GDGPG regions, suggesting that although the first Ca^{2+} is bound to the internal D residue, the second one is coordinated by serine. Differences in Ca^{2+} binding capacity of the two peptides indicated the different assembly pathways. The tight Ca^{2+} binding h9e has more compact structure and less hydrophobic area exposure than h5e (Figure 4.1g, h), which may explain the morphological difference of their supramolecular aggregation and why hydrogel formed in h9e but not h5e

To further understand the contribution of each sequence region for hydrogel formation, we divided the h9e sequence into three regions: the relatively hydrophobic part FLIVI, the relatively hydrophilic part GPGGDGPGD, and the critical GSII segment, and designed a series of peptides by modifying each region (Table 4.3). The peptide h5SIIe designed by removing the glycine residue from the GSII segment exhibited the matrix morphology in aqueous solution (Figure 4.1b). Unlike hydrogel of h9e or insoluble particles of h5e, h5SIIe aggregated into semitransparent particles in the presence of Ca^{2+} or in acidic solution. This phenomenon suggested that the conformation freedom provided by the glycine residue should be another critical factor for peptide correct assembly. Next, two relative inflexible segments, IIVI and PP^D, were selected to replace GSII segment for peptide h5IIVIe and h5PP^De. According to the conformational properties of amino acid residues, IIVI is a hydrophobic and linear structure, but PP^D is a sharp turning motif. The peptide h5IIVIe has similar matrix morphology as h5e (Figure 4.1c), and aggregates as insoluble particles in the presence of Ca^{2+} or in acidic solution. Surprisingly, the peptide h5PP^De was soluble in DI water without any pH adjustment. The amorphous morphology presented in TEM images of h5PP^De (Figure 4.1d), indicate the assembly of peptide molecules when the sharp turning h5PP^De fold the hydrophobic region and the hydrophilic region as a hairpin structure (Figure 4.1i). Except h9e, none of these peptides formed hydrogel. Both the correct packing of peptide monomers with Ca^{2+} and the conformation freedom between the hydrophobic and hydrophilic segments of peptides played important roles for hydrogel forming capability.

In addition, two other peptides, L5GSIIe, h5GSIIK10 were designed by retaining the GSII motif and substituting the h5 segment of h9e with LLLLL or replacing the eD_2 segment of h9e with KKKKKKKKKK, respectively. These two sequences formed viscous solution or hydrogel with low modules. The storage module of 5mM L5GSIIe is 21.6 ± 0.3 Pa in Ca^{2+} solution and that of 5mM h5GSIIK10 is 55.0 ± 0.9 Pa in basic pH, both of which were much smaller than the storage module of the h9e hydrogel, 1560.0 ± 13.0 Pa (h9e Ca^{2+} hydrogel) and 2863.7 ± 27.8 Pa (h9e acidic hydrogel), formed at the same concentration (Figure 4.3a). Here, the hydrophobic sequences h5 which could provide the high adhesion shear strength and eD_2 which has ion binding and fiber forming propensity display a great potential to improve the mechanical strength of this hydrogel. When we replaced both h5 and eD_2 segments of h9e, the peptide L5GSIIK10 did not form hydrogel in aqueous solution. These findings suggest that h9e, designed from rational combination of two native segments, is a unique hydrogel-forming sequence.

The h9e formed hydrogels in Ca^{2+} solution as well as at acidic pH (Figure 4.2a, c). In Ca^{2+} solution, the pepide molecules self-assembled into nanofibers which further corss-link into a matrix structure as a hydrogel (Figure 4.2b). In contrast, h9e formed a hydrogel with higher G' than h9e Ca2+ gel (Figure 4.3a, at 2.5 mM peptide concentration) in acidic conditions, the nanofibers of which aggregated parallelly and entangle for a network (Figure 4.2d). The circular dichroism (CD) spectra (Figure 4.2e) suggested that h9e adopted predominantly β-sheet in Ca^{2+} solution, whereas a more random structure was detected in the acidic solution, which has much lower intensity of CD spectra as well, suggesting the disordered chain conformations of h9e acidic hydrogel. Figure 4.2f shows amide I and amide II region of FTIR spectra of h9e Ca^{2+} and acidic hydrogels. The major amide I peak of both hydrogels appeared at 1625 cm^{-1}, indicating that the peptide adopts mainly the β-sheet structure. In addition, some random structures represented by a small peak at 1659 cm^{-1}were observed in the acidic h9e hydrogel. Normally, stable chain conformations are considered as essential factors in the formation and strength of hydrogels [12], however, h9e acidic hydrogel, which even have higher storage modulus than h9e Ca^{2+} hydrogels at concentration lower than 5 mM (Figure 4.3a), does not follow this common rule. Combinding the morphological and secondary structural data suggests that the peptide monomeric structure not only affects the peptide self-assembly into nanofiber structure but also relates to the interaction of nanofibers.

A storage moduli (G') of the h9e acidic gel is about 10 times higher than that of the h9e Ca^{2+} gel at 2.5 mM peptide concentration (Figure 4.3a). The difference in G' between these two hydrogels became smaller as peptide concentration increased. For example, at 10 mM, G' of the h9e Ca^{2+} gel was about 9,000 Pa, which was even higher than that of the h9e acidic gel (about 8,000 Pa). The dramatically increase of G' of h9e Ca2+ gel with peptide concentration may be contributed by its highly order secondary structure formation which made the self-assembly of peptides more compact and nanofibers crossing more tightly at higher concentration. The effect of the molar ratio of Ca^{2+} and peptide on the G' of h9e Ca^{2+} gel was also tested (Figure 4.4) and the G' was found to be higher than 300 Pa when the ratio higher than 1. In a temperature profile test, G' of the h9e Ca^{2+} hydrogel increased 10 fold as temperature increased from 5 to 90 ℃, however, G' of the h9e acidic hydrogel decreased as temperature increased and dropped to 1,000 Pa at 75 ℃ (Figure 4.3b). The G' of h9e Ca^{2+} hydrogel was reversible based on the changing of temperature within the range from 2 to 80 ℃ (Figure 4.3c). The changes of the storage moduli according to the fluctuation of temperature were not observed in the h9e acidic hydrogel. The shear thinning and rapid recovery of mechanical strength was found only in the h9e Ca^{2+} hydrogel (Figure 4.4d). Hydrogels underwent a serial of amplitude sweep tests. There were 10 s to 60 s delay between every two test cycles. Gel became like pure liquid ($G'' > G' \approx 0$) under 500% strain oscillation. After 10 s of the first cycle, 75 to 80% of the hydrogel strength was recovered. Percentage of strength recovery increased as the delay time increased and reached 100% recovery by 60 s. Under the same process, the strength of the h9e acidic hydrogel did not recover in this short time period (Figure 4.3e). The property of hydrogel strength recovery within 60 s after shear-thinning suggests the h9e Ca^{2+} hydrogel has large potential for biomedical application.

This is our first report of two types of hydrogels with distinct mechanical properties created from a peptide with the same primary structure. According to published studies, changing an amino acid in certain positions could result in peptide hydrogels with different mechanical strength,[29] thermal response[30, 31] or recovery property.[14] Because these changes in primary structures could facilitat molecular folding and cross-linking of peptide fibers. The distinct properties of these two h9e hydrogels suggest that peptide molecule with the same primary structure, such as h9e peptide, could undergo different molecular self-assembling

pathways to form hydrogel. The nanofiber structure, inter-fiber interaction and mechanical properties of hydrogel materials could be controlled by different external parameters.

Ions Na^+, Mg^{2+}, and Zn^{2+} at the same concentration of Ca^{2+} (100 mM) were also studied with h9e. In these three ion solutions, h9e formed hydrogels with different G' (Figure 4.5a). The h9e Na^+ hydrogel had physical properties similar to those of the h9e Ca^{2+} hydrogel (Figure 4.5b, c). However, h9e formed a soft hydrogel in Mg^{2+} solution. In Zn^{2+} solution, h9e formed a hard hydrogel as it did in h9e acidic gel. The rapid shear strength recovery property was not found in h9e Mg^{2+} or h9e Zn^{2+} hydrogels (Figure 4.5d, e).

4.5 Conclusions

According to the objective of this chapter, we rationally used two native functional sequences from spider silk and a trans-membrane motif of human muscle calcium channel to design and synthesize novel peptides that were sensitive to Ca^{2+}. The h9e peptide (sequence: FLIVI-GSII-GPGGDGPGGD) could self-assemble into hydrogel under the triggerments of Ca^{2+} or acidic pH solution. However, eD_2 (sequence: GPGGDGPGGD) alone or tailored with hydrophobic segments (i.e., h5 = FLIVI) was not able to form hydrogels. The turning function of GSII played a key role, altering the molecular assembly pathways of h9e for hydrogel formation. In acidic conditions, h9e formed hard hydrogels that had a storage modulus (G') 10 times stronger than that of the hydrogel formed in Ca^{2+} solution (at 2.5 mM peptide concentration). The G' of h9e acidic hydrogel was weakened upon heating, whereas the G' of h9e Ca^{2+} hydrogel increased as temperature increased and was reversible in the temperature range of at 2 to 80 ℃. The h9e Ca^{2+} hydrogel was shear-thinning and had 100% recovery within 1 min. These distinct physical properties between h9e acidic hydrogel and h9e Ca^{2+} hydrogel suggest that a peptide's molecular assembly pathways and degree of nanofiber cross-linking could be induced by external parameters such as pH and metal ions. The h9e has great potential for drug delivery and tissue engineering applications.

4.6 Acknowledgments

We thank Dr. Dan Boyle (Department of Biology, Kansas State University) for TEM and LSCM images, Dr. Michal Zolkiewski (Department of Biochemistry, Kansas State University) for CD use, Dr. Duy Hua (Department of Chemistry, Kansas State University) for HPLC use, and the University of Kansas Mass Spectrometry Lab for mass spectrometric analysis. Funding

for this work was provided by the Targeted Excellence Program and Center for Biobased Polymers by Design at Kansas State University. Contribution no. 10-127-J from the Kansas Agricultural Experiment Station. MS/MS experiments were performed at the W. R. Wiley Environmental Molecular Sciences Laboratory (EMSL), a national scientific user facility sponsored by the U.S. DOE of Biological and Environmental Research and located at the Pacific Northwest National Laboratory.

4.7 References

1. Lee, K. Y.; Mooney, D. J. Hydrogels for tissue engineering. Chem. Rev. 2001, 101, 1869-1879.

2. Langer, R.; Tirrell, D. A. Designing materials for biology and medicine. Nature 2004, 428, 487-492.

3. Zhang. S.; Greenfirld, M. A.; Mata, A.; Palmer, L. C.; Bitton, R.; Mantei, J. R. et al. A self-assembly pathway to aligned monodomain gels. Nature Mater. 2010, 9, 594-601.

4. Cushing, M. C.; Anseth, K. S. Hydrogel cell cultures. Science 2007, 316, 1133-1134.

5. Anderson, D. G.; Burdick, J. A.; Langer, R. Smart Biomaterials. Science 2004, 305, 1923-1924.

6. Koutspoulos, S.; Unsworth, L. D.; Nagai, Y.; Zhang, S. Controlled release of functional proteins through designer self-assembling peptide nanofiber hydrogel scaffold. Proc. Natl. Acad. Sci. 2009, 106, 4623-4628.

7. Zhang, S. Hydrogels wet or let die. Nature Mater. 2004, 3, 7-8.

8. Jeong, B.; Bae, Y. H.; Lee, D. S.; Kim, S. W. Biodegradable block copolymers as injectable drug-delivery systems. Nature 1997, 388, 860-862.

9. Zawaneh, P. N.; Singh, S. P.; Padera, R. F.; Henderson, P. W.; Spector, J. A.; Putnam, D. Design of an injectable synthetic and biodegradable surgical biomaterial. Proc. Natl. Acad. Sci. 2010, 107, 11014-11019.

10. Petka, W. A.; Harden, J. L.; McGrath, K. P.; Wirtz, D.; Tirrell, D. A. Reversible hydrogels from self-assembling artificial proteins. Science 1998, 281, 389-392.

11. Aggeli, A.; Bell, M.; Boden, N.; Keen, J. N.; Knowles, P. F.; McLeish, T. C. B. et al. Responsive gels formed by the spontaneous self-assembly of peptides into polymeric β-sheet tapes. Nature 1997, 386, 259-262.

12. Nowak, A. P.; Breedveld, V.; Pakstis ,L.; Ozbas, B.; Pine, D. J.; Pochan, D.; Deming, T. J. Rapidly recovering hydrogel scaffolds from self-assembling diblock copolypeptide amphiphiles. Nature 2002, 417, 424-428.

13. Schneider, J. P.; Pochan, D. J.; Ozbas, B.; Rajagopal, K.; Pakstis, L.; Kretsinger, J. Responsive hydrogels from the intramolecular folding and self-assembly of a designed peptide. J. Am. Chem. Soc. 2002, 124, 15030-15037.

14. Aulisa, L.; Dong, H.; Hartgerink, J. D. Self-assembly of multidomain peptides: sequence variation allows control over cross-linking and viscoelasticity. Biomacromolecules 2009, 10, 2694-2698.

15. Salick, D. A.; Pochan, D. J.; Schneider, J. P. Design of an injectable β-hairpin peptide hydrogel that kills methicillin resistant staphylococcus aureus. Adv. Mater. 2009, 21, 4120-4123.

16. Kisiday, J.; Jin, M.; Kurz, B.; Hung, H.; Semino, C.; Zhang, S. et al. Self-asssembling peptide hydrogel fosters chondrocyte extracellular matrix production and cell division: implications for cartilage tissue repair. Proc. Natl. Acad. Sci. 2002, 99, 9996-10001.

17. Caplan, M. R.; Moore, P. N.; Zhang, S.; Kamm, R. D.; Lauffenburger, D. A. Self-assembly of a β-sheet protein governed by relief of electrostatic repulsion relative to van der waals attraction. Biomacromolecules 2000, 1, 627-631.

18. Saiani, A.; Mohammed, A.; Frielinghaus, H.; Collins, R.; Hodson, N.; Kielty, C. M. et al. Self-assembly and gelation properties of α-helix versus β-sheet forming peptides. Soft Matter 2009, 5, 193-202.

19. Cavalli, S.; Albericio, F.; Kros, A. Amphiphilic peptides and their cross-disciplinary role as building blocks for nanoscience. Chem. Soc. Rev. 2010, 39, 241-263.

20. Zhang, S. Fabrication of novel biomaterials through molecular self-assembly. Nat. Biotechnol. 2003, 21, 1171-1178.

21. Hardy, J. G,; Römer, L. M.; Scheibel, T. R. Polymeric materials based on silk proteins. Polymer, 2008, 49, 4309-4327.

22. Yang, M.; Yamauchi, K.; Kurokawa, M.; Asakura, Design of silk-like biomaterials inspired by mussel-adhesive protein. T. Tissue Eng. 2007, 13, 2941-2947.

23. Scotter, A. J.; Guo, M.; Tomczak, M. M.; Daley, M. E.; Campbell, R. L.; Oko, R. L.; Bateman, D. A. Chakrabartty, A. Sykes, B. D.; Davies, P. L. Metal ion-dependent, reversible, protein filament formation by designed beta-roll polypeptides. BMC Struct. Biol. 2007, 7, 63.

24. Huang, H.; Sun, X. Rational design of responsive self-assembling peptides from native protein sequences. Biomacromolecules 2010, 11, 3390-3394.

25. Shen, X.; Mo, X.; Moore, R.; Frazier, S. J.; Iwamoto, T.; Tomich, J. M. et al. Adhesion and structure properties of protein nanomaterials containing hydrophobic and charged amino acids. J. Nanosci. Nanotechnol. 2006, 6, 837-844.

26. Mo, X.; Hiromasa, Y.; Warner, M.; Al-Rawi, A. N.; Iwamoto, T.; Rahman, T. S. et al. Design of 11-residue peptides with unusual biophysical properties: induce secondary structure in the absence of water. Biophys. J. 2008, 94, 1807-1817.

27. Teesch, L. M.; Adams, J. Intrinsic interactions between alkaline-earth metal ions and peptides: a gas-phase study. J. Am. Chem. Soc. 1990, 112, 4110-4120.

28. Nemirovskiy, O. V.; Gross, M. L. Determination of calcium binding sites in gas-phase small peptides by tandem mass spectrometry. J. Am. Soc. Mass. Spectrom. 1998, 9, 1020-1028.

29. Branco, M. C.; Nettesheim, F.; Pochan, D. J.; Schneider, J. P.; Wagner, N. J. Fast dynamics of semiflexible chain networks of self-assembled peptides. Biomacromolecules 2009, 10, 1374-1380.

30. Banwell, E. F.; Abelardo, E. S.; Adams, D. J.; Birchall, M. A.; Corrigan, A.; Donald, A. M.; Kirkland, M.; Serpell, L. C.; Butler, M. F.; Woolfson, D. N. Rational design and application of responsive alpha-helical peptide hydrogels. Nat. Mater. 2009, 8, 596-600.

31. Pochan, D. J.; Schneider, J. P.; Kretsinger, J.; Ozbas, B.; Rajagopal, K.; Haines, L. Thermally reversible hydrogels via intramolecular folding and consequent self-assembly of a de novo designed peptide. J. Am. Chem. Soc. 2003, 125, 11802-11803.

Figure 4.1 Synthetic peptides in aqueous solution.

a-c. TEM images of h5e (a) h5SIIe (b) and h5IIVIe (c) integrations respectively, **d.** TEM image of micelle-like structure of h5PPDe, **e.** needle shape nanofibres of h9e, **f.** MS fragments of h5e and h9e, **g-i.** assembly of amphiphilic peptides (g: linear peptide, h: peptide with flexible turning segment, i: peptide with sharp turning; blue: hydrophobic segment, red: hydrophilic segment, yellow: turning segment).

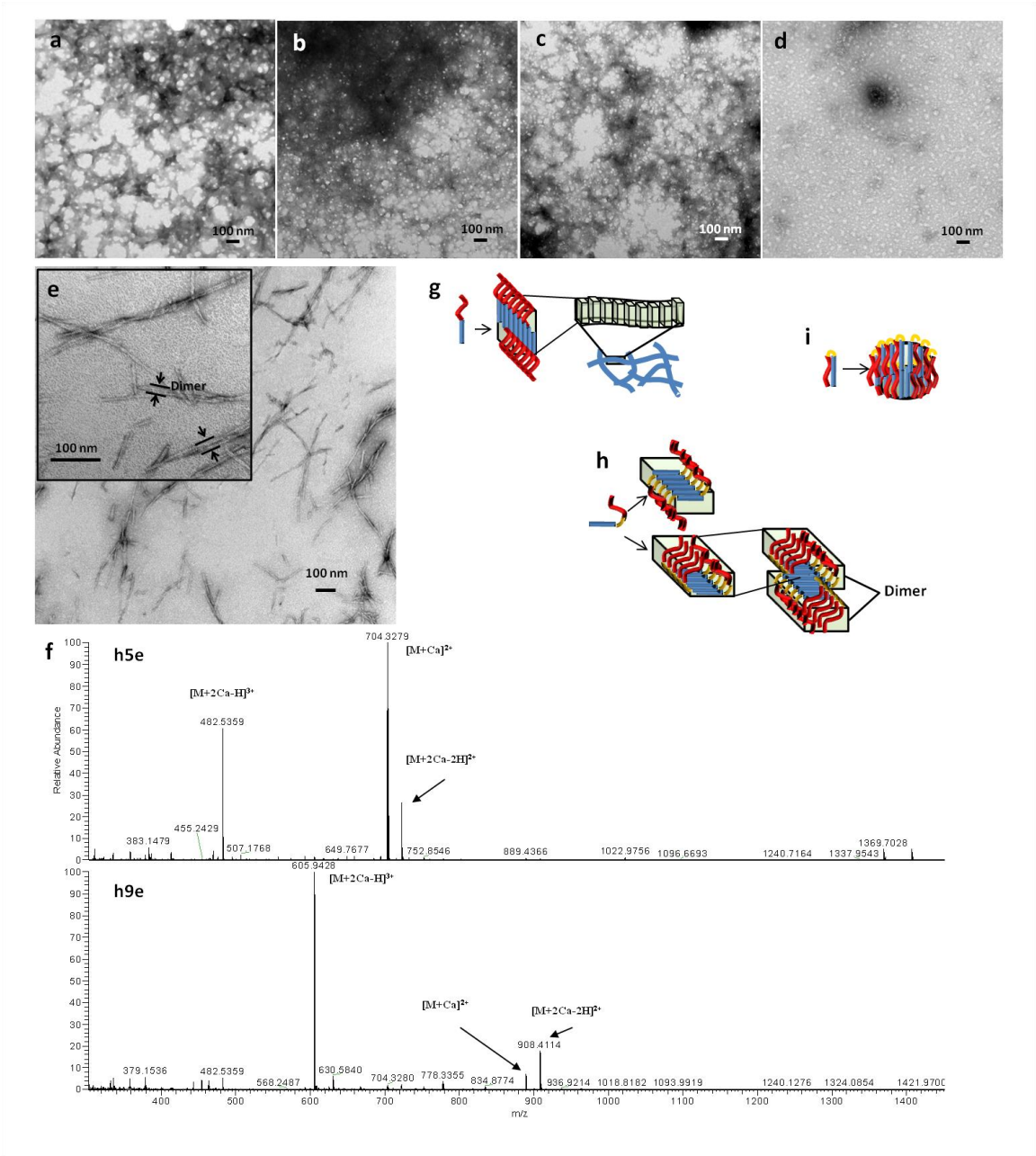

Figure 4.2 Morphological and structure properties of h9e Ca^{2+} and acidic hydrogel.
a, c. pictures of h9e Ca2+ (a) and acidic hydrogel (c), **b, d.** TEM, images of h9e Ca2+ (b) and acidic (d) hydrogels, **e.** CD spectra of h9e Ca2+ and h9e acidic hydrogels (solid: h9e acidic hydrogel, open: h9e Ca2+ hydrogel) **f.** FTIR of h9e Ca2+ (black) and acidic (red) hydrogels.

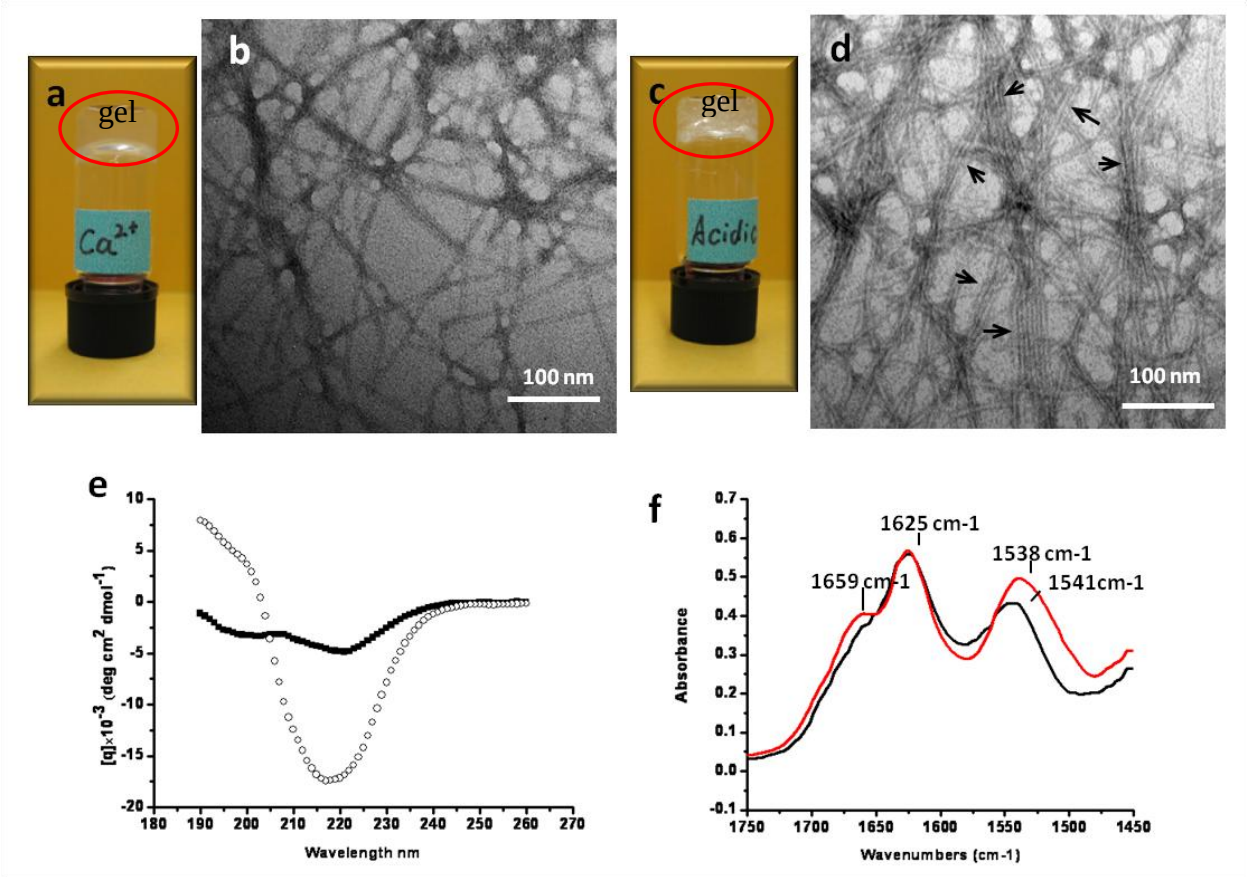

Figure 4.3 Rheological and thermal properties of h9e Ca^{2+} and acidic hydrogels.

a. G' of h9e Ca2+ and h9e acidic hydrogels. (solid: h9e Ca2+ gel, open: h9e acidic gel. Peptide concentration: black square: 2.5 mM, red circle: 5 mM, blue triangle: 10 mM) **b.** Temperature profile test of h9e Ca2+ and h9e acidic hydrogels. (solid: h9e acidic hydrogel, open: h9e Ca2+ hydrogel. Temperature: black: 5 ℃, red: 20 ℃, blue: 37 ℃, yellow: 50 ℃, green: 75 ℃, purple: 90℃) **c.** Thermal reversible of G' of h9e Ca2+ hydrogel (black: 2 ℃, red; 80 ℃) **d, e.** G' and G'' values of h9e Ca2+ (d) and acidic (e) hydrogel under 4 amplitude sweep shear circles, time interval between each cycle was 10, 30 and 60 s, respectively (black: G'; red: G'').

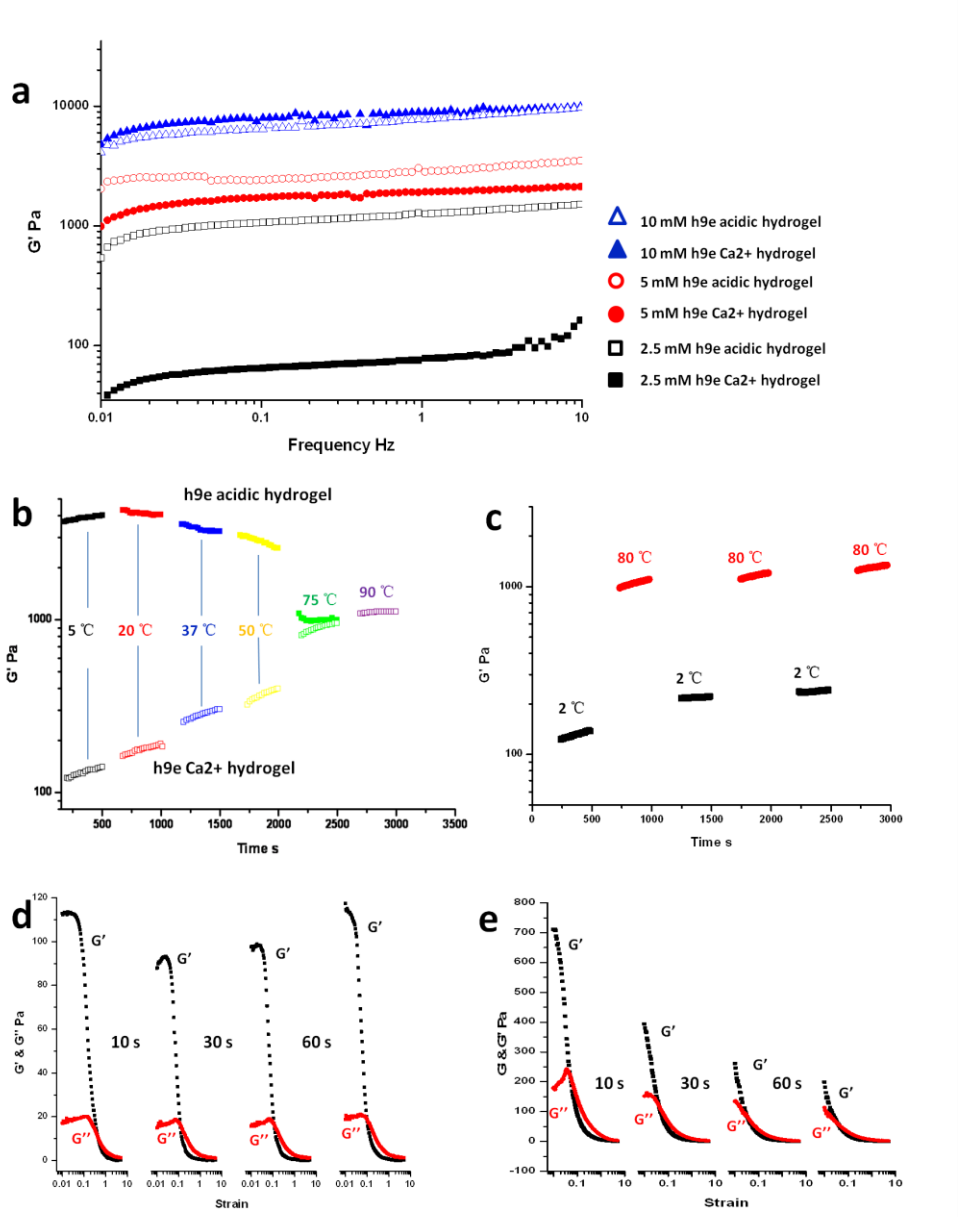

Figure 4.4 G' of h9e Ca^{2+} hydrogels with different molar ratio of Ca^{2+} to peptide.

(Molar ratio of Ca2+ to h9e: 0.1 (black), 1 (red), 10 (blue), 100 (green))

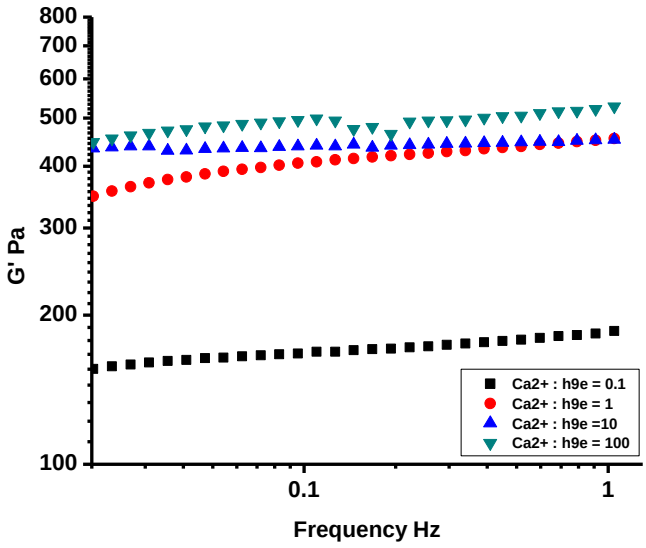

Figure 4.5 Physical properties of h9e hydrogel in Zn^{2+}, Na^{+} and Mg^{2+} solutions.
a. G' of h9e Zn2+ (blue), Na+ (black) and Mg2+ (red) hydrogels. (peptide concentration 0.005M) **b.** Temperature profile test of h9e Na2+ hydrogel. (Temperature: black: 5 ℃, red: 20 ℃, blue: 37 ℃, yellow: 50 ℃, green: 75 ℃, purple: 90℃) **c.** G' and G'' values of h9e Na+ hydrogel under 4 amplitude sweep shear circles, time interval between each cycle was 10, 20 and 30 s, respectively (black: G'; red: G''). **d.** G' and G'' values of h9e Mg2+ hydrogel under 4 amplitude sweep shear circles, time interval between each cycle was 10 s, 1 min and 5 min, respectively (black: G'; red: G''). **e.** G' and G'' values of h9e Zn2+ hydrogel under 4 amplitude sweep shear circles, time interval between each cycle was 10 s, 1 min and 5 min, respectively (black: G'; red: G'').

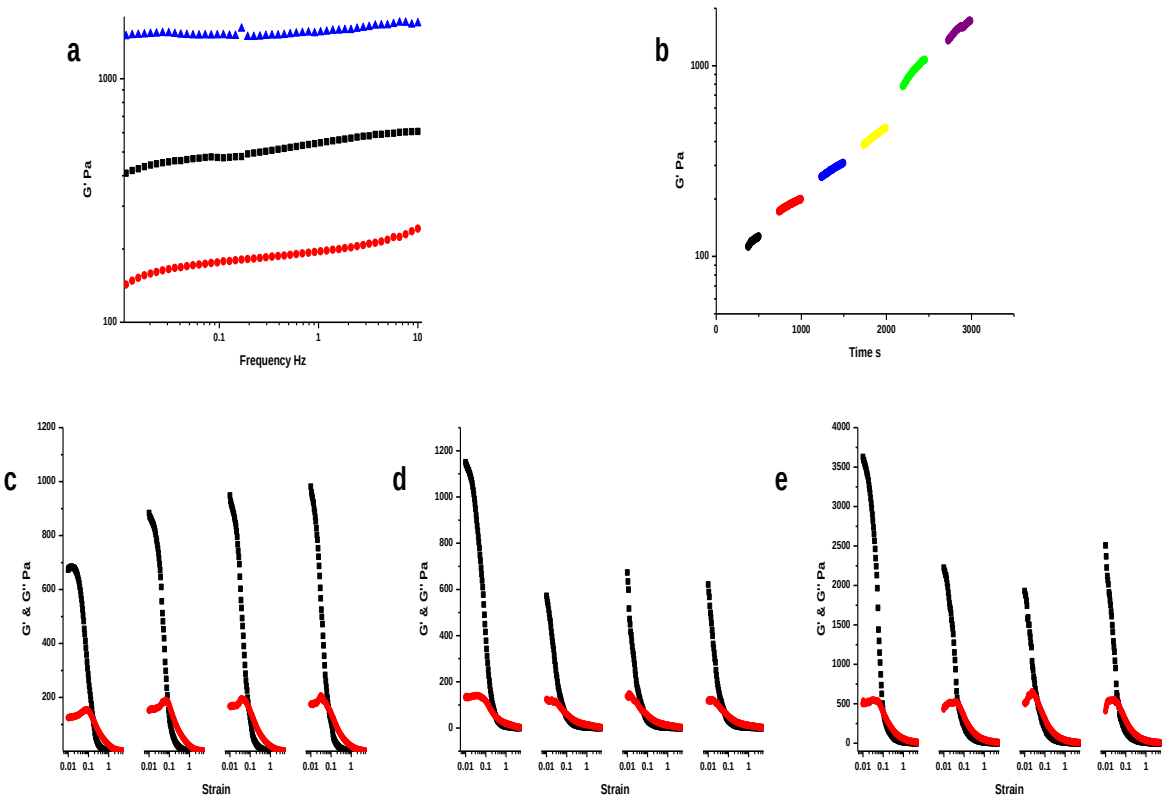

Table 4.1 Fragmentation behavior of several precursor ions observed in the ESI spectra of the h5e peptide (M).

Precursor		$[M+H+Ca]^{3+}$ (m/z 469.891)		$[M+2Ca-H]^{3+}$ (m/z 482.54)		$[M+Ca]^{2+}$ (m/z 704.33)	
Fragments		*N-terminal*	*C-terminal*	*N-terminal*	*C-terminal*	*N-terminal*	*C-terminal*
1	F						
2	L	**a_2; b_2** [a)]	$[y_{14}-H+Ca]^{2+}$	**a_2; b_2**	$[y_{14}-3H+2Ca]^{2+}$	a_2	
3	I	b_3	**$[y_{13}-H+Ca]^{2+}$**		**$[y_{13}-3H+2Ca]^{2+}$** $[y_{13}-3H+2Ca-H2O]^{2+}$	b_3	
4	V		**$[y_{12}-H+Ca]^{2+}$**		$[y_{12}-3H+2Ca]^{2+}$	a_4; b_4	$[y_{12}-H_2O-2H+Ca]^{+}$
5	I						$[y_{11}-H_2O-2H+Ca]^{+}$
6	G		$[y_{10}-H+Ca]^{2+}$				$[y_{10}-2H+Ca]^{+}$ $[y_{10}-H_2O-2H+Ca]^{+}$
7	P						$[y_9-H_2O-2H+Ca]^{+}$
8	G					$[b_8-2H+Ca]^{+}$	
9	G			**$[c_9-H+Ca]^{2+}$**		**$[c_9-H+Ca]^{2+}$** $[c_9-2H+Ca]^{+}$	
10	D					**$[b_{10}-H+Ca]^{2+}$** $[a_{10}-H+Ca]^{2+}$ **$[b_{10}-2H+Ca]^{+}$** $[c_{10}-2H+Ca]^{+}$	
11	G					$[b_{11}-2H+Ca]^{+}$	**y_5** **$[y_5-H+Ca]^{+}$**
12	P					$[b_{12}-H+Ca]^{2+}$	y_4
13	G	$[b_{13}-H+Ca]^{2+}$				$[b_{13}-H+Ca]^{2+}$	
14	G	$[b_{14}-H+Ca]^{2+}$				**$[b_{14}-H+Ca]^{2+}$** $[a_{14}-H+Ca]^{2+}$	
15	D						

a) Abundant fragments are shown in bold.

Table 4.2 Fragmentation behavior of several precursor ions observed in the ESI spectra of the h9e peptide (M).

Precursor		$[M+2Ca-H]^{3+}$ (m/z 605.948)		$[M+H+Ca]^{3+}$(m/z 593.299)		$[M+Ca]^{2+}$ (m/z 889.444)		$[M+2Ca]^{4+}$ (m/z 454.713)	
Fragments		*N-terminal*	*C-terminal*	*N-terminal*	*C-terminal*	*N-terminal*	*C-terminal*	*N-terminal*	*C-terminal*
1	F								
2	L	**a_2; b_2**	$[y_{18}+2Ca-3H]^{2+}$	**a_2; b_2**	$[y_{18}+Ca-H]2+$			a_2	
3	I	b_3	**$[y_{17}+2Ca-3H]^{2+}$**	b_3	**$[y_{17}+Ca-H]2+$ $[z_{17}+Ca-2H]2+$**	b_3		b_3	
4	V	b_4	**$[y_{16}+2Ca-3H]^{2+}$**	b_4	**$[y_{16}+Ca-H]2+$**	b_4		a_4; **b_4**	$[y_{16}+2Ca-3H]^{2+}$
5	I		**$[y_{15}+2Ca-3H]^{2+}$**		$[y_{15}+Ca-H]2+$				$[y_{15}+2Ca-3H]^{2+}$
6	G		$[y_{14}+2Ca-3H]^{2+}$						$[y_{14}+2Ca-2H]^{3+}$ $[y_{14}+2Ca-3H-H_2O]^{2+}$ **$[y_{14}+2Ca-3H]^{2+}$**
7	S							$[a_7+Ca-3H]^{2+}$ **$[a_7+Ca-H]^{2+}$** **$[b_7+Ca-H]^{2+}$**	$[y_{13}+2Ca-3H]^{2+}$
8	I								$[y_{12}+Ca-H]^{2+}$ $[y_{12}+2Ca-3H]^{2+}$
9	I								
10	G							**$[b_{16}-H+Ca]^{2+}$**	
11	P								
12	G								
13	G					$[a_{13}+Ca-H]^{2+}$ $[b_{13}+Ca-H]^{2+}$ $[c_{13}+Ca-H]^{2+}$			
14	D					**$[b_{14}+Ca-H]^{2+}$** $[b_{14}+Ca-H-H_2O]^{2+}$		$[b_{14}-H+Ca]^{2+}$	
15	G					$[b_{15}+Ca-H]^{2+}$			**$[y_5+Ca-H]^{2+}$**
16	P								
17	G								
18	G					$[b_{16}+Ca-H]^{2+}$			
19	D								

Table 4.3 Sequences of synthesis.

Peptide	**Sequence**	**in Ca^{2+} solution or acidic solution**
h5e	FLIVI-GPGGDGPGGD	insoluble particles
h9e	FLIVI-GSII-GPGGDGPGGD	strong hydrogel
h5SIIe	FLIVI-SII-GPGGDGPGGD	gel-like particles
h5IIVIe	FLIVI-IIVI-GPGGDGPGGD	insoluble particles
h5PP^{D}e	FLIVI-PP^{D}-GPGGDGPGGD	liquid
L5GSIIe	LLLLL-GSII-GPGGDGPGGD	weak hydrogel
h5GSIIK10	FLIVI-GSII-KKKKKKKKKK	weak hydrogel

Chapter 5 - Conformational Flexibility and pH Effects in Anisotropic Growth of Sheet-like Assembly by Amphiphilic Peptides[3]

5.1 Abstract

Peptide-based biomaterials have many potential applications in tissue engineering, drug delivery, cosmetic product, and other areas. One of the key challenges for design of functional biomaterials is to control the supramolecular assembly morphology via physical properties of the peptide monomer and experimental conditions. In this study, we exploited a series of amphiphilic diblock model peptides to demonstrate the possibility of controlling the supra-assembly morphology (sheet, fiber or sphere) through modulating peptide turning sequence flexibility and pH. Although these designed peptides have different structures as monomers, a combination of experiment and simulation revealed importance of conformational flexibility differences. Importantly, such differences can be correlated to the peptide's ability to form sheet-like assemblies. Substantial conformational heterogeneity appears to be required for anisotropic growth of sheet-like materials, likely by reducing the kinetic rate of peptide assembly. Conversely, increasing the assembly rate, such as through promoting hydrophobic collapse of peptide aggregation by neutralizing net charges at high pH, might hinder the growth of the sheet morphology as predicted by computer simulation. Together, our study suggests the importance of peptide conformational flexibility and pH in modulation of the peptide supramolecular assembly morphology.

5.2 Introduction

Self-assembling peptides are attractive building blocks for higher-order supramolecular architectures (supramolecule: a complex of molecules held together by noncovalent bonds) via bottom-up approaches.[1,2] Because of their bio-compatibility and sensitive responses to different

[3] Result have been submitted. Huang, H.; Ganguly, D.; Chen, J.; Sun, X. S. Conformational flexibility and pH effects in anisotropic growth of sheet-like assembly by amphiphilic peptides. Biopolymer: Peptide Science, in submit.

environmental conditions, peptide-based biomaterials are suitable for many applications.[3-10] Successful design of these biomaterials relies on precise control of the peptide supramolecular assembly morphology.

Formation of peptide supramolecular assemblies can be influenced by monomeric peptide properties and a complex array of environmental factors such as pH, temperature and solvent conditions.[11-13]With an improved understanding of the physical controls of single peptide properties, hydrophobic interactions and collapse have been considered as one of the most important factors for peptide self-assembly.[14,15] Therefore, amphiphilic peptides with clear hydrophobic and hydrophilic domains are preferred for most rational peptide design to form highly ordered secondary structure.[16-18] Under an environmental condition compatible for order structures, such amphiphilic peptides could spontaneously aggregate into fiber or sheet-like morphology as an effect of fast and stable hydrophobic collapse of either the fatty acid tails, coiled-coil interactions or alternation of charged and non-charged amino acid.[19-24] However, the effect of conformation flexibility between the hydrophobic and hydrophilic domains on peptide supramolecular assembly morphology is rarely discussed. In our recent study of a hydrogel forming peptide,[25] a 4-residue flexible linker segment (GSII) between the hydrophobic and hydrophilic functional domains turned out to be very important for peptide self-assembling into nanofibre and further crossing as gel matrix. Without this flexible linker, peptides assemble into ribbon structures and lose gel-forming properties. While, replacing GSII with a sharp turning segment, $P^{D}P$, leads to spherical morphology in aqueous solution.[25] Based on these observations, we hypothesized that that the conformation freedom between the hydrophobic and hydrophilic domains is correlated with peptide assembly morphology. Nevertheless, rational control of the morphology of supramolecular assemblies has remained a key challenge for rational design of functional biomaterials. In particular, one of the outstanding challenges is to more directly relate the sequence and structural properties of monomers (and experimental conditions) to the final supramolecular assembly morphology.

In this study, our objective is to used a set of rationally designed amphiphilic peptides (Table 5.1) derived from L5K10 (LLLLLKKKKKKKKK) as model systems to determine the function role of the conformation flexibility between hydrophobic and hydrophilic domains on peptide assembly morphology.[26] Turning sequences with different conformational flexibility such as GSII and $P^{D}P$ were first inserted between the L5 and K10 domains to explore their effect

on growth of peptide self-assembly morphologies. Computer simulations coupled with CD and FTIR were used to provide atomistic structural characterization of peptide monomers and to rationalize observed morphological differences of supramolecular assemblies formed by these peptides. The initial analysis suggested that conformational flexibility of monomeric peptides could be strongly correlated with the final assembly morphology, especially for sheet-like morphology. As recent report of an aqueous self-assembly of amphiphilic peptoid polymers into free-floating sheet,[27] the mechanism of sheet formation involves a fast complexation of the globular aggregated state followed by slowly re-ordering into sheet structure. Such process allows maximizing aromatic interactions, electrostatic attraction, and minimizing the exposure of hydrophobic groups to water. We assumed that the increase in conformational flexibility of an amphiphilic peptide sequence would result in slower aggregation kinetics with re-ordering of globular aggregates for anisotropic growth of sheet-like morphology. Directly monitoring of the morphological growth of L5GSIIK10 as well as hydrophobic interaction analysis between peptide and high-density polyethylene (HDPE) would provide further evidence to prove this hypothesis. In addition, we gradually increased the conformation flexibility by replacing the GSII turn with generic ones consisting of one to four glycines, and examined the monomer conformational properties and supramolecular assembly morphologies. Meanwhile, we have also tested another prediction of the kinetic control hypothesis, that enhancing peptide-peptide interactions, such as through charge neutralization at high pH (10 mM NaOH), could accelerate aggregation and hinder the formation of sheet-like morphology. The results of these additional experiments proved to be fully consistent with the kinetics mechanism, supporting the notion that control of supramolecular assembly morphology might be achieved by regulating the aggregation kinetics through modulating the peptide conformational flexibility and aggregation propensity.

5.3 Experimental Section

5.3.1 Materials

N,N-Dimethylformamide (DMF), Trifluoroacetic Acid (TFA), Piperidine, N,N-Diisopropylethylamine (DIEA) and Triisopropylsilane (TIS) were purchased from Sigma-Aldrich (Milwaukee, WI). N-Methylpyrrolidinone (NMP), Anhydrous Ether, Dichloromethane (DCM) were purchased from Fisher Biotech (Fair Lawn, NJ). Rink Amide MBHA Resin, 2-(1H-

Benzotriazole-1-yl)-1,1,3,3-tetramethyluronium Hexafluorophosphate (HBTU) and all protected amino acids were purchased from EMD Biosciences (San Diego, CA). N-Hydroxybenzotriazole (HOBT) was purchased from CEM (Matthews, NC).

5.3.2 Peptide Synthesis

Peptides were synthesized on a CEM Liberty microwave peptide synthesizer (CEM Corporation, Matthews, NC) according to the automated base-labile 9-fluorenylmethoxycarbonyl (Fmoc) strategy with Fmoc-protected amino acids (EMD Biosciences, San Diego, CA). Peptides were cleaved using 95% trifluoroacetic acid (Sigma-Aldrich, Milwaukee, WI), 2.5% triisopropylsilane (Sigma), and 2.5% deionized water. After synthesis, peptides were washed three times with anhydrous ether (Fisher Biotech, Fair Lawn, NJ), dissolved in acetonitrile and deionized water (50/50 v/v). The peptide solution was freezed in a -80 ˚C refrigerator overnight and then was freeze-dried for 48 hours by using the Labconco freeze dry system (Labconco, Kansas City, MO). The pH value of the peptide in water solution was 3.6. Molecular weight of the synthesized peptide was confirmed by matrix-assisted laser desorption/ionization time-of-flight mass spectroscopy on an Ultraflex II instrument (Bruker Daltronics, Billerica, MA). The peptide purity wa confirmed by a Beckman System Gold high performance liquid chromatography (HPLC, Beckman Coulter, Inc., Fullerton, CA) on a phenomenex synergi 4 μ Hydro-RP column (Phenomenex, Inc., Torance, CA) with the following gradient: 10-90% B in 20 min (A: 99.9% H_2O, 0.1% TFA; B: 90% acetonitrile, 9.9% H_2O, 0.1% TFA).

5.3.3 Transmission Electron Microscopy (TEM)

Lyophilized peptide powders were dissolved in deionized water and 10 mM NaOH solution, respectively, with the final peptide concentration of 5 mM. The solutions were placed in a 4 ^{o}C refrigerator overnight for peptide anisotropic aggregation. Peptide solutions were prepared on carbon-coated 200-mesh copper grids (Electron Microscopy Sciences, Fort Washington, PA) and stained with 2% (w/v) uranyl acetate (Ladd Research Industries, Inc., Burlington, VT) for 60 s at ambient conditions before imaging. To observe the morphological growth of L5GSIIK10, the peptide was dissolved in water or 10 mM NaOH solution right before TEM test. 20 μL peptide solution was sampled to obsorb onto copper grids for every 30 min. The samples were imaged with a CM100 TEM (FEI Company, Hillsboro, OR) at 100 kV accelerating voltage. The digital camera system is a Hamamatsu digital camera model C8484-05G. The

particle size was measured by using Image J software (rsbweb. nih. gov) with more than 10 measurements.

5.3.4 Circular Dichroism (CD) Spectroscopy

The CD spectra of peptide solutions were recorded at ambient conditions using a Jasco J-815 spectrometer with a 1mm pathlength cell (Jasco Corporation, Tokyo, Japan). Peptides were dissolved in deionized water and 10 mM NaOH solution at initial concentration of 1 mM. Then the solutions were diluted by adding deionized water to reach the final 200 μM peptide concentration in both neutral and basic (2 mM NaOH) solutions. To test the secondary structure change of L5GSIIK10 with time, the peptide was dissolved in water or 10 mM NaOH solution at 1 mM concentration right before CD test. For every 30 min, 200 μL of the 1 mM peptide solution was sampled and diluted to 200 μM with deionized water. CD spectra were recorded at room temperature from 190 to 260 nm with 1 nm bandwidth and 50 nm min^{-1} scanning speed, then averaged over five accumulations. The secondary structure of each peptide was interpreted according to the pure secondary structures of protein reported by Brahms & Brahms[28].

5.3.5 Fourier Transform Infrared Spectroscopy (FTIR)

1 mM peptide solutions with deionized water and 10 mM NaOH were place in a -80 ℃ refrigerator overnight, then freeze-dried. The FTIR spectra of lyophilized peptide powders were recorded on a PerkinElmer spectrum 400 FT-IR/FT-NIR spectrometer (PerkinElmer Inc, Waltham, MA) in the range of wavenumbers from 400-4000 cm-1. The accumulation was 32 scans and the peaks were identified by deconvolution.[29]

5.3.6 Contact Angle Anlysis

10 wt % peptide solutions were prepared in deionized water and 10 mM NaOH respectively. The solutions were stocked in room temperature for overnight and analyzed by an optical contact angle meter (CAM 100, KSV Instruments, Ltd., Helsinki, Finland) with the sessile drop method. The HDPE was selected as a hydrophobic surface substrate. Two-sample t-test was used to analyze difference between water and NaOH solution of each peptide. P values less than 0.05 were considered statistically significant.

5.3.7 Viscosity Analysis

The L5GSIIK10 peptide solutions were prepared in deionized water or 10 mM NaOH at peptide concentration of 1%, 4% and 10% (w/v)at room temperature overnight. The viscosity was determined on a rheometer system C-VOR 150 (Malvern instruments, Malvern, Worcestershire WR141XZ, United Kingdom) with 20 mm diameter parallel plate geometry through a single shear model. The test was operated at 25 ℃ temperature with 0.05/s shear rate and 500 μm gap size.

5.3.8 Computer Simulation

Atomistic replica exchange molecular dynamics (REX-MD) simulations were carried out in an optimized GBSW implicit solvent protein force field[30] to characterize the conformational properties of monomeric peptides. REX is an advanced sampling technique that has proven very powerful in simulating protein conformational equilibrium.[31] The basic idea is to simulate multiple independent replicas of the system at different temperatures. Periodically, replicas attempt to exchange simulation temperatures according to a Metropolis criterion that preserves the detailed balance and ensures proper canonical ensembles at all temperatures. The resulting random walk in the temperature space helps the system to avoid being kinetically trapped in states of local energy minima and thus enhances conformational sampling. Implicit treatment of solvent reduces the system size about tenfold compared to traditional explicit solvent simulation, and thus further facilitates sampling of accessible conformations.[32] Importantly, this optimized GBSW force field is able to reproduce the experimental structures and stabilities of a wide range of helical peptides, β-hairpins, and mini-proteins.[30] The same force field also has been applied successfully to describe the conformational equilibria of several proteins under stable and unstable conditions.[33-37] Therefore, the force field is particularly suitable for modeling highly unstructured peptides such as those investigated in this study.

The REX-MD simulations were performed using the Multiscale Modeling Tools for Structural Biology (MMTSB) toolset[38] along with CHARMM.[39,40] For each peptide, an extended conformation was first generated using CHARMM, and then used to initiate a 28-ns REX-MD simulation. For each REX-MD run, eight replicas were distributed exponentially within a temperature range of 300 to 500K. Exchange of simulation temperatures between neighboring replicas was attempted after every 2 ps. Analyses were conducted based on the structure

ensembles sampled at 300K using CHARMM. All properties examined in this work are well converged (see Figure 5.1), and the final distributions reported are derived from the last 20 ns of sampling.

5.4 Results and Discussion

Table 5.1 lists the sequences and molecular weight of amphiphilic peptides studied. Although these peptides have the same hydrophobic and hydrophilic domains, the difference in conformational flexibilities introduced by the turning segments significantly influence the peptide monomer structure (Figure 5.2), such as radius of gyration, distance between the N and C termini, and angle between these two domains, which are further correlated to aggregation kinetics and the finial supramolecular assembly morphology. Under neutral pH, lysine residues are positively charged. The amphiphilic peptide L5K10 showed an amorphous aggregation of the interconnected ribbon network in water (Figure 5.3a). The electrostatic repulsion of charged polylysine domain was believed to contribute to the fast orientation of peptide monomers. Similar as other fiber-like morphology of peptide-based materials,[41] separation of hydrophobic and hydrophilic domains helps peptides rapid hydrophobic collapse. This aggregation through hydrophobic interaction could minimize the exposure of hydrophobic groups to aqueous environment. The CD spectrum (Figure 5.4a) shows that L5K10 has a largely random coil secondary structure in solution, with a negative peak at 196 nm. In addition, the shoulder at 215 nm is indicative of some β-turn conformation, which is confirmed by the 1668 cm^{-1} peak showing in the FT-IR data (Figure 5.4c). Even though γ-branched hydrophobic amino acids such as leucine have a substantial propensity to form α-helical conformations,[42-44] L5 as a short domain next to the oligolysine segment could remain disordered.[44, 45]

With the flexible turning segment GSII inserted between L5 and K10 domains, peptide L5GSIIK10 assembled into a flat sheet-like morphology in aqueous solution (Figure 5.3c). Analysis of the higher magnification (inset of Figure 5.3c) revealed that formation of this flat sheet structure might be based on the anisotropic aggregation of the peptide molecules. This is different from other reported sheet assemblies built from a highly ordered arrangement of molecular monomers.[27,46] For example, a 16 residue peptide EAK16 $((AEAEAKAK)_2)$[46] was found to spontaneously assemble as an insoluble macroscopic membrane with the addition of salt in water. These peptides adopted a stable β-sheet structures which then stacked into sheet-like

morphology under the complementary ionic bonds between lysine and glutamic acid as well as the hydrophobic bonds between antiparallel holdings of alanine residues.[46] Instead of stabilizing the monomer structure for rapid hydrophobic attraction, in our case, the flexibility of the GSII turning segment seems to increase the heterogeneity of peptide monomeric structure, which may disturb the peptide arrangement and slow the aggregation kinetics. The spectra data supports the change in secondary structure: the shift of the peak from 1668 to 1654 cm^{-1} in FT-IR (Figure 5.4c) further suggests a decrease of β-turn structure and a simultaneous increase of α-helical conformation. Interestingly, with the fixed and sharp truning segment, L5P^{D}PK10 assembles into spherical aggregates of 20 to 150 nm diameter in aqueous solution (Figure 5.3e). It has been recognized that spherical aggregation is one of the most common strategies to effectively embed hydrophobic domain for rapid peptide self-assembly.[47-49] Also, amphiphilic peptide with cone shape structure has been reported having a spherical assembly tendency.[50] The P^{D}P segment appears to restrict the angle between L5 and K10 and force the peptide to adopt a cone shape. A small increase in intensity of a positive peak at 215 nm in CD spectrum (Figure 6.3a) supports the elevation of the β-turn structure.

To further understand the observed difference in assembly morphology, we combined an implicit solvent protein force field and REX-MD advanced sampling to calculate atomistic conformational ensembles of monomeric peptides in aqueous solution. Key conformational properties derived from the calculated ensembles are summarized in Figure 5.5. Clearly, in agreement with the CD measurements, all three peptides are largely disordered with small residual secondary structures, with L5K10 displaying the highest β-content (Figure 5.5c-d). However, important differences in conformational heterogeneity exist among these three peptides. In particular, both L5K10 and L5P^{D}PK10 display narrow distributions of the angle between L5 and K10 segments (see Figure 5.5 caption for the angle definition), centered around 60 °and 40 °, respectively (Figure 5.5a). In contrast, monomeric L5GSIIK10 was predicted to adopt a much more heterogeneous ensemble of conformations, with two dominant angles between L5 and K10 near 60 °and 120 °. Consistent with the angle distribution, L5GSIIK10 is the least compact with the largest radius of gyration compared to L5K10 and L5P^{D}PK10 (Figure 5.5b). These differences in the conformational properties of monomeric peptides suggest that the conformational flexibility of an amphiphilic peptide, as modulated by the turning sequence, might play a key role in controlling the morphology of supramolecular assembly. With greater

conformational heterogeneity (and chain entropy), peptide like L5GSIIK10 should assemble at a slower rate compared to L5K10 and L5P^{D}PK10, and such reduced assembly kinetics may be required for anisotropic growth to form the observed sheet morphology.

To test the importance of kinetics in control of the assembly morphology, we first characterized peptide assemblies in 10 mM NaOH. Higher pH deprotonates lysine side chains and reduces the electrostatic repulsion between peptides. Consequently, one expects greater aggregation propensity and higher growth rates, which should discourage growth anisotropic assemblies with slow aggregation rate such as the sheet morphology but promote the fiber or spherical-like morphology which is preferred for rapid hydrophobic collapse. Indeed, for L5GSIIK10, the flat sheet structure observed under neutral pH was replaced by filament amorphous aggregation (Figure 5.3d). While real-time monitoring of the continuous aggregation process is challenging, we used TEM to image the morphological evolution of the peptide aggregates under both neutral and high pH conditions every 30 minutes after the sample preparation (Figure 5.6). The results show that, immediately after fresh sample preparation (time=0 min), the L5GSIIK10 peptides were distributed as amorphous structures, with some aggregations (Figure 5.6a). With 30 minutes' incubation time (t=30 min), peptide molecules appeared to associate with each other and more aggregations were observed (Figure 5.6a). Likely due to the electrostatic repulsion between positively charged lysine side chains, these aggregates appear able to remain largely dispersed in the solution for substantial period. At t=60 min, amorphous aggregates appeared to conglomerate to form flat amorphous structures, which formed flat, sheet-like assemblies at time=120 min (Figure 5.6a). Interesting, such transition phenomena from sphere to sheet has also been reported in a peptoid polymer with 36 residues[27]: at initial mixing, hydrophobic collapse and electrostatic attraction lead to a rapid formation of spheres; after 4 hours, some spheres begin to form a planar sheet-like structure; and this structure finally re-organizes into a well-defined sheet by 6 hours of mixing. In this study, we suggest that the conformational flexibility along with hydrophobic collapse and electrostatic repulsion, which relates to the aggregation kinetics, could be one of the most important factors influencing the rapid aggregation and slow re-ordering process for sheet-like morphology. In contrast, the L5GSIIK10 peptide quickly formed an extended aggregate network after it was dissolved in 10 mM NaOH solution (Figure 5.6b), and formed the filament structure within 30 minutes. Similar rapid aggregations were observed for L5K10 and L5P^{D}PK10 peptides to form fiber and

spherical-like morphologies in aqueous solution with or without pH adjustment (Figure 5.3b,f and Figure 5.7). In L5K10 solution, nanofibers with 10 nm in width and from 100 nm up to several micrometers in lengths were found (Figure 5.3b). While, the L5P^{D}PK10 still maintained its spherical structure with nearly uniform size distribution between 10 and 40 nm (Figure 5.3f) in 10 mM NaOH. The secondary structure (Figure 5.4b, d) of both peptides in water and NaOH solution are β structure dominating with some α-helical structure of L5K10 in basic condition by showing the peak at 1653 cm^{-1} in FT-IR. The secondary structure of peptide has no direct relation with the TEM observation but confirms the peptide monomeric structure from computer simulation.

Interestingly, the CD spectrum (Figure 5.8a) suggests that the secondary structure of L5GSIIK10 peptide did not change with time during the assembly processes in either water or NaOH solution. Similar random structures were dominated in both conditions by showing the negative peaks at 197 nm and 199 nm, respectively. Although the slight higher order structure performed in NaOH solution, which may because the decrease of the electrostatic repulsion, this structural similarity is consistent with the notion of kinetics-induced morphological change. Therefore, the hydrophobic collapse, one of the most significant factors to dominate the peptide assemble kinetics, was expected to largely contribute to the growth rates and morphological differences of L5GSIIK10 peptide in water and NaOH solution.

To demonstrate this, the contact angles of L5GSIIK1 solutions on a hydrophobic HDPE surface were measured. The hydrophobic-hydrophobic interaction between peptide and HDPE surface not only affect their solid and liquid wetting but also reflect the peptide-peptide hydrophobic collapse in solution.[51,52] For L5GSIIK10, the contact angle was significant higher in NaOH solution than that in water (Figure 5.8b), which suggests more hydrophilic groups (charged oligolysine segment, K10) were oriented toward water phase in neutral condition, leading to a better wetting between water and peptide attached HDPE surface (Figure 5.8c). On the other hand, the deprotonated lysine side chains of L5GSIIK10 in NaOH solution promoted the peptide-peptide interaction through oligolysine segments (Figure 5.8c). The higher contact angle was induced by a greater number of oligolysine segments in contact with the HDPE hydrophobic surface. This result reflects the stronger hydrophobic collapse of L5GSIIK10 peptides in NaOH solution and is consistent with their faster growth rate. In contrast, both L5K10 and L5PPK10 presented higher contact angle values in either water or NaOH solution

(Figure 5.8b). The contact angle of each L5K10 and L5PPK10 was around 73 degree and had no significant differences ($p > 0.05$) in either water or NaOH solution, which is consistent with their partial morphological preservation (Figure 5.3b, f). Figure 5.8d shows that the viscosity of L5GSIIK10 in NaOH solution increased with peptide concentrations, indicating the expansion of its fiber like network structure.[53, 54] In contrast, the viscosity of L5GSIIK10 in water decreased with peptide concentrations (Figure 5.8d). The electrostatic repulsion and lower growth rate allow peptides flat sheet to arrange into a stable compact or folding structure, which reduced the shear resistance of the solution.

According to the discussion above, the conformational flexibility introduced by the turning sequences such as GSII between hydrophobic and hydrophilic domains might play an important role on the kinetics of peptide anisotropic assembly or rearrangement, and consequently result in the flat sheet morphology. To further validate this mechanism, we chose to insert different number of glycine residues between L5 and K10 segments as a direct way of gradually modulating the peptide conformational flexibility and, consequently, assembly kinetics and final morphologies. Four sequences, L5GK10, L5G2K10, L5G3K10, and L5G4K10 (Table 5.1), were examined. CD spectrum suggested all four peptides had partial β-turn structure by showing peaks at 196 and 215 nm (Figure 5.9a). This β-content secondary conformation was further supported by FT-IR with a peak around 1630 cm^{-1} and a broad peak from 1640 to 1670 cm^{-1} (Figure 5.9c). Both CD and FT-IR are fully consistent with the predictions from atomistic simulations (Figure 5.10c-d). The simulation further predicted that the distribution of angles between L5 and K10 at neutral pH was around 20 ° for L5GK10, and gradually increases and becomes more heterogeneous with longer glycine inserts (Figure 5.10a). In particular, only L5G4K10 peptide displays conformational flexibility similar to that of peptide L5GSIIK10. Therefore, one would predict that only L5G4K10 might be capable of forming sheet-like assemblies. Indeed, in water under neutral pH, spherical aggregates of 10 to 50 nm in diameter were found in both L5GK10 and L5G2K10 solutions (Figure 5.11a, c), where L5G2K10 aggregates appeared to be slightly more amorphous than L5GK10. Anisotropic growth is more evident with an increasing number of glycine residues, and the flat sheet structure was obtained in L5G4K10 solution (Figure 5.11g). Similar to the case of L5GSIIK10, the sheet-like assembly is susceptible to elevated assembly rates such as when induced by higher pH. In 10 mM NaOH, all four peptides formed a ribbon network (Figure 5.11b, d, f, h), and ribbon widths increased

with the number of glycine residues. The shift of peaks from 1630 to 1624 cm^{-1} and appearance of the peak at 1674 cm^{-1} in FT-IR indicate the secondary structure of these four peptides performed more β structures in 10 mM NaOH solution (Figure 5.9d). The structure change was also confirmed with the CD spectrum data by showing the shoulder at 221 nm (Figure 5.9b). These data further support that turning sequence flexibility and pH modulation of amphiphilic peptides can modulate the morphology of supramolecular assembly by regulating the aggregation kinetics.

5.5 Conclusions

The conformational properties of monomeric peptides were modulated by inserting linker regions with different levels of flexibility between the hydrophobic and hydrophilic domains of a series of diblock amphiphilic peptides. The important relationship between the conformational flexibility of individual peptides and the supramolecular morphologies of peptide aggregations was revealed by a combination of experiment and simulation: the propensity of the anisotropic aggregation of flat sheet structure increases with greater conformational heterogeneity of the monomer state. We suggest that the kinetics of peptide aggregation play a key role in controlling the morphology of supramolecular assembly. For example, increasing assembly rates such as those induced by high pH suppressed sheet-like assembly. Our current work not only yields new insights into devising rational strategies to modulate peptide supramolecular assembly mophology, but also provides a set of novel model systems for future mechanistic investigation of peptide aggregation and self-assembly.

5.6 Acknowledgments

We thank Dr. Dan Boyle (Department of Biology, Kansas State University) for TEM use, Dr. John Tomich (Department of Biochemistry, Kansas State University) for CD use, and the University of Kansas Mass Spectrometry Lab for HPLC and mass spectrometric analysis. Funding for this work was provided by the Targeted Excellence Program and Center for Biobased Polymers by Design at Kansas State University, and by the National Science Foundation through a CAREER Award (MCB 0952514) to Jianhan Chen. This work is contribution no. 11-268-J from the Kansas Agricultural Experiment Station.

5.7 References

1. Toksoz, S.; Guler, M. O. Self-assembled peptide nanostructrures. Nano Today 2009, 4, 458-469.

2. Liu, J.; Zhao, X. Design of self-assembling peptides and their biomedical applications. Nanomedicine 2011, 6, 1621-1643.

3. Cavalli, S.; Albericio, F.; Kros, A. Amphiphilic peptides and their cross-disciplinary role as building blocks for nanoscience. Chem. Soc. Rev. 2010, 39, 241-263.

4. Zhang, S. Nat. Fabrication of novel biomaterials through molecular self-assembly. Biotechnol. 2003, 21, 1171-1178.

5. Langer, R.; Tirrell, D. A. Designing materials for biology and medicine. Nature 2004, 428, 487-492.

6. Lee, K. Y.; Mooney, D., J. Hydrogels for Tissue Engineering. Chem Rev. 2001, 101, 1869-1879.

7. Zhao, X; Zhang, S. Designer self-assembling peptide materials. Macromol. Biosci. 2007, 7, 13-22.

8. Jabbari, E. Bioconjugation of hydrogels for tissue engineering. Curr. Opin. Biotechnol. 2011, 22, 655-660.

9. Kyle, S; Aggeli, A.; Ingham, E.; McPherson, M. J. Production of self-assembling biomaterials for tissue engineering. Trends Biotechnol. 2009, 27, 423-433.

10. Mooney, B. J.; Fairman, R. Peptides as materials. Curr. Opin. Struct. Biol.2009, 19, 483-494.

11. Kanazawa, H.; Okano, T. Temperature-responsive chromatography for the separation of biomolecules. J. Chromatogr. A 2011, 1218: 8738-8747.

12. Sato, K.; Yoshida, K.; Takahashi, S.; Anzai, J. pH- and sugar-sensitive layer-by-layer films and microcapsules for drug delivery. Adv. Drug Deliv. Rev. 2011, 63: 809-821.

13. Roy, S.; Lessing, J.; Meisl, G.; Ganim, Z.; Tokmakoff, A.; Knoester, J.; Jansen, T. L. C. Solvent and conformation dependence of amide I vibrations in peptides and proteins containing proline. J. Chem. Phys. 2011, 234507-234517.

14. Vaitheeswaran, S.; Chen, J.; Thirumalai, D. Hydrophobic and ionic-interactions in bulk and confined water with implications for collapse and folding of proteins. J. Stat. Phys. 2011, 145, 276-292.

15. Taraballi, F.; Campione, M.; Sassella, A.; Vescovi, A.;Paleari, A.; Hwang, W.; Gelain, F. Effect of functionalization on the self-assembling propensity of β-sheet forming peptides. Soft Matter 2009, 5: 660-668.

16. Matson, J. B.; Stupp, S. I. Self-assembling peptide scaffolds for regenerative medicine. Chem. Commun. 2012, 48:26-33.

17. Chen, C.; Hu, J.; Zhang, S.; Zhou, P.; Zhao, X.; Xu, H.; Zhao, X.; Yaseen, M.; Lu, J. Molecular mechanisms of antibacterial and antitumor actions of designed surfactant-like peptides. Biomaterials, 2012, 33: 592-603.

18. Ryan, D.M.; Nilsson, B. L. Self-assembled amino acids and dipeptides as noncovalent hydrogels for tissue engineering**.** Polym. Chem. 2012, 3: 18-33

19. Rajangam, K.; Arnold, M. S.; Rocco, M. A.; Stupp, S. I. Peptide Amphiphile Nanostructure-Heparin Interactions and their Relationship to Bioactivity. Biomaterials. 2008, 29, 3298-3305.

20. Dagads, Y. S.; Tombuloglu, A.; Tekinay, A. B.; Dana, A.; Guler M. O. Interfiber interactions alter the stiffness of gels formed by supramolecular self-assembled nanofibers. Soft Matter 2011, 7, 3524-3532.

21. Banwell, E. F.; Abelardo, E. S,.;Adams, D. J.; Birchall, M. A.; Corrigan, A.; Donald, A. M.; Kirkland, M.; Serpell, L. C.; Butler, M. F.; Woolfson, D. N. Rational design and application of responsive α-helical peptide hydrogels. Nature Mater. 2009, 8, 596-600.

22. Bellomo, E. G.; Wyrsta, M. D.; Pakstis, L.; Pochan, D. J.; Deming, T. J. Stimuli-responsive polypeptide vesicles by conformation-specific assembly. Nat. Mater. 2004, 3, 244-248.

23. Branco, M. C.; Nettesheim, F.; Pochan, D. J.; Schneider, J. P.; Wagner, N. J. Fast Dynamics of Semiflexible Chain Networks of Self-Assembled Peptides. Biomacromolecules 2009, 10, 1374-1380.

24. Saiani, A.; Mohammed, A.; Frielinghaus, H.; Collins, R.; Hodson, N.; Kielty, C. M.; Sherratt, M. J.; Miller, A. F. Self-assembly and gelation properties of α-helix *versus* β-sheet forming peptides. Soft Matter 2009, 5, 193-202.

25. Huang, H.; Shi, J.; Laskin, J.; Liu, Z.; McVey, D. S.; Sun, X. Design of a shear-thinning recoverable peptide hydrogel from native sequences and application for influenza H1N1 vaccine adjuvant. Soft matter, 2011, 7, 8905-8912.

26. Amino acid Lysine with a long hydrophobic aliphatic chain is not purely polar; however, the L5K10 peptide serial with one end (K10) much more polar than the other (L5) should be still amphiphilic. The implicit solvent simulations indeed suggest that the peptides have strong tendencies to adopt collapse forms despite of heavily charged K10 side chains.

27. Nam, K. T.; Shelby, S. A.; Choi, P. H.; Marchiel, A. B.; Chen, R.; Tan, L.; Chu, T. K.; Mesch, R. A.; Lee, B.; Connolly, M. D.; Kisielowski, C.; Zuckermann, R. N. Free-floating ultrathin two-dimensional crystals from sequence-specific peptoid polymers. Nat. Mater. 2010, 9, 454-460.

28. Brahms, S.; Brahms, J. Determination of protein secondary structure in solution by vacuum ultraviolet circular dichroism. J. Mol. Biol. 1980, 138: 149-178.

29. Pistorius, M. A.; DeGrip, W.J. Deconvolution as a tool to remove fringes from an FT-IR spectrum. Vib. Spectrosc. 2004, 36, 89-95.

30. Chen, J. H.; Im, W. P.; Brooks, C. L. Balancing Solvation and Intramolecular Interactions: Toward a Consistent Generalized Born Force Field. J. Am. Chem. Soc, 2006, 128, 3728-3736.

31. Sugita, Y.; Okamoto, Y. Replica-exchange molecular dynamics method for protein folding. Chem. Phys. Lett.1999, 314, 141-151.

32. Chen, J. H.; Brooks, C. L.; Khandogin, J. Recent advances in implicit solvent based methods for biomolecular simulations. Curr. Opin. Struc. Biol. 2008, 18, 140-148.

33. Khandogin, J.; Chen, J. H.; Brooks, C. L. Exploring atomistic details of pH-dependent peptide folding. Proc. Natl. Acad. Sci. USA. 2006, 103, 18546-18550.

34. Khandogin, J.; Brooks, C. L. Linking folding with aggregation in Alzheimer's β-amyloid peptides. Proc. Natl. Acad. Sci. USA. 2007, 104, 16880-16885.

35. Khandogin, J.; Raleigh, D. P.; Brooks, C. L. Folding Intermediate in the Villin Headpiece Domain Arises from Disruption of a N-Terminal Hydrogen-Bonded Network. J. Am. Chem. Soc. 2007, 129, 3056-3057.

36. Chen, J. H. Intrinsically Disordered p53 Extreme C-Terminus Binds to S100B(ββ) through "Fly-Casting". J. Am. Chem. Soc. 2009, 131, 2088-2089.

37. Ganguly, D.; Chen, J. Atomistic details of the disordered states of KID and pKID. Implications in coupled binding and folding. J. Am. Chem. Soc. 2009, 131, 5214-5223.

38. Feig, M.; Karanicolas, J.; Brooks, C. L. MMTSB Tool Set: enhanced sampling and multiscale modeling methods for applications in structural biology. J. Mol. Graph. Model. 2004, 22, (5), 377-395.

39. Brooks, B. R.; Bruccoleri, R. E.; Olafson, B. D.; States, D. J.; Swaminathan, S.; Karplus, M. CHARMM: A program for macromolecular energy, minmimization, and dynamics calculations. J. Comput. Chem. 1983, 4, 187-217.

40. Brooks, B. R.; Brooks, C. L.; Mackerell, A. D.; Nilsson, L.; Petrella, R. J.; Roux, B.; Won, Y.; Archontis, G.; Bartels, C.; Boresch, S.; Caflisch, A.; Caves, L.; Cui, Q.; Dinner, A. R.; Feig, M.; Fischer, S.; Gao, J.; Hodoscek, M.; Im, W.; Kuczera, K.; Lazaridis, T.; Ma, J.; Ovchinnikov, V.; Paci, E.; Pastor, R. W.; Post, C. B.; Pu, J. Z.; Schaefer, M.; Tidor, B.; Venable, R. M.; Woodcock, H. L.; Wu, X.; Yang, W.; York, D. M.; Karplus, M. CHARMM: The Biomolecular Simulation Program. J. Comput. Chem. 2009, 30, 1545-1614.

41. Carullaa, N.; Zhou, M.; Arimon, M.; Gairi, M.; Giralt, E.;Robinson, C. V.; Dobson, C. M. Experimental characterization of disordered and ordered aggregates populated during the process of amyloid fibril formation. Proc. Natl. Acad. Sci. USA 2009, 106: 7828-7833.

42. Nowak, A. P.; Breedveld, V.; Pakstis, L.; Ozbas, B.; Pine, D. J.; Pochan, D.; Deming, T. J. Rapidly recovering hydrogel scaffolds from self-assembling diblock copolypeptide amphiphiles. Nature 2002, 417, 424-428.

43. Xiong, H.; Buckwalter, B. L.; Shieh, H.; Hecht, M. H. Periodicity of polar and nonpolar amino acids is the major determinant of secondary structure in self-assembling oligomeric peptides. Proc. Natl. Acad. Sci. 1995, 92, 6349-6353.

44. Baumann, M. K.; Textor, M.; Reimhult, E. Understanding self-assembled amphiphilic peptide supramolecular structures from primary structure helix propensity. Langumir 2008, 24, 7645-7647.

45. Deming, T. J. Polypeptide hydrogels *via* a unique assembly mechanism. Soft Matter 2005, 1, 28-35.

46. Zhang, S.; Holmes, T.; Lockshin, C.; Rich, A. Spontaneous assembly of a self-complementary oligopeptide to form a stable macroscopic membrane. Proc. Natl. Acad. Sci. 1993, 90, 3334-3338.

47. Xu, X. D.; Jin, Y.; Liu, Y.; Zhang, X. Z.; Zhuo, R. X. Self-assembly behavior of peptide amphiphiles (PAs) with different length of hydrophobic alkyl tailsColloid Surface B 2010, 81: 329-335.

48. Huang, H.; Sun, X. Rational design of responsive self-assembling peptides from native protein sequences. Biomacromolecules, 2010, 11: 3390-3394.

49. Grzybowski, B. A.; Wilmer, C. E.; Kim, J.; Browne, K. P.;Bishop, K. J. M. Self-assembly: from crystals to cells. Soft Matter 2009, 5: 1110-1128.

50. Khoe, U.; Yang, Y.; Zhang, S. Self-assembly of nanodonut structure from a cone-shaped designer lipid-like peptide surfactant. Langmuir 2009, 25, 4111-4114.

51. Shera, J. N.; Sun, X. S. Effect of Peptide Sequence on Surface Properties and Self-Assembly of an Amphiphilic pH-Responsive PeptideBiomacromolecules 2009, 14, 2446-2450.

52. Yamamoto, H.; Sakai, Y.; Ohkawa, K. Synthesis and wettability characteristics of model adhesive protein sequences inspired by a marine mussel. Biomacromolecules 2000, 1, 543-551.

53. Ortman, K. C.; Agarwal, N.; Eberle, A. P. R.; Baird, D. G.; Wapperom, P.; Giacomin, A. J. Transient shear flow behavior of concentrated long glass fiber suspensions in a sliding plate rheometer. J. Non-Newton. Fluid Mech. 2011, 166: 884-895.

54. Fletcher, N. L.; Lockett, C. V.; Dexter, A. F. A pH-responsive coiled-coil peptide hydrogel. Soft Matter 2011, 7:10210-10218.

Figure 5.1 Convergence key conformational properties from REX-MD simulations. Peptides L5K10 (panels a & b) and L5GGGGK10 (panels c & d) are selected to represent the least and most flexible cases. The data show that the distributions are very similar using either the last 10 or 20 ns of REX-MD trajectories.

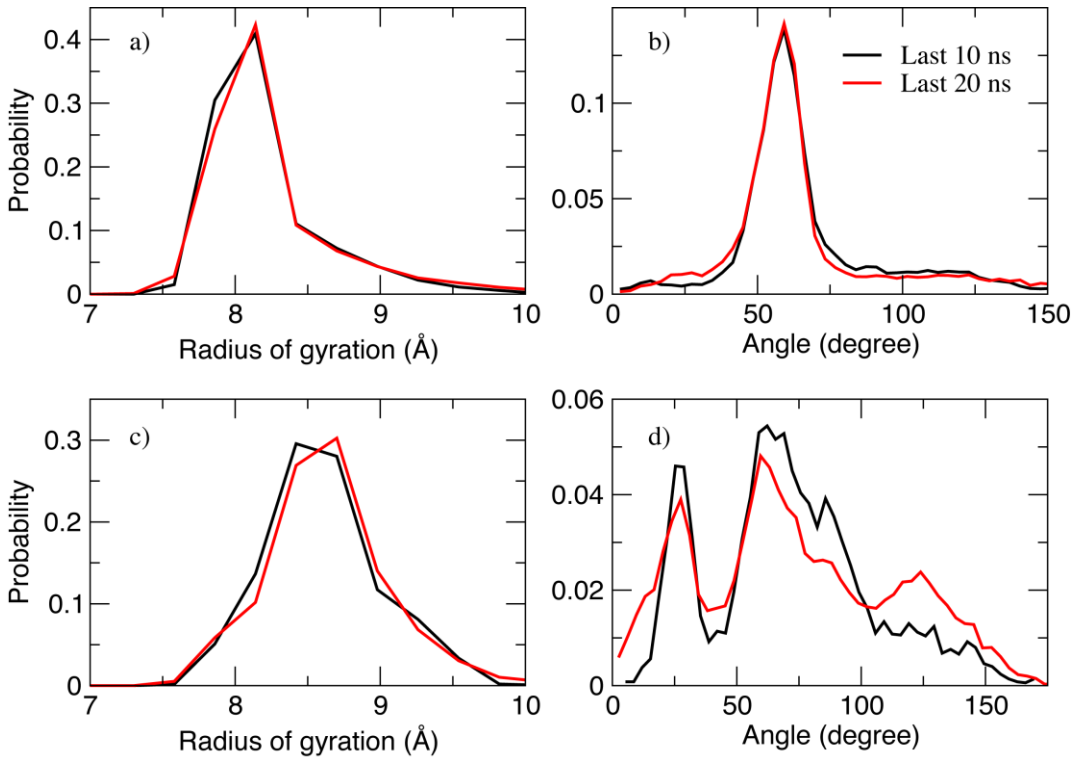

Figure 5.2 Ensembles of 10 representative monomer structures for each peptide listed in Table 5.1.

a. L5K10; **b.** L5GSIIK10; **c.** L5PDPK10; **d.** L5GK10; **e.** L5G2K10; **f.** L5G3K10; **g.** L5G4K10. In all figures, the N-terminal leucine residues are colored in purple, the C-terminal lysine residues in cyan, and the turns in green. All structures within the ensemble have been aligned using the five luecine resides. These ensembles illustrate the underlying conformational heterogeneities quantified by the probability distributions of the angles between L5 and K10 shown in Fig. 3 and Fig. 7.

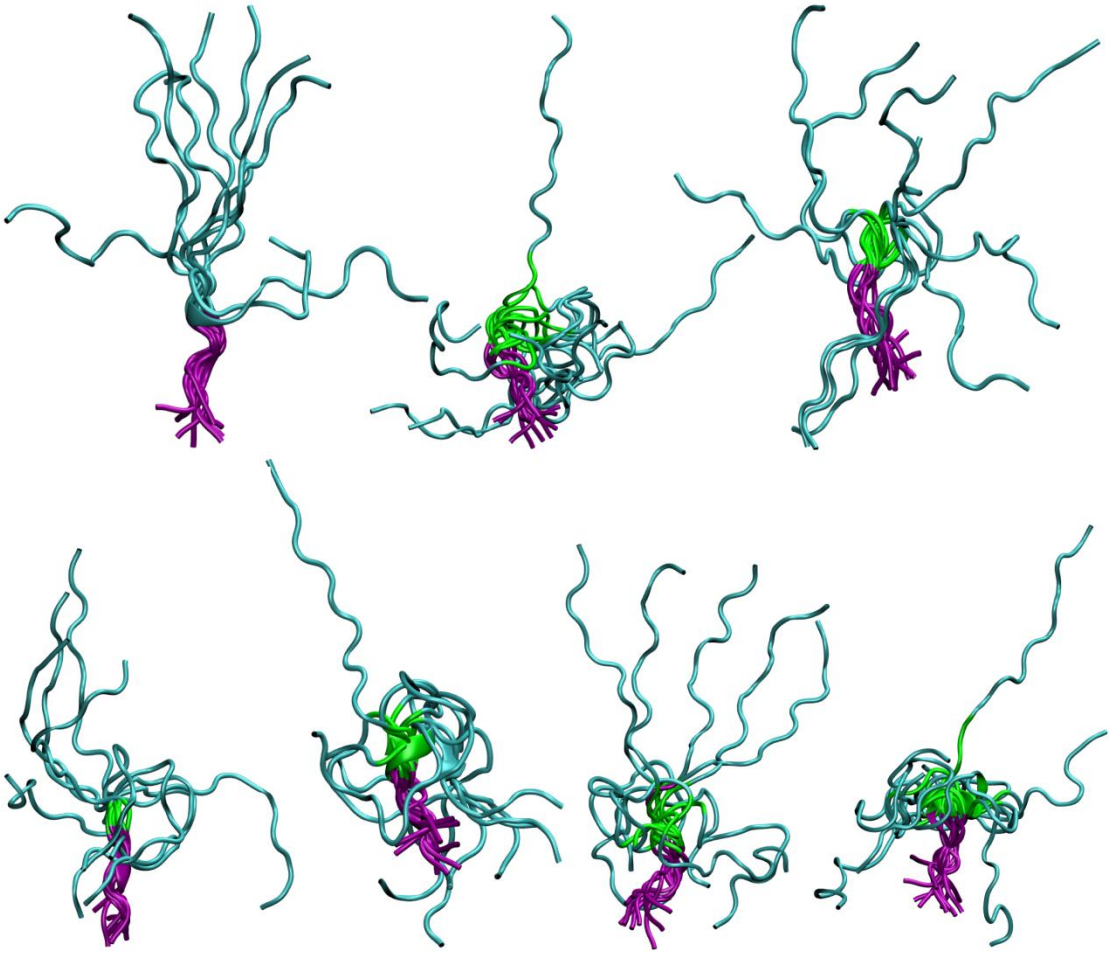

Figure 5.3 TEM images of peptide solutions in both water and 10 mM NaOH.

a. ribbon network of L5K10 in water, **b.** Nanofiber of L5K10 in basic condition, **c.** flat sheet structure of L5GSIIK10 in water, **d.** nanofiber aggregation of L5GSIIK10 in basic condition, **e., f.** spherical morphology of L5PDPK10 in both water (e) and 10 mM NaOH (f).

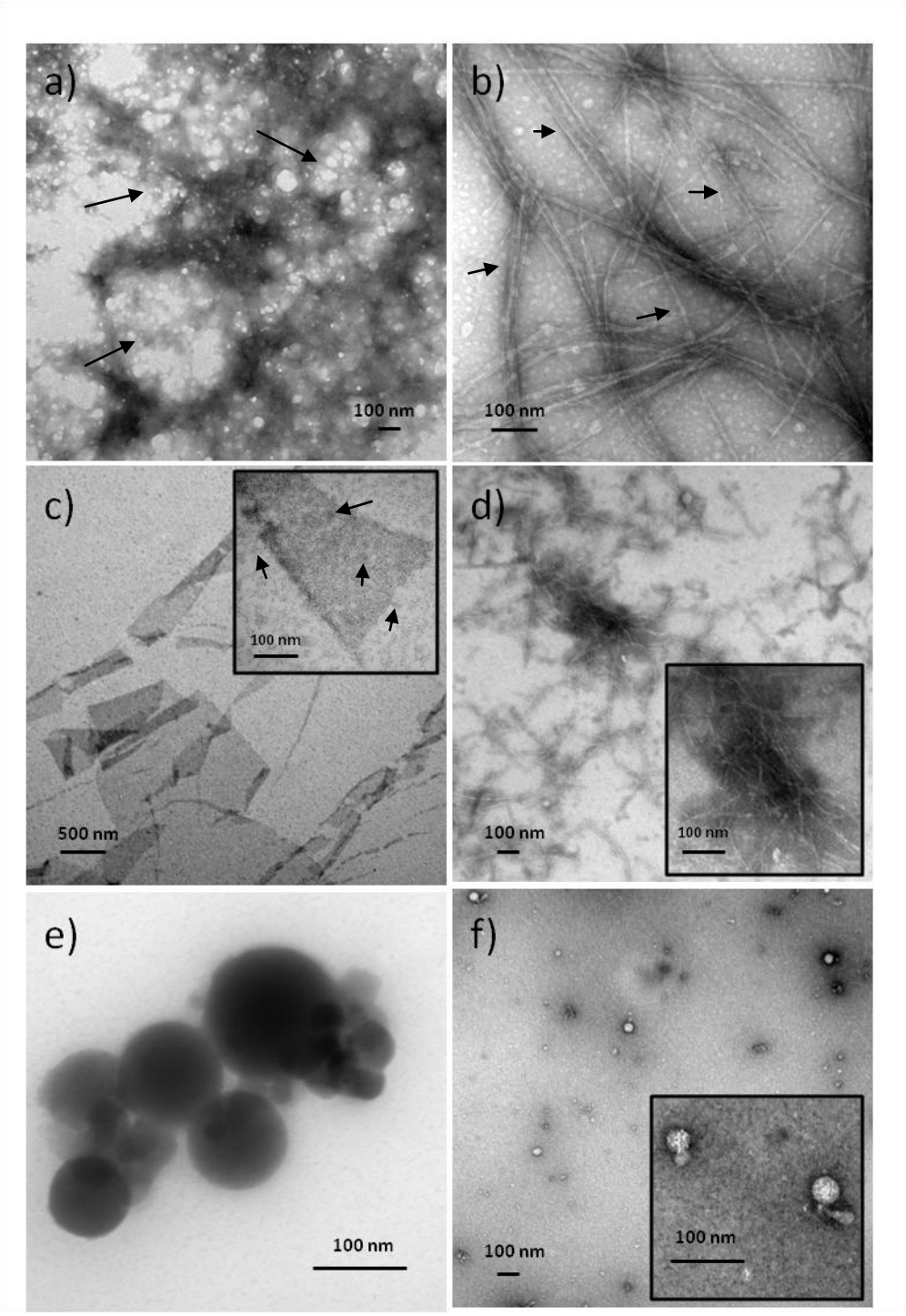

Figure 5.4 Secondary structure of peptides L5K10, L5GSIIK10, and L5PDPK10 in both neutral and basic conditions.

a, b. CD spectrum of peptides in water (a) and 10 mM NaOH (b), **c., d.** FT-IR analysis of peptides in neutral (c) and basic condition (d). (Each CD spectrum is the average value of five accumulations with 50 nm min-1 scanning speed).

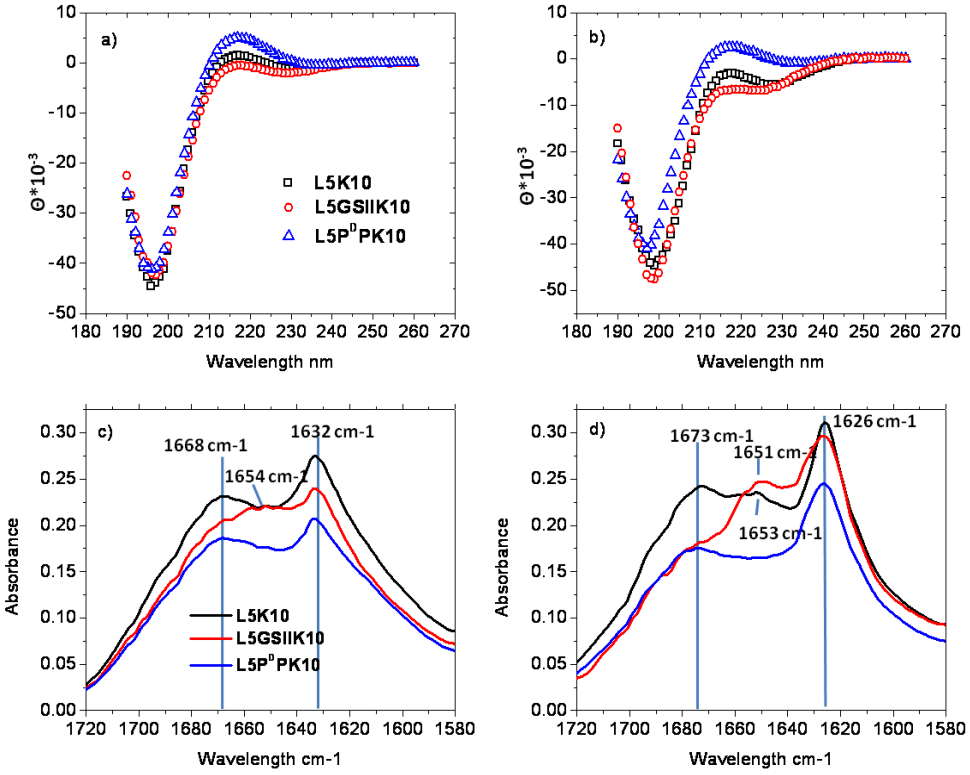

Figure 5.5 Key conformational properties of monomeric L5K10, L5GSIIK10, and L5PDPK10 in aqueous solution from REX-MD simulations.

a. radius of gyration, **b.** angle between L5 and K10, **c.** fraction of helical residues, and **d.** fraction of β-residues. The angle between L5 and K10 is calculated as the angle formed between the vector from Cα of the fifth leucine residue to the center of mass of L5 segment and a second vector from Cα of the first lysine residue to the center of mass of K10 segment.

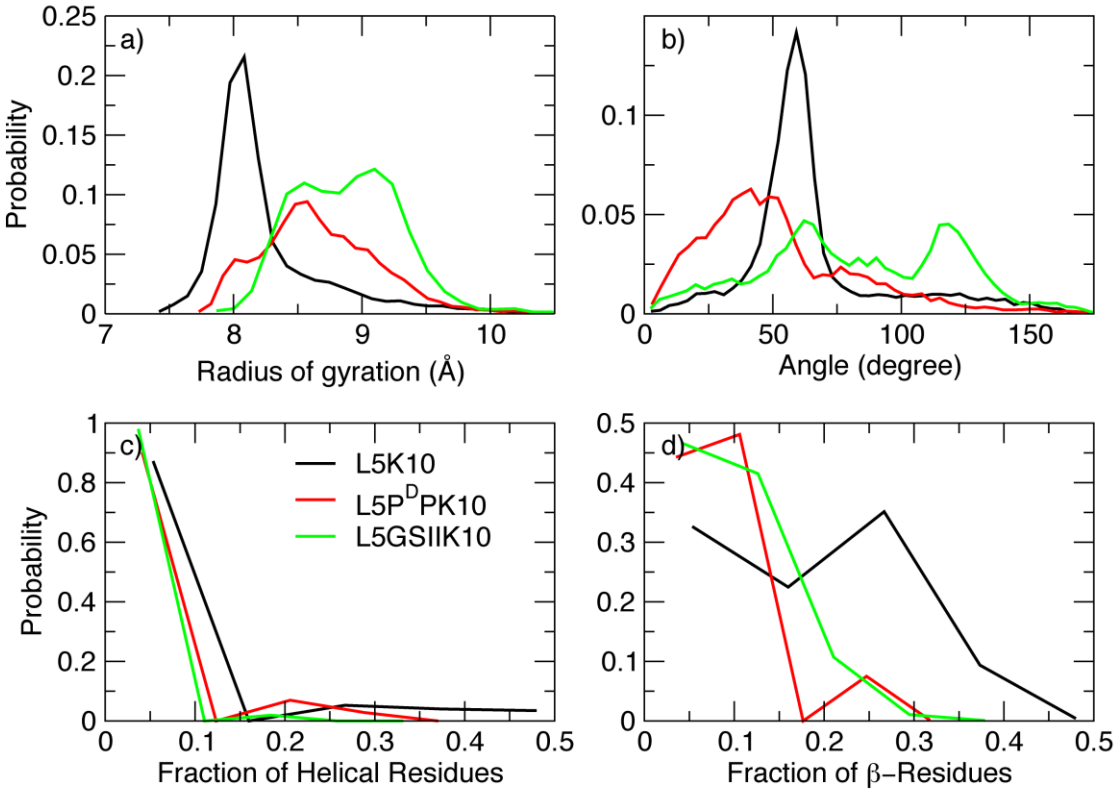

Figure 5.6 TEM images of L5GSIIK10 morphological growth in both water and 10 mM NaOH.

a. growth of flat sheet morphology of L5GSIIK10 in water from 0 min to 120 min, **b.** growth of fiber like amorphous morphology of L5GSIIK10 in NaOH solution from 0 min to 30 min.

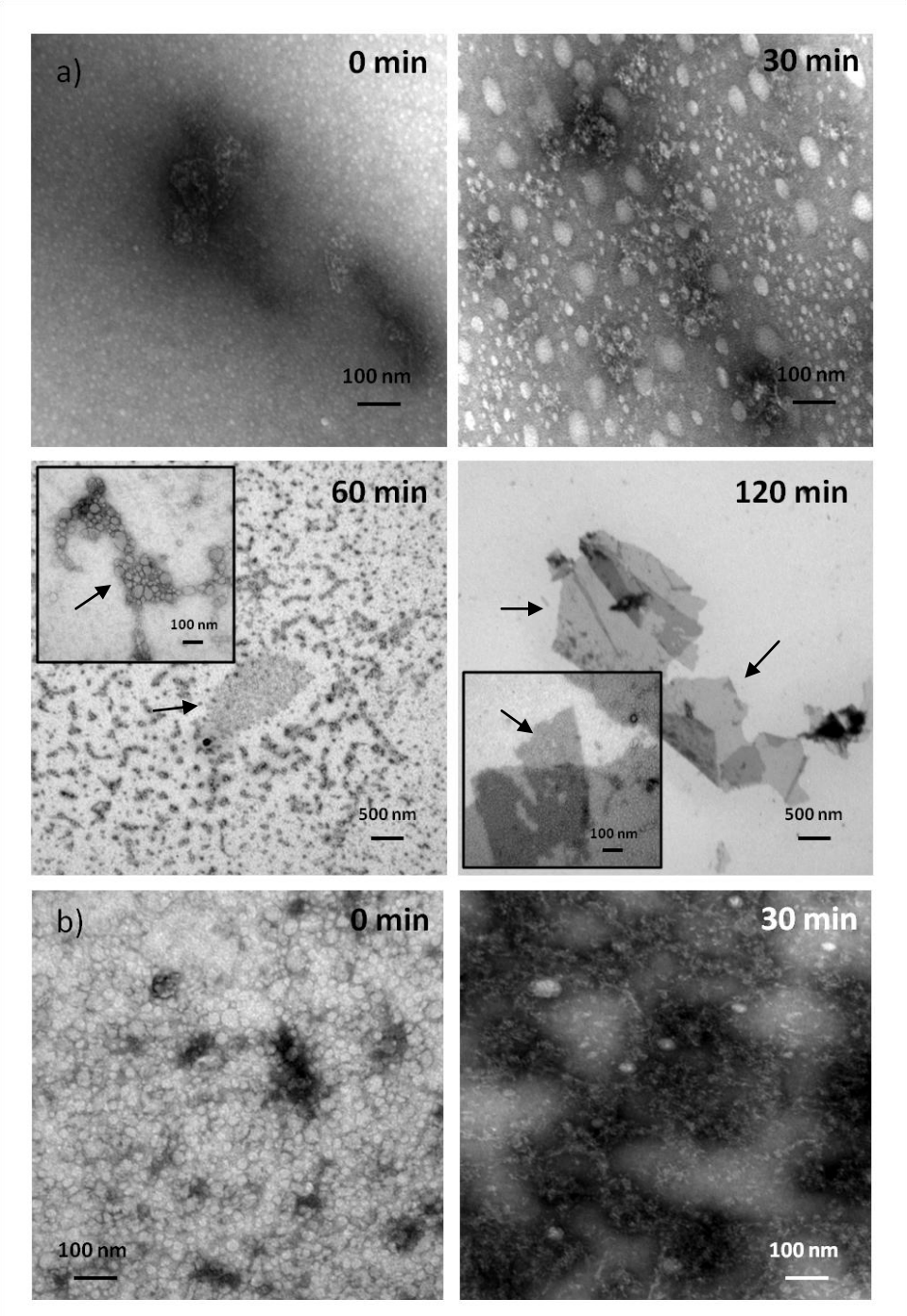

Figure 5.7 TEM images of L5K10 and L5PDPK10 morphological growth in water.
a., b. growth of fiber-like morphology of L5K10 in water from 30 min to 60 min; the finial morphology was stable at 60 min, **c., b.** growth of spherical morphology of L5PDPK10 in water from 0 min to 30 min; the finial morphology was stable within 30 min after mixing.

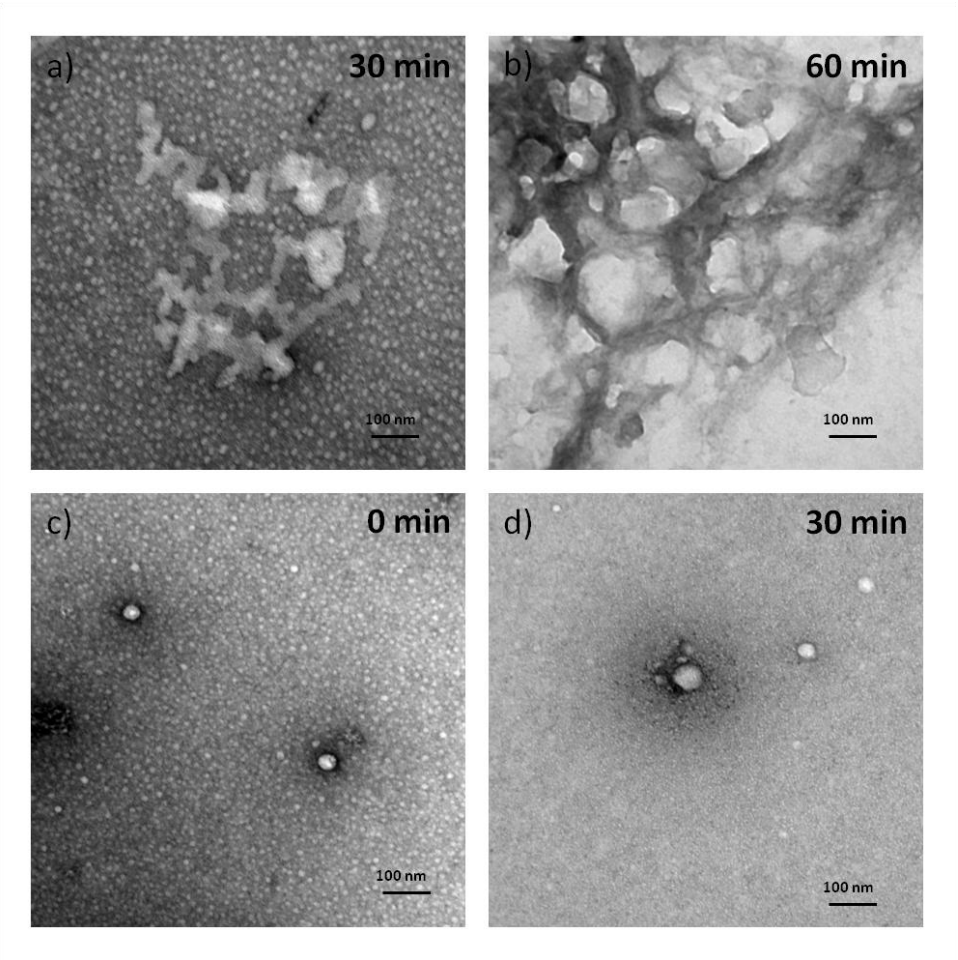

Figure 5.8 Secdonary structure, contact angle and viscosity of peptide in water and NaOH solution.

a. CD spectrum of L5GSIIK10 during the assembly processes, **b.** contact angle of L5K10, L5GSIIK10 and L5PDPK10 on HDPE (*p < 0.05), **c.** proposed mechanism of hydrophobic-hydrophobic association of L5GSIIK10 and HDPE surface, **d.** viscosity of L5GSIIK10 with 1%, 4% and 10% (w/v) concentrations in water and NaOH solution.

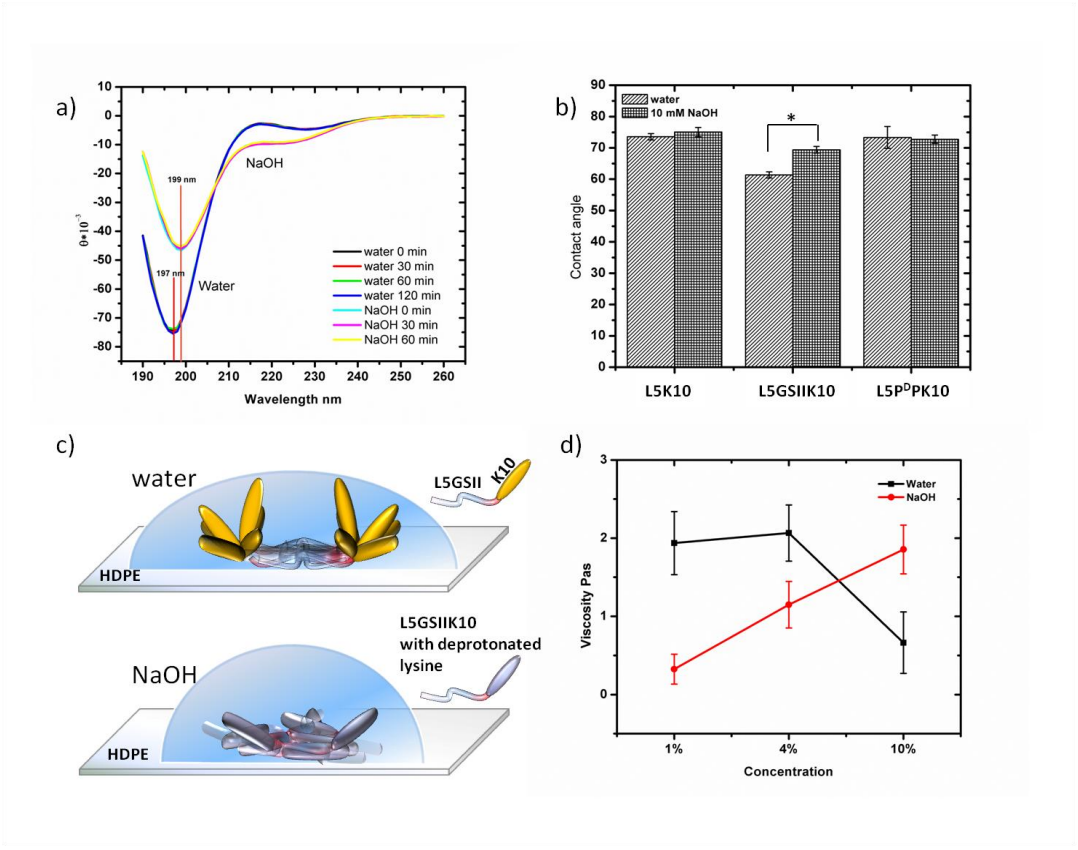

Figure 5.9 Secondary structure of peptides L5GK10, L5G2K10, L5G3K10, and L5G4K10 in both neutral and basic conditions.

a., b. CD spectrum of peptides in water (a) and 10 mM NaOH (b), **c., d.** FT-IR analysis of peptides in neutral (c) and basic condition (d). (Each CD spectrum is the average value of five accumulations with 50 nm min-1 scanning speed).

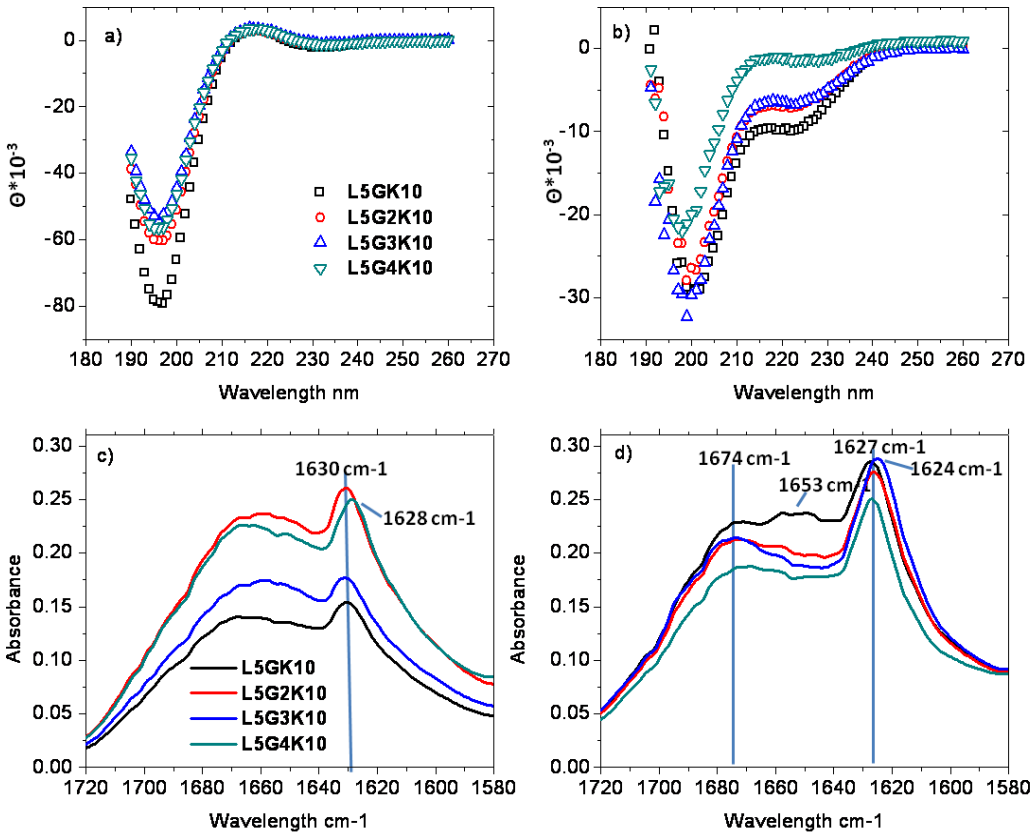

Figure 5.10 Key conformational properties of monomeric L5K10, L5GK10, L5GGK10, L5GGGK10 and L5GGGGK10 in aqueous solution from REX-MD simulations.

a. radius of gyration, **b.** angle between L5 and K10, **c.** fraction of helical residues, and **d.** fraction of β-residues. The angle between L5 and K10 is calculated as the angle formed between the vector from Cα of the fifth leucine residue to the center of mass of L5 segment and a second vector from Cα of the first lysine residue to the center of mass of K10 segment.

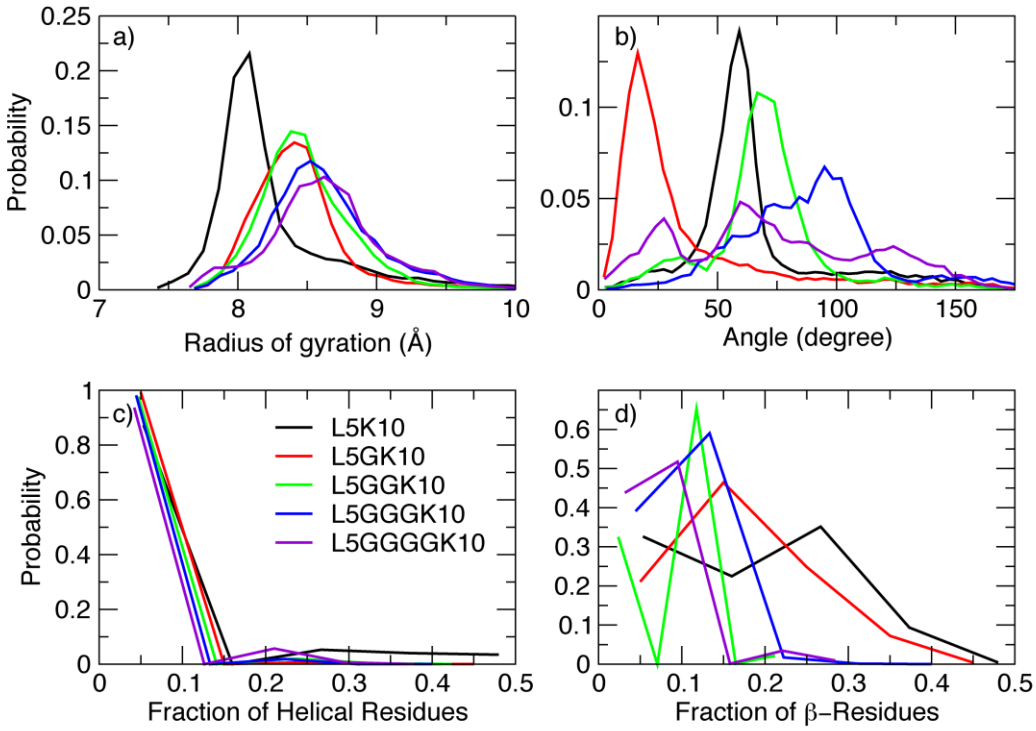

Figure 5.11 TEM images of peptides L5GK10, L5G2K10, L5G3K10 and L5G4K10 in both water and 10 mM NaOH.

a., c. spherical structure of L5GK10 (a) and L5G2K10 (c) in water, **b., d., f., h.** ribbon networks of L5GK10 (b), L5G2K10 (d), L5G3K10 (f) and L5G4K10 (h) in 10 mM NaOH with the widths increasing for more glycine residues, **e.** amorphous aggregation of L5G3K10 in water, **g.** flat sheet structure of L5G4K10 in water.

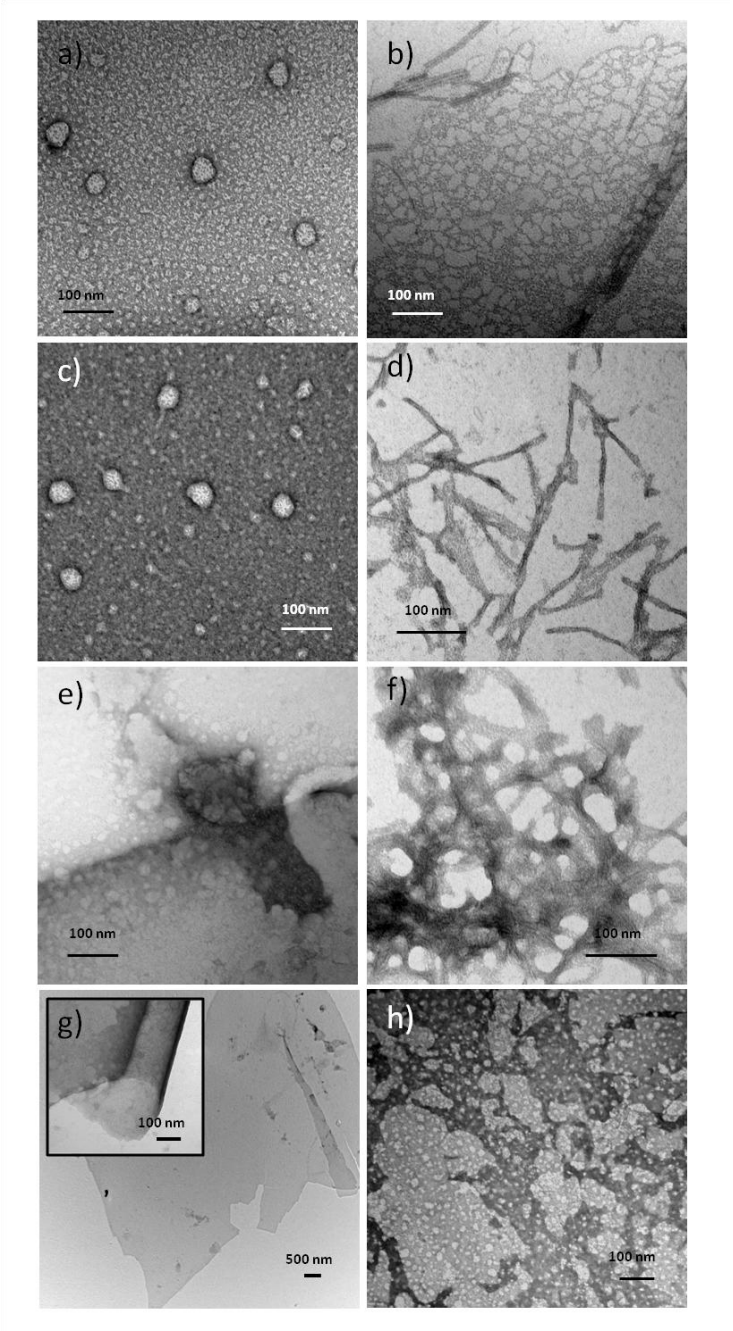

Table 5.1 Sequence and molecular weight of synthesis peptides with different turning segments.

Peptide name	Sequence	Molecular weight (Da)	Potential Flexibility
L5K10	LLLLL-KKKKKKKKKK	1864	Fixed turning
L5GSIIK10	LLLLL-GSII-KKKKKKKKKK	2235	Flexible turning
L5P^{D}PK10	LLLLL-P^{D}P-KKKKKKKKKK	2059	Sharp fixed turning
L5GK10	LLLLL-G-KKKKKKKKKK	1922	Fixed turning
L5G2K10	LLLLL-GG-KKKKKKKKKK	1979	Fixed turning
L5G3K10	LLLLL-GGG-KKKKKKKKKK	2036	Little flexible turning
L5G4K10	LLLLL-GGGG-KKKKKKKKKK	2093	Flexible turning

Chapter 6 - Structural Transformation and Physical Properties of a Hydrogel Forming Peptide Studied by NMR and TEM[4]

6.1 Abstract

Peptide-based hydrogels are attractive biological materials. Study of their self-assembly pathways from their monomer structures is important not only for undertaking the rational design of peptide-based materials, but also for understanding their biological functions and the mechanism of many human diseases relative to protein aggregation. In this paper, we have monitored the conformation, morphological and mechanical properties of a hydrogel-forming peptide during hydrogelation in different dimethylsulfoxide (DMSO)/H_2O solutions. The peptide shows nanofiber morphologies in DMSO/H_2O solution with a ratio lower than 4:1. Increased water percentage in the solution enhanced the hydrogelation rate and gel strength. 1D and 2D proton nuclear magnetic resonance (NMR) and electron microscopy studies performed on the peptide in DMSO/H_2O solution with different ratios indicate that the peptide monomer tends to adopt a more helical structure during the hydrogelation as DMSO/H_2O ratio is reduced. Interestingly, at the same DMSO/H_2O ratio, adding Ca^{2+} not only promotes peptide hydrogelation and gel strength, but also leads to special shear-thinning and recovery properties of the hydrogel. Without changing the peptide conformation, Ca^{2+} binds to the charged Asp residues and induces the change of interfiber interactions that play an important role in hydrogel properties.

6.2 Introduction

Peptide-based hydrogel is an attractive material for biological applications in tissue engineering, drug delivery, 3D cell culture (matrix substract for cell growth), and so on.[1-3] Understanding of how do the peptide, conformations, assembly properties, and dynamic behaviors respond to external parameters has led to the rational novel design of various peptide

[4] Results have been accepted. Huang, H.; Herrera, A. I.; Luo, Z.; Prakash, O.; Sun, X. S. Structural transformation and physical properties of a hydrogel forming peptide studied by NMR, TEM and dynamic rhemeter. Biophysical Journal, in press.

biomaterials.[4, 5] Recently, most artificial peptide hydrogels have been achieved by synthesizing peptide sequences with alternating charged and non-charged amino acids or blocks of hydrophobic and hydrophilic copolymers.[3, 6, 7] These designs allow the peptide monomers to fold into stable α-helical or β-sheet structures that separate the hydrophobic domain from the hydrophilic domain within a monomer. With hydrophobic association, peptide monomers (with filament forming potential) assemble as nanofibers and further cross-link to a network through interfiber interactions. The nanofiber and hydrogel-like formations in native systems such as collagen,[8] extracellular matrices, and the aggregation of amyliod peptides in Alzheimer's disease have characteristics similar to those of artificial peptides, but the formations rely on different protein sequences.[8-12] Because of the close relation of molecular function and molecular assembling structure, studying the self-assembly pathways of these native molecules is importent in understanding their biological functions and the mechanism of many human diseases.

In addition, many novel peptide designs have successfully incorporated biofunctionality, biocompatibility, and biodegradability into peptide hydrogel by modifying amino acid building blocks.[13-17] These biological properties have stimulated the development of hydrogels as injectable systems for potential biomaterial applications. Most prevalent injectable hydrogels have been designed as free-flowing solutions (such as MatrixGel). After syringe injection into the target location, the sol-gel transition of these peptide solutions could be triggered by physiological pH, temperature, or even photo-initiated hydrogelation. However the free-flowing injected system could cause the leakage of gel precursor solutions into neighboring tissue or the bloodstream.[18, 19] Since 2002, Pochan, Schneider, and coworkers have been developing a series of β-hairpin peptide hydrogels with special shear-thinning and rapid recovery properties[16, 20, 21] that provide an alternate strategy for injectable hydrogel therapies. The hydrogel scaffolds are fractured into small domains under proper shear stress, which leads to the Newtonian flowing properties. When the shear ceases, these hydrogel domains immediately percolate and cross-link into a network and recover the hydrogel behavior.

Interestingly, we found similar mechanical reversible properties in a peptide hydrogel from our laboratory in 2010.[22] The peptide sequence FLIVIGSIIGPGGDGPGGD (h9e) was designed from two peptide sequences taken from two functional native proteins: the FLIVIGSII segment of human muscle L-type calcium channel[23] and the $(GPGGX)_n$ segment of β-spiral motif of spider flagelliform silk protein[24, 25]. Asp was selected in X positions for Ca^{2+}-sensitive

nanofiber formation.[5] The h9e peptide could be induced to form two distinct hydrogels by adding Ca^{2+} (100 mM) and adjusting pH, respectively, and only the h9e Ca^{2+} hydrogel exhibited the special shear-thinning and rapid recovery properties.[22] This phenomenon excluded the effect of sequence difference on hydrogel properties and led us to focus on the effect of the peptide monomer self-assembly pathway and interfiber interactions on hydrogel shear thinning and rapid recovery properties. The native sequence of this peptide was outside the model of the regular artificial amphiphilic peptide; therefore, predicting a proposed self-assembly pathway from its primary and secondary structure became difficult. Thus, the objective of this chapter is to undertake the conformational study of the peptide monomer to understand the assembly of a peptide hydrogel and its interfiber interactions. We hypothesized that the h9e peptide could fold into an amphiphilic monomeric structure which self-assembles into nanofilament through hydrophobic interaction. We also hypothesized that the Ca^{2+} ions could affect the the interfiber interactions, which relate to the mechanical properties of peptide hydrogel.

Initially, we tried to use proton NMR spectroscopy to monitor the conformational changes of peptide monomers during the gel-forming process in water-based solutions, but the short gelling time and the semi-solid state of the hydrogel caused broadening of proton resonances along with a strong water peak and made the NMR assignment impossible. To solve this problem, 100% DMSO was selected to dissolve h9e peptide in this study (h9e peptide could dissolve in 100% DMSO as a liquid solution, DMSO could be mixed with water). By adding H_2O, we slowly converted the h9e DMSO solution into hydrogel and maintained the DMSO:H_2O ratio lower than 4:1 (v/v). The hydrogelation time and gel strength depended on the DMSO:H_2O ratio. Proton NMR spectroscopy, transmission electron microscopy (TEM), and rheological studies of h9e peptide in different DMSO:H_2O ratios revealed the conformational, morphological, and mechanical changes during hydrogel formation. In addition, we added Ca^{2+} (see experimental section for Ca^{2+} concentration) to the h9e DMSO/H_2O solution to enhance hydrogel formation. Similar to a water-based solution, Ca^{2+} promoted shear-thinning and rapid recovery properties in the DMSO/H_2O solution by exhibiting faster recovery and a higher recovery strength percentage in mechanical studies. Further studies of the peptide hydrogel in different Ca^{2+} concentrations (0-30 mM) emphasized that, besides the peptide monomer assembly into the individual nanofibers, interfiber interactions were another important factor contributing to physical properties of peptide hydrogel.

6.3 Experimental Section

6.3.1 Materials

N,N-Dimethylformamide (DMF), trifluoroacetic acid (TFA), piperidine, N,N-diisopropylethylamine (DIEA), triisopropylsilane (TIS), calcium chloride ($CaCl_2$), and dimethylsulfoxide (DMSO) were purchased from Sigma-Aldrich (Milwaukee, WI). N-Methylpyrrolidinone (NMP), anhydrous ether, and dichloromethane (DCM) were purchased from Fisher Scientific (Pittsburgh, PA). Rink Amide MBHA resin, 2-(1H-Benzotriazole-1-yl)-1,1,3,3-tetramethyluronium hexafluorophosphate (HBTU), and all protected amino acids were purchased from EMD Biosciences (San Diego, CA). N-Hydroxybenzotriazole (HOBT) was purchased from CEM (Matthews, NC). Deuterium Oxide (D_2O), sodium deuteroxide (NaOD), and deuterated dimethyl sulfoxide (DMSO-D6) were purchased from Cambridge Isotopes Laboratories (Andover, MA).

6.3.2 Peptide Synthesis and Hydrogel Preparation

The h9e peptide was synthesized according to a previously published protocol. Briefly, based on the base-labile 9-fluorenylmethoxycarbonyl (Fmoc) strategy, peptides were synthesized on an automated CEM Liberty microwave peptide synthesizer (CEM Corporation, Matthews, NC) with Rink amide resin and Fmoc-protected amino acids. The N-terminal Fmoc group was final-deprotected. The resin-bound peptides were side-chain-deprotected and cleaved using TFA/TIS/water (95/2.5/2.5 v/v). After cleavage, peptides were precipitated and washed three times with anhydrous ether. The peptide was dried in air overnight and dissolved in acetonitrile and deionized water (50/50 v/v). The peptide solution was freezed in a -80 ˚C refrigerator overnight and then was freeze-dried for 48 hours by using the Labconco freeze dry system (Labconco, Kansas City, MO). Molecular weight of the synthesized peptide was confirmed by matrix-assisted laser desorption/ionization time-of-flight mass spectroscopy on an Ultraflex II instrument (Bruker Daltronics, Billerica, MA). The peptide purity wa confirmed by a Beckman System Gold high performance liquid chromatography (HPLC, Beckman Coulter, Inc., Fullerton, CA) on a phenomenex synergi 4μ Hydro-RP column (Phenomenex, Inc., Torance, CA) with the following gradient: 10-90% B in 20 min (A: 99.9% H_2O, 0.1% TFA; B: 90% acetonitrile, 9.9% H_2O, 0.1% TFA).

Lyophilized peptide was completely dissolved in 100% DMSO with a peptide concentration of 6 mM. For hydrogel preparation, the ratioes of DMSO:H2O were adjust to 9:1, 4:1, and 7:3 (v/v) respectively. After these adjustments, the final peptide concentration was 3 mM). Peptide solutions were hydrogelated at room temperature. To prepare h9e hydrogel with Ca^{2+}, 100 mM $CaCl_2$ was first dissolved in 100% DMSO, then added to h9e solution for the finial molar ratioes of Ca^{2+}:peptide were 1:1, 2:1, and 10:1, respectively. Water was then added into the Ca^{2+} and peptide mixture to adjust the final DMSO:water ratio to 9:1, 4:1, and 7:3 (v/v).

6.3.3 Transmission Electron Microscopy (TEM)

TEM samples were prepared by a negative staining method as follows: (1) prepare staining solution of 2 wt.% uranyl acetate in water and place a drop (~100 μl) of the aqueous solution onto parafilm surface; (2) glow discharge TEM Cu grids (carbon coated); (3) place a small drop of the sample solution (~ 5 μl) onto the top surface of the TEM grids for 1 min; (4) flip the TEM grids upside down and let it float on the top surface of the staining solution for 20 s; (4) pick up the TEM grids and dry in air. The TEM work was carried out using a FEI Tecnai G^2 F20 with field emission gun (FEG), at a accelerating voltage of 200 kV. In order to reduce image intensity and improve contrast, all images were acquired by using a Gatan Image Filter (GIF) which wilter away the inelastic scattering electrons. . The particle size was measured by using Image J software (rsbweb. nih. gov) with more than 10 measurements.

6.3.4 Nuclear Magnetic Resonance (NMR)

The 1D and 2D ^1H-^1H NMR experiments were performed on a Varian 500 NMR System (Varian Inc., now Agilent Technologies, Palo Alto, CA) equipped with a 5 mm cryogenic triple-resonance inverse detection pulse field gradient probe operating at 499.84 MHz for ^1H frequency. 2D- ^1H-^1H Total Correlation Spectroscopy (TOCSY) and NOE Spectroscopy (NOESY) data was acquired in phase-sensitive (States-TPPI) mode into 2000 t2 and 256 t1 points with spectral width of 13 ppm in each dimension, and 4 transients per increment. Spin-lock time of 80 ms at a B1 field strength of 7.0 KHz was used for TOCSY experiments, and mixing times of 200 ms and 400 ms were used for NOESY experiments. All experimental data were zero-filled to 4K data points in the t2 dimension, and, when necessary, the spectral resolution was enhanced by Lorenzian-Gaussian apodization. DMSO-D6 peak (2.5 ppm for 25 ℃) was considered a reference for chemical shift assignements. Data processing was done

using VnmrJ2.2c (Varian Inc., now Agilent Technologies, Palo Alto, CA) and analyzed using Sparky – NMR Assignment and Integration software.[26]

6.3.5 Structure Calculations

Structure calculations were performed using standard methods based on the unambiguously identified and classified NOE crosspeaks. NOE peaks were assigned an inter-proton distance constrain range based on their peak intensities; values given to each category of crosspeaks were: strong (1.8-2.7 Å), medium (1.8-3.5 Å), weak (1.8-4.0 Å) (27). Upper distance limits for NOEs involving methyl protons and non-stereo specifically assigned methylene protons were corrected appropriately for center averaging.

The assigned distance constraints were used as input in the calculation of peptide structures starting from an extended structure. The initial extended structure was created from the amino acid sequence using the program Crystallography & NMR System (CNS) version 1.1. CNS uses both a simulated annealing protocol and molecular dynamics to produce low-energy structures with the minimum distance constraint violations. From 100 generated structures, a subset of structures with the lowest overall energies and lesser dihedral angle violation were selected as representative structures.

6.3.6 Oscillational Rheology Test

A C-VOR 150 rheometer system (Malvern instruments, Malvern, Worcestershire, United Kingdom) was used to determine the storage and loss moduli (G′ and G″, respectively) of h9e hydrogels with a 20-mm diameter parallel plate geometry and 500 μm gap size at 25 ℃. The peptide DMSO/H_2O solution was placed on the measuring system immediately after mixing for a gel-forming rate test. Single frequency (1 Hz) and steady shear strain (1%) were selected for a 2-h test. To determine the shear-thinning and recovery capability of the hydrogel, the peptide in 70% DMSO solution was incubated at room temperature overnight for hydrogelation, then transferred to a lower measuring plate for a 1-h, single-frequency test (1 Hz, 1% strain). The hydrogel was disturbed using 1 Hz frequency and 500% shear strain for 1 min. Afterward, resetting the instrument parameters took 1 min, and the hydrogel moduli during the reassembly period were measured under 1 Hz frequency and 1% shear strain for 1 h. The amplitude sweep test (strain from 1 to 500%, 1Hz frequency) was conducted multiple times to determine hydrogel

recovery capability after it was destroyed. Four testing circles were applied in this measurement, and the hydrogel recovery time between every two circles was 1, 5, and 10 min.

6.4 Results and Discussion

The peptide h9e dissolved in 100% DMSO. Adding H_2O to the h9e DMSO solution allowed the peptides to pack into their corresponding nanofiber structure (Figure 6.1d) in an orderly fashion and induced the self-supported hydrogel formation when the DMSO:H_2O ratio was lowered to 4:1. This hydrogelation process was enhanced by increasing the water percentage (Figure 6.1). For example, when DMSO:H_2O ratio was 4:1, hydrogel formation took about 48 h. This process was completed within 2 h at a DMSO:H_2O ratio of 7:3 and lowered to 50 min when the DMSO:H_2O ratio reached 1:1. The morphological properties of peptide solutions with different DMSO:H_2O ratios observed by TEM confirmed this hydrogelation process. Figure 6.1a shows a diffuse amorphous morphology of h9e peptide in 100% DMSO. The peptides dispersed in the visual field without obviously ordered aggregation. This amorphous morphology was maintained with more anisotropic aggregations of individual peptides when DMSO:H_2O ratio was 9:1 (Figure 6.1b). The 90% DMSO h9e solution was in a free-flowing liquid state for more than 1 month after it was prepared. The nanofiber morphology with about 5 nm diameter appeared at 80% DMSO h9e solution (Figure 6.1c) and became denser when the DMSO:H_2O ratio was decreased to 7:3 (Figure 6.1d).

To further understand the molecular conformation changes during peptide hydrogelation, 1D and 2D NMR experiments were performed at the Biomolecular NMR facility, using a 500MHz NMR instrument equipped with a 5 mm triple resonance cryogenic probe, which allowed the assignment of the proton resonances of peptide in DMSO/H_2O solution at increasing water concentration. Based on the proton resonance assignments in both 2D ^{1}H-^{1}H TOCSY and NOESY spectra of h9e in 100% DMSO (Figure 6.2), the calculated monomeric structure of the h9e peptide (Figure 6.3a) showed a helical conformation with the C-terminal residues bent back into the helix, thus allowing the potentially charged side-chains of the Asp residues to come into proximity. Analysis of the predicted surface of the monomeric peptide (Figure 6.3a) structures presented segregation of the hydrophobic (gray color) and hydrophilic side chains (red color). In addition, the Chemical Shift Index (CSI) for the alpha protons of each amino acid residue in

different DMSO:H_2O ratio solutions was calculated (Figure 6.3b) as an indicator of the peptide backbone conformation. In 100% DMSO, a more β-sheet-like structure appeared for the hydrophobic residues (Leu-2, Ill-3, Val-4 and Ill-5) of the N terminal compared with the helix or turn-like structure present for the non-hydrophobic residues of the C terminal. With increasing water concentration, the peptide solution became more and more gel-like, and the backbone conformation of the whole monomeric peptide was inclined to adopt a more helix-like structure. Especially in the N terminal region, the significant decrease of CSI. values for residue Leu-2 to Ile-9 indicated the change of this β-strand-like domain segment into a turn- or twist-like structure. Interestingly, unlike most native or artificial hydrogel peptides in which a stable β-sheet like molecular structure is preferred for hydrogelation [28-30], this helix-like structure-induced hydrogelation is rarely seen in a native protein sequence-based peptide. Although the segregation of the hydrophobic and non-hydrophobic side-chains of the monomeric h9e structure was observed in terminal-to-terminal direction in 100% DMSO solution, the top view (Figure 6.3a and c) of the calculated peptide structure showed that both the side chains of the hydrophobic residues (gray color of Figure 6.3c) and the potentially charged Asp residues (red color of Figure 6.3c) were crowded to one side perpendicular to the terminal-to-terminal direction. We suggest that on adding water to the h9e DMSO solution, along with peptide hydrogelation, the backbone conformational changes caused turning of the hydrophobic domain and bent some of their side-chains perpendicular to the terminal-to-terminal direction from one side to the other and resulted in extension of the terminal-to-terminal distance (Figure 6.3c), which further separates the hydrophobic and potentially charged segment in both directions. The stacked hydrophobic interactions benefited from this further segregation and may have contributed the assembly of the peptide monomers to the nanofiber (Figure 6.3e). The calculated monomeric structure of the h9e peptide in 100% DMSO was about 1.67 nm in width and 1.92 nm in length (Figure 6.3d), which could extend to more than 2 nm in length during the hydrogelation. Therefore, according to the hydrophobic stacked peptide assembly pathway, a 4-5 nm nanofiber diameter could be expected (Figure 6.3e). The 5 nm nanofiber diameter observed under TEM (Figure 6.1c) matched this expectation quite well. The rheological tests of h9e DMSO/H_2O solutions further demonstrated the morphological and conformational properties of peptide hydrogelation (Figure 6.3f). During the 2-h test, 90% DMSO h9e solution remained in liquid form and showed very weak elastic modulus (G′, about 0 Pa). With increasing water concentration, the G′ of peptide solution with

70% DMSO increased slowly and reached about 80 Pa at the end of the test. For h9e peptides in 50% DMSO solution, the G′ reached 100 Pa within 50 min and kept increasing within the test time, indicating the much faster formation of the self-support hydrogel with stronger gel strength.

Further studies were focused on the shear-thinning and rapid recovery properties of h9e hydrogel with Ca^{2+} ions. Similar to the water-based h9e solution, peptides in DMSO/H_2O solution responded to Ca^{2+} and exhibited a significant decrease in hydrogelation time with Ca^{2+}. For example, with 50 mM Ca^{2+}, the hydrogelation time of 5 mM h9e peptide in 80% DMSO solution was 30 min compared with 2 days for that without Ca^{2+}. The TEM observation of h9e peptide with Ca^{2+} (the molar ratio of peptide:Ca^{2+} is 1:10) in different DMSO:H_2O ratio solutions demonstrated that these metal ions triggered nanofiber-forming promotion (Figure 6.4). In 100% DMSO solution, there were anisotropic aggregations of individual peptides with Ca^{2+} (Figure 6.4a). These aggregations became fiber-like morphologies when DMSO was reduced to 90% (Figure 6.4b), and the nanofiber morphology was observed then the water concentration in the DMSO/H_2O solvent was increased (Figure 6.4c and d). The Ca^{2+}-induced hydrogel has stronger gel strength of identical peptide concentration to that without Ca^{2+} in the same DMSO/H_2O solution. To explore the hydrogel shear-thinning and recovery properties, we selected 5 mM h9e peptides in 80% DMSO solution with 50 mM Ca^{2+} and in 50% DMSO solution, which have similar gel strength of 225 Pa and 315 Pa, respectively (Figure 6.4e and f). An amplitude sweep test was conducted four times for both hydrogels with increasing shear strain from 1% to 500% within 5 min each time. After each cycle, we waited 0.5, 1, and 10 min, respectively, for hydrogel recovery. Both hydrogels had been completely disturbed into liquid form at the end of each cycle by showing a G′ close to zero. After shear stress ceased, only about 20% gel strength could recover for hydrogel in 50% DMSO in 0.5 min, and this recovery percentage did not change even with longer waiting time. In contrast, the percentage of recovery gel strength increased with waiting time for hydrogel in 80% DMSO with Ca^{2+}, which appeared around 70% recovery after 10 min (Figure 6.4e). These results suggest that, like hydrogel in an aqueous environment, [22] the construction of h9e hydrogel with Ca^{2+} presents a much faster reassemble capability than that without Ca^{2+} after mechanical disturbance in DMSO/H_2O solution. According to the NMR result, the peptide fold into an amphiphilic structure which

could self-assemble into nanofilament structure through hydrophobic callopse. Here, the promotion of the hydrogel formation and the increase of the hydrogel strength indicate that binding the hydrophilic region of the peptide monomer with Ca^{2+} may further help the peptide self-assembly.

To further understand why the Ca^{2+} ions could promote shear-thinning and rapid recovery properties in h9e hydrogel, different concentrations of Ca^{2+} ions were added to 3 mM h9e peptide DMSO solutions. DMSO:H_2O ratio was adjusted to 7:3 for all solutions. The rheological data (Figure 6.5a) show that, with 3 mM Ca^{2+} concentration, the peptide has a hydrogelation rate almost identical to that without Ca^{2+} within the first 2 h of testing time; however, after a 12-h gelling process, the stable gel strength of 3 mM h9e with 3 mM Ca^{2+} is around 450 Pa, which is much higher than 80 Pa of that without Ca^{2+} (stable gel strength before shear thinning of Figure 6.5b). With 30 mM Ca^{2+} concentration, h9e peptides increase dramatically in their hydrogelation rates (Figure 6.5a) and achieve over 1000 Pa in gel strength. After 12 h incubation at 4 ^{o}C in a refrigerator, all three hydrogels were allowed to stabilize at 25 ^{o}C with a 1% test shear strain for 1 h, and were then disturbed using 500% shear strain for 1 min. Afterward, another 1 min was taken to reset the instrument parameter and the gel recovery was tested using 1% shear strain for 2 h. Without Ca^{2+}, only about 30% of the gel was recovered during a 1-min waiting time (Figure 6.5b). The recovery rate of this hydrogel was very slow, and restored only about 40% after 2 h. With Ca^{2+}, the gel strength recovered much faster. For example, during the 1-min waiting time, about 60 and 75% gel strengths were recovered for hydrogel with 3 mM and 30 mM Ca^{2+}, respectively. After 2 h, close to 80% gel strengths of both hydrogels could be recovered. Interestingly, the effect of Ca^{2+} on h9e peptide hydrogelation was observed only when the water percentage was high enough to promote peptide assembly into hydrogel. In 100% or 90% DMSO, h9e solutions were still in liquid form, even after adding high concentrations of Ca^{2+} and a long incubation period. On the other hand, there was no significant change in the α proton CSI of h9e peptide in 70% DMSO solution with 0, 3, or 6 mM Ca^{2+} (Figure 6.5c), which indicates the almost identical monomeric structure of peptides in these solutions. This phenomenon suggests that the conformational promotion of peptide monomeric structure is the primary requirement for peptide self-assembly into hydrogel. When the required structure is stable, h9e peptides may follow a similar pathway for nanofiber assembly, and the surrounding Ca^{2+} ions may promote

this hydrophobic stacked interaction by capturing the charged Asp residues on the opposite site and further affect the interfiber interactions of peptide hydrogel.

The effect of Ca^{2+} charge screening on mechanical properties of other types of peptide hydrogels has been reported.[31-33] The research suggests that, besides the strength of individual nanofibers, interfiber interactions, which are relative to the charge screen of Ca^{2+}, were considered important contributors to gel stiffness. Therefore, in addition to the differences in the rheological data presented above, the morphological properties of interfiber interactions of hydrogel with/without Ca^{2+} were also observed. Figure 6.6a shows the unbent nanofiber of h9e hydrogel in 70% DMSO without Ca^{2+}. Most junction points of nanofibers of this 3D network are static points (binding through non-colavent attraction on the surface of nanofibers), where the non-covalent attractive interactions such as hydrogen bonding, hydrophobic, or van der Walls interactions dominate the bunch between nanofibers (Figure 6.6d). Such junctions cannot reform after they are broken, which may relate to the mechanical irreversibility of the corresponding hydrogel. In contrast, bent nanofibers were observed in h9e 70% DMSO hydrogel with 3 mM Ca^{2+} (Figure 6.6b). Although some static junctions remained, most nanofibers in this hydrogel network were held together by nanofiber entanglements (Figure 6.6e). According to the data of mechanical test (Figure 6.5b), compared with the bunch of nanofibers in static points, the entanglement crossings of nanofibers with enough fiber length might be healed much more easily after they were broken. Increasing the Ca^{2+} concentration to 30 mM rendered the entanglements of nanofibers even more obvious with rare static junctions (Figure 6.6c & f). High-magnification TEM images (Figure 6.6g & h) show that the nanofiber of hydrogel with 3 mM Ca^{2+} is composed of two individual fibers, which indicates a stack of two fibers (Figure 6.6i). Higher Ca^{2+} concentration (30 mM) occupied most charged Asp residues on the nanofiber surface, which affected the interfiber interaction and led to individual fibers with 5-nm diameter (Figure 6.6j). The higher occupation of Ca^{2+} on the surface may prevent the attracted interactions between nanofibers at static junctions.

6.5 Conclusions

As our hypothesis, the h9e peptide presents an amphiphilic structural property with C-terminal proximity of potentially charged Asp residues in DMSO solution. With increasing water

concentration in a DMSO/H_2O solvent mixture, the peptide monomer tends to adopt a more helical structure, which enhances the stacked hydrophobic interactions for nanofiber formation. Peptides self-assemble into nanofiber morphology when the DMSO:H_2O ratio is lower than 4:1. The hydrogelation rate and gel strength are improved when water percentage is increased. With the same DMSO:H_2O ratio, Ca^{2+} could enhance hydrogelation rate and stable gel strength and cause the peptide hydrogel to exhibit special shear-thinning and rapid recovery properties. Instead of changing the peptide monomeric structure, Ca^{2+} occupies the charged Asp residues on fiber surface and further influences the interfiber interactions of peptide hydrogel. Compared with static junctions of nanofibers of hydrogel in 70% DMSO without Ca^{2+}, entanglement crossings of nanofibers hold the networks of peptide hydrogel with Ca^{2+}, which may play an important role in hydrogel shear thinning and rapid recovery property. This study helps us understand the assembly pathways of peptide monomers into their corresponding nanofiber structures and may lead to the development of new biological materials with controlled stiffness and shearing-respondent behaviors.

6.6 Acknowledgments

We thank the University of Kansas Mass Spectrometry Lab for HPLC and mass spectrometric analysis, and Microscopy and Imaging Center of Texas A&M University for TEM images. NMR instrumentation at KSU was funded by NIH grant (S10-RR 025441). This project was partially supported by KSU Targeted Excellence Program and KSU Research Foundation Scholarship Program, and is contribution no. 12-288-J from the Kansas Agricultural Experiment Station.

6.7 References

1. Hauser, C. A. E.; Zhang, S. Designer self-assembling peptide nanofiber biological materials. Chem. Soc. Rev. 2010, 39, 2780–2790.

2. Langer, R.; Tirrell, D. Designing materials for biology and medicine. Nature 2004, 428, 487–492.

3. Zhao, X.; Pan, F.; Xu, H.; Yaseen, M.; Shan, H.; Hauser, C. A. E.; Zhang, S.; Lu, J. R. Molecular self-assembly and applications of designer peptide amphiphiles. Chem. Soc. Rev. 2010, 39, 3480–3498.

4. Aluri, S.; Janib, S. M.; Mackay, J. A. Environmentally responsive peptides as anticancer drug carriers. Adv. Drug Deliv. Rev. 2009, 61, 940–952.

5. Huang, H.; Sun, X. S. Rational design of responsive self-assembling peptides from native protein sequences. Biomacromolecules 2010, 11, 3390–3394.

6. Luo, Z., Wang, S.; Zhang, S. Fabrication of self-assembling D-form peptide nanofiber scaffold d-EAK16 for rapid hemostasis. Biomaterials 2011, 32, 2013–2020.

7. Hule, R.; Nagarkar, R.; Hammouda, B.; Schneider, J.; Pochan, D. Dependence of self-assembled peptide hydrogel network structure on local fibril nanostructure. Macromolecules. 42009, 2, 7137–7145.

8. Dvir, T.; Timko, B. P.; Kohane, D. S.; Langer, R. Nanotechnological strategies for engineering complex tissues. Nature Nanotechnology. 2011, 6, 13–22.

9. Okuyama, K. High-resolution structures of collagen-like peptides [(pro-pro-gly)(4)-xaa-yaa-gly-(pro-pro-gly)(4)]: Implications for triple-helix hydration and hyp(X) puckering. Biopolymers, 2009, 91, 361–372.

10. Eyrich, D.; Brandl, F.; Apple, B.; Wiese, H.; Maier, G. Wenzel, M. Staudenmaier, R.; Goepferich, A.; Blunk, T. Long-term stable fibrin gels for cartilage engineering. Biomaterials, 2007, 28, 55–65.

11. Hrd, T. Protein engineering to stabilize soluble amyloid β-protein aggregates for structural and functional studies. The FEBS J. 2011, 278, 3884–3892.

12. Friedman, R. Aggregation of amyloids in a cellular context: Modelling and experiment. Biochem. J. 2011, 438, 415–426.

13. Ruoslahti, E. Targeting tumor vasculature with homing peptides from phage display. Semin. Cancer Biol. 2000, 10, 435–442.

14. Yang, M.; Yamauchi, K.; Kurokawa, M.; Asakura, T. Design of silk-like biomaterials inspired by mussel-adhesive protein. Tissue Eng. 2007, 13, 2941–2947.

15. Bunick, C. G.; Nelson, M. R.; Mangahas, S.; Hunter, M. J.; Sheehan, J. H.; Mizoue, L. S.; Bunick, G. J. Chazin, W. J. Designing sequence to control protein function in an EF-hand protein. J. Am. Chem. Soc. 2004, 126, 5990–5998.

16. Branco, M. C.; Pochan, D. J.; Wagner, N. J.; Schneider, J. P. The effect of protein structure on their controlled release from an injectable peptide hydrogel. Biomaterials, 2010, 31, 9527–9534.

17. Garty, S.; Kimelman-Bleich, N.; Hayouka, Z.; Cohn, D.; Friedler, A.; Pelled, G.; Gazit, D. Peptide-modified "smart" hydrogels and genetically engineered stem cells for skeletal tissue engineering. Biomacromolecules 2010, 11, 1516–1526.

18. Haines-Butterick, L.; Rajagopal, K.; Branco, M.; Salick, D.; Rughani, R.; Pilarz, M.; Lamm, M. S.; Pochan, D. J.; Schneider, J. P. Controlling hydrogelation kinetics by peptide design for three-dimensional encapsulation and injectable delivery of cells. Proc. Natl. Acad. Sci. U. S. A. 2007, 104, 7791–7796.

19. Chang, C.; Kuo, T.; Lin, C.; Chou, C.; Chen, K.; Lin, F.; Liu, H. Tissue engineering-based cartilage repair with allogenous chondrocytes and gelatin-chondroitin-hyaluronan tri-copolymer scaffold: A porcine model assessed at 18, 24, and 36 weeks. Biomaterials, 2006, 27, 1876–1888.

20. Schneider, J.; Pochan, D.; Ozbas, B.; Rajagopal, K.; Pakstis, L.; Kretsinger, J. Responsive hydrogels from the intramolecular folding and self-assembly of a designed peptide. J. Am. Chem. Soc. 2002, 124, 15030–15037.

21. Nowak, A., Breedveld, V.; Pakstis, L.; Ozbas, B.; Pine, D.; Pochan,D.; Deming, T. Rapidly recovering hydrogel scaffolds from self-assembling diblock copolypeptide amphiphiles. Nature 2002, 417, 424–428.

22. Huang, H.; Shi, J.; Laskin, J.; Liu, Z.; McVey, D. S.; Sun, X. S. Design of a shear-thinning recoverable peptide hydrogel from native sequences and application for influenza H1N1 vaccine adjuvant. Soft Matter, 2011, 7, 8905–8912.

23. Shen, X.; Mo, X.; Moore, S.; Frazier, S.; Iwamoto, T.; Tomich, J.; Sun, X. Adhesion and structure properties of protein nanomaterials containing hydrophobic and charged amino acids. Journal of Nanoscience and Nanotechnology. 2006, 6, 837–844.

24. Hayashi, C. Y.; Lewis, R. V. Spider flagelliform silk: Lessons in protein design, gene structure, and molecular evolution. BioEssays. 2001, 23, 750–756.

25. Lammel, A.; Schwab, M.; Slotta, U.; Winter, G.; Scheibel, T. Processing conditions for the formation of spider silk microspheres. ChemSusChem. 2008, 15, 413–416.

26. www.cgl.ucsf.edu/home/sparky

27. Wthrich, K.; Billeter, M.; Braun, W. Pseudo-structures for the 20 common amino acids for use in studies of protein conformations by measurements of intramolecular proton-proton distance constraints with nuclear magnetic resonance. J. Mol. Biol. 1983, 169, 949–961.

28. Zhao, Y.; Yokoi, H.; Tanaka, M.; Kinoshita, T.; Tan, T. Self-assembled pH-responsive hydrogels composed of the RATEA16 peptide. Biomacromolecules 2008, 9, 1511–1518.

29. Rapaport, H.; Grisaru, H.; Silberstein, T. Hydrogel scaffolds of amphiphilic and acidic beta-sheet peptides. Advanced Functional Materials 2008, 18, 2889–2896.

30. Wu, L.; Yang, J.; Kopecek, J. Hybrid hydrogels self-assembled from graft copolymers containing complementary β-sheets as hydroxyapatite nucleation scaffolds. Biomaterials 2011, 32, 5341–5353.

31. Kopecek, J.; Yang, J. Peptide-directed self-assembly of hydrogels. Acta Biomaterialia. 2009, 5, 805–816.

32. Dagdas, Y.; Tombuloglu, A.; Tekinay, A.; Dana, A.; Guler, M. Interfiber interactions alter the stiffness of gels formed by supramolecular self-assembled nanofibers. Soft Matter. 2011, 7, 3524–3532.

33. Toksoz, S.; Mammadov, R.; Tekinay, A.; Guler, M. Electrostatic effects on nanofiber formation of self-assembling peptide amphiphiles. J. Colloid Interface Sci. 2011, 356, 131–137.

Figure 6.1 TEM images of h9e peptide in 70-100% DMSO solutions without Ca^{2+}.

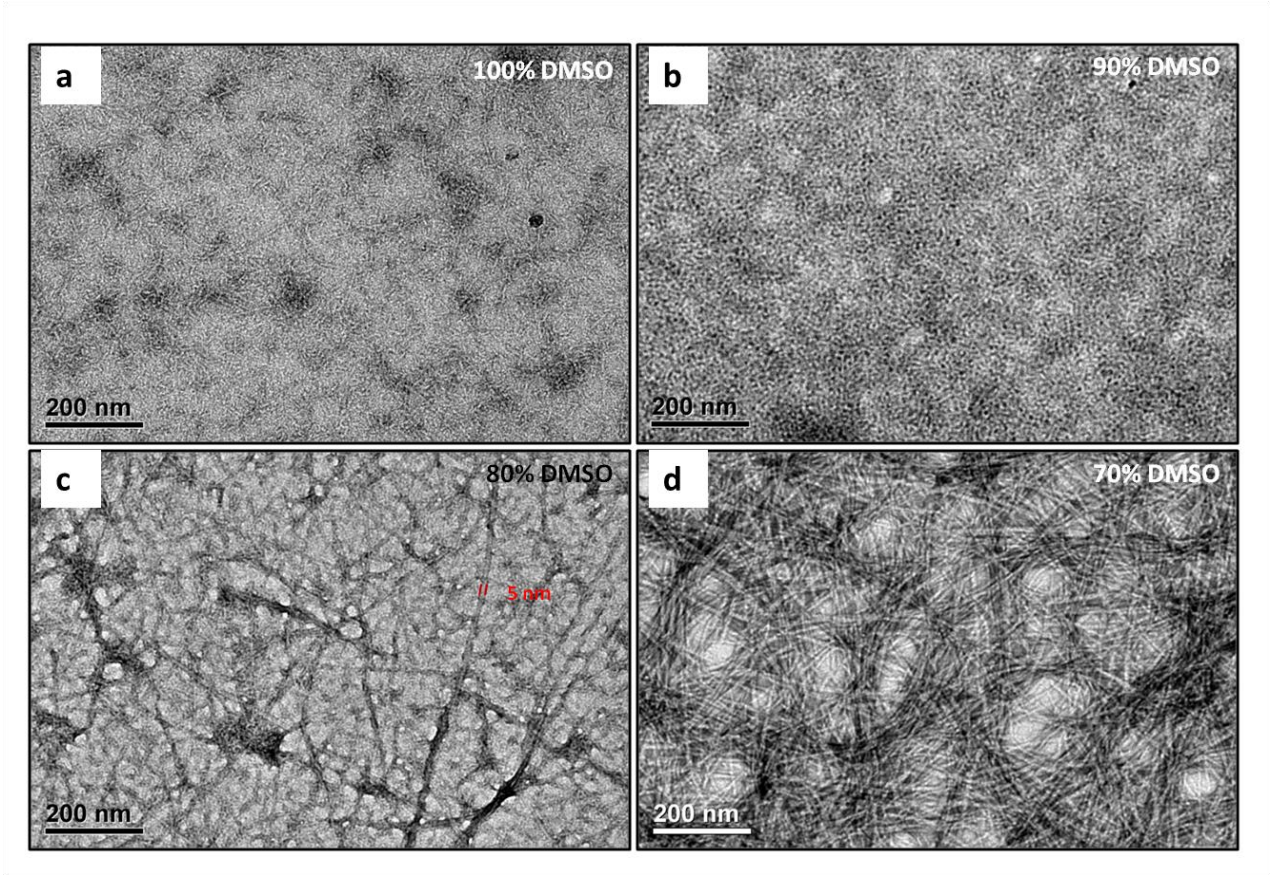

Figure 6.2 TOCSY and NOESY of h9e in 100% DMSO.

a. TOCSY spectra of h9e in 100% DMSO show resonance assignments in the HN-Hα, HN-Side chain and Side Chain-Side Chain regions. **b.** Sample of NOESY spectra showing assignments of NOESY peaks in the HN-Hα and HN-HN regions.

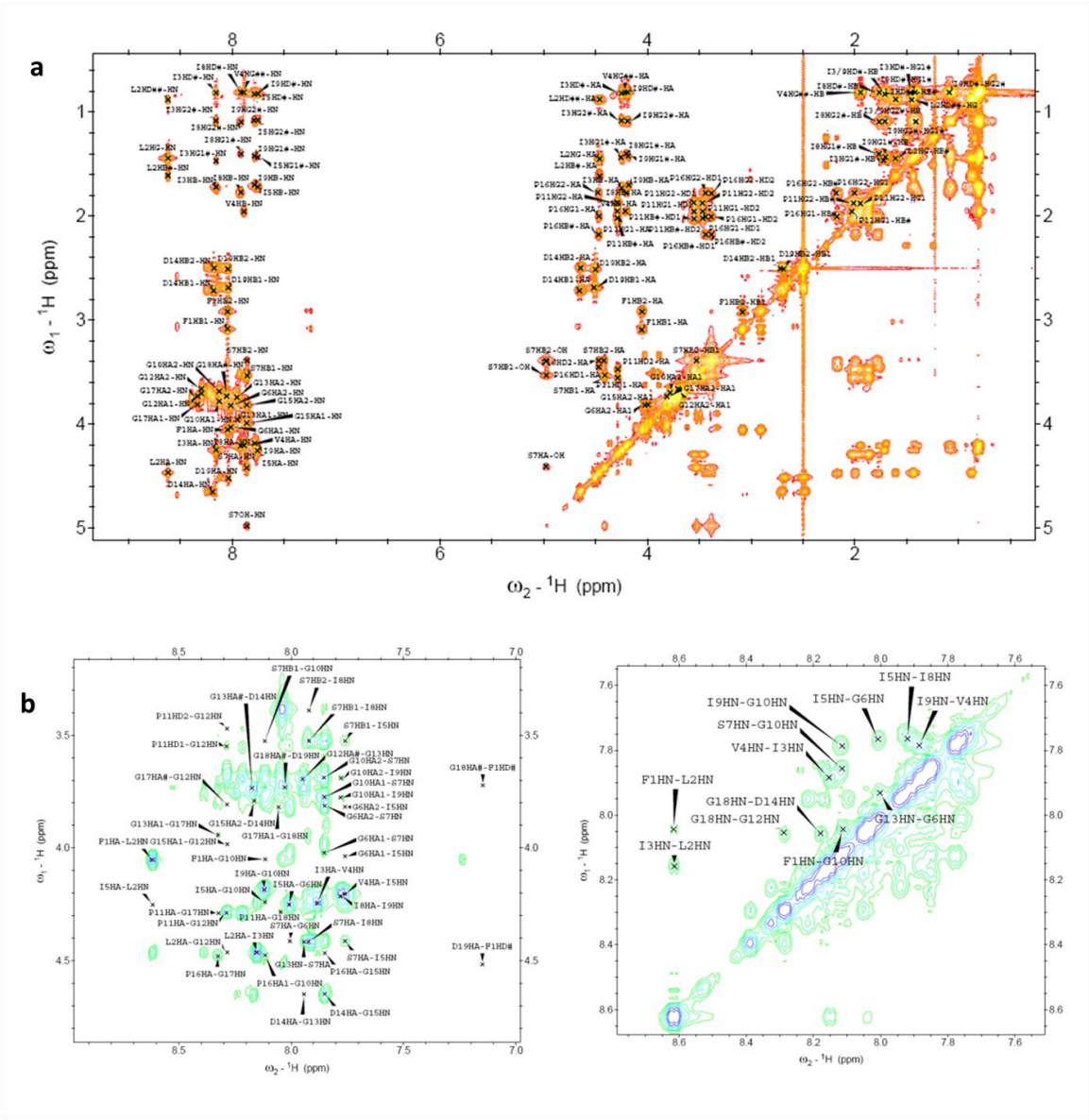

Figure 6.3 Monomeric study of peptide hydrogelation.

a. Calculated monomeric structure of h9e in 100% DMSO (hydrophobic, non hydrophobic and Asp side-chains colored as gray, green, and red, respectively). **b.** Chemical Shift Index for peptide in 70-100% DMSO solution without Ca^{2+}. **c.** Increasing water concentration of DMSO/H2O solvent mixture induces the helix turning of peptide backbone, which leads to a further segregation of hydrophobic (gray) and hydrophilic (red) domains. **d.** Molecular size of h9e peptide in 100% DMSO. **e.** Proper stacked hydrophobic interactions contribute to peptide assembly for nanofiber formation. **f.** Mechanical property of peptides in 90, 70, and 50% DMSO during the first 2 h of hydrogelation.

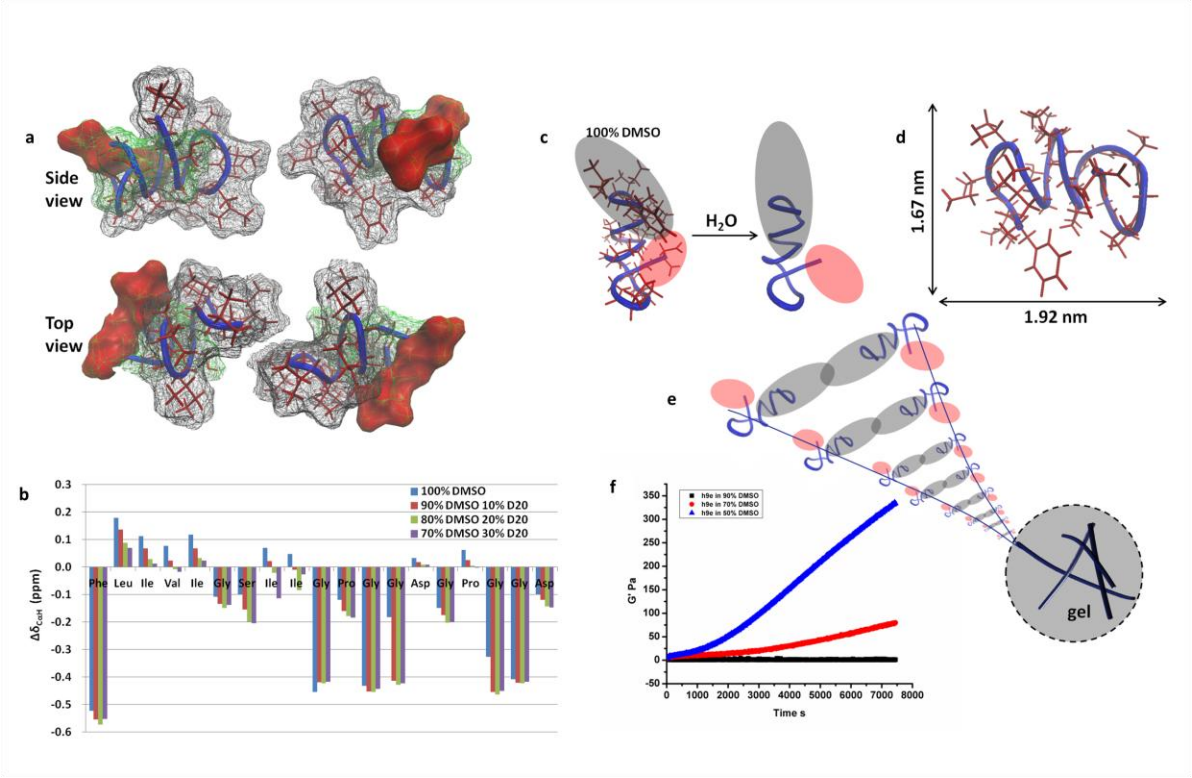

Figure 6.4 Morphological and rheological properties of h9e peptide in DMSO/H2O solution with Ca^{2+}

a-d. TEM images of 3 mM h9e peptide in 70-100% DMSO solution with 30 mM Ca^{2+}. **e.** Amplitude sweep test of 5 mM h9e with 50 mM Ca^{2+} in 80% DMSO solution with 1 to 500% shear strain. **f.** Amplitude sweep test of 5 mM h9e without Ca2+ in 50% DMSO solution with 1 to 500% shear strain.

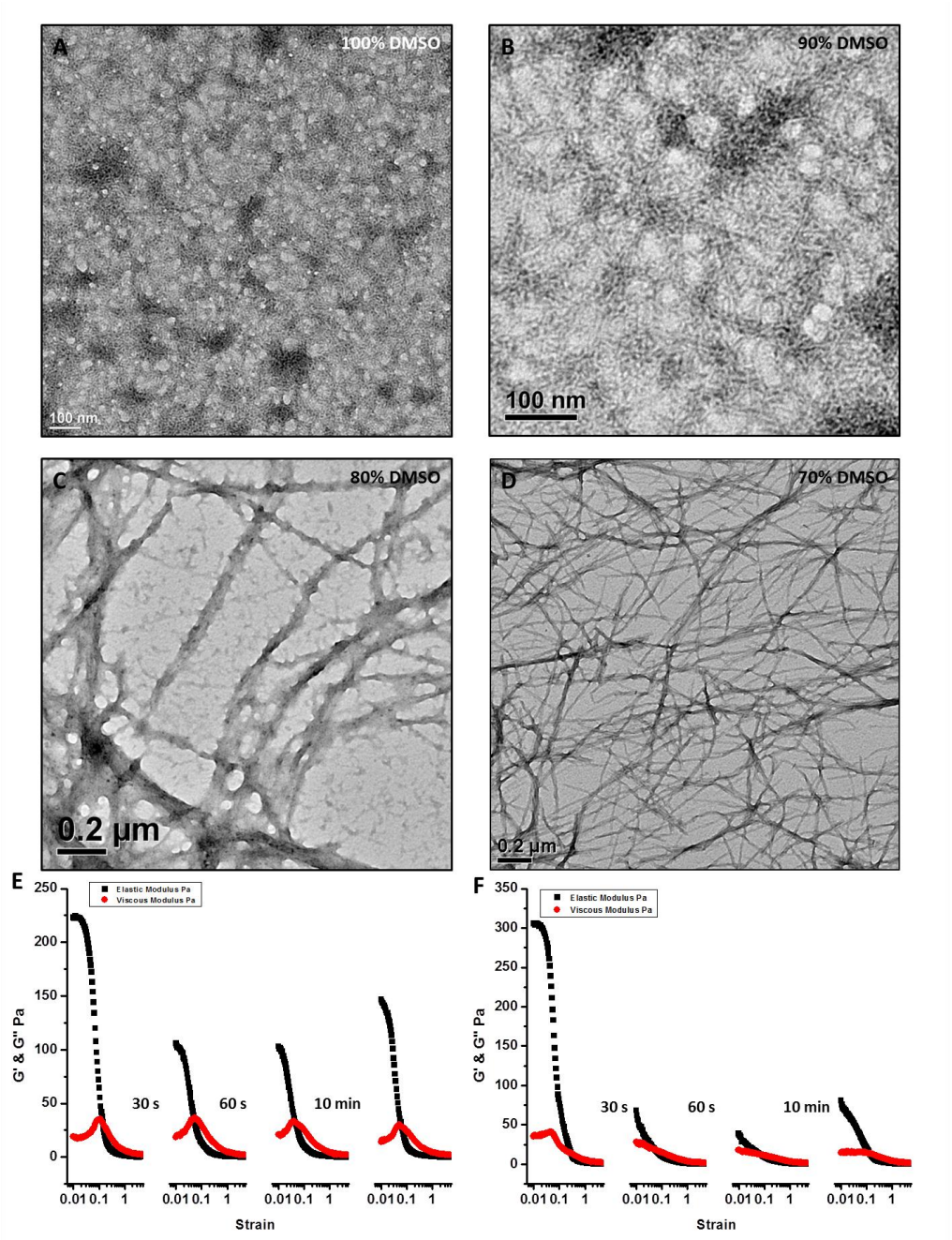

Figure 6.5 Mechanical and monomeric structural properties of h9e peptide in 70% DMSO solution with/without Ca^{2+}.

a. G′ of h9e hydrogel in 70% DMSO solution with 0, 3, and 30 mM Ca^{2+}. **b.** Shear-thinning and recovery properties of h9e hydrogel in 70% DMSO solution with 0, 3, and 30 mM Ca^{2+}. **c.** Chemical Shift Index of h9e peptide in 70% DMSO solution with 0, 3, and 30 mM Ca^{2+}.

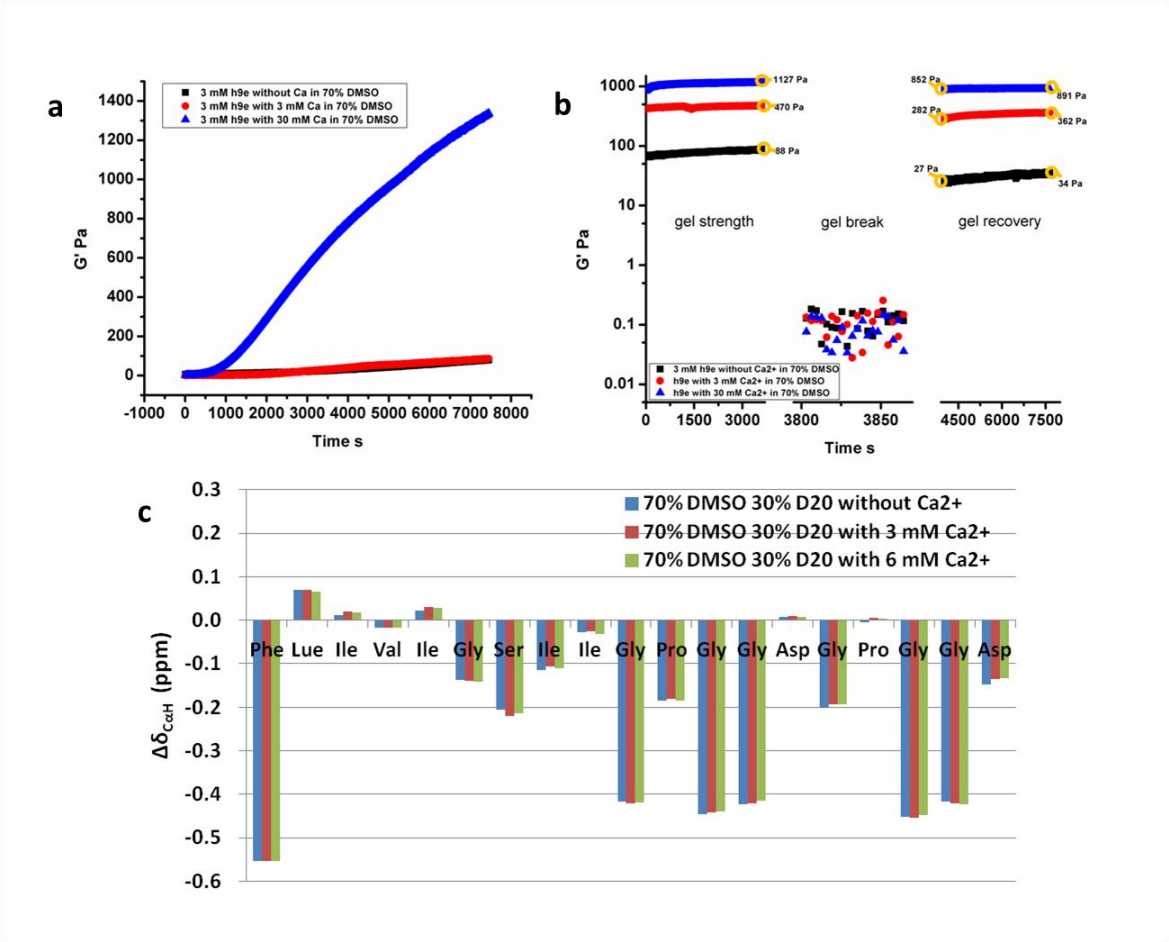

Figure 6.6 Morphological properties of interfiber interactions of h9e hydrogel in 70% DMSO solution with/without Ca^{2+}.

a., d. Nanofibers with various fiber lengths of hydrogel without Ca^{2+} showing static junctions (yellow circle). **b., e.** Both entanglements (red circle) and static junctions (yellow circle) were observed in peptide hydrogel with 3 mM Ca^{2+}. **c., f.** The peptide network was held by entanglements (red circle) of hydrogel with 30 mM Ca^{2+}. **g., i.** Nanofiber of h9e hydrogel with 3 mM Ca^{2+} is composited by stacking of two individual fibers. **h., j.** Ca^{2+} occupying most charged Asp residue on fiber surface leads to nanofiber with 5 nm diameter of hydrogel with 30 mM Ca^{2+}.

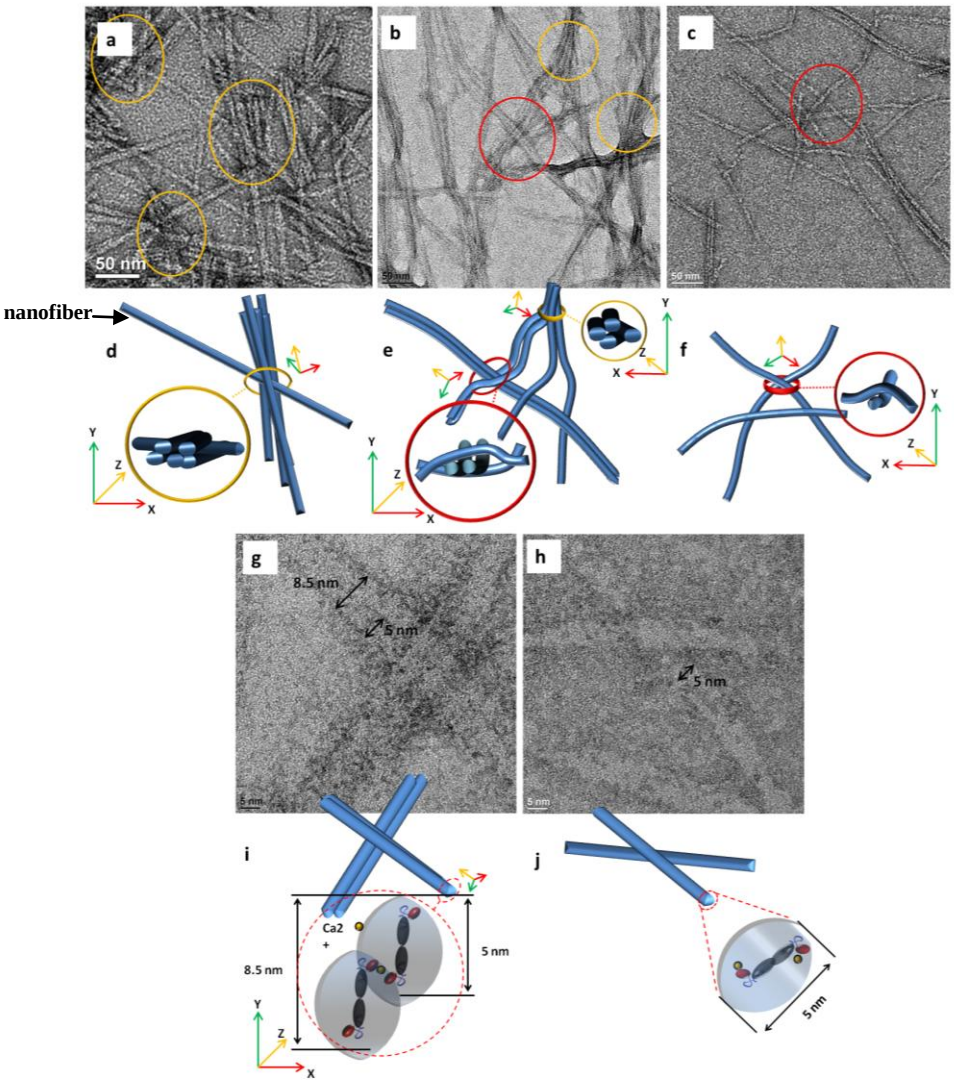

Chapter 7 - Physiological Properties of an Injectable Peptide Hydrogel for 3D Cell Culture with Easy Cell Cluster Recovery[5]

7.1 Abstract

Physiological conditions such as neutral pH, physiological temperature are very important for cell growth. Most existing pre-gelated solutions for cell culture are limited by their extreme condition such as acidic or basic pH or cold or hot temperatures during hydrogelation. Here, we report an injectable peptide hydrogel that shows superior physiological properties as an *in vitro* matrix for three-dimensional (3D) cell culture and provides a tool for physiology- and pathophysiology-related studies. The 3D matrix of hydrogel was accomplished by mixing a peptide solution directly with a cell culture medium without pH or temperature adjustment. According to its specific shear-thinning and quick reassembly rheological properties, this hydrogel can be delivered multiple times via pipette. Human epithelial cancer cells, MCF-7, are encapsulated homogeneously in the hydrogel matrix during hydrogelation and grow as colony-like clusters (reminiscent of real tumors) in 3D. More crucially, after incubation, cell clusters can be isolated from the 3D hydrogel matrix through a simple diluting and centrifuging procedure. These unique physiological properties make this peptide hydrogel a potentially great biological material for 3D cell culture and other biomedical applications.

7.2 Introduction

Two-dimensional (2D) substrates, such as tissue culture polystyrene, make an enormous contribution to modern *in vitro* cell studies; however, traditional 2D platforms cannot accurately mimic the complex 3D architecture of the extracellular matrix (ECM) where native cells reside.[1-4] In 2D culture, the monolayer cells are surrounded by bulk media which contains homogenous concentration of nutrients and growth factors, yielding a flat and stretched morphology.[5] Recent studies have shown that the morphological differences of cells cultured in 2D and 3D can also exhibit several striking differences in subtle cellular processes such as proliferation, apoptosis, differentiation, gene expression, migration, and drug sensitivities.[6-9] On the other hand, the

[5] Huang, H.; Sun, X. S.; Boyle, D.; Nguyen, T. A. Physiological properties of an injectable peptide hydrogel for 3D cell culture with easy cell cluster recovery. in preparation

biological *in vivo* 3D systems, such as animal models, are expensive and time-consuming. Therefore, advanced *in vitro* 3D model systems are needed to offer an alternative to 2D systems and to mimic the complexity of the ECM and the physiological relevance of an *in vivo* biological system.

In the last few decades, hydrogel scaffolds have attracted more and more attention in an attempt to mimic *in vivo* conditions for cell culture. The biocompatible nanofiber network enables a hydrogel matrix with high water content that provides a promising architecture for 3D cell growth and introduces a number of desirable cellular microenvironment characteristics: 3D spatial support for cell growth; cell migration; and facile transportation of oxygen, nutrients, waste, and soluble factors.[10-16] Natural hydrogels are commonly derived from natural ECM or other biological components such as collagen, fibrin, hyaluronic acid, chitosan, and alginate. Although these natural hydrogels inherit various bioactive growth factors that promote cellular functions and enhance cell viability and proliferation,[17-20] these biochemical presentations introduce complex influence factors for cell physiological and pathophysiological studies[21] and restrict the applications of these culture systems to special cell lines. For example, a commercially available protein hydrogel (i.e., matrigel matrix) is constructed by a protein source extracted from the Engelbreth-Holm-Swarm (EHS) mouse sarcoma, which is a tumor rich in ECM proteins. Beside 60% laminin, 30% collagen Ⅳ, and 8% entactin, this matrix also contains several types of growth factors from the nature of the EHS tumor. In addition, some physical properties of the natural hydrogel matrix scaffold, such as fiber size, pore size, and mechanical strength, are not easily modified due to their fixed protein structures. For instance, the pore size of alginate hydrogel is 50-200 μm, which is much larger than most normal cell sizes (~10 μm). Such large pore size makes this hydrogel perform as a 2D substrate with curvature rather than an effective 3D matrix. Like many other synthetic biomaterials,[22-24] peptide hydrogel is highly reproducible and has properties that are predictably manipulated. Since Shuguang Zhang discovered the self-assembling peptide scaffold EAK16 in the early 1990s, design of peptide-based biological materials has been advancing rapidly.[25-29] By changing a single amino acid of the peptide sequence, peptide hydrogel could be modified to have various biological activities and functions.[30-32]

In addition, encapsulating cells into the hydrogel matrix is a critical step to introduce 3D spatial support for cell growth. For a convenient and effective encapsulation, cells should be

added simultaneously with the initialization of hydrogelation.[33, 34] Therefore, to ensure cells survive comfortably during gel formation, mild and cyto-compatible hydrogel-forming conditions are preferred. At present, according to environmental sensitivity, the sol-gel transformation of widely used peptide/protein hydrogels (i.e., puramatrix gel, hydromatix peptide hydrogel, and matrigel) are triggered by adjusting pH or temperature. A sudden change in conditions, such as more acidic pH (pH 2-3) or colder temperature (below 10 ˚C) than cells can tolerant, brings new challenges for cell encapsulation. Media may need to be changed several times to balance the pH of solutions, and every tool, piece of glassware, and medium needs to be chilled to ensure the gelator is in liquid form before mixing.

The objective of this study is to make a peptide hydrogel for 3D cell culture by directly mixing the peptide solution (h9e, FLIVIGSIIGPGGDGPGGD, at neutral pH) with Minimum Essential Medium (MEM, with 10% FBS). We hypothesized that without introducing any additional gel forming buffer or adjusting environmental pH or temperature, the h9e peptide provides a convenient and mild hydrogel forming process and allows cells to be surrounded by their culture medium during cell encapsulation. The mechanical properties of the h9e-MEM hydrogel architecture and its reassembly capability for potential injectable biomaterial were characterized through a series of rheological tests. Furthermore, a breast cancer cell line, MCF-7, was selected to grow in 3D in the h9e-MEM hydrogels with 1-3 mM peptide concentrations. Cell morphologies and their distribution in the hydrogel matrix were observed using biomedical microscopy and scanning electron microscopy (SEM). According to the special shear-thinning and rapid recovery property of this hydrogel matrix, we also hypothesized that this hydrogel could be used as an injectable material[35-37] and cells could be isolated from the hydrogel matrix by simple pipetting procedure. It has been a great challenge to isolate the 3D cultured cells from some currently used hydrogel matrixes:[21] either adding cell recovery buffer or reversing the sol-gel transformation by changing the environmental factors back to acidic pH or cold temperature may threaten the survival of the 3D cultured cells. Thus, this peptide hydrogel not only presents a convenient and effective process for cell encapsulation, but also provides an easy and safe cell isolation for further cell physiological and pathophysiological studies.

7.3 Experimental Section

7.3.1 Materials

N,N-Dimethylformamide (DMF), Trifluoroacetic acid (TFA), piperidine, N,N-Diisopropylethylamine (DIEA), Triisopropylsilane (TIS), paraformaldehyde, glutaraldehyde, 0.4 % Trypan blue, and insulin were purchased from Sigma-Aldrich (Milwaukee, WI). N-Methylpyrrolidinone (NMP), anhydrous ether, dichloromethane (DCM), and sodium bicarbonate were purchased from Fisher Scientific (Pittsburgh, PA). Rink Amide MBHA Resin, 2-(1H-Benzotriazole-1-yl)-1,1,3,3-tetramethyluronium Hexafluorophosphate (HBTU), and all protected amino acids were purchased from EMD Biosciences (San Diego, CA). N-hydroxybenzotriazole (HOBT) was purchased from CEM (Matthews, NC). Sodium pyruvate, non-essential amino acids, MEM with Eagle's salts, and TrypLE Express trypsin solution were purchased from Invitrogen (Carlsbad, CA). Fetal bovine serum (FBS) was purchased from Atlanta Biologicals (Lawrenceville, CA).

7.3.2 Peptide Synthesis and Hydrogelation

The h9e peptide was synthesized according to a previously published protocol[38]. Briefly, peptides were synthesized on an automated CEM Liberty microwave peptide synthesizer (CEM Corporation, Matthews, NC) according to the base-labile 9-fluorenylmethoxycarbonyl (Fmoc) strategy with Rink amide resin and Fmoc-protected amino acids. After final N-terminal Fmoc group deprotection, the resin-bound peptides were side-chain-deprotected and cleaved using TFA/TIS/water (95/2.5/2.5 v/v). Peptides were precipitated and washed three times with anhydrous ether, dissolved in acetonitrile and deionized water (50/50 v/v). The peptide solution was freezed in a -80 ˚C refrigerator overnight and then was freeze-dried for 48 hours by using the Labconco freeze dry system (Labconco, Kansas City, MO). The pH value of the peptide in water solution was 3.6. Molecular weight of the synthesized peptide was confirmed by matrix-assisted laser desorption/ionization time-of-flight mass spectroscopy on an Ultraflex II instrument (Bruker Daltronics, Billerica, MA). The peptide purity wa confirmed by a Beckman System Gold high performance liquid chromatography (HPLC, Beckman Coulter, Inc., Fullerton, CA) on a phenomenex synergi 4μ Hydro-RP column (Phenomenex, Inc., Torance, CA) with the following gradient: 10-90% B in 20 min (A: 99.9% H_2O, 0.1% TFA; B: 90% acetonitrile, 9.9% H_2O, 0.1% TFA).

Lyophilized peptide was added to 100 mM sodium bicarbonate (pH=8) and completely dissolved by magnetic stirring for 3 h with a final peptide concentration of 10 mM. For hydrogelation, peptide solution was added into MEM with 10% FBS and the mixture was hand-shaken for about 10 seconds. The peptide hydrogel formed within 15 min at room temperature with final peptide concentration of 1, 2, and 3 mM.

7.3.3 Oscillational Rheology Test

The storage and loss moduli (G' and G'', respectively) of h9e hydrogels were determined on a C-VOR 150 rheometer system (Malvern instruments, Malvern, Worcestershire WR141XZ, United Kingdom) with a 20-mm diameter parallel plate geometry and 500 μm gap size. To mimic cell physiological conditions, all rheological tests were performed at 37 ℃ unless otherwise specified. The peptide and MEM (with/without cells) mixture was placed on the measuring system immediately after mixing for a gel-forming rate test. Single frequency (1 Hz) and steady shear strain (1%) were selected for a 1-h test. To determine the hydrogel reassembly capability, the peptide and MEM mixture was incubated at room temperature overnight for hydrogelation, then transferred to a lower measuring plate for a 10-min, single-frequency test (1 Hz, 1% strain) for stabilization. The hydrogel was broken using 1 Hz frequency and 500% shear strain for 1 min. Afterward, resetting the instrument parameters took 1 min, and the hydrogel moduli during the reassembly period were measured under 1 Hz frequency and 1% shear strain for 1 h. The amplitude sweep test (strain from 1 to 500%, 1Hz frequency) was conducted multiple times to determine hydrogel reassembly capability after every time it was destroyed. Four testing circles were applied in this measurement and the hydrogel recovery time between every two circles was 1, 5, and 10 min. Furthermore, to test the response to different environmental temperatures, the peptide hydrogel was measured under a temperature profile test with steady oscillatory frequency (1 Hz) and strain (1%). The temperature was adjusted from 4 ℃ to 50 ℃ for two testing circles. For each circle, the instrument's heating or cooling processes took 5 min, then another 5 min to arrive at the setting temperature (4 ℃ or 50 ℃). To determine the G' and G'' of hydrogel during cell isolation, 3 mM peptide hydrogel was diluted 15 times with MEM. After thorough mixing, the diluted solution was tested under 1 Hz frequency and 1% shear strain at 4 ℃ for 1 h.

7.3.4 Cell Culture

MCF-7 cells were selected for this study to grow as cell colony in hydrogel matrix (to *in vitro* mimic the real tumor for drug testing in future). The cells were maintained in T-75 cm^2 tissue culture flasks (Greiner Bio-one, Begium) at 37 ℃ in 5% (v/v) CO_2 in MEM medium with 10% (v/v) FBS, 1 mM sodium pyruvate, 17.9 mM sodium bicarbonate, 0.01 mg/mL insulin, and 1% (v/v) non-essential amino acid. The medium was changed every other day and cells were routinely passed using trypsin (Invitrogen).

7.3.5 Culturing Cells in h9e Hydrogel

The h9e solution was sterilized by UV irradiation (254 nm) for 30 min before cell encapsulation. MCF-7 cells were detached from the flask using trypsin and pelleted by centrifugation for 5 min at 2000 rpm and 4 ℃. The supernatant was removed and pelleted cells were re-suspended in MEM. The numbers of cells were counted using a cellometer (Auto T4, Nexcelom Bioscience, Lawrence, MA). About 2.8×10^5 cells were seeded into each well of a 12-well culture plate (Becton Dickinson Labware, Franklin Lakes, NJ) and 100 to 300 μL of h9e peptide solution (10 mM) was then added to make the final volume of the mixture 1 mL and peptide concentrations 1 to 3 mM. The mixture was thoroughly mixed by pipetting the mixture three times, and the culture plate was then placed in a 37 ℃ incubator (Thermo Scientific, Asheville, NC) for approximately 30 min. After hydrogelation, another 1 mL of MEM was carefully added to the top of the hydrogel to prevent drying during long-term incubation. Part of the top medium (600 μL, the liquid phase) was changed every 2 days to reduce cell loss and provide fresh nutrition for cells embedded in the hydrogel matrix. Cells cultured on plastic substracte of 12-well culture plates were used as the control. The morphological of the cells cultured in on plastic plate verse h9e hydorgel were determined using an inverted microscope (Nikon Eclipse TE2000-U, Kanagawa, Japan) at days 1, 3, 5, and 7.

7.3.6 Scanning Electron Microscopy (SEM)

The morphologies of h9e hydrogels as well as MCF-7 cells cultured in h9e hydrogels were observed by FESEM. The hydrogel samples with cells were fixed in a 2% paraformaldehyde and 2% glutaraldehyde mixture for 30 min before dehydration and critical point drying. Samples were then sputter-coated (Desk II Sputter/etch Unit, Denton Vaccum, Moorestown, NJ) 3 times (12 seconds each time) with 100% Pt. The hydrogel samples were

dehydrated in a serial ethonal concentration of 50% (v/v) to 100% (v/v) at 5% steps. The samples were immersed in ethonal for 15 min per step. The samples were then critical point dryed (Samdri-790B, Tousimis Research Corp., Rockville, MD). The SEM observation was carried out with an FEI, Nova NanoSEM 430 (Hillsboro, ON) at 5 kV and through a lens detector. The particle size was measured by using Image J software (rsbweb. nih. gov) with more than 10 measurements.

7.3.8 Cell Isolation

To isolate the cells from the hydrogel matrix, 2 mL MEM was added to each hydrogel cell culture in the 12-well plate. The total 4 mL solution was thoroughly mixed by using a pipette and transferred to a centrifuge tube. An additional 4 mL MEM was added to wash the cell culture well and was collected in the centrifuge tube, then 1 mL trypsin solution was added to the well, which allowed cells to detach from the well. The plate was incubated at 37 ℃ for 5 min and the solution was collected into the centrifuge tube again. The centrifuge tube was placed on ice. Another 6 mL MEM was added to the centrifuge tube for a final volume of 15 mL. The solution was thoroughly mixed by using pipette and cells were pelleted by centrifugation for 5 min at 2000 rpm and 4 ℃. The supernatant was removed and the cell pellet was re-suspended with 2 mL MEM. A 20 μL cell re-suspension was add into a cell counting chamber (Nexcelom Bioscience, Lawrence, MA) and counted by cellometer (Auto T4, Nexcelom Bioscience, Lawrence, MA). To test the cell viability, 100 μL 0.4% Trypan blue was added into 100 μL cell re-suspension for 10 min, then 20 μL cells/Trypan blue mixture was add into a cell counting chamber was and counted by cellometer (Auto T4, Nexcelom Bioscience, Lawrence, MA).

7.3.9 Statistical Analysis

A two-sample t-test was used to analyze the difference among the various treatments. P value of less than 0.05 was considered statistically significant.

7.4 Results and Discussion

The 10 mM h9e peptide was placed in 100 mM $NaHCO_3$, and the solution's final pH was around 7.5. To initiate hydrogelation, 100 μl peptide solution was added to 900 μL MEM medium (with 10% FBS) and mixed by gentle hand-shaking for 10 seconds or pipette mixing

(withdraw and infuse) three times to form 1 mL mixture with 1mM (0.17% w/v) peptide concentration (Figure 7.1a). Because h9e is a Ca^{2+} sensitive peptide,[38] a proposed mechanism of MEM-induced h9e self-assembly (Figure 7.1a) suggests that after MEM was added, the Ca^{2+} ions from the medium immediately attached to the ion-binding sites of peptides, which enhanced peptide self-organization into nanofibers, which further interlaced as a scaffold of the hydrogel matrix. The SEM image of Figure 7.1a presents the morphology of the nanofiber network of hydrogel matirx.

Incorporation of drugs, proteins, or cells into hydrogel during gel formation is considered one of the most effective ways to introduce these compounds into *in vivo* biological systems.[33, 34] However, to ensure homogenous distribution of drugs, proteins, or cells in hydrogel matrix, peptides should assemble as a nanofiber network in a relatively short period with sufficent strength to hold the suspended molecules. To determine the peptide gel-formation rate, we prepared hydrogels with three concentrations, 1 mM (0.17% w/v), 2 mM (0.34% w/v), and 3 mM (0.51% w/v), in MEM. The solutions were measured at 37 ℃ immediately after mixing. Figure 7.1b shows an exponential increase in storage modules (Pa) from time zero upto around 900 s. After that time poin, the storage modules reached a plateau over the 1-h test period. With increasing concentration of h9e, 1mM, 2 mM and 3 mM the storage modules reached a plateau of 100, 400 and 700 Pa, respectively. This data clearly shows that h9e formed a stable hydrogel after 900 s and that the concentration of h9e has a direct affect on the strength of the hydrogel. A similar result was observed when cells (1×10^6 cells/mL) were suspended in MEM and then had peptide solution for 1-3 mM hydrogels added (Figure 7.1c), indicating that the cells didn't change the rate or strength of hydrogelation. FESEM images (Figure 7.1d, e) indicated that the hydrogel architecture was built by entanglement of nanofibers; however, the lower-concentration hydrogel (1 mM, Figure 7.1d) shows a relatively less density of nanofiber networkcompared with the greater density of nanofiber network of the higher-concentration hydrogel (3 mM Figure 7.1e). Because a higher nanofiber density may exhibit stronger mechanical strength, this visual evidence of different nanofiber density of hydrogels with different concentrations further supports their strength differences.

For tissue regeneration and controlled release of drug delivery applications, delivering hydrogel-encapsulating molecules from *in vitro* to *in vivo* via syringe injection is critical to the success of a 3D matrix.[31,37,39] For this purpose, the peptide hydrogel must exhibit shear-thinning

behavior (transfer from solid phase into liquid phase) under the applied shearing force, yet reassemble quickly to retain the 3D encapsulation of molecules after injection.[40]. The reassembly ability of MEM-induced h9e hydrogel was assessed by a dynamic rheological test: 1-3 mM peptide hydrogels were prepared at room temperature overnight, then transferred to a measuring system and stabilized for 10 min. By shear-thinning at 500% strain for 1 min, all three hydrogels were converted to a liquid state, showing a G' lower than 0.2 Pa (Figure 7.2a). Shear stress encountered during syringe delivery is much lower than this measuring system and causes the hydrogel to become a low-viscosity gel. After shear-thinning stopped and we waited 1 min to reset instrument parameters, hydrogel recovery was monitored using 1% shear strain for 1 h. The data in Figure 7.2a show that after the 1-min waiting time, about 80% of hydrogel G' was recovered. The G' of hydrogel at all three concentrations stiffened further with time, and 100% gel strength recovery was observed within the 1-h recovery test.

To determine whether the hydrogel could maintain this quick reassembly capability even after shear-thinning many times, the hydrogel was measured under an amplitude sweep test conducted multiple times. Four testing circles were applied in this measurement, and shear strain was increased from 1% to 500% within 5 min for each circle. After that, we waited 1, 5, and 10 min, respectively, for hydrogel recovery. Figure 7.2b suggests that although the hydrogel architecture was completely broken into liquid form (G' < 0.2 Pa) at the end of each circle, quick reassembly persisted (G' > 80, 100, 300 Pa for 1 mM, 2 mM and 3 mM h9e hydrogel respectively) even after shear-thinning multiple times. We also found that the percentage of recovery G' increased with waiting time and that the hydrogel reassembly rate related to hydrogel concentrations. For example, with waiting time of 1 min, about 73% (70 Pa), 76% (130 Pa), and 88% (320 Pa) of the gel strengths were recovered for 1, 2, and 3 mM hydrogel, respectively, but after three shear-thinning circles and 10 min waiting, 83% (80Pa, 1 mM), 84% (144 Pa, 2 mM), and 100% (363 Pa, 3 mM) of the gel strength were recovered (Figure 7.2b). The higher reassembly rate is most likely caused by the more compact matrix structure of hydrogel due to higher peptide concentration (3 mM) (Figure 7.1e), where some non-covalent gel network cross-links remain intact and the broken nanofiber groups are close to each other, making rebuilding the cross-links easy.[41] Based on these rheological properties, we could deliver this MEM-induced h9e hydrogel multiple times and inject it via pipette or syringe without permanently destroying the hydrogel architecture (Figure 7.2c).

For biological study, temperatures between 4 ℃ and 37 ℃ are commonly applied for many standard operational procedures for molecule storage; therefore, the response of the high-water-content hydrogel materials to these temperature variations has a large impact on their practical applications. The rheological temperature profile test was performed to address this challenge. We adjusted the temperature from 4 ℃ to 50 ℃ for two testing circles. Figure 7.2d shows that the G' of hydrogels moves along with temperature and performs 2-3 times higher at 50 ℃ than that at 4 ℃. This thermal response is reversible according to the hydrogel heating and cooling circles (Figure 7.2d) and provides us positive information for using this peptide hydrogel as a 3D cell culture: the hydrogel matrix is stiffened for cell encapsulation when it remains at 37 ℃, but is weakened at 4 ℃ for cell isolation using standard centrifuge method.

The 3D cell culture matrices were prepared by directly adding peptide solution into MCF-7 cell suspension. The mixture was incubated 30 min at 37 ℃ for the hydrogel to firm completely. Another 1 mL MEM medium was carefully added to the top of the hydrogel to preserve the moisture for long-term incubation. The top medium was changed every other day to provide embedded cells fresh nutrition. The inverted microscope images of MCF-7 cells in h9e hydrogel (Figure 7.3a) shows that the colony-like structure suggests the 3D division of a single seeded cell, and the neighboring clusters also show the tendency to merge. In contrast, the MCF-7 cells cultured in a plastic plate attached to the bottom of the plastic plate and presented a flat-shaped morphology (Figure 7.3b). Some cultured cells floated on top of the cell-attached layer and appeared as a sphere shape.

FESEM images reveal the attachment of cells and the surrounding hydrogel matrix (Figure 7.4). Figure 7.4b is a protruding cell cluster from the nanofiber scaffold. Given a close observation of the cell surface, layers of dense nanofiber network were observed on the surface of cells (Figure 7.4a), indicating that the cluster of cells grows inside out by self-division. The expanding cells force the surrounding hydrogel matrix to collapse into layers of nanofiber network and attach to the cell surface. The interface character of the cell surface and the surrounding hydrogel matrix (Figure 7.4c) suggest that the hydrogel matrix promotes the cell attachment by providing a scaffold environment on which cells could stably settle.

For further cell physiological and pathophysiological studies, cells need to be isolated from the hydrogel matrix after cultured. According to the rheological study above, h9e hydrogel architecture can be destroyed under mechanical stress. Therefore, the hydrogel matrix can be

converted to liquid through a simple shearing procedure, which allows cells to be isolated before hydrogel architecture is reassembles. As mentioned before, the fast reassembly property of this hydrogel is correlated to the peptide concentration. To ensure enough time for cell isolation, the sheared hydrogel with 3D cultured cells then needs to be diluted while maintained at a low environmental temperature. To further confirm this cell isolation hypothesis, we diluted a 3 mM peptide hydrogel 15 times with MEM. The final peptide concentration was 0.2 mM. After thorough mixing with a pipette, the G' and G'' of this solution were determined by a 1 Hz single frequency rheological study with 1% shear strain. The experimental temperature was set at 4 ℃, the same as that used for cell centrifugation. Figure 7.5b indicates that after dilutions, the hydrogel was converted to Newtonian liquid showing that both G' and G'' were around 0 Pa for the first 200 seconds. The G' then increased to 9 Pa within the first 10 min; however, it quickly dropped to 5 Pa and stayed at the same level as G'' for the remaining test. This phenomenon suggests that although the peptide has the tendency to reassemble, its solid strength is too weak to resist a slight disturbance, even shear stress from 1% strain. The diluted solution become stable as a low-viscosity liquid and would not reform as a hydrogel (Figure 7.5b) within the time domain for the centrifuge isolation process. Besides, the shear stress encountered during centrifugation is much higher than 1% shear strain, which keeps the hydrogel solution in low-viscosity liquid form and makes cell isolation from this solution even easier.

In practice, we diluted a cell's encapsulating peptide hydrogel 15 times with MEM (Figure 7.5a) and thoroughly mixed using a pipette (see cell isolation and cell viability in the Experimental section for details). The cells/peptide/MEM mixture was converted to a liquid. After 5 min centrifugation at 4 ℃, the cells were clearly separated from the peptide/MEM solution into a small pellet, which was observed at the bottom of the centrifuge tube (Figure 7.5a).

This peptide hydrogel provides a convenient method of isolating cells from the 3D hydrogel matrix. The next question is what percentage of cells in the hydrogel matrix could be collected from this method and whether they are viable after extraction. To address this question, 1.5×10^5 cells were seeded in 3mM h9e hydrogel and isolated using the above method after 30 min incubation. Cell viability before encapsulation and after isolation was compared (Figure 7.5c, d). Based on the mean value of three measurements, about 97% of viable cells were re-collected from the hydrogel matrix. The statistical analysis suggests no significant difference in

viable cell number before encapsulation and after isolation (Figure 7.5c, d). These results confirmed that the cell isolation method for this h9e peptide hydrogel is safe and effective for biological studies.

7.5 Conclusions

In this study, we reported a convenient and effective peptide hydrogel system for 3D cell culture. With physiological conditions and surrounded by cell growth medium, MCF-7 cells were encapsulated during the mild and cyto-compatible hydrogelation process simply by adding a peptide solution to the cell suspension of MEM. At physiological pH, the formation of hydrogel with controlled time and gel strength can be modulated by changing the temperature or peptide concentration. The specific shear thinning and rapid recovery rheological properties of hydrogel allow us to inject or deliver this hydrogel material via syringe or pipette multiple times. Unlike the attached flat morphology of cells in a plastic plate culture, cells residing in peptide hydrogel adopt growing and merging clustered structures that are reminiscent of real tumors. More advantageously, the hydrogel architecture can be disrupted by pipette mixing and further converted to a liquid form through dilution with MEM. This property provides a convenient method to isolate 3D cultured cells effectively from the hydrogel matrix by centrifugation, which makes the monitoring of viable and non-viable cells easier for *in vitro* 3D cell culture. This peptide hydrogel could be an advanced functional material for 3D cell culture for various further biomedical studies.

7.6 Acknowledgments

We thank Mr. Kent Hampton (Department of Entomology, Kansas State University) for SEM sample preparation, the University of Kansas Mass Spectrometry Lab for HPLC and mass spectrometric analysis, and the Confocal Microfluorometry and Microscopy Core of NIH P20RR017686. This project was partially funded by KSU Targeted Excellence Program and KSU Research Foundation Scholarship Program as well as the contribution (no. 12-181-J) from the Kansas Agricultural Experiment Station.

7.7 References

1. Zhang, S. Designer self-assembling peptide nanofiber scaffolds for study of 3-D cell biology and beyond. Adv. Can. Res. 2008, 99, 335-362.

2. Dvir, T.; Timko, B. P.; Kohane, D. S.; Langer, R. Nanotechnological strategies for engineering complex tissues. Nat. Nanotechnol. 2011, 6, 13-22.

3. Perez-Castillejos, R. Replication of the 3D architecture of tissues RID F-5656-2010. Materials Today 2010, 13, 32-41.

4. Kyle, S.; Aggeli, A.; Ingham, E.; McPherson, M. J. Production of self-assembling biomaterials for tissue engineering. Trends Biotechnol. 2009, 27, 423-433.

5. Tibbitt, M. W.; Anseth, K. S. Hydrogels as Extracellular Matrix Mimics for 3D Cell Culture. Biotechnol. Bioeng. 2009, 103, 655-663.

6. Gurski, L. A; Jha, A. K.; Zhang, C.; Jia, X.; Farach-Carson, M. C. Hyaluronic acid-based hydrogels as 3D matrices for in vitro evaluation of chemotherapeutic drugs using poorly adherent prostate cancer cells. Biomaterials 2010, 31, 4248-4248.

7. Feder-Mengus, C.; Ghosh, S.; Reschner, A.; Martin, I.; Spagnoli, G. C. New dimensions in tumor immunology: what does 3D culture reveal? Trends Mol. Med. 2008, 14, 333-340.

8. Engler, A. J.; Sen, S.; Sweeney, H. L.; Discher, D. E. Matrix elasticity directs stem cell lineage specification. Cell 2006,126, 677-689.

9. Liu, S. Q.; Tay, R.; Khan, M.; Ee, P. L. R.; Hedrick, J. L.; Yang, Y. Y. Synthetic hydrogels for controlled stem cell differentiation. Soft Matter 2010, 6, 67-81.

10. Shea, L.; Smiley, E.; Bonadio, J.; Mooney, D. DNA delivery from polymer matrices for tissue engineering. Nat. Biotechnol. 1999, 17, 551-554.

11. Levenberg, S.; Huang, N.; Lavik, E.; Rogers, A.; Itskovitz-Eldor, J.; Langer, R. Differentiation of human embryonic stem cells on three-dimensional polymer scaffolds. Proc. Natl. Acad. Sci. U. S. A. 2003,100, 12741-12746.

12. Silva, G.; Czeisler, C.; Niece, K.; Beniash, E.; Harrington, D.; Kessler, J.; Stupp, S. Selective differentiation of neural progenitor cells by high-epitope density nanofibers. Science 2004, 303, 1352-1355.

13. Peppas, N.; Hilt, J.; Khademhosseini, A.; Langer, R. Hydrogels in biology and medicine: From molecular principles to bionanotechnology. Adv. Mater. 2006, 18, 1345-1360.

14. Lee, K.; Mooney, D. Hydrogels for tissue engineering. Chem. Rev. 2001, 101, 1869-1879.

15. Drury, J.; Mooney, D. Hydrogels for tissue engineering: scaffold design variables and applications. Biomaterials 2003, 24, 4337-4351.

16. Mather, M. L.; Tomlins, P. E. Hydrogels in regenerative medicine: towards understanding structure-function relationships. Regenerative Medicine 2010, 5, 809-821.

17. Azab, A.; Orkin, B.; Doviner, V.; Nissan, A.; Klein, M.; Srebnik, M.; Rubinstein, A. Crosslinked chitosan implants as potential degradable devices for brachytherapy: In vitro and in vivo analysis. J. Controlled Release 2006,111, 281-289.

18. Eyrich, D.; Brandl, F.; Appel, B.; Wiese, H.; Maier, G.; Wenzel, M.; Staudenmaier, R.; Goepferich, A.; Blunk, T. Long-term stable fibrin gels for cartilage engineering. Biomaterials 2007, 28, 55-65.

19. Barralet, J.; Wang, L.; Lawson, M.; Triffitt, J.; Cooper, P.; Shelton, R. Comparison of bone marrow cell growth on 2D and 3D alginate hydrogels. J. Mater. Sci.-Mater. Med. 2005, 16, 515-519.

20. Dawson, E.; Mapili, G.; Erickson, K.; Taqvi, S.; Roy, K. Biomaterials for stem cell differentiation. Adv. Drug. Deliv. Rev. 2008, 60, 215-228.

21. Cushing, M. C.; Anseth, K. S. Hydrogel cell Cultures. Science 2007, 316, 1133-1134.

22. Bryant, S.; Anseth, K. Hydrogel properties influence ECM production by chondrocytes photoencapsulated in poly(ethylene glycol) hydrogels. J. Biomed. Mater. Res. 2002, 59, 63-72.

23. Chirila, T.; Constable, I.; Crawford, G.; Vijayasekaran, S.; Thompson, D.; Chen, Y.; Fletcher, W.; Griffin, B. Poly(2-Hydroxyethyl Methacrylate) Sponges as Implant Materials - Invivo and Invitro Evaluation of Cellular Invasion. Biomaterials 1993, 14, 26-38.

24. Sawhney, A.; Pathak, C.; Hubbell, J. Bioerodible Hydrogels Based on Photopolymerized Poly(ethylene Glycol)-Co-Poly(alpha-Hydroxy Acid) Diacrylate Macromers Rid A-9266-2008. Macromolecules 1993, 26, 581-587.

25. Zhang, S.; Lockshin, C.; Cook, R.; Rich, A. Unusually Stable Beta-Sheet Formation in an Ionic Self-Complementary Oligopeptide. Biopolymers 1994, 34, 663-672.

26. Hauser, C. A. E.; Zhang, S. Designer self-assembling peptide nanofiber biological materials. Chem. Soc. Rev. 2010, 39, 2780-2790.

27. Cavalli, S.; Albericio, F.; Kros, A. Amphiphilic peptides and their cross-disciplinary role as building blocks for nanoscience. Chem. Soc. Rev. 2010, 39, 241-263.

28. Branco MC, Pochan DJ, Wagner NJ, Schneider JP. The effect of protein structure on their controlled release from an injectable peptide hydrogel. Biomaterials 2010, 31, 9527-9534.

29. Rapaport, H.; Grisaru, H.; Silberstein, T. Hydrogel Scaffolds of Amphiphilic and Acidic beta-Sheet Peptides. Adv. Fun. Mate. 2008, 18, 2889-2896.

30. Chawla, K.; Yu, T.; Liao, S. W.; Guan, Z. Biodegradable and Biocompatible Synthetic Saccharide-Peptide Hydrogels for Three-Dimensional Stem Cell Culture. Biomacromolecules 2011, 12, 560-567.

31. Salick, D. A.; Pochan, D. J.; Schneider, J. P. Design of an Injectable beta-Hairpin Peptide Hydrogel That Kills Methicillin-Resistant Staphylococcus aureus. Adv. Mater. 2009, 21, 4120-4123.

32. Shah, R. N.; Shah, N. A.; Lim, M. M. D. R.; Hsieh, C.; Nuber, G.; Stupp, S. I. Supramolecular design of self-assembling nanofibers for cartilage regeneration. Proc. Natl. Acad. Sci. U. S. A. 2010, 107, 3293-3298.

33. Haines-Butterick, L.; Rajagopal, K.; Branco, M.; Salick, D.; Rughani, R.; Pilarz, M.; Lamm, M. S.; Pochan, D. J.; Schneider, J. P. Controlling hydrogelation kinetics by peptide design for three-dimensional encapsulation and injectable delivery of cells. Proc. Natl. Acad. Sci. U. S. A. 2007, 104, 7791-7796.

34. Zhang, S.; Greenfield, M. A.; Mata, A.; Palmer, L. C.; Bitton, R.; Mantei, J. R.; Aparicio, C.; Cruz, M. O.; Stupp, S. I. A self-assembly pathway to aligned monodomain gels. Nature Mat. 2010, 9, 594-601.

35. Nowak, A.; Breedveld, V.; Pakstis, L.; Ozbas, B.; Pine, D.; Pochan, D.; Deming, T. Rapidly recovering hydrogel scaffolds from self-assembling diblock copolypeptide amphiphiles. Nature 2002, 417, 424-428.

36. Schneider, J.; Pochan, D.; Ozbas, B.; Rajagopal, K.; Pakstis, L.; Kretsinger, J. Responsive hydrogels from the intramolecular folding and self-assembly of a designed peptide. J. Am. Chem. Soc. 2002, 124, 15030-15037.

37. Yu, L.; Ding, J. Injectable hydrogels as unique biomedical materials. Chem. Soc. Rev. 2008, 37, 1473-1481.

38. Huang, H.; Shi, J.; Laskin, J.; Liu, Z. McVey DS, Sun XS. Design of a shear-thinning recoverable peptide hydrogel from native sequences and application for influenza H1N1 vaccine adjuvant. Soft Matter 2011, 8905-8912.

39. Balakrishnan, B.; Jayakrishnan, A. Self-cross-linking biopolymers as injectable in situ forming biodegradable scaffolds. Biomaterials 2005, 26, 3941-3951.

40. Yan, C.; Pochan, D. J. Rheological properties of peptide-based hydrogels for biomedical and other applications. Chem. Soc. Rev. 2010, 39, 3528-3540.

41. Yan, C.; Altunbas, A.; Yucel, T.; Nagarkar, R. P.; Schneider, J. P.; Pochan, D. J. Injectable solid hydrogel: mechanism of shear-thinning and immediate recovery of injectable beta-hairpin peptide hydrogels. Soft Matter 2010, 6, 5143-5156.

Figure 7.1 Peptide hydrogelation in MEM.

a. MEM-induced h9e peptide self-assembling hydrogelation (proposed mechanism of peptide self-assembly with Ca2+; SEM image showing the nanofiber scaffold of the hydrogel matrix). **b.** Storage modulus G' of 1, 2, and 3 mM peptide hydrogel during the hydrogelation at 37 °C. **c.** Storage modulus G' of 1, 2, and 3 mM peptide with 1 ×106 cells/mL in MEM during the hydrogelation at 37 °C. **d.** SEM image of 1 mM peptide hydrogel. E. SEM image of 3 mM peptide hydrogel.

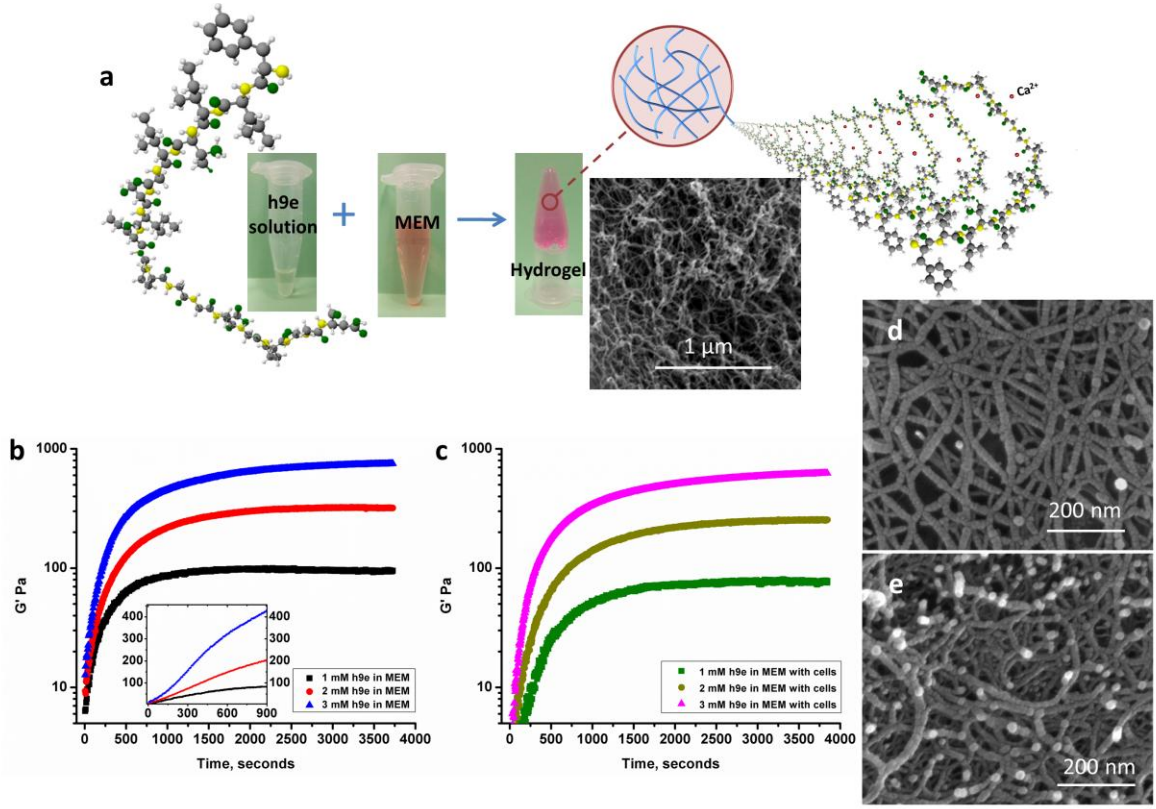

Figure 7.2 Dynamic rheological study of h9e hydrogel.

a. Storage modulus G' of shear-thinning and recovery test of 1, 2, and 3 mM peptide hydrogel. **b.** Four times amplitude sweep test with shear strain from 1% to 500% and 1-, 5-, and 10-min breaks. **c.** Peptide hydrogel was delivered via pipette multiple times; hydrogel was shear-thinned but reassembled quickly without permanently destroying the hydrogel architecture. **d.** Temperature profile test of 1-, 2-, and 3-mM peptide hydrogel between 4 °C and 50 °C.

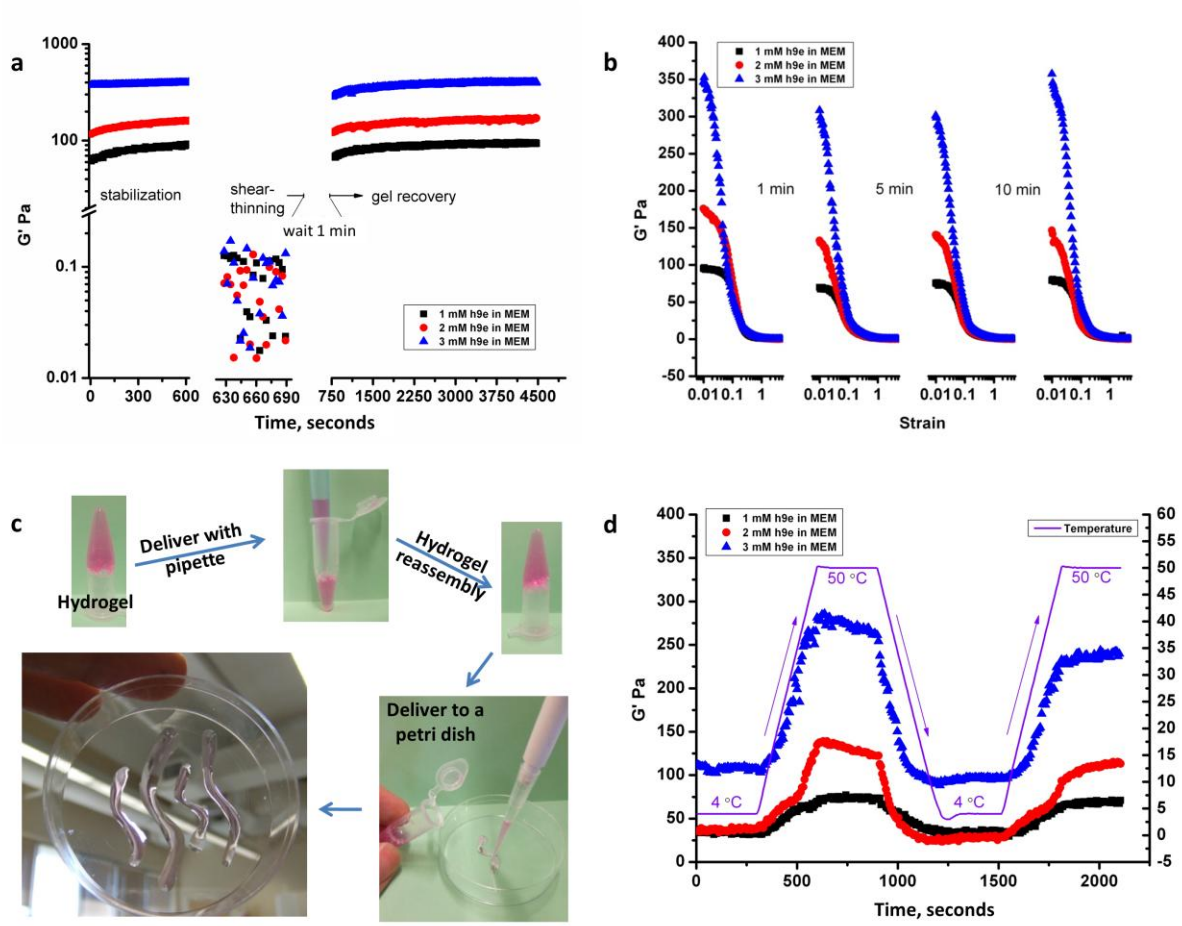

Figure 7.3 Culturing cells in h9e hydrogel.

a. Morphology of cluster cell in 3D hydrogel matrix over 5 days. **b.** Morphology of cell growth on 2D plastic monolayer over 5 days.

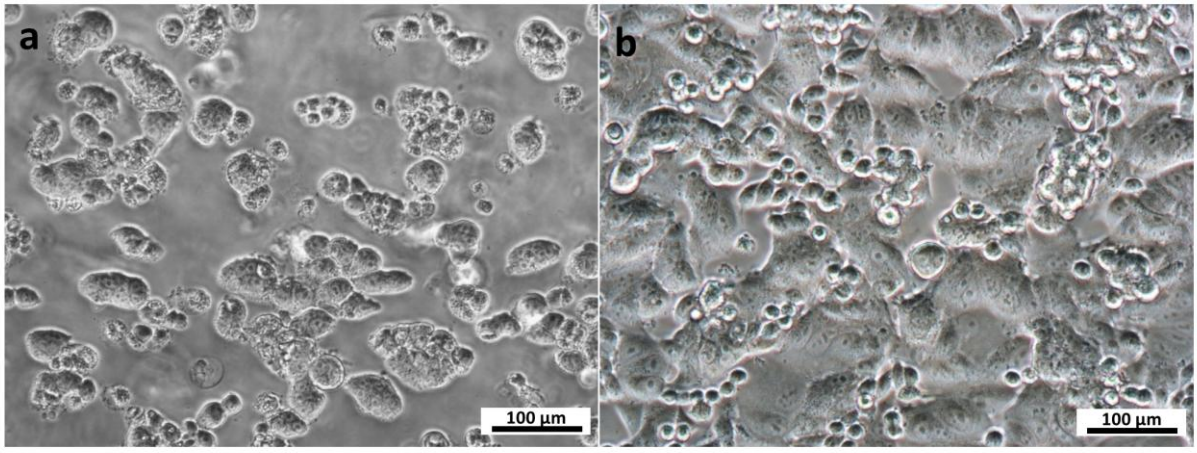

Figure 7.4 SEM images of cell cluster in 3D hydrogel matrix.

a. Nanofiber network coating on cell surface. **b.** A protruding cell cluster from the nanofiber scaffold. C. Interface of the cell surface and the surrounding hydrogel matrix.

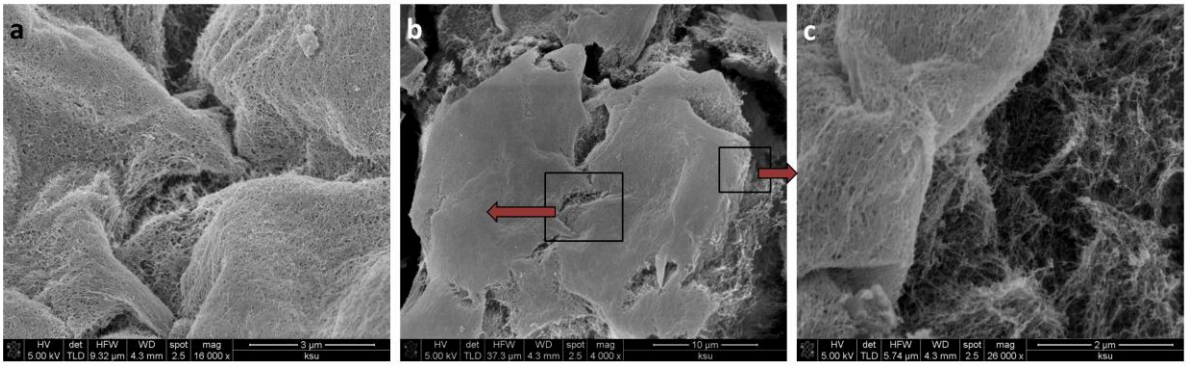

Figure 7.5 Cell isolation from hydrogel matrix.

a. Cells encapsulating peptide hydrogel diluted in MEM and cells pelleted with 5 min centrifugation at 4 ^{o}C. **b.** Storage (G') and loss (G'') moduli of hydrogel diluted 15 times at 1 Hz frequency and 1% shear strain at 4 ^{o}C for 1 h. **c.** Viable cells before cell encapsulation and after cell isolation. **d.** Cell viability before cell encapsulation and after cell isolation. *p < 0.05, n=3, error bars represent standard deviation.

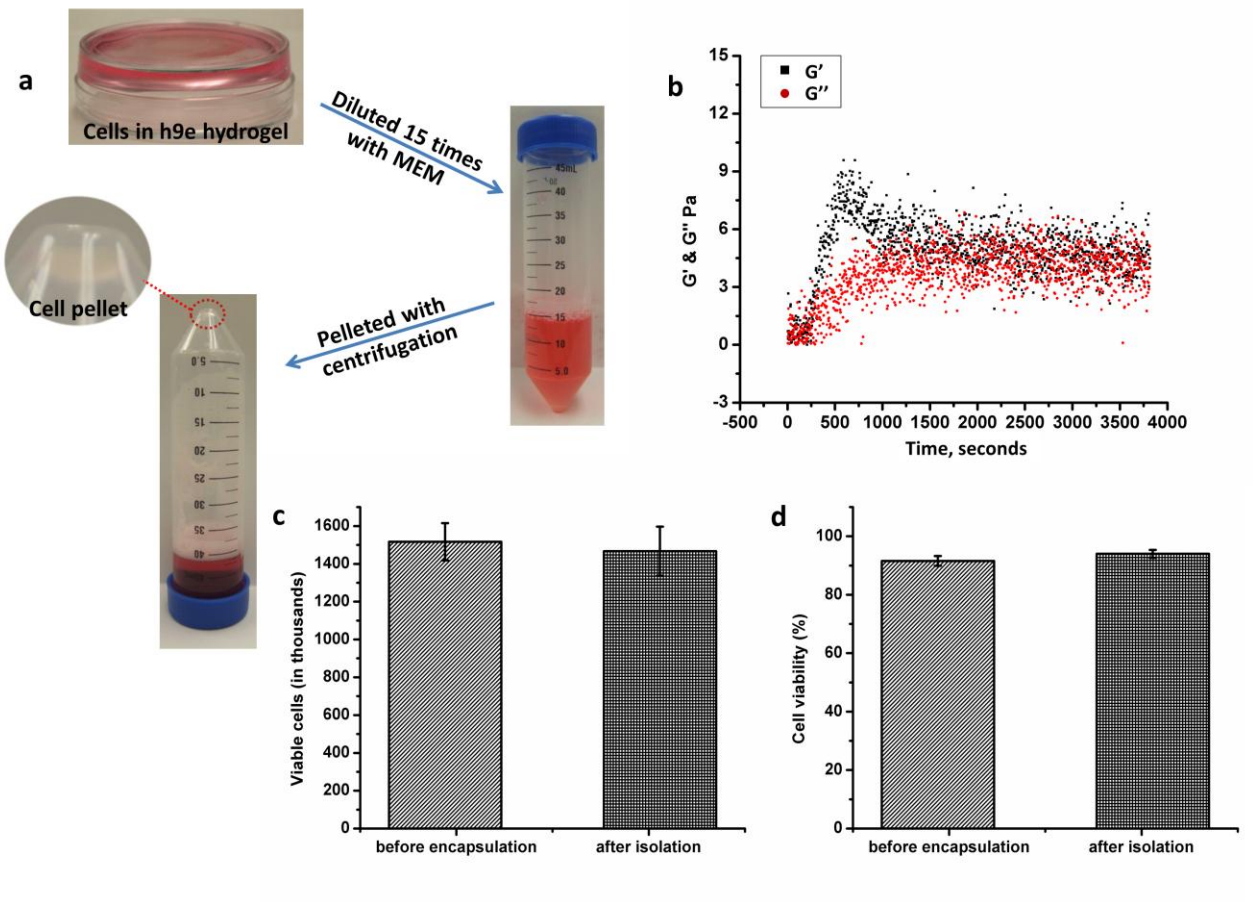

Chapter 8 - Study Albumin Triggered Hydrogel Forming Process

8.1 Abstract

A specific albumin that triggered the peptide self-assembly pathway was found in this study. Peptide molecules could bind the surface of albumin molecules and lead to a highly ordered self-organization. Albumin concentration controlled the hydrogel forming rate and related to the final mechanical strength. The critical concentration of both peptide and albumin is required for this specific hydrogel forming process. Further understanding this specific peptide self-assembly pathway will lead to a new class of rational designed biomaterials for bread applications.

8.2 Introduction

Because of its distinct three-dimensional network, peptide hydrogel not only provides an *in vitro* environment that mimics the extracellular matrix condition for 3D cell culture but also acts as an auxiliary carriers for targeted drug or gene delivery and biomolecular controlled release.[1-3] With the rapid development of peptide hydrogel for biomedical applications, the mild method to trigger the peptide solution into hydrogel has attracted more attentions to apply these materials.[4-6] In our resent study, we found that the h9e peptides could spontaneously organize into an injectable hydrogel material under the trigger of Bovine Serum Albumin (BSA) or Human Serum Albumin (HSA) without adding any other metal ions or adjusting environmental pH or temperature. This is the first time a rationally designed peptide has been found to self-assemble into hydrogel through binding with albumin molecules. The objective of this study is to understand how albumin triggers h9e peptide self-assembly into hydrogel. We hypothesized that albumin will help the peptide molecules aggregate orderly; the storage module of hydrogel as well as the hydrogel forming rate are affected by peptide and albumin concentration. Because albumin is the most abundant protein in human serum and is considered one of the most important proteins for molecular transportation, pH balance, and maintaining osmotic pressure,[7, 8] hydrogel formed through albumin binding has great potential for a wide range applications.

8.3 Experimental Section

8.3.1 Peptide Synthesis and Hydrogel Preparation

Peptides were synthesized on a CEM Liberty microwave peptide synthesizer (CEM Corporation, Matthews, NC) based on the automated base-labile 9-fluorenylmethoxycarbonyl (Fmoc) strategy with Fmoc-protected amino acids (EMD Biosciences, San Diego, CA). Peptides were cleaved with 95% trifluoroacetic acid (Sigma-Aldrich, Milwaukee, WI), 2.5% triisopropylsilane (Sigma), and 2.5% deionized water. The crude peptides were washed three times with anhydrous ether (Fisher Biotech, Fair Lawn, NJ). After that, peptides were dissolved in acetonitrile and distilled (DI) water (50/50 v/v). The peptide solution was freezed in a -80 ˚C refrigerator overnight and then was freeze-dried for 48 hours by using the Labconco freeze dry system (Labconco, Kansas City, MO). The pH value of the peptide in water solution was 3.6. Molecular weight of the synthesized peptide was confirmed by matrix-assisted laser desorption/ionization time-of-flight mass spectroscopy on an Ultraflex II instrument (Bruker Daltronics, Billerica, MA). The peptide purity wa confirmed by a Beckman System Gold high performance liquid chromatography (HPLC, Beckman Coulter, Inc., Fullerton, CA) on a phenomenex synergi 4 μ Hydro-RP column (Phenomenex, Inc., Torance, CA) with the following gradient: 10-90% B in 20 min (A: 99.9% H_2O, 0.1% TFA; B: 90% acetonitrile, 9.9% H_2O, 0.1% TFA).

For albumin triggered hydrogel, 10 mM (1.74 wt %) peptide was first dissolved in 100 mM $NaHCO_3$ solution. BSA and HSA were dissolved in water with 5 wt % concentration. The peptide solution and albumin solution were then mixed at a different ratio for final mixtures of 1, 2, 3 mM h9e peptide with albumin from 0.1 to 5 wt %.

8.3.2 Transmission Electron Microscopy (TEM)

Peptide solutions were prepared by a negative strain method. 20 μl peptide solution was placed on Formvar/carbon-coated 200-mesh copper grids (Electron Microscopy Sciences, Fort Washington, PA) for 1 min. We removed the extra solution and float the TEM grids on the top surface of 2% (w/v) uranyl acetate (Ladd Research Industries, Inc., Burlington, VT) for 60 s at ambient conditions. We picked up the TEM grids and dried them before imaged. The samples were observed with a CM100 TEM (FEI Company, Hillsboro, OR) at 100 kv.

8.3.3 Oscillational RheologyTest

The storage, G', and loss, G'', moduli of h9e hydrogels with different peptide/albumin ratio were measured on a rheometer system C-VOR 150 (Malvern instruments, Malvern, Worcestershire WR141XZ, United Kingdom) with a 20 mm diameter parallel plate test system. All rheological tests were tested at 37 ℃. To determine the hydrogel forming rate, the peptide and albumin mixture was placed in the measuring system immediately after preparation and tested by a single frequency (1 Hz) method with steady shear strain (1%) for 1 hour

8.4 Results and Discussion

During the study of h9e peptide for 3D cell culture, we found that h9e peptide solution could be directly added into Minimum Essential Medium (MEM) with 10% serum and transform into a self-supporting hydrogel matrix within 1 min; however, using MEM without serum did not stimulate solution-to-hydrogel transitions effectively. This supports out hypothesis that some component of serum, possibly albumin, can cause h9e to form a hydrogel. This phenomenon was further tested in other cell culture mediums such as Dulbecco's modified Eagle's medium (DMEM), Roswell Park Memorial Institute medium (RPMI) and Leibovitz medium (L-15). Because serum is a complex combination, we focus on one of its most abundant component, albumin. Albumin contains charged groups and several surface binding domains, which has great potential to bind with peptide molecules and enhance the self-assembly process. . Interestingly, the hydrogel formation of h9e peptide in a serum-free N2B27 supplemented 2i medium with 1 wt% albumin confirmed our assumption.

To demonstrate this albumin induced peptide self-assembly pathway, we prepared h9e/BSA and h9e/HSA mixtures and observed under TEM. Peptide nanofiber binds on the surface of both albumins (Figure 8.1). Figure 8.1a shows the BSA attached the peptide nanofibers. Similarly, Figure 8.1b exhibits peptide nanofibers touching the surfaces of HSA. These observations confirm the interactions of h9e peptide and albumin molecules. In addition, the hydrogel forming process was monitored by a rheological test. Figure 8.2a presents the storage modulus (G') change of 3 mM h9e peptide solution right after mixing with 5% BSA. In contrast to 3 mM h9e solution or 5% BSA solution that performed as a Newtonian liquid during the 30 min test, the mechanical strength of h9e/BSA mixture kept increasing within the first 500

s and reached a stable G' around 200 Pa. The relationship of h9e peptide and BSA was further tested by testing the mechanical strength and hydrogel forming rate of 3 mM h9e with BSA ranging from 0.1 wt % to 5 wt %. Figure 8.2b shows an interesting phenomenon: the finial strength of the h9e/BSA hydrogel with the same peptide concentration does not linearly correspond to the BSA concentration. For example, after 2 hours of testing, the G' of peptide with 0.1 wt % BSA is about 110 Pa. The G' increased to over 900 Pa for peptide hydrogel with 0.5 wt % BSA but reduced in gradient to 680 Pa and 200 Pa for peptide with 1 wt% and 5 wt % BSA respectively. On the other hand, the enlarged screen (Figure 8.2c) of the first 500 s of data shows that the increasing rate of G' is consistent with the BSA concentration, which indicates that albumin helps peptide molecules self-assemble into hydrogel.As we suggested in our previous study that the kinetic is a key factor for peptide self-assembly, relatively lower BSA concentration may allow a slower assembly rate for peptides and lead to a better nanostructural arrangement for a stronger mechanical strength. The mixtures of different peptide concentrations (1-3 Mm) with constant BSA concentration (1wt%) were also studied. Higher peptide concentration leads to stronger and faster hydrogel formation (Figure 8.2d). A solution of 1 mM peptide with 1 wt % BSA performed like a Newtonian liquid after a 2 hour-test, suggesting that a critical peptide and BSA concentration may exist for this hydrogel forming process. A similar phenomenon has been found in the h9e/HSA mixture (Figure 8.3). Hydrogel was formed when 3 mM h9e peptide was mixed with 5 wt % HAS (Figure 8.3a). The hydrogel strength and forming rate were more sensitive to the HSA concentration compared with the h9e/BSA mixture. Hydrogel did not form when peptide concentration was 1 mM or HSA concentration was 0.5 wt %, which again suggests the concentration requirement of both compounds for h9e/HSA hydrogel formation (Figure 8.3 b, c). The differences between the storage modelus of hydrogel triggered by BSA and HSA need to be further studied.

Albumin triggered peptide self-assembly is a unique and interesting property. This needs to be further studied by characterizing the peptide-albumin binding site, understanding how peptide-albumin binding help the molecular self-assembly process and determining the critical concentration for stable hydrogel formation via this process. With better understanding of this peptide self-assembly pathway, many functional peptide could be designed and a wide range of biomedical applications are waiting for them.

8.5 Conclusions

The h9e peptide could self-assemble into hydrogel with the help of BSA and HSA. The association between the peptide nanofibers and albumin molecules were observed under TEM. The mechanical study suggests that hydrogel formation could be triggered right after mixing a peptide solution with albumin. The hydrogel formation rate is related to the albumin concentration in that the higher albumin concentration leads to faster hydrogel formation; however, a relatively lower concentration may allow a better peptide molecular organization for stronger mechanical strength. The critical concentration of both peptide and albumin is needed for this hydrogel forming pathway.

8.6 Acknowledgments

We thank the University of Kansas Mass Spectrometry Lab for HPLC and mass spectrometric analysis. This project was partially funded by the KSU Targeted Excellence Program and the KSU Research Foundation Scholarship Program.

8.7 References

1. Zha, L.; Banik, B.; Alexis, F. Stimulus responsive nanogels for drug delivery. Soft Matter 2011, 7, 5908-5916.

2. Branco, M. C.; Pochan, D. J.; Wagner, N. J.; Schneider, J. P. The effect of protein structure on their controlled release from an injectable peptide hydrogel. Biomaterials 2010, 31, 9527-9534.

3. King, W. J.; Mohammed, J. S.; Murphy, W. L. Modulating growth factor release from hydrogels via a protein conformational change. Soft Matter 2009, 5, 2399-2406.

4. Garty, S.; Kimelman-Bleich, N.; Hayouka, Z.; Cohn, D.; Friedler, A.; Pelled, G.; Gazit, D. Peptide-Modified "Smart" Hydrogels and Genetically Engineered Stem Cells for Skeletal Tissue Engineering. Biomacromolecules 2010, 11, 1516-1526.

5. Chawla, K.; Yu, T.; Liao, S. W.; Guan, Z. Biodegradable and Biocompatible Synthetic Saccharide-Peptide Hydrogels for Three-Dimensional Stem Cell Culture. Biomacromolecules 2011, 12, 560-567.

6. Xu, C.; Kopecek, J. Self-assembling hydrogels. Polymer Bulletin 2007, 58, 53-63.

7. Curry, S.; Mandelkow, H.; Brick, P.; Franks, N. Crystal structure of human serum albumin complexed with fatty acid reveals an asymmetric distribution of binding sites. Nature 1998, 5, 827-835

8. Dennis, M.; Zhang, M.; Meng, G.; Kadkhodayan, M.; Kirchhofer, D.; Combs, D.; Damic, L. A. Albumin binding as a general strategy for improving the pharmacokinetics of proteins. J. Bio. Chem. 2002, 277, 35035-35043.

Figure 8.1 TEM image of peptide albumin mixture: a. h9e/BSA mixture, b. h9e/HSA mixture.

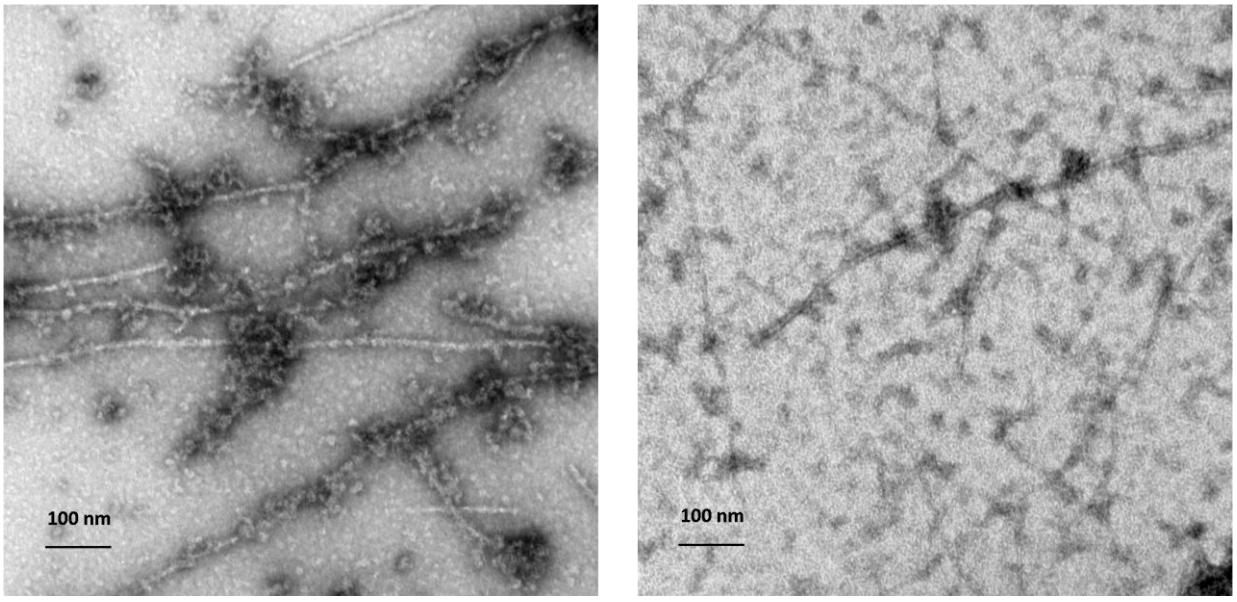

Figure 8.2 Mechanical properties of h9e/BSA hydrogel.

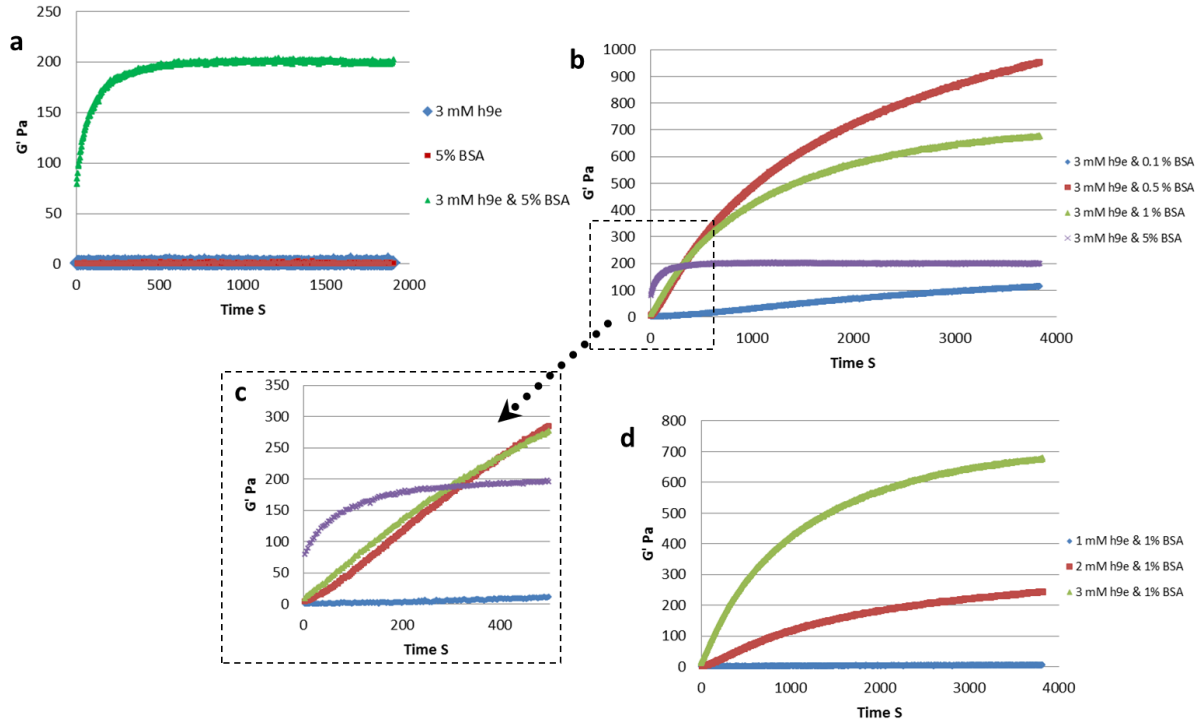

Figure 8.3 Mechanical properties of h9e/HSA hydrogel.

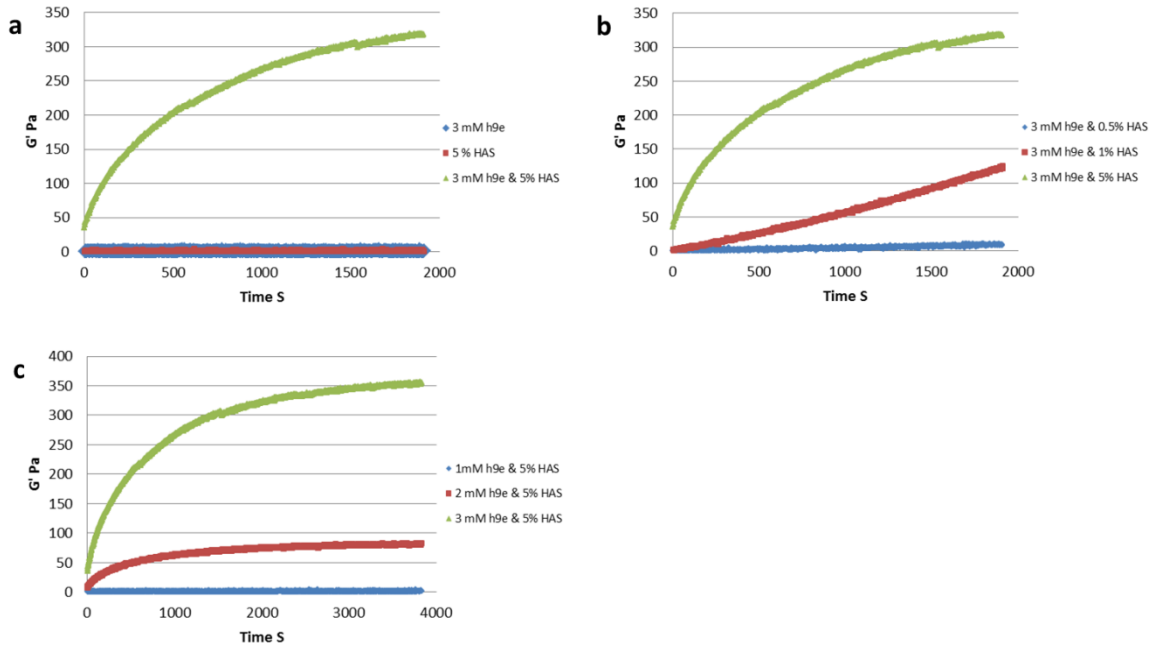

Chapter 9 - Conclusions and Recommendations

9.1 Conclusions

With the motivation of promoting understanding of the self-assembly pathways of peptide monomers for rational design of functional biomaterial, this study began by combining two identified functional sequences of native protein for a novel Ca^{2+} sensitive nanofiber-forming peptide. This peptide was further developed into a hydrogel-forming sequence by introducing a strong hydrophobic domain at the N-terminus. With in-depth modification of peptide primary structure as well as characterization of the structural, morphological and mechanical properties during hydrogel formation, some key factors for controlling peptide self-assembling pathways and some specific trigger methods for peptide sol-gel transition have been identified. At the end, some potential applications of these controllable hydrogel forming peptides were exploited as 3D cell culture. Here, we conclude the major discoveries during this study.

A novel peptide, eD_2, was designed by rationally combining two native functional sequences from spider silk and calcium-binding motifs. This peptide was a β-spiral structure and inherited properties of both model sequences by showing nanofiber morphology under the trigger of Ca^{2+}. The specific Ca^{2+} responsive behavior of this peptide was further demonstrated by changing solution pH, adding other metal ions, and mutating the model sequence. These properties indicated eD_2 could be used as a nanofiber-introducing motif under the help of Ca^{2+}.

Selecting a functional hydrophobic sequence, FLIVIGSII (h9), from a trans-membrane motif of a human muscle calcium channel to add at the N-terminus of eD_2, a new peptide h9e performed Ca^{2+}-sensitive hydrogel forming properties; however, eD_2 alone or tailored with hydrophobic segments (i.e., h5 = FLIVI) was not able to form hydrogels, which indicated the turning function of GSII played a key role to alter the molecular assembly pathways of h9e for hydrogel formation. Beside the Ca^{2+} trigger, acidic pH would also lead to h9e hydrogel formation. At 2.5 mM peptide concentration, the storage modulus (G') of h9e acidic hydrogel was 10 times stronger than that of h9e Ca^{2+} hydrogel. In addition, h9e Ca^{2+} hydrogel has some specific properties such as thermal stability up to 80 ℃, G' reversibility at the temperature range from 2 to 80 ℃ and shear-thinning and rapid recovery mechanical strength. These distinct

physical properties suggest the great potential of h9e peptide for drug delivery and tissue engineering applications.

To further exploit the effect of conformational properties of monomeric peptides, especially the turning segment between hydrophobic and hydrophilic domains for final peptide physical properties, a series of diblock amphiphilic peptides were designed by inserting turning regions with different levels of flexibility. Demonstrated by the experimental data as well as computer simulation, the close relationship between the conformational flexibility of individual peptides and the supramolecular morphologies of peptide aggregations was revealed: greater conformational heterogeneity of a peptide monomer would lead to a higher propensity of anisotropic aggregated flat sheet formation. Kinetics, affected by peptide monomeric conformation and solution environment, was suggested to play a key role in controlling the peptide self-assembly pathway.

The study of h9e hydrogel forming process through NMR, TEM and rheometer demonstrated that, in the DMSO/H_2O solution, the h9e peptide presents an amphiphilic structural property with C-terminal proximity of potentially charged Asp residues and tends to adopt a more helical structure during hydrogel formation. Adding Ca^{2+} to the peptide solution could enhance the hydrogelation rate and lead to a more stable gel strength with shear-thinning and rapid recovery property; however, Ca^{2+} ions did not change the peptide monomeric structure. Instead, they occupy the charged Asp residues on fiber surface and affect hydrogel interfiber interactions. The entanglement crossings of nanofibers may play an important role in hydrogel injectable mechanical property.

Furthermore, we used h9e peptide hydrogel for 3D cell culture of a breast cancer cell, MCF-7. By directly mixing cells with peptide solution and the cell suspension of MEM, cells were homogeneously encapsulated in h9e hydrogel. The hydrogel forming rate and finial mechanical strength can be adjusted by changing medium temperature or peptide concentration. Cells residing in peptide hydrogel adopt growing and merging clustered structures that resemble real tumors. Because of the specific shear thinning and rapid recovery rheological properties of h9e hydrogel, the mixture could not only be injected or delivered via syringe or pipette multiple times but also allowed to isolate 3D cultured cells effectively from the hydrogel matrix by simply pipetting and diluting with MEM medium. This isolating process is convenient, safe, and

suggests the great advantage of using this peptide hydrogel for 3D cell culture and other biomedical studies.

In addition, inspired by hydrogel formation in serum containing cell culture medium, we identified a unique albumin induced self-assembly pathways for h9e hydrogel formation. Through binding on the surface of albumin molecules, peptides could be triggered to form hydrogel matrix right after mixing with albumin solution. The hydrogel formation rate is related to the albumin concentration, and a relatively lower concentration may allow better peptide self-assembly to form a hydrogel with stronger mechanical strength. This hydrogel-forming pathway is also dependent on the critical concentration of both peptide and albumin.

The information provided in this study not only yields a successful model for rationally designed biomaterials from native functional sequences and helps to understand the peptide's spontaneous organization for hydrogel formation, but also inspires a novel pathway to induce peptide self-assembly via native molecules for future peptide-based materials designed for biomedical applications.

9.2 Recommendations

Future studies of this project could consider the following points:

1. Study the binding site between h9e peptide and albumin molecules. Understand the structural complementary for albumin and h9e association and how this binding helps peptide molecular self-assembly for hydrogel formation. Identify the critical residues of h9e primary structure and build the peptide structural model for future design of peptides with albumin-binding triggered self-assembly property. Further understand the self-assembly kinetic on mechanical properties and nanofiber morphology of peptide hydrogel materials. Design albumin binding peptides with different assembling capability such as micelle, nanofiber and nanosheet for drug delivery, and hemostat and biosensor applications.
2. Study the molecules with different sizes, charges, and morphologies diffused into and released from the peptide hydrogel matrix to better understand how nutrient supplies or drug treatment for 3D cultured cells in the hydrogel matrix and molecules are released for hydrogel targeted delivery. Further modify h9e peptide to yield different biophysical properties such as cell adhesion, pore size, gel

strength, and molecular conjugation capability for different applications. Apply h9e hydrogel series as 3D cell culture for different cell types. Use them for drug delivery systems including the oral administration of h9e/drug solution because the h9e peptide could form hydrogel in acidic stomach conditions.

3. Study the adjuvant (drug delivery) mechanism of h9e peptide. Several possibilities such as the peptide-cell binding hypothesis, the antigen controlled release hypothesis, and the peptide-cell penetrating hypothesis need to be considered in this study. Apply this peptide series for different animal and human vaccine systems.